University of California
Santa Barbara

Thermal Behavior of Holographic Quantum Field Theories

A dissertation submitted in partial satisfaction
of the requirements for the degree

Doctor of Philosophy
in
Physics

by

Eric Mefford

Committee in charge:

Professor Gary T. Horowitz, Chair
Professor David Berenstein
Professor David Weld

June 2018

The Dissertation of Eric Mefford is approved.

Professor David Berenstein

Professor David Weld

Professor Gary T. Horowitz, Committee Chair

June 2018

Thermal Behavior of Holographic Quantum Field Theories

To Chili

Acknowledgements

First, I would like to thank my advisor Gary Horowitz for his support and mentorship during my graduate career. Throughout my time at UCSB, Gary has consistently encouraged me to become a strong independent scientist. This has served his previous students well (congratulations, Netta, on your new faculty position!) and has made me feel very proud of my work. This is best illustrated in my first two papers where, when it came time to publish, he insisted being listed second against convention [1] or that I should publish the paper myself [2]. Finally, he helped fund trips to TASI in Boulder, GR21 in New York, and a workshop in Benasque, Spain, so that I could meet and collaborate with other researchers in the field. I hope one day to be as good a teacher and advisor as he has been to me.

Second, I would like to thank Professors Don Marolf and Joe Polchinski. Don has been both a collaborator, a string theory teacher, and a useful resource in my endless confusion with entanglement entropies. Joe was a wonderful mentor and teacher who inspired me and the entire physics community. In addition, he served on my advancement committee and helped organize the TASI summer school in Boulder. I would also like to thank Professors Kengo Maeda and Akihiro Ishibashi, whose visit to Santa Barbara started an exciting set of collaborations which have continued since our first project. They are wonderful collaborators who have taught me how to be respectful and encouraging even when the graduate student on the collaboration (me) is wrong. I would also like to thank David Berenstein and David Weld for serving on my committee.

Next, I would like to thank Edgar Shaghoulian. Edgar has been a mentor for me in physics longer than anyone else. At Stanford, he was my TA in junior year, helped

oversee my undergraduate thesis the next summer, and we were co-TA's my senior year. My first year of grad school, he spent a few months at UCSB during the great firewall debates of 2012-2013 and the next year, came to UCSB as a post-doc. We finally found a way to collaborate during his last year here. He has always been a good friend, advisor, and collaborator and while it is at times frustrating, his constant assumption that I am wrong forces me to be a better scientist and explain things in clearer, more concise terms.

I would like to thank many graduate students who have been friends and mentors during my time at UCSB. I would first like to thank Kevin Kuns. He and I spent many hours teaching ourselves group theory, tetrad formalism, and the renormalization group to answer problem sets in our first year courses. Kevin has been a great housemate and friend and is my go-to resource for quantum field theory and LIGO and the reliable source for finding good Indian food. I would like to thank Benson Way, Gavin Hartnett, and Netta Engelhardt, for leading the way for me as Gary's previous students and for teaching me numerics and much of what I know about General Relativity. I would like to thank Alex Miller for her friendship and for her amazing ability to become friends with new physicists and to let me tag along. I would like to thank Milind Shyani for being my backup resource for QFT, for being a hilarious person whose never-ending happiness inspires me to never take things too seriously, but mostly for the new gray hairs I grew in the days leading up to our paper submission.

Finally, I could not have done this without my friends and family. Jason Iaconis, Andrew Dunsworth, Scott Haselschwardt, and Nick Noll shared my passion for surfing and helped keep me sane during my graduate career. I must thank Bishnu and

Bhaskar making the day to day tasks of Naomi and my lives easier during the last couple of years. My parents Ivan and Ruth, brothers Tyler and Eric, sisters Caitlin and Melissa have always been there for me especially during some of the more trying times over the last few years and I could not have done this without them. Finally, there are not enough thanks in the world that I can give to Naomi. She is my inspiration and the most caring, strongest person I know.

Curriculum Vitæ

Eric Mefford

Education

2018	Ph.D. in Physics (Expected), University of California, Santa Barbara.
2015	M.A. in Physics, University of California, Santa Barbara.
2012	B.Sc. in Physics with Honors and Distinction, Stanford University

Publications

"Sparseness bounds on local operators in holographic CFT_d"
E. Mefford, E. Shaghoulian, M. Shyani
[arXiv:1711.03122]

"Holographic stress-energy tensor near the Cauchy horizon inside a rotating black hole"
A. Ishibashi, K. Maeda, E. Mefford
Phys. Rev. D **96** 024005 (2017) [arXiv: 1703.09743 [hep-th]]

"Time-independent wormholes"
Z. Fu, D. Marolf, E. Mefford
JHEP **1612**, 021 (2016) [arXiv: 1610.08069 [hep-th]]

"Entanglement Entropy in Jammed CFTs"
E. Mefford
JHEP **1709**, 006 (2017) [arXiv:1605.09369 [hep-th]]

"Simple holographic insulator"
E. Mefford and G.T. Horowitz
Phys. Rev. D **90** 084042, (2014)

Abstract

Thermal Behavior of Holographic Quantum Field Theories

by

Eric Mefford

This dissertation investigates thermal holographic quantum field theories dual to gravitational systems with black holes. This study has relevance for experimental physics in a lab or near an astrophysical black hole as well as for the structure of higher dimensional quantum field theories. The dissertation begins with an introduction to AdS/CFT, entanglement entropy, and numerical methods.

The next two chapters explore constraints on holographic quantum field theories with a semi-classical dual. In chapter two, a scalar field is used to construct an "extended wormhole" that connects two identical asymptotic regions and is globally static. Mutual information of identical regions in the two boundary CFTs show that the expanded throat corresponds to rapid thermalization in the field theory. In the third chapter, a finite temperature phase transition in the gravitational path integral is used to constrain the spectrum of charged, spinning operators in the dual thermal CFT.

The fourth and fifth chapters are concerned with the study of thermal quantum field theories around black holes. In chapter four, the holographic dual of a zero-temperature quantum field theory on a finite temperature Reissner-Nordström black hole background is constructed. The entanglement entropy of annular regions in the field theory explains a phenomenon called "jamming," in which heat flow is impeded

due to strong interactions. In chapter five, the holographic dual to a quantum field theory on the interior of a doubly-spinning Myers-Perry black hole is constructed. The null energy along the Cauchy horizon diverges negatively, indicating singular behavior and providing evidence for strong cosmic censorship.

The sixth chapter constructs the holographic dual to a strongly interacting metal with charged bosonic excitations. Such a field theory is a candidate system to describe the pseudogap phase of the high temperature superconductors. Experiments on these systems exhibit a metal-insulator transition at zero temperature and power-law conductivities at low temperature. On the gravity side, a domain wall potential for a scalar field interpolates between UV and IR conformally invariant spacetimes with different length scales. The dimension of the scalar controls the temperature and frequency dependence of the low temperature conductivity.

Contents

Curriculum Vitae **viii**

Abstract **ix**

1 Introduction **1**
1.1 AdS/CFT basics 7
1.2 Entanglement Entropy 23
1.3 Numerics 38
1.4 Permissions and Attributions 51

2 Time-independent wormholes **53**
2.1 Introduction 53
2.2 Thin Wall Solutions 55
2.3 Smooth Solutions 63
2.4 Discussion 72
2.5 Acknowledgements 75
2.6 Appendix: No solutions with smooth scalar potentials 75

3 Sparseness bounds on local operators in holographic CFT_d **79**
3.1 Introduction 79
3.2 Method for obtaining bounds 84
3.3 Bounds on operators 88
3.4 BPS, cosmic censorship, and sparseness bounds 110
3.5 Comments on the high-lying spectrum 114
3.6 Conclusion 118
3.7 Appendix A: Black hole entropy from deconfining phase transitions . 120
3.8 Appendix B: AdS_5, AdS_6, and AdS_7 details 121

4 Entanglement entropy in jammed CFTs **134**
4.1 Introduction . . . 134
4.2 Quantum Stress Tensors in Spherically Symmetric Static Spacetimes . 142
4.3 Numerical Construction of RN Boundary Black Holes . . . 147
4.4 Boundary Stress Tensor . . . 155
4.5 Entanglement Entropies of Droplets . . . 164
4.6 Discussion . . . 185
4.7 Acknowledgments . . . 187
4.8 Appendix: Stress Tensor Expansion . . . 187

5 Holographic stress-energy tensor near the Cauchy horizon inside a rotating black hole **201**
5.1 Introduction . . . 201
5.2 Derivative expansion method . . . 205
5.3 The holographic stress-energy tensor . . . 214
5.4 Numerical results . . . 218
5.5 Conclusion and discussions . . . 231
5.6 Acknowledgments . . . 233
5.7 Appendix: $\mathcal{P}(r)$, $\mathcal{S}(r)$, $\mathcal{R}(r)$, and $\mathcal{Q}(r)$ . . . 234

6 Simple holographic insulator **238**
6.1 Introduction . . . 238
6.2 The Model . . . 241
6.3 Conductivity . . . 248
6.4 Discussion . . . 256
6.5 Acknowledgments . . . 260

Bibliography **261**

Chapter 1

Introduction

This dissertation comprises some investigations into holographic quantum field theories that I have carried out over the last five years. These quantum field theories are broadly characterized as infinitely strongly interacting gauge theories with an infinite number of colors at finite temperature. Given that the perturbative methods of the mid-twentieth century [3] have been unable to fully tackle the problem of quantum chromodynamics (QCD), a theory where the dimensionless coupling is large but finite and the number of colors is three [4], it may seem surprising that one can ask questions about a theory in which these quantities go to infinity. However, we find within string theory a remarkable duality in which these limits lead to great simplifications when questions are rephrased in the language of gravity [5].

This duality, which is often called AdS/CFT or gauge/gravity duality, initially identified the four-dimensional $U(N)$ gauge theory $\mathcal{N} = 4$ super-Yang Mills with a classical supergravity theory in five-dimensional anti-de Sitter space in the limit that N and the field theory coupling are taken to infinity. Since this discovery, physicists

have identified supersymmetric gauge theories in other dimensions d, which in the strong coupling and large N limit can be described by classical supergravity in $d+1$ dimensions [5]. Nature, it seems, views gravity and quantum field theory as two limits of the same theory, hence the denotation *duality*. In fact, many physicists now believe that gravity in asymptotically $(d+1)$-dimensional anti-de Sitter space is always dual to a d-dimensional quantum field theory, at least in some limit.

For a given spacetime, the precise details of the dual quantum field theory, phrased in the variables of fields and a Lagrangian, is not known and in some cases such a description might not even exist [6]. Nevertheless, physicists believe that all observables of the theory, phrased in terms of the expectation values of local and non-local operators, for instance correlation functions and entanglement entropies, can be calculated on the gravitational side of the duality using a translational dictionary [7, 8]. This dictionary is frequently compared to a Rosetta Stone because it holds the key to deciphering the mysteries of strongly coupled gauge theories and of quantum gravity and, like the existing Rosetta Stone, it is incomplete.

In my graduate work, I have tried to both test and discover new entries in the dictionary, as in chapters 2 and 3. These investigations explore the class of spacetimes which may have holographic dual quantum field theories and the class of quantum field theories which may have holographic dual Einstein gravity spacetimes. These chapters emphasize the role that finite temperature plays in constraining the duality. I have also applied the holographic duality to novel quantum systems, using known entries in the dictionary to learn about thermal quantum field theories as in chapters 4, 5, and 6. This follows a long trend in high energy research, in which physicists have used the duality to similarly study applications to condensed matter [9], the quark-

gluon plasma at RHIC [10], turbulence and fluid dynamics [11], and confinement in gauge theories [12].

The first aspect of the research presented here has been to explore the boundaries of the AdS/CFT correspondence. Working with Donald Marolf and Zicao Fu, we constructed static extended wormhole spacetimes, discussed in chapter 2. The exteriors to the wormhole are AdS-Schwarzschild black holes dual to an entangled pair of thermal QFTs but are *not* dual to the known thermofield double state (TFD) [13]. One can only see this by looking at both boundaries simultaneously; any one-sided observable must agree with the TFD. Hence, extra degrees of freedom must be hidden inside the wormhole. This work raises an interesting question as to whether such spacetimes should be allowed by the gauge/gravity duality as such a state cannot be constructed via a Euclidean path integral. In fact, mutual information, a measure of correlations between the two conformal field theories, shows that the system has already traced over degrees of freedom inside the wormhole.

In chapter 3, with Edgar Shaghoulian and Milind Shyani, we found criteria for CFTs to have a classical gravity dual. Ubiquitous among AdS spacetimes with compact boundaries is the presence of a thermal phase transition between competing saddles of the Euclidean path integral [12] indicating a discontinuous jump in the free energy of a large-N gauge theory from $\mathcal{O}(N^0)$ to $\mathcal{O}(N^k)$. We were especially interested in the fixed temperature, angular velocity, and electric potential ensemble. Here, the competing phases are rotating, thermal, vacuum AdS, and a charged rotating large black hole. The gravitational phase transition bounds the number of allowed CFT states at a given energy, spin, and charge, $\rho(E, Q, J) \lesssim \exp[\beta_c(E - \Phi_c Q - \Omega_c J)]$, with universal but non-trivial values for $\beta_c, \Phi_c, \Omega_c$. At large central charge, our bound

agrees with the Cardy formula for $d = 2$ (previously obtained in [14]) and gives an independent derivation of horizon entropy for black holes at the phase transition in higher dimensions. Furthermore, our bound rules out weakly coupled holographic theories which require a higher density of states.

In most applications, AdS/CFT gives a gravitational description for interacting QFTs on a fixed background manifold, typically chosen to be Minkowski space or a sphere. On these simple spaces, field theory calculations may be performed analytically, as with topological quantities which can be calculated at weak coupling, e.g. [15]. If one accepts the validity of the duality, one may explore the same QFTs on more exotic backgrounds, most compelling of which are black holes. An important step in this direction was the construction of a spacetime dual to a CFT on a Schwarzschild black hole, nicknamed a "black droplet" [16]. Intriguingly, while the black hole had an associated Hawking temperature, the CFT far from the black hole was at zero temperature. The lack of thermal equilibrium in the boundary theory resembles a phenomenon known from soft condensed matter known as "jamming."

To understand the jamming of the CFT, I constructed new black droplet spacetimes dual to CFTs on Reissner-Nordström (RN) black hole backgrounds, discussed in chapter 4. Schwarzschild black droplets have only one parameter, the mass, which controls the temperature; but, because of the scale invariance of the field theory, all black holes are conformally equivalent. The charge of RN black holes allows for variable black hole temperatures, including zero temperature extremal horizons. In these spacetimes, entanglement entropy and radial dependence of the quantum stress tensor provide complementary pictures of the jamming. Both are minimized at finite distances from the horizon, indicating localized degrees of freedom near the event

horizon uncorrelated with those far away. In the extremal limit, an effect called the Gross-Ooguri phase transition indicates that the vacuum state of a CFT has finite size excitations. Similar to monopole confinement, this transition effectively screens thermal transport away from the localized excitation. At higher temperatures, the size of excitations near the horizon increases due to thermal fluctuations; however, far from the black hole, entanglement entropy remains independent of temperature.

In chapter 5, Akihiro Ishibashi, Kengo Maeda, and I explored the interiors of black droplets to investigate the quantum instability of Cauchy horizons. There was evidence that Cauchy horizons must be unstable both classically and quantum mechanically [17, 18, 19] but these argument were classical or neglected interactions in the QFT. In our work, we asked if non-perturbative effects and strong interactions affect this picture. Using a derivative expansion (also called a blackfold expansion) we constructed the bulk dual to a CFT inside an equally spinning five dimensional Myers-Perry black hole. Within this context, the quantum stress tensor shows diverging negative energy, which shows that interactions do not fix the instability, and upholds strong cosmic censorship [20].

Particularly fascinating is the application of gauge/gravity to strongly coupled condensed matter systems. In the thirty years since the discovery of high T_c superconductivity (SC) by Bednorz and Müller [21], little progress has been made in providing a field theoretic description. Spectroscopic studies of cuprate superconductors indicate that rather than the phonon-electron interactions responsible for conventional SC, high T_c must involve strong electron-electron interactions and antiferromagnetism. As electrons (or holes) are doped into these materials, a quantum phase transition occurs between an antiferromagnetic insulator and a superconduc-

tor. Near the critical point, a third phase called the pseudogap appears with small but nonzero occupation of states near the Fermi surface. Contrary to conventional SC, in this state, it's believed that Cooper pair formation and SC condensation are not simultaneous [22]. An understanding of this phase is believed to hold the key to understanding high T_c, though a QFT description is still lacking.

Near the underlying quantum phase transition, the system is described by a conformal field theory and this problem lends itself well to the gauge/gravity duality. My advisor, Gary Horowitz, and I found a simple model that shares some features with the pseudogap, discussed in chapter 6. On the gravity side, preformed pairs are modeled by a neutral scalar field propagating near a black hole. The scalar field condenses due to a relevant deformation in the field theory and is coupled to a $U(1)$ gauge field. Introducing a Higgs-type potential gives rise to vanishing conductivity at zero temperature, while above zero temperature, thermal fluctuations produce the standard metallic Drude conductivity. Intriguingly, we were also able to recreate the conductivity response of a "Bose metal" which is thought to be a toy model for the pseudogap.

Each of the following chapters has been published elsewhere and was written for an audience familiar with the holographic dictionary. To facilitate their reading to the general physics audience and to make this thesis as self-contained as possible, the remainder of this introduction will lay out the basics of Maldacena's arguments for the existence of a holographic duality. Then, there will be a small discussion of some entries in the holographic dictionary, particularly expectation values for operators and entanglement entropies. Finally, much of my work has used numerics to solve the gravitational equations of motion. I will also give a short introduction to these

methods.

1.1 AdS/CFT basics

Modern holography often uses the general features of AdS/CFT clearly delineated by Maldacena in [5]. The practice of applying general features of holography is frequently called "bottom up" holography since it assumes the existence of a quantum field theory dual to a particular asymptotically anti-de Sitter spacetime. Whether such a field theory exists is an open question, though most physicists in the field believe it to be true since the field theory can be defined by correlation functions calculable through the holographic dictionary. Two natural extensions of this question are whether there exist field theories dual to every spacetime and similarly whether a particular quantum field theory has a semi-classical holographic dual. Some of these questions will be addressed in chapters 2 and 3.

Before we travel too far into the unknown, however, it will be useful to lay out the canonical duality: $\mathcal{N} = 4$ super Yang-Mills with gauge group $U(N)$ on four-dimensional Minkowski space and type IIB classical supergravity in $AdS_5 \times S_5$. This duality is especially convenient because many quantities in $\mathcal{N} = 4$ do not get renormalized as the coupling changes so that the duality can be subjected to non-trivial checks. Furthermore, there are consistent truncations of the supergravity theory to classical Einstein gravity in AdS_5, a theory that we know much about. Finally, this example is "top down," which means that we begin with string theory and a configuration of branes and then take limits of certain parameters and use known string theory dualities to argue in favor of the field theory and gravitational theory being

dual. This means that presumably we can vary these parameters in other directions and the field theory will remain dual to the gravitational theory, but in limits where one is simpler than the other. This is a major goal of holography, as it may lead to major insights into quantum gravity. Let's see how it works.

We begin with type IIB superstring theory in ten-dimensional Minkowski space. This theory is a theory of closed and open strings with both fermionic and bosonic excitations. The excitations are along the two dimensional string worldsheet which is embedded in the ambient ten-dimensional space. The specific notation type IIB means that the fermions have different boundary conditions depending on whether they propagate left or right along the open strings. Perhaps unsurprisingly, the representation theory for how symmetries of the two dimensional string excitations manifest in the ten dimensional space leads to a collection of fields with specific spacetime symmetries. The closed string, bosonic excitations, lead to a scalar called the dilaton, a two form, and a spin-2 particle called the *graviton*. The fermionic excitations lead to a collection of $p+1$-form gauge fields. For the IIB theory, the gauge fields have odd p, while for the IIA theory, the gauge fields have even p. These two are related by a duality called T-duality which interchanges the boundary conditions of the fermions.

Like in normal quantum field theory, the gauge fields are associated with potentials for particular charged operators in the theory and they have an underlying gauge symmetry due to the antisymmetry of the p-form. However, unlike the photon, for example, which is associated with the pointlike electron, $(p+1)$-form gauge fields are associated with p-dimensional objects called Dp-branes whose charge is given by

$$Q_p = \mu_p \int_S dA_{p+1} \tag{1.1}$$

where S is a $8-p$ dimensional surface surrounding the Dp-brane. In this way, a ten-dimensional electron would be analogous to a D0-brane and it would satisfy a Gauss's law through an 8-dimensional sphere. The "D" in the name Dp-brane stands for Dirichlet because the branes are the endpoints for open strings and their location serves as a boundary condition. The string is free to move along the Dp-brane and gives rise to $(p+1)$-dimensional quantum field theory that lives on the brane world-volume. The field content for the field theory descends from the field content of the ten-dimensional string theory whose symmetry is broken by the Dirichlet boundary condition. In particular, there will be $9-p$ scalar fields describing the location of the brane in the ambient spacetime and there will be a gauge field plus fermionic fields on the brane. Branes also have finite energy due to their tension and will backreact on the ambient spacetime. In the string picture, this is because closed strings are emanated from the brane and their excitations include the graviton.

When multiple branes are present, things get very interesting. The scalars which describe the location of the brane now must carry two extra indices that label the branes to which each of the open string ends are attached. These indices are like the color indices of adjoint valued scalars in a gauge theory. In fact, when N branes are well separated, the scalars commute and the field theory on the branes is just a $U(1)^N$ gauge theory. However, when the branes become coincident, this commutation breaks down, the open strings become massless, and the field theory on the brane becomes $U(N)$. This is like "de-Higgsing" the theory. Furthermore, the N coincident branes backreact more strongly on the surrounding geometry. A quantum field theory on the branes and a gravitational theory away from the branes are indications that we are getting close to the AdS/CFT correspondence! All that is left is taking limits.

Here is the recipe:

Consider N parallel $D3$ branes separated by a distance r. Take the decoupling limit

$$\alpha' \to 0, \quad U \equiv \frac{r}{\alpha'} \text{ fixed.} \tag{1.2}$$

Here α' is the string scale, related to the string length $\alpha' = l_s^2$, and the tension in the string $T = 1/2\pi\alpha'$. In this limit, the branes become coincident so that the string becomes infinitely heavy and excitations are supressed away from the branes. In this limit the theory decouples to four dimensional $\mathcal{N} = 4$ super-Yang Mills on the brane and closed ten-dimensional IIB string theory away from the branes. The field theory limit can be checked by comparing the field content as well as the symmetries after Higgsing the theory.

Next, solving the string equations of motion for N parallel D3 branes gives the backreacted metric [23],

$$ds^2 = f^{-1/2} dx_{||}^2 + f^{1/2}(dr^2 + r^2 d\Omega_5^2) \tag{1.3}$$

where

$$f = 1 + \frac{4\pi g N \alpha'^2}{r^4} \tag{1.4}$$

and the string coupling constant is g, related to the expectation value of the dilaton.

The branes source a self-dual five-form flux,

$$F_5 = 2\alpha' \sqrt{4\pi g N}\,(\epsilon_5 + *\epsilon_5) \tag{1.5}$$

which is the exterior derivative of the four-form gauge field discussed earlier. In the decoupling limit the metric (1.3) becomes

$$ds^2 = \alpha' \left\{ \frac{U^2}{\sqrt{4\pi g N}} dx_{||}^2 + \sqrt{4\pi g N}\frac{dU^2}{U^2} + \sqrt{4\pi g N} d\Omega_5^2 \right\} \tag{1.6}$$

This metric is $AdS_5 \times S_5$. In this limit the radius of the five-sphere is constant and equal to

$$\frac{L_{AdS}}{l_s} = (4\pi g N)^{1/4}. \tag{1.7}$$

The supergravity approximation is valid as long as $L_{AdS} \gg l_s$ so that we can neglect α' corrections to the string action. This limit is equivalent to

$$gN \gg 1. \tag{1.8}$$

Consistency under "S-duality," which takes $g \to 1/g$, requires that $N \gg 1$. A similar way to see this is to note that the leading term in the string action

$$\mathcal{L} = \frac{1}{g^2 l_s^8} \int d^{10}x \sqrt{g}(R + ... \tag{1.9}$$

is just the Einstein-Hilbert action so that the Planck length

$$l_p \sim (g l_s^4)^{1/4} \tag{1.10}$$

implies the separation of scales,

$$\frac{L_{AdS}}{l_p} \sim N^{1/4} \gg 1 \quad \text{and} \frac{L_{AdS}}{l_s} \sim (gN)^{1/4} \gg 1. \tag{1.11}$$

Returning to the field theory, the Yang-Mills coupling is related to the string coupling as

$$g_{YM}^2 = 2\pi g. \tag{1.12}$$

The supergravity approximation corresponds to

$$N g_{YM}^2 \gg 1, \quad N \gg 1. \tag{1.13}$$

This is the 't Hooft limit of the gauge theory on the brane, where planar diagrams dominate the $1/N$ perturbative expansion. In this limit, the coupling in the gauge field is large. The final step is to realize that the symmetries of AdS_5, namely $SO(4,2)$ correspond exactly to the conformal symmetry of four-dimensional $\mathcal{N} = 4$ super Yang-Mills. The $SO(6)$ rotational symmetries match onto the $SO(6)$ R-symmetry of the adjoint scalars of $\mathcal{N} = 4$ super Yang-Mills. In the string theory description, it is these six scalars that describe the locations of the D3-branes in the transverse six dimensions. Gauge symmetries in the field theory translate to global symmetries in

the gravitational theory and there is likewise a correspondence between fields in the gravitational and gauge theories. In chapter 3, we will emphasize the impact of strong coupling and large N on the spectrum of operators. These limits lead to a gap to "stringy," high spin states which become infinitely heavy as $N \to \infty$ and to a sparse spectrum of primary operators with small anomalous dimensions.

That's all there is to it! To summarize, in the decoupling limit where the string length is taken very small and a large number of D3 branes are taken to coincide, the same string theory has two descriptions. One is a strongly coupled, planar limit of a superconformal four-dimensional quantum field theory with gauge group U(N). Neglecting the five sphere, the other is a semi-classical five-dimensional gravitational theory in anti-de Sitter space. The two descriptions are the same string theory and are hence dual.

The dream of many physicists is to find a way to move away from the large N, large 't Hooft limit. Since quantum effects in the bulk are controlled by an expansion in Newton's constant, they are subleading in $1/N$. However, as N becomes finite, these effects become more important. If one could find an example in which this limit is well controlled, then perturbative quantum field theory in d dimensions could give great insights into $(d+1)$-dimensional quantum gravity. Many theories have quantities that do not scale with the coupling, and these quantities have provided non-trivial checks of the duality and new insights into the nature of quantum gravity. Some of those results will be discussed in the next section. There has been recent success in an exactly solvable one-dimensional quantum field theory [24, 25] which has given insights into quantum gravity near extremal black holes as one can move away from the infinite coupling limit.

1.1.1 Some entries in the dictionary

To use the duality, we must develop the "dictionary" that translates between the language of the gravitational theory and the quantum field theory. The dictionary has many entries [8], some of which will be discussed thoroughly in the following chapters. However, it will be useful to illustrate the example of a minimally coupled bulk scalar field, dual to a scalar operator in the field theory, to better understand what follows. Consider the following action for a scalar field in AdS_{d+1},

$$S = \frac{1}{16\pi G_{d+1}} \int d^{d+1}x\sqrt{-g}\left[-\frac{1}{2}(\nabla\phi)^2 - \frac{m^2}{2}\phi^2\right]. \tag{1.14}$$

We will attempt to solve the equations of motion for this theory in the "probe limit," or when the scalar field does not backreact on the spacetime. For simplicity, we will look at Poincaré-AdS, with metric

$$ds^2 = \frac{L^2}{z^2}\left[-dt^2 + dz^2 + dx_i dx^i\right] \tag{1.15}$$

where $z = 0$ is the conformal boundary and the extremal horizon is at $z \to \infty$. The scalar equation of motion is

$$\begin{aligned} m^2\phi &= \frac{1}{\sqrt{-g}}\partial_\mu\left(\sqrt{-g}\partial^\mu\phi\right) \\ &= (1-d)z\partial_z\phi + z^2\partial_z^2\phi + z^2(k_i k^i - \omega^2)\phi. \end{aligned} \tag{1.16}$$

One can convert this to a simple Schrödinger equation via the substitution

$$\phi \to \sqrt{\frac{L^{d-1}}{\text{Vol}}} z^{(1-d)/2} \psi. \tag{1.17}$$

where Vol is the volume of the boundary spacelike hypersurface. Now the equation of motion reads

$$(-\partial_z^2 + V(z))\psi = \omega^2 \psi \tag{1.18}$$

with

$$V(z) = k^2 + \frac{1}{z^2}\left(L^2 m^2 - \frac{d^2-1}{4}\right). \tag{1.19}$$

For $k = 0$ and $\omega^2 > 0$, the solution to this equation is

$$\psi(z) = \sqrt{z}\left(c_1 J_a(\omega z) + c_2 Y_a(\omega z)\right), \quad a^2 = L^2 m^2 + \frac{d^2}{4} \tag{1.20}$$

where J_a and Y_a are Bessel functions. Note that a is real for $m^2 > -d^2/4L^2$. This is called the Breitenlohner-Freedman bound and scalar fields below this bound are unstable as we will see in chapter 6. Our solution must have a bounded Klein-Gordon norm,

$$\begin{aligned} < \phi, \phi > &= -i \int_\Sigma d^d x \sqrt{\gamma} n^i (\phi \nabla_i \phi^\dagger - \phi^\dagger \nabla_i \phi) \\ &= 2\omega \int dz |\psi|^2 < \infty \end{aligned} \tag{1.21}$$

where Σ is a spacelike hypersurface with unit normal n^μ and induced metric γ_{ij}. In the second line, we have chosen Σ to be a fixed time slice and used eq. (1.17). Note that the energy of the scalar field is

$$E = -\int_\Sigma d^d x \sqrt{\gamma} n^\mu \xi^\mu T_{\mu\nu} = \omega^2 \int dz |\psi|^2 \tag{1.22}$$

where $\xi^\mu = \partial_t$ is the timelike Killing vector and

$$T_{\mu\nu} = \nabla_\mu \phi \nabla_\nu \phi - \frac{g_{\mu\nu}}{2}\left[(\nabla\phi)^2 + m^2\phi^2\right] \tag{1.23}$$

is the gravitational stress tensor. Hence the finite Klein-Gordon norm is equivalent to finite energy. Finally, we also require that there is no energy flux across the conformal boundary at $z = 0$, which is to say,

$$0 = \int dt d^{d-1}x \sqrt{-h} l^\mu \xi^\nu T_{\mu\nu}\Big|_{z=0} = \int dt d^{d-1}x \left(\frac{z}{L}\right)^{1-d} \partial_t\phi\partial_z\phi. \tag{1.24}$$

Again using eq. (1.17) and integrating by parts, we can show that our fields must satisfy

$$\psi_{\omega_1}\partial_z\psi^\dagger_{\omega_2} - \psi^\dagger_{\omega_2}\partial_z\psi_{\omega_1} = 0 \tag{1.25}$$

where $\psi_{\omega_1} = \frac{1}{2\pi}\int dt e^{-i\omega_1 t}\psi(t)$ is just a Fourier transform. Normalizeability and zero flux pick out just one of the solutions from eq. (1.20. This is

$$\psi(z) \sim cJ_a(\omega z) \to \frac{c}{\Gamma(1+a)}\left(\frac{z}{2}\right)^a \quad \text{as} \quad z \to 0. \tag{1.26}$$

In other words, $\psi(z)$ scales as a power of z as the conformal boundary is approached. This scaling must be related to the dimension of the dual conformal operator.

To see this, we will demonstrate how the previous solution serves as the Green's function for the Klein-Gordon equation [26]. Consider a massless field with $a = d/2$. Next, note that we can use the conformal symmetry of AdS to take all points x_i on the boundary to a single point P,

$$x_i \to \frac{x_i}{z^2 + x_i x^i}. \tag{1.27}$$

The asymptotic form for ϕ is

$$\phi \to c\frac{z^d}{(z^2 + x_i x^i)^d} \tag{1.28}$$

For all points $x_i \neq 0$, $\phi(z = 0) = 0$ but ϕ diverges when $z = 0$. Choosing the constant c appropriately, ϕ can be a delta function. Sourcing the Klein-Gordon equation on the boundary then leads to a solution in the bulk

$$\phi(z, x^a) = c\int d^d x \frac{z}{(z^2 + |x^a - x^{a'}|^2)^d}\phi_0(x^a). \tag{1.29}$$

As $z \to 0$, $\phi \to \phi_0$. Furthermore, the action for the scalar field can be expressed on-shell as

$$I(\phi) = \frac{cd}{2}\int_{z=0} d^d x d^d x' \frac{\phi_0(x^a)\phi_0(x^{a'})}{|x^a - x^{a'}|^{2d}}. \tag{1.30}$$

This scales like the two-point function of a conformal primary $\mathcal{O}$ of dimension d. This

is clear considering the following argument; if ϕ_0 serves as a source in the field theory, then it appears in the generating functional of the boundary theory as

$$Z(\phi_0) = \langle \int d^d x \phi_0 \mathcal{O} \rangle \tag{1.31}$$

so that $\mathcal{O}$ must have dimension $d/2$. It is clear that this leads to the same two-point function as eq. (1.30).

Frequently, however, we want the expectation value for an operator, for instance the electric current in chapter 6. When there exists a bulk black hole whose horizon is at a finite z_0, then both modes of ϕ are normalizeable in the bulk, and

$$\phi(z) \sim \phi_0 + \mathcal{O} z^d. \tag{1.32}$$

Massive scalars and higher spin fields behave in very similar ways. For a massive spin s particle, the exponents in the large z expansion are

$$\Delta_\pm = -s + \frac{d}{2} \pm \sqrt{m^2 L^2 + \frac{d^2}{4}}. \tag{1.33}$$

In chapter 6, we will see a specific example of this for the electric current and a complex scalar and discuss how things change when we deform the boundary theory. In chapters 4 and 5, we use the dictionary to calculate the stress tensor of the boundary field theory. There, the boundary metric serves as a source for $\langle T_{\mu\nu} \rangle$. As a nice check of the recipe, the dimension for the stress-tensor is d, as it should be in a conformal field theory.

There is a beautiful structure to anti-de Sitter space, some of which we will ex-

plore in the next section. Much has been learned by viewing AdS in the embedding space formalism [27], where the spacetime is thought of as a hyperboloid in $(d+2)$ dimensional Minkowski space satisfying

$$-T_1^2 - T_2^2 + \sum_{i=1}^{d} X_i^2 = L^2. \tag{1.34}$$

From this perspective, one can obtain the global extension of AdS as well as many exciting submanifolds [28]. At the same time, the following chapters contain detailed descriptions of these spacetimes as well as new solutions, and so in this section, we will forego much of the detail. A nice review is in [7, 29]. Because it is useful, we will mention the global properties of AdS. Global AdS is the maximally symmetric spacetime of constant negative curvature,

$$R_{\mu\nu} = \frac{2\Lambda}{d-1} g_{\mu\nu}. \tag{1.35}$$

It is the solution to the Einstein-Hilbert action with cosmological constant

$$\Lambda = -\frac{d(d-1)}{2L^2}. \tag{1.36}$$

The metric for this global AdS_{d+1}

$$ds^2 = -(\frac{r^2}{L^2} + 1)dt^2 + \frac{dr^2}{\frac{r^2}{L^2} + 1} + r^2 d\Omega_{d-1}^2 \tag{1.37}$$

and the conformal boundary is at $r \to \infty$. Near the boundary, we can write the

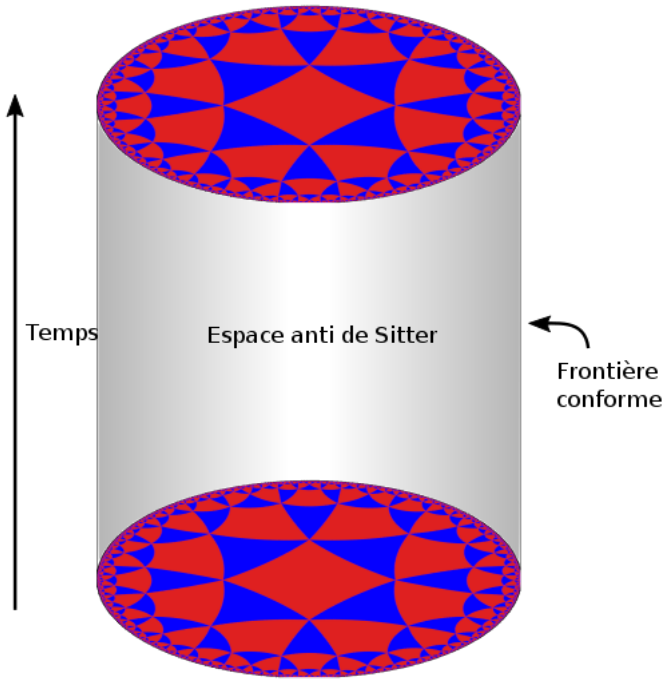

Figure 1.1: A graphical depiction of global AdS, where the boundary is $\mathbb{R} \times S^{d-1}$. Regions of constant area are depicted within the interior of the cylinder. The text is in French in honor of my upcoming postdoctoral position in Paris. Figure created by Ariel Provost and accessed via Wikimedia Commons.

metric as

$$ds^2 = L^2 \frac{dr^2}{r^2} + \frac{r^2}{L^2}(-dt^2 + L^2 d\Omega_{d-1}^2) \tag{1.38}$$

so that the boundary metric is conformally equivalent to a $(d-1)$ sphere cross time. The typical picture of AdS is of a cylinder where constant time slices are the Poincaré disc as in figure 1.1. These asymptotics will be important in chapter 3. From the

embedding formalism, we obtain this metric as

$$T_1 = \sqrt{L^2 + r^2}\cos(t/L) \tag{1.39}$$

$$T_2 = \sqrt{L^2 + r^2}\sin(t/L)$$

$$X_i = r\hat{\phi}_i, \quad \sum_i \hat{\phi}_i^2 = 1. \tag{1.40}$$

Radial light rays sent into the interior will reach the other side in

$$\Delta t = 2\int_0^\infty \frac{L^2 dr}{r^2 + L^2} = L\pi \tag{1.41}$$

while light rays sent along the equator of the sphere reach the opposite side in

$$\Delta t = L\int_0^\pi d\phi = L\pi. \tag{1.42}$$

These are the same! Thus, causality in AdS behaves similar to causality on the boundary.

On the other hand, there exist so-called bulk point singularities [30], where points on the boundary are all null separated from a single point in the bulk, but the boundary points are not null separated. These singularities appear in n-point Lorentzian correlation functions on the boundary and require $n > d + 2$. These singularities capture how locality in the bulk theory is manifested in the field theory, and they have been proposed as a tool to reconstruct the bulk metric [31]. Since the light cone serves as the boundary of timelike trajectories in the bulk, it is clear that massive particles can never reach the boundary, as discussed earlier. For completeness, we

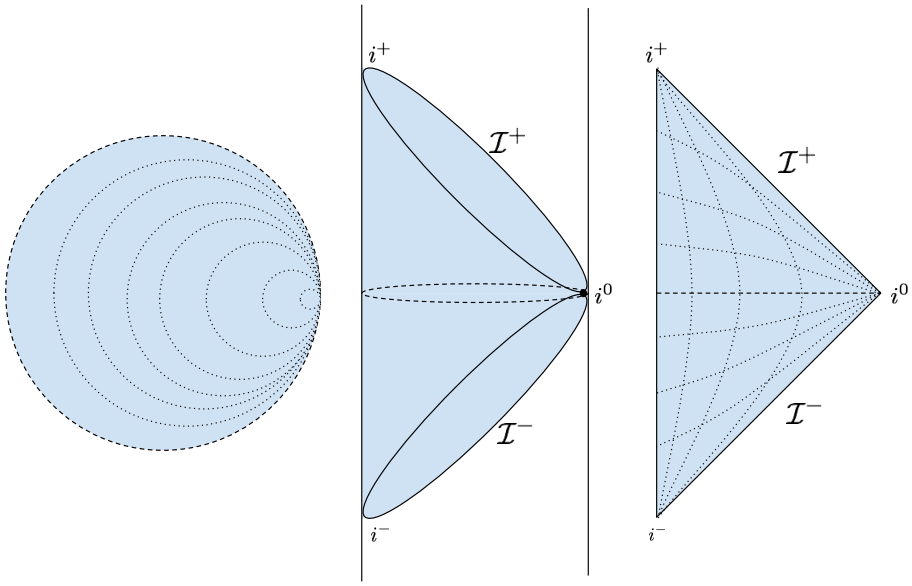

Figure 1.2: In the middle, the region of global AdS covered by Poincaré coordinates is shown in blue. Asymptotic infinity on the boundary and the point $z \to \infty$ coincide. On the left, a single time slice of global AdS is shown with surfaces of constant z shown in dotted lines. As $z \to \infty$ the size of the circle vanishes and coincides with i^0. On the right, the Penrose diagram for Minkowski space is shown. This is the metric on the boundary of Poincaré AdS.

also include the embedding for the Poincaré metric discussed earlier,

$$\begin{aligned} T_1 &= \frac{L^2}{2r}(1 + \frac{r^2}{L^4}(L^2 + x_i x^i - t^2)), \\ T_2 &= \frac{r}{L}t, \\ X_i &= \frac{r}{L}x_i, \quad i \in \{1, ..., d-1\} \\ X_d &= \frac{L^2}{2r}(1 + \frac{r^2}{L^4}(-L^2 + x_i x^i - t^2). \end{aligned} \tag{1.43}$$

From this perspective, the region of global AdS these coordinates cover is illustrated in figure 1.1.

AdS/CFT has opened the door to an exciting new way to study quantum gravity

and strongly coupled field theories. For the purposes of my graduate work, the duality has proved especially useful in bottom-up applications to strongly coupled thermal gauge theories. This included strongly coupled thermal field theories near black hole horizons and in an analogue of the pseudogap phase of high temperature superconductors. In chapters 4, 5, 6, I used techniques of the duality to explore quantum field theories where perturbative techniques had been lacking. One of the most intriguing areas of study that is difficult with perturbative quantum field theory is entanglement entropy. This is discussed in the next section.

1.2 Entanglement Entropy

Recently, there has been much excitement over the study of the entanglement entropy of a subregion in the boundary quantum field theory. Much has been learned about the nature of quantum field theories and quantum gravity by considering the relationship of this quantity to the geometry of the bulk gravitational theory. In fact, were it not for Maldacena's observation of the limits of type IIB string theory, the relation of entanglement entropy and geometry could still be considered convincing evidence for the holographic nature of quantum gravity [32, 33]. The reason for this is the striking relationship between the area of a black hole's event horizon and its thermodynamic entropy,

$$S_{BH} = \frac{A}{4G\hbar}. \tag{1.44}$$

This result was arrived at from mathematical properties of black holes, such as the requirement that classically, the area of an event horizon monotonically increases and

from the semi-classical analysis of quantum fields near the event horizon [29, 34, 35].

Conventional statistical mechanics emphasizes that thermodynamic entropy is an extensive quantity, yet if this S_{BH} counts the number of microstates of the black hole, then the states of the underlying fields in a sense live in one fewer dimension. The relationship between entropy and area becomes strengthened when one thinks of the black hole quantum mechanically. First, neglecting subtleties about topology and exotic systems [36], the ground states of a quantum field theory exhibit an area law entropy [37]. Second, while the original arguments for S_{BH} used classical general relativity, quantum corrections including higher curvature terms do not modify the area law, but instead renormalize G [38, 39, 40]. Furthermore, there is reason to believe that associated with specific null surfaces called light sheets, there is a corresponding entropy in spacetime that scales as the area [41].

Perhaps it is not surprising, then, that entanglement entropy of a holographic quantum field theory should also be given by an area, though fitting with the duality, the area is of a minimal surface in the AdS spacetime and the appropriate Newton's constant is the higher dimensional one, because as we saw earlier, it counts the number of flavors in the field theory. This is summarized in the celebrated Hubeny-Rangamani-Ryu-Takayanagi formula for the entanglement entropy of a region A,

$$S(A) = \frac{\text{Area}(\Sigma_A)}{4G_{d+1}\hbar} \tag{1.45}$$

where Σ_A is the codimension-2 extremal surface in the bulk that is anchored to the boundary at ∂A [42, 43]. This is shown for a black hole spacetime with global AdS asymptotics in figure 1.2.

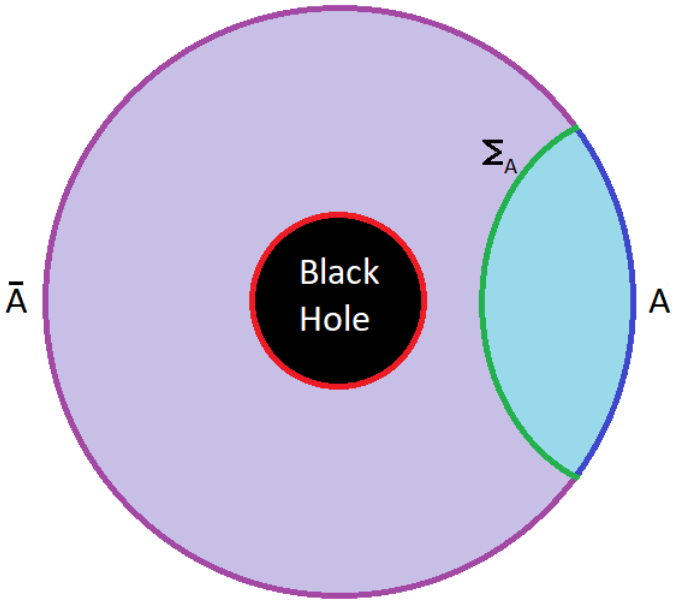

Figure 1.3: The entanglement entropy for a subregion A (blue) is given by the area of a codimension-2 minimal surface Σ_A (green) through the formula eq. (1.45). The entropy for the complementary region $\bar{A}$ (purple) is given by the area of Σ_A plus the area of the bulk black hole event horizon (red). This is because the minimal surface must satisfy a homology constraint: the region plus the minimal surfaces must completely bound a region of the bulk. For A, this is in light blue, while for $\bar{A}$ this is in light purple.

Let's discuss some properties of the entanglement entropy. First, the entanglement entropy is typically defined as the von Neumann entropy associated with a reduced density matrix for a region A,

$$S_{VN}(\rho_A) = -\mathrm{Tr}\rho_A \ln \rho_A. \tag{1.46}$$

Likewise, the reduced density matrix for a region A is obtained by tracing out all degrees of freedom outside of the region A

$$\rho_A = \mathrm{Tr}_{\bar{A}}\rho. \tag{1.47}$$

There are many subtleties associated with this density matrix, the most important of which is the fact that a true quantum field theory may not be factorizeable [44, 45]. Nevertheless, a fundamental principle of a relativistic field theory is locality, and so spatial decomposition should be possible as in eq. (1.47).

The second subtlety is that correlations in a quantum field theory are UV divergent. In a sense, this is why the entanglement entropy of a ground state satisfies an area law; most of the correlations are across the boundary of the region ∂A. Thus, for any finite quantity, we need a UV regulator ϵ. We can organize the divergences in such a state by computing a local integral over ∂A,

$$S \sim \int d^{d-2}\sigma\sqrt{h}\mathcal{F}(h,K) \tag{1.48}$$

where h is the induced metric on the surface ∂A and K is the extrinsic curvature. The function $\mathcal{F}$ is a sum of all linearly independent scalars that can be constructed out of these two functions and their derivatives. Importantly, derivatives come in pairs, so the generic entropy of the subregion A will go as

$$S \sim a_{d-2}\left(\frac{L}{\epsilon}\right)^{d-2} + a_{d-4}\left(\frac{L}{\epsilon}\right)^{d-4} + ... + a^* \log\left(\frac{L}{\epsilon}\right) + s. \tag{1.49}$$

In this expression, L is some length scale associated with A, s is the UV finite piece of the entanglement entropy, and a^* only appears for even d. We will later see that a^* is a universal constant associated with the field theory [46]. In this expression, it is clear that the leading order term is proportional to the area of ∂A and for gravitational fields, its divergence is evidence of a loop expansion which renormalizes G.

To show how eq. (1.46) captures the entanglement of a subsystem, consider the

prototypical entangled state, a Bell pair,

$$|\psi\rangle = \frac{1}{\sqrt{2}} \{|\uparrow\rangle |\downarrow\rangle - |\downarrow\rangle |\uparrow\rangle\} . \tag{1.50}$$

The density matrix for this state is $\rho = |\psi\rangle \langle\psi|$. Tracing out the second qubit gives

$$\rho_1 = \mathrm{Tr}_2 \rho = \sum_{i \in \uparrow,\downarrow} \langle i| \rho |i\rangle = \frac{1}{2} \{|\uparrow\rangle \langle\uparrow| + |\downarrow\rangle \langle\downarrow|\} \tag{1.51}$$

so that the von Neumann entropy is

$$S_1 = -2 \left(\frac{1}{2} \ln(1/2) \right) = \ln 2. \tag{1.52}$$

Compare this to the von Neumann entropy of the original system

$$S_{12} = - \left(\frac{1}{2} \ln(1/2) + \frac{1}{2} \ln(1/2) - \frac{1}{2} \ln(1/2) - \frac{1}{2} \ln(1/2) \right) = 0. \tag{1.53}$$

Note that the original system can be thought of as part of a larger system in which $\rho_> = \rho \otimes \mathbb{I}_{env}$. We see that the entanglement entropy of the entire Bell pair system with the environment vanishes as expected since they are not entangled. On the other hand, the entanglement entropy of each qubit with the other is non-vanishing and equal, which is expected since the qubits are entangled. This leads to a nice property of the von Neumann entropy,

$$S(\rho) \geq 0 \tag{1.54}$$

and vanishes only for pure states: states which can be written

$$\rho = |\psi\rangle \langle\psi| . \tag{1.55}$$

Furthermore, if we start with a pure state and trace out a subsystem, we have

$$S(\rho_A) = S(\rho_{\bar{A}}). \tag{1.56}$$

as we saw for the qubit subsystems. There are some subtleties with eq. (1.54) in quantum field theories, as the regularized entropy, which comes from subtracting the UV divergences, may be negative, but the area term always dominates the true (divergent) entropy and is positive.

Now, let's slightly modify our qubit system to be a "thermal system." Consider the two-site Ising model

$$H = \sum_i U\sigma_i^2 - h\sigma_i. \tag{1.57}$$

The eigenstates are $|\uparrow\uparrow\rangle, |\downarrow\downarrow\rangle, \text{span}(|\uparrow\downarrow\rangle, |\downarrow\uparrow\rangle)$ with energies

$$E_{\uparrow\uparrow} = U - 2h, \quad E_{\downarrow\downarrow} = U + 2h, \quad E_{\downarrow\uparrow} = E_{\uparrow\downarrow} = U \tag{1.58}$$

The thermal density matrix for this system is

$$\rho_\beta = \frac{1}{Z} \sum e^{-\beta E_i} |i\rangle \langle i| \tag{1.59}$$

where Z is

$$Z = \sum_j e^{-\beta E_j}. \tag{1.60}$$

The entanglement entropy is

$$\begin{aligned} S(\beta) &= \frac{1}{Z}\left[\sum_i e^{-\beta E_i}\beta E_i + \log Z\right] \\ &= \frac{1}{Z}\left(4e^{-\beta U}\cosh(\beta h)\left[\beta U\cosh(\beta h) - 2\beta h\sinh(\beta h)\right] + \log Z\right) \end{aligned} \tag{1.61}$$

In the first line, we see that the entanglement entropy for a thermal density matrix agrees with the thermodynamic entropy, as expected. As opposed to a pure state, the thermal system does not have vanishing entropy. Tracing out the second qubit gives the reduced density matrix

$$\rho_1 = \frac{1}{Z}\left\{\left[e^{-\beta(U-2h)} + e^{-\beta U}\right]|\uparrow\rangle\langle\uparrow| + \left[e^{-\beta(U+2h)} + e^{-\beta U}\right]|\downarrow\rangle\langle\downarrow|\right\}. \tag{1.62}$$

The entanglement entropy of this state is

$$S_1 = S(\beta) + \frac{4}{Z}e^{-\beta U}\cosh(\beta h)\left\{\beta h\sinh(\beta h) - \cosh(\beta h)\ln(2\cosh[\beta h])\right\}. \tag{1.63}$$

From the symmetry of the problem, we have

$$S_1 = S_{\bar{1}} < S(\beta). \tag{1.64}$$

For pure states the entropy of a subsystem was greater than for the whole system,

but for the thermal state it is less. One might have expected that the entropy of a subsystem should always be greater than the whole system, but it turns out that the true inequality that must be satisfied is called subadditivity. For two subsystems A and B the entropies must satisfy

$$S(A \cup B) \leq S(A) + S(B). \tag{1.65}$$

For a pure state, this just says $S(A) = S(\bar{A}) \geq 0$, which we already knew. For a mixed state, like the thermal state we just investigated, where $S_1 < S(\beta)$, this says that $2S_1 \geq S(\beta)$ which is clearly satisfied above. Hence a decrease in entanglement entropy for a subsystem is not necessarily unusual. If on the other hand, if subadditivity or its generalizations were violated, that would be a sign of major problems in a theory. This seems to be the case for our current understanding of black hole evaporation [47]. The quantity

$$I(A : B) = S(A) + S(B) - S(A \cup B) \tag{1.66}$$

is called the mutual information and is strictly positive. We study this in chapter 2.

Entanglement entropies of subsystems have been found to satisfy many such inequalities. For instance a generalization of subadditivity is strong subadditivity for three subsystems,

$$S(A \cup B \cup C) + S(B) \leq S(A \cup B) + S(B \cup C) \tag{1.67}$$

and there are further generalizations to more systems. There is also the Araki-Lieb

inequality

$$S(A \cup B) \geq |S(A) - S(B)| \tag{1.68}$$

which can be used to bound the entanglement of a system from above and below. There is currently an active research program into finding all the inequalities satisfied by a given number of subsystems [48].

In chapters 2 and 4, mutual information and relative entropies are used to investigate two holographic systems. The relative entropy is a way to compare the entropies between two states ρ and σ. It states that the relative entropy of ρ relative to σ is

$$S(\rho||\sigma) = -\mathrm{Tr}\rho \ln \sigma + \mathrm{Tr}\rho \ln \rho. \tag{1.69}$$

In words, it is the failure in $\ln \rho$ and $\ln \sigma$ to overlap. Not surprisingly, this quantity satisfies certain inequalities including positivity,

$$S(\rho||\sigma) \geq 0 \tag{1.70}$$

and monotonicity

$$S(\mathcal{N}(\rho)||\mathcal{N}(\sigma)) \leq S(\rho||\sigma) \tag{1.71}$$

where $\mathcal{N}$ is a completely positive trace preserving operation on a density matrix. A

nice example is

$$S(\rho_{AB}||\sigma_{AB}) \leq S(\rho_A||\sigma_A) \tag{1.72}$$

for two subsystems A and B. This can be used to prove strong subadditivity as well as the monotonicity of mutual information,

$$I(A:BC) \geq I(A:B). \tag{1.73}$$

It is important to state that thermal systems can be "purified" by coupling them to an auxiliary system. An example of this is the thermofield double state, discussed in chapter 2. This is a pure state obtained by coupling the Hilbert space of a system, $\{|n\rangle_1\}$ to an identical Hilbert space $\{|n\rangle_2\}$ and forming the following linear combination,

$$|TFD\rangle = \frac{1}{Z(\beta)} \sum_n e^{-\beta E_n/2} |n\rangle_1 |n\rangle_2 . \tag{1.74}$$

The density matrix is $\rho = |TFD\rangle \langle TFD|$. When one system is traced over, we get a thermal density matrix,

$$\rho_1 = \sum_m \langle m|_2 |TFD\rangle \langle TFD| |m\rangle_2 = \frac{1}{Z(\beta)} \sum_n e^{-\beta E_n} |n\rangle_1 \langle n|_1 . \tag{1.75}$$

This has a very interesting holographic dual, a maximally extended static black hole, that is discussed in chapter 2.

Many of the properties of entanglement entropies are naturally encoded into holog-

raphy. In the following we will use AdS_3 as an example because its boundary is a $1+1$ dimensional conformal field theory with many nice properties. Let's consider entanglement entropy for an interval on the boundary, $x \in [-\frac{l}{2}, \frac{l}{2}]$. As argued earlier, from the field theory we expect

$$S(L) \sim a^* \log(\frac{l}{\epsilon}) + s. \tag{1.76}$$

In fact, since we expect a^* to be a universal constant and $S(L)$ counts the states of the system, a^* should scale as the central charge c of the CFT. This is correct. For a $1+1$ CFT, we know [49, 50],

$$S(L) = \frac{c}{3} \log(\frac{l}{\epsilon}) + s. \tag{1.77}$$

Furthermore, s is typically associated with topological states, as in the case of a one-dimensional spin chain [51].

In AdS_3, minimal surfaces for the region x are geodesics which minimize the length functional

$$\mathcal{L} = 2L_{AdS} \int_{\epsilon}^{z_{max}} \frac{dz}{z} \sqrt{x'(z)^2 + 1} \tag{1.78}$$

where we will see that $\epsilon \ll 1$ serves as a UV cutoff and z_{max} is where the geodesic intersects $x = 0$. The solution to the equations of motion is

$$x(z) = \sqrt{\frac{l^2}{4} - z^2}. \tag{1.79}$$

so that $z_{max} = l/2$. Using the HRRT formula, the entanglement entropy is

$$S = \frac{\mathcal{L}}{4G_3} = \frac{L}{2G_3} \log(\frac{l}{\epsilon}) \tag{1.80}$$

as expected for a $1+1$ dimensional CFT with no topological sector. Interestingly, in this formula, we can identify the central charge of the CFT in gravitational language,

$$c = \frac{3}{2G_3} \tag{1.81}$$

which is known as the Brown-Henneaux central charge [52] due to realizations that the symmetries of three-dimensional anti-de Sitter generate a conformal algebra with the same central charge.

Holographic proofs of entanglement inequalities are fun because they have nice geometric arguments. We used one in chapter 2 and they have proved especially useful in the literature [53, 54, 55, 56, 57]. A nice example is the proof of strong subadditivity as shown in 1.2. This figure can be modified slightliy for higher dimensions where strong subadditivity is still upheld.

The Ryu-Takayanagi formula also gives a nice bulk description for the form of divergences in the entanglement entropy. Choosing a bulk cutoff $z = \epsilon$ to evaluate the area of the minimal surface, the entanglement entropy has a form

$$S \sim \frac{L^{d-1}}{4G} \int_{\epsilon}^{zmax} \frac{dz}{z^{d-1}} \mathcal{G}(z^2, h, K) \tag{1.82}$$

where again h and K are the induced metric and extrinsic curvature of the boundary of the field theory subregion. Importantly, $\mathcal{G}$ is a function only of z^2. Near the

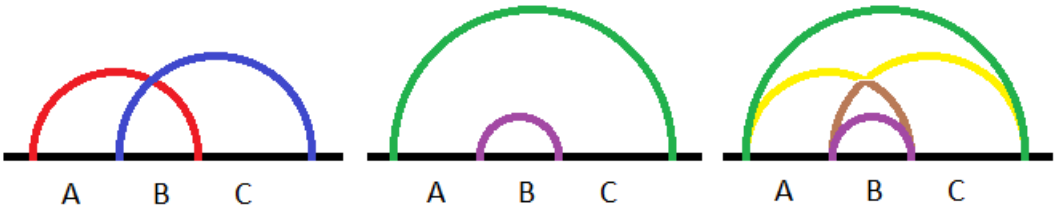

Figure 1.4: In this figure, there are three boundary subregions, A, B, C as well as their unions. For any boundary subregion that is continuous, we know the minimal surface is a semicircle. These are drawn on the left for $A \cup B$ (red), $B \cup C$(blue) and in the middle and the right for $A \cup B \cup C$ (green) and B purple. Strong subadditivity says that $S(A \cup B) + S(B \cup C) \geq S(A \cup B \cup C) + S(B)$. This is easily seen in the panel on the right, where the surfaces in the leftmost panel are redrawn but with their colors changed. The yellow curve meets $z = 0$ at $\partial(A \cup B \cup C)$ but is not the minimal surface for that subregion. Likewise, the brown curve meets the boundary at ∂B but is not the minimal surface for that region. Hence their areas must be larger than the true minimal surfaces and strong subadditivity is proven.

boundary, we can expand this function and find

$$S \sim \frac{L^{d-1}}{4G_{d+1}} \left[\frac{\mathcal{G}(0)}{z^{d-2}} + \frac{d\mathcal{G}(0)/dz^2}{z^{d-4}} + ... + \frac{d^{d/2-1}\mathcal{G}(0)}{dz^{d/2-1}} \log(\epsilon) + s \right] \tag{1.83}$$

and we also see that the log term only exists for even d. Furthermore, with certain symmetries, one can find the generic form for these divergences in terms of the boundary surface [58].

Thermal states are especially nice in the geometric picture as their bulk duals correspond to regular black holes. In these states, the bulk has a horizon at $z \sim T$, so the minimal surface can extend only that deep (there are proofs that these horizons serve as barriers [59]). In this picture, for small regions on the boundary, the entanglement entropy is very similar to that of the vacuum (dual to a zero temperature bulk horizon). This means that the UV divergences are the same for thermal states

and the vacuum on the same field theory manifold. However, for sufficiently large regions, the minimal surface spends most of its time hugging the horizon. The entanglement entropy then differs in its finite piece. We expect the vacuum subtracted entanglement entropy—that is the entanglement entropy of the thermal state minus the entanglement entropy of the vacuum state for the same boundary region—to have a form

$$\Delta S \sim \frac{1}{G_{d+1}} \mathrm{Vol(A)} T^d \tag{1.84}$$

which is the correct volume law scaling for a thermal system. Furthermore the $z \sim T$ relation shows that the thermal length scale serves as an IR cutoff to any non-extensive behavior of the entanglement. This is expected as the required periodicity in the Euclidean section of the field theory and bulk washes out correlations above the thermal scale.

The behavior of entanglement in the black hole background also emphasizes the manner in which the extra dimension manifests the renormalization group. Anti-de Sitter space has an infinite redshift because of the divergent warp factor near the conformal boundary. Particles in the bulk must have increasingly large energies, or low masses, to probe closer and closer to the conformal boundary. In fact, as we saw in the scalar field example, any massive scalar field has a solution near $z \to 0$ of the form z^{Δ_+} which vanishes and so these fields never reach the boundary. In this manner, $1/z$ is related to the mass-scale in the theory. That is the reason divergences in the entanglement entropy, related to UV correlations in the field theory, come from the $z \to 0$ region. That is also why the bulk horizon washes out correlations for

$L \gtrsim 1/T$. This is the renormalization scale below which thermal fluctuations wash out all correlations.

Finally, the bulk black holes make clear that the minimal surfaces must satisfy a homology constraint. That is, the boundary of the interior of the minimal surface is the subregion A and the minimal surface itself. It is clear that this is satisfied for the AdS_3 system we looked at previously. However, for compact boundaries, as in the case of the BTZ black hole [60], for regions larger than roughly half the boundary, the minimal surface will be disconnected. Part of the surface will look like minimal surfaces for the complement $\bar{A}$ and another piece will be the horizon of the black hole itself, which is a minimal surface because it has zero expansion, see figure 1.2.

The homology constraint is important because it upholds the fact that thermal states are dual to black holes. From statistical mechanics and dimensional analysis, we expect that the entropy of the whole boundary for a thermal state scales as the volume of the boundary times the inverse temperature β^d. In the bulk, this is proportional to the area of the bulk black hole. This lends itself nicely to interpretations of the black hole entropy formula since each microstate of the black hole should be dual to a single pure state on the boundary. Their thermal ensemble should then reproduce the entropy formula. This idea has been investigated [61] and in a sense has been used to actually reproduce the black hole entropy from the field theory [62]. In chapter 3, we use this idea to impose bounds on the number of states at a fixed energy, charge, and spin in holographic conformal field theories.

1.3 Numerics

In each of the following chapters, non-linear differential equations make analytic methods prohibitive and numerical methods must be used. There are many numerical methods for solving differential equations and each is particularly suited to a certain task. This section will only cover the basics of numerics. More complete references are in [63, 64].

1.3.1 Finite-differencing

Finite differencing or Runge-Kutta methods are well-suited to solving initial value problems. In these methods, one starts at the initial boundary, for instance a t_0 surface in a dynamical process, with a boundary condition

$$y(t_0) = y_0 \tag{1.85}$$

and approximates the solution to a differential equation

$$\sum_{m=1} a_n \frac{d^m y}{dt^m} = f(t, y) \tag{1.86}$$

at a later time t. For instance, consider the first-order simple differential equation

$$\frac{dy}{dt} = f(t, y) \tag{1.87}$$

With an approximation y_n for the actual solution $y(t_n)$ at some time t_n, we can approximate the solution y_{n+1} at time $t_{n+1} = t_n + h$ by

$$\begin{aligned} y_{n+1} &= y_n + \frac{h}{6}(k_1 + 2k_2 + 2k_3 + k_4) \\ k_1 &= f(t_n, y_n), \\ k_2 &= f(t_n + \frac{h}{2}, y_n + \frac{k_1}{2}) \\ k_3 &= f(t_n + \frac{h}{2}, y_n + \frac{k_2}{2}) \\ k_4 &= f(t_n + h, y_n + k_3). \end{aligned} \tag{1.88}$$

This method is called "RK-4" or the classical Runge-Kutta. If we had perfect knowledge of the solution, then we could find the error in this method to be

$$e_{n+1} = y(t_{n+1}) - y(t_n) - \frac{h}{6}(k_1 + 2k_2 + 2k_3 + k_4) \tag{1.89}$$

which can be shown to be of order $\mathcal{O}(h^5)$ for each step and of order $\mathcal{O}(h^4)$ for the full computation. Runge-Kutta methods with more stages, or points between t_n and t_{n+1} used in the approximation, can achieve lower errors of $\mathcal{O}(h^p)$ with $s \geq p + 1$.

Finite differencing methods have the advantage that they are easy to implement and find a solution but can become computationally expensive for a given precision. More advanced techniques involve adapting the step size and precision as the code runs. Such techniques proved especially useful in the landmark simulation of the Gregory-Laflamme instability [65, 66] as well as in generation of gravitational waveforms [67]. In boundary value problems, however, finite differencing can be difficult. Typically, one must "shoot" for a solution by tuning the initial data until one ob-

tains the correction condition at the other boundary, as was performed in the first application of holography to superconductivity [68].

1.3.2 Pseudospectral

For boundary value problems, it is often more useful to use pseudospectral methods. We will explain these by using the following differential equation as an example,

$$E(y(x)) = \mathcal{D}(x, \frac{d^{(m)}}{dx^m})y(x) = 0 \tag{1.90}$$

with boundary conditions

$$\begin{aligned} \mathcal{B}(x, \frac{d^{(m)}}{dx^m})y(x)\Big|_{x=x_0} &= 0 \\ \mathcal{C}(x, \frac{d^{(m)}}{dx^m})y(x)\Big|_{x=x_f} &= 0 \end{aligned} \tag{1.91}$$

In these expressions $\mathcal{B}, \mathcal{C}$, and $\mathcal{D}$ are differential operators and $y(x)$ is the function we are trying to find. To solve this numerically, one first discretizes the numerical domain, $x \in [a, b]$ into a set of N points, $x_1 = a, ..., x_N = b$. Then, at each point, the function $y(x)$ is approximated as $y_i = y(x_i)$. In this way, the function $y(x)$ becomes a rank-N vector,

$$y(x) \to \vec{y} = \begin{bmatrix} y_1 \\ y_2 \\ \cdots \\ y_N \end{bmatrix} \tag{1.92}$$

Next, the differential operator can be approximated by matrices over the grid. For a given grid structure, there are expressions for $\frac{d}{dx}, \frac{d^2}{dx^2}, ...$ but typically it suffices to use just

$$\frac{d}{dx} \to D^{(1)} = \begin{pmatrix} D_{11} & D_{12} & ... & D_{1N} \\ D_{21} & D_{22} & ... & D_{2N} \\ ... & ... & ... & ... \\ D_{N1} & D_{N2} & ... & D_{NN} \end{pmatrix} \tag{1.93}$$

and then

$$\frac{d^{(m)}}{dx^m} \to D^{(m)} \approx \underbrace{D^{(1)} \cdot D^{(1)} \cdot \ ... \ \cdot D^{(1)}}_{m \text{ times}}. \tag{1.94}$$

In this way, derivatives are discretized. For example

$$\frac{dy}{dx} \to (y')_i = \sum_j (D^{(1)})_{ij} y_j. \tag{1.95}$$

To illustrate how this may work for a simple differential equation, consider

$$\frac{d^2y}{dx^2} + x \, \frac{dy}{dx} + 2x^2 = 0. \tag{1.96}$$

We want to construct the differential operator

$$\mathcal{D} = \frac{d^2}{dx^2} + x\frac{d}{dx} + 2x^2. \tag{1.97}$$

Writing everything in index form, the rows of the matrix representing this operator are

$$\mathcal{D}_{ij} = D^{(2)}_{ij} + x_i D^{(1)}_{ij} + 2x_i^2 \mathbb{I}_{ij} \tag{1.98}$$

where $D^{(2)} = D^{(1)} \cdot D^{(1)}$ and the differential equation is

$$\mathcal{D}_{ij} y_j = 0. \tag{1.99}$$

In row form, it is clear how to implement the boundary conditions. Just replace the first and last rows by the corresponding matrix equation of the boundary condition. In this way, the full differential equation with boundary conditions imposed is

$$\begin{pmatrix} \mathcal{B}_{11} & \mathcal{B}_{12} & ... & \mathcal{B}_{1N} \\ \mathcal{D}_{21} & \mathcal{D}_{22} & ... & \mathcal{D}_{2N} \\ ... & ... & ... & ... \\ \mathcal{D}_{(N-1)1} & \mathcal{D}_{(N-1)2} & ... & \mathcal{D}_{(N-1)N} \\ \mathcal{C}_{N1} & \mathcal{C}_{N2} & ... & \mathcal{C}_{NN} \end{pmatrix} \begin{pmatrix} y_1 \\ y_2 \\ ... \\ y_N \end{pmatrix} = 0 \tag{1.100}$$

Now, we are ready to solve our differential equations. In linear algebra form, eq. (1.99) looks like a set of coupled polynomials whose roots are the solutions to the differential equation. Thus, we should treat our differential equation like a polynomial and find its roots using a numerical algorithm like the Newton-Raphson relaxation method.

The method is as follows. Consider some guess for a solution $y^{(0)}(x)$ which differs

from the true solution $y(x)$ by an amount $\Delta^{(0)}y(x)$. Then, we may write

$$0 = E[y(x)] = E[y^{(0)}(x)] + \left.\frac{\delta E}{\delta y(x)}\right|_{y=y^{(0)}} \Delta^{(0)}y(x) + ... \tag{1.101}$$

If we are near a solution, we can neglect the higher order terms and solve for $\Delta^{(0)}y(x)$,

$$\left.\frac{\delta E}{\delta y(x)}\right|_{y=y^{(0)}} \Delta^{(0)}y(x) = -E[y^{(0)}(x)]. \tag{1.102}$$

This gives us a new guess for the solution

$$y^{(1)} = y^{(0)}(x) + \Delta^{(0)}y(x) \tag{1.103}$$

which differs from $y(x)$ by $\Delta^{(1)}y(x)$. We can solve for $\Delta^{(1)}y(x)$ in terms of $y^{(1)}(x)$, thereby obtaining a new approximation $y^{(2)}(x)$. We continue this process k-times until we obtain a $\Delta^{(k)}$ smaller than some chosen precision. Typically, this precision is chosen to be the floating point precision of the computer and is less than 10^{-12}. One benefit of pseudospectral methods over finite differencing is that their precision scales exponentially in the number of grid points [63] and is thus less computationally expensive.

Finally, we implement eq. (1.102) on the computer by constructing the differential operator

$$\left.\frac{\delta E}{\delta y(x)}\right|_{y=y^{(i)}} \rightarrow \mathcal{F}^{(i)} \tag{1.104}$$

and solving the matrix equation

$$\mathcal{F}^{(i)}\Delta^{(i)}\vec{y} = -\mathcal{D}^{(i)}\vec{y}^{(i)} \tag{1.105}$$

and solving for $\Delta^{(i)}\vec{y}$ iteratively. For my computations, this process was easily implemented by the built-in `NSolve` function in Mathematica.

In addition to exponential convergence, pseudospectral methods are easy to adapt to coupled differential equations and partial differential equations. For coupled differential equations, for instance

$$\begin{aligned} \mathcal{D}^{(1)}y(x) + \mathcal{D}^{(2)}z(x) &= 0 \\ \mathcal{D}^{(3)}y(x) + \mathcal{D}^{(4)}z(x) &= 0 \end{aligned} \tag{1.106}$$

we can combine $y(x)$ and $z(x)$ into a vector function $Y(x) = \{y(x), z(x)\}$ and the differential operators are the elements of a 2×2 matrix $\mathbb{D}(x)$. Clearly, the numerical analog of this is to construct a rank-$2N$ vector,

$$Y = \begin{pmatrix} y_1 \\ y_2 \\ \cdots \\ y_N \\ z_1 \\ \cdots \\ z_N \end{pmatrix} \tag{1.107}$$

and an analogous matrix, $\bar{D}$, representing $\mathbb{D}(x)$.

Partial differential equations can be constructed similarly. First construct an $M \times N$-point grid with each point (x, y) labelled by (x_i, y_j). Then, a function $z(x, y)$ can be turned into a vector

$$z(x,y) \to z = \begin{pmatrix} z_{11} \\ \cdots \\ z_{1N} \\ z_{21} \\ \cdots \\ z_{2N} \\ \cdots \\ z_{M1} \\ \cdots \\ z_{MN} \end{pmatrix} \tag{1.108}$$

Partial derivatives are constructed in a similar way to total derivatives, but must accommodate the new index structure,

$$\frac{\partial}{\partial x} \to D_x^{(1)} \otimes I_y, \quad \frac{\partial}{\partial y} \to I_x \otimes D_y^{(1)}. \tag{1.109}$$

One must also be careful to respect the index structure of Y to implement boundary conditions in $\bar{D}$, but it is straightforward.

Last but not least, the actual form of the differentiation matrices and grids must be mentioned. There are two choices that are based on the symmetries of the problem.

If the differential equation has some periodicity, then the appropriate grid is evenly spaced,

$$x_i = x_{min} + (x_{max} - x_{min})\frac{i-1}{N-1}. \tag{1.110}$$

The differentiation matrix for this grid is

$$D^{(1)}_{ij} = f'_N(x_i - x_j) \tag{1.111}$$

where

$$f_N(x) = \frac{\sin(\frac{N}{2}\frac{x}{L})}{N\tan(\pi x/L)}. \tag{1.112}$$

If the system is not periodic, then one chooses a Chebyshev grid,

$$x_i = \frac{x_{min} + x_{max}}{2} + \frac{x_{min} - x_{max}}{2}\cos\left(\frac{(i-1)\pi}{N-1}\right). \tag{1.113}$$

Define

$$a_i = \prod_{j\neq i}(x_i - x_j). \tag{1.114}$$

Then

$$\begin{aligned} D^{(1)}_{ii} &= \sum_{j\neq i}\frac{1}{x_i - x_j} \\ D^{(1)}_{ij} &= \frac{a_i}{a_j}\frac{1}{x_i - x_j} \end{aligned} \tag{1.115}$$

Pseudospectral methods are the most common technique that I use in my research and they are gaining widespread traction in numerical relativity, having recently overtaken finite differencing as the state of the art in generation of gravitational waveforms especially with the "Simulating Extreme Spacetimes" group [69].

1.3.3 The Einstein-de Turck Equation

In holography, one is often trying to solve the equations of motion for classical fields on a fixed gravitational background, or as we do in chapter 6, solve for the backreacted gravitational solution which slightly modifies an existing metric. However, one can go further and ask about the existence of new solutions to the Einstein equations which are asymptotically locally anti-de Sitter. Unfortunately, analytic solutions are limited by the requirement of a large amount of symmetry and few solutions are known. On the other hand, because the Einstein equations can be phrased as a boundary value problems, the pseudospectral numerical methods just discussed are well-suited to the task of finding solutions. But, there is a catch. While it is known that the Einstein equations have a well-posed initial value formulation [20], the evolution equations are hyperbolic. For boundary value problems, one requires elliptic equations. Simple examples of hyperbolic and elliptic equations are the wave equation and Poisson's equation, respectively.

To put the Einstein equations into an elliptic form, we can use the gauge symmetry of the Einstein equations. We fix the gauge by introducing an auxiliary field, a "background metric," $\bar{g}_{\alpha\beta}$, which serves as a Lagrange multiplier. The new (vacuum)

Einstein equations, called the "Einstein-de Turck" equations, have the form

$$R_{\mu\nu} - \frac{2\Lambda}{d-1} g_{\mu\nu} - \nabla_{(\mu}\xi_{\nu)} = 0 \tag{1.116}$$

where

$$\xi^{\mu} = g^{\alpha\beta}\left(\Gamma^{\mu}_{\alpha\beta} - \bar{\Gamma}^{\mu}_{\alpha\beta}\right) \tag{1.117}$$

is the "de-Turck vector" constructed from the Christoffel symbols of $\bar{g}$. When the Einstein-de Turck equation is satisfied and

$$\xi^2 = 0, \tag{1.118}$$

the Einstein equations are satisfied simultaneously. This equation can be modified to include matter in a straightforward manner.

Solutions of the Einstein-de Turck equation with $\xi^2 \neq 0$ are termed "Ricci solitons." Given certain conditions on the metric, for instance imposing stationarity or staticity, one can demonstrate that the norm of the de Turck satisfies a maximum principle and sufficient boundary conditions will rule out Ricci solitons [63, 70]. Here we reproduce the argument for a static spacetime.

The contracted Bianchi identity, applied to the Einstein-de Turck equation, says that any solution must also satisfy

$$\nabla^2\xi_{\mu} + R_{\mu}{}^{\nu}\xi_{\nu} = 0. \tag{1.119}$$

We define

$$\phi = \xi^2 \tag{1.120}$$

which is non-negative in static spacetimes. Rewriting the Einstein-de Turck equation in terms of this scalar, and using the Bianchi identity

$$\nabla^2\phi + \xi^\mu \partial_\mu \phi = -2\Lambda\phi + 2(\nabla_\mu \xi_\nu)(\nabla^\mu \xi^\nu) \geq 0. \tag{1.121}$$

The last inequality is true for asymptotically anti-de Sitter or asymptotically flat spacetimes where $\Lambda \leq 0$. The left hand side of this equation satisfies a maximum principle for smooth, connected, Riemannian manifolds $\mathcal{M}$ with boundary $\partial\mathcal{M}$. Our static spacetime is just the Lorentzian continuation of such a manifold, so this maximum principle continues to hold. The maximum principle states

$$\begin{aligned} &i)\ \ \phi \text{ may attain its maximum only on the boundary } \partial M \\ &ii)\ \ \text{the outer normal gradient } \partial_n\phi > 0 \text{ at such a maximum.} \end{aligned} \tag{1.122}$$

Since $\phi \geq 0$ everywhere in the interior, if $\phi = 0$ on $\mathcal{M}$, then $\phi = 0$ everywhere from (i). One can also impose $\partial_n\phi \leq 0$ on $\partial\mathcal{M}$ to ensure no Ricci soliton.

In asymptotically AdS spacetimes, it is clear that the conformal boundary and spatial infinity correspond to true boundaries of the Riemannian manifold. For applications to finite temperature quantum field theory, it is useful to have a black hole horizon in the bulk. In Euclidean signature, this is a point where the $U(1)$ Euclidean

time circle smoothly caps off. Any such metric can be cast in the form

$$g = -T^2 r^2 dt^2 + A^2 (dr + r\beta_\alpha dx^\alpha)^2 + \gamma_{\alpha\beta} dx^\alpha dx^\beta \tag{1.123}$$

where the horizon is at $r = 0$. For a smooth manifold, the functions T, A, γ must be functions only of ω^2 and x^α and we require that

$$\left.\frac{T}{A}\right|_{r=0} = \kappa \tag{1.124}$$

where, upon $t \to -i\tau$

$$\tau = \tau + \frac{2\pi}{\kappa}. \tag{1.125}$$

If we choose the reference metric to be in the same class as equation (1.123) and have the same smoothness conditions, a direct calculation shows that $\partial_r \phi = \phi = 0$ at $r = 0$. In this way, the non-extremal horizon serves as a "fictitious boundary" that satisfies the maximum principle. Furthermore, the $U(1)$ symmetry of the Euclidean section can be easily modified to $SO(n)$ and the same arguments can be made to show that an axis of rotational symmetry can also serve as a fictitious boundary where $\phi = 0$. Of course, on this boundary, the analogous κ to eq. (1.124) must be unity. Finally, extremal bulk horizons serve as true boundaries, but can also be shown to satisfy a maximum principle.

After seeing the basic mechanism for AdS/CFT, including example observables of scalar two-point functions and entanglement entropies, the following chapters should be more clear. When a new observable or novel boundary conditions are intro-

duced, a somewhat pedagogical discussion will follow. Nevertheless, the concepts follow straightforwardly from those discussed in the introduction. Hopefully, the remainder of this dissertation will convince the reader that simple applications of the gauge/gravity duality have enormous power to teach us about the physical world, whether it is the behavior of quantum fields near black holes, high temperature superconductors, or exotic new laboratories like wormholes or higher-dimensional quantum field theories.

1.4 Permissions and Attributions

1. The content of chapter 2 is the result of a collaboration with Zicao Fu and Donald Marolf, and has previously appeared in the Journal of High Energy Physics [71]. It is reproduced here with the permission of the International School of Advanced Studies (SISSA), Trieste, Italy. `https://jhep.sissa.it/jhep/help/JHEP/CR_OA.pdf`

2. The content of chapter 3 is the result of a collaboration with Edgar Shaghoulian and Milind Shyani, and has previously appeared online at the arXiv [72]. It will appear in the Journal of High Energy Physics and is reproduced here with the permission of the International School of Advanced Studies (SISSA), Trieste, Italy. `https://jhep.sissa.it/jhep/help/JHEP/CR_OA.pdf`

3. The content of chapter 4 has previously appeared in the Journal of High Energy Physics [2]. It is reproduced here with the permission of the International School of Advanced Studies (SISSA), Trieste, Italy. `https://jhep.sissa.it/jhep/help/JHEP/CR_OA.pdf`

4. The content of chapter 5 is the result of a collaboration with Akihiro Ishibashi and Kengo Maeda, and has previously appeared in the journal Physical Review D [73]. It is reproduced here with permission from the publisher, the American Physical Society: `http://journals.aps.org/copyrightFAQ.html#thesis` See `http://publish.aps.org/info/terms.html` for the official copyright transfer agreement.

5. The content of chapter 6 is the result of a collaboration with Gary Horowitz, and has previously appeared in the journal Physical Review D [1]. It is reproduced here with permission from the publisher, the American Physical Society: `http://journals.aps.org/copyrightFAQ.html#thesis` See `http://publish.aps.org/info/terms.html` for the official copyright transfer agreement.

Chapter 2

Time-independent wormholes

2.1 Introduction

The familiar Kruskal wormhole has an exact Killing symmetry often called a time-translation. But as illustrated in figure 2.1 (left) for the asymptotically AdS case, this symmetry displaces one asymptotic region forward in time while shifting the other asymptotic region toward the past. As a result, non-local quantities that compare the two boundaries do in fact change under the asymptotic symmetry that shifts both boundaries toward the future. Such quantities are commonly studied in AdS/CFT and include both boundary-to-boundary two-point functions and mutual informations between the two boundaries. The resulting time-evolutions were described in e.g. [74] and [75].

Below, we explore whether Einstein-Hilbert gravity coupled to familiar matter sources might allow wormholes with a Killing symmetry that translates *both* ends in the same direction. Since topological censorship [76, 77] requires wormholes to have

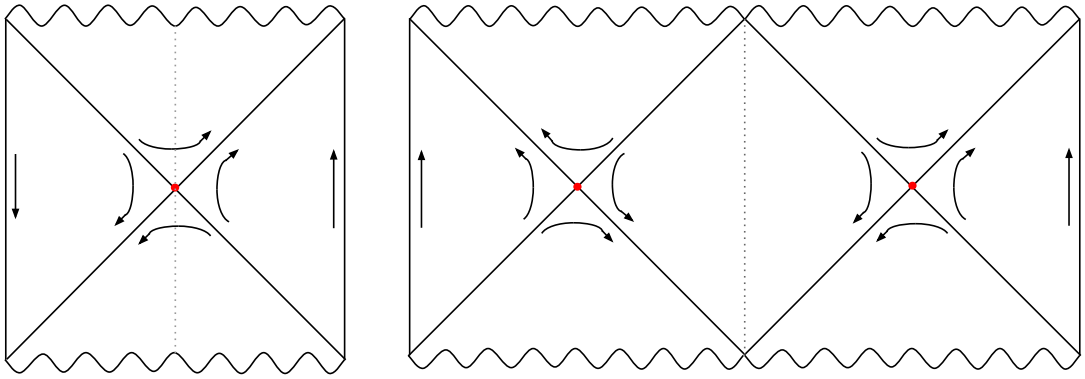

Figure 2.1: Sketches of conformal diagrams for the familiar two-sided Kruskal-AdS wormhole (left) and what we call time-independent wormholes (right). In the Kruskal case the Killing symmetry moves one boundary forward in time while shifting the other backward. But on the right the Killing symmetry acts as a future-directed time-translation on both boundaries. On the left, the Killing horizon has only a single bifurcation surface, while the Killing horizon of the right figure has two (red dots). Both spacetimes have Z_2 reflection symmetries about the dotted vertical lines. On the left, this reflection changes the sign of the time translation Killing field, while it leaves the Killing field invariant on the right.

horizons, and since the Killing symmetry must resemble a flat-space boost transformation near the horizon bifurcation surface, such spacetimes should have conformal diagrams resembling figure 2.1 (right), or more generally should have Killing horizons with an even number of bifurcation surfaces in the $t = 0$ hypersurface.

For simplicity, we study wormholes with spherical symmetry. Birkhoff's theorem then forbids vacuum solutions of this form in Einstein-Hilbert gravity. Physically, the issue is that the interior of the wormhole tends to collapse, destroying the presumed-static region shown in the middle of the wormhole at right in figure 2.1. We solve this problem by coupling gravity to a scalar field. The repulsive gravity generated by either positive-tension scalar domain walls or positive scalar potentials (which effectively act as local positive cosmological constants) allow the desired static region

to exist.

Section 2.2 constructs and studies asymptotically-AdS such solutions in the thin wall approximation. The resulting spacetimes are similar in many ways to the single-asymptotic region black holes with de Sitter interiors found in [74]. Interestingly, the holographic mutual information between the two boundaries always vanishes when considering regions smaller than half of either boundary.

We then consider spacetimes sourced by smooth scalar fields in section 2.3. We show that time-independent wormhole solutions exist when the scalar potential $V(\phi)$ is chosen to behave like $\phi^2(\log \phi)^3$ near a local minimum; i.e., while the solutions are smooth, the scalar potentials are only C^1 as functions of ϕ. Examples are constructed numerically. Again, the holographic mutual information between the two boundaries always vanishes when considering regions smaller than half of either boundary. That singular potentials are required is shown in section 2.6; scalar fields with smooth potentials cannot support our time-independent wormholes. We close with some final discussion in section 2.4. In particular, we comment on the status of such solutions with respect to gauge/gravity duality and also with respect to recent discussions of the possible role of complexity in gauge/gravity duality [78, 79, 80, 81].

2.2 Thin Wall Solutions

We begin in section 2.2.1 by constructing thin wall versions of the time-independent wormholes shown at right in figure 2.1. We then briefly analyze the holographic mutual information defined by these wormholes in section 2.2.2 and note that in a certain sense they are already thermalized at any finite t.

2.2.1 A cut and paste construction

It is straightforward to assemble the desired time-independent wormholes by cutting two copies of Kruskal-AdS (fig. 2.1 left) along a timelike surface defined by orbit of the symmetry group (a constant r surface) and then sewing the two larger pieces together other along a thin positive-tension domain wall. This domain wall then becomes the dotted line in right diagram in figure 2.1 and is left invariant under the reflection symmetry.

To proceed, recall the D dimensional AdS-Schwarzschild metric

$$ds^2 = -\left(1 - \frac{\omega_D M}{r^{D-3}} + \frac{r^2}{\ell^2}\right) dt^2 + \frac{1}{1 - \frac{\omega_D M}{r^{D-3}} + \frac{r^2}{\ell^2}} dr^2 + r^2 d\Omega^2, \tag{2.1}$$

where $\omega_D = \frac{16\pi G_D}{(D-2)S_{D-2}}$ and $S_{D-2} = \frac{2\pi^{\frac{D-1}{2}}}{\Gamma\left(\frac{D-1}{2}\right)}$. A timelike constant r surface has unit normal $n^a = \sqrt{1 - \frac{\omega_D M}{r^{D-3}} + \frac{r^2}{\ell^2}} \left(\frac{\partial}{\partial r}\right)^a$. Its extrinsic curvature $K_{ab} = \frac{1}{2}\pounds_n h_{ab}$ is thus

$$K_{ab} dx^a dx^b = \frac{1}{2}\sqrt{1 - \frac{\omega_D M}{r^{D-3}} + \frac{r^2}{\ell^2}} \left[-\left((D-3)\frac{\omega_D M}{r^{D-2}} + \frac{2r}{\ell^2} \right) dt^2 + 2r d\Omega^2 \right]. \tag{2.2}$$

We wish to consider relativistic domain walls with surface stress tensor $\hat{T}_{ab} = -\sigma h_{ab}$ in terms of the (constant) tension σ and the induced metric h_{ab}. Here we use the conventions of [20] in which h_{ab} is a degenerate tensor in the full spacetime such that $h^a{}_b$ is the projector onto the vector space tangent to the wall. The full stress-energy tensor T_{ab} is proportional to $\hat{T}_{ab}$, but contains an extra delta-function localizing the stress-energy on the wall. Given the Z_2 symmetry of figure 2.1 (right), the Israel junction conditions (see e.g. [82]) require $\hat{T}_{ab} \propto K_{ab}$, and thus $\frac{g_{tt}}{g_{\Omega\Omega}} = \frac{K_{tt}}{K_{\Omega\Omega}}$.

This relation is satisfied if and only if

$$r_{\rm wall}^{D-3} = \frac{D-1}{2}\omega_D M. \tag{2.3}$$

The junction condition then gives $K_{ab} = \frac{4\pi G_D \sigma}{D-2} h_{ab}$ so that

$$\sigma = \frac{D-2}{4\pi G_D r_{\rm wall}} \sqrt{1 - \frac{\omega_D M}{r_{\rm wall}^{D-3}} + \frac{r_{\rm wall}^2}{\ell^2}} \tag{2.4}$$

is positive as desired.

This completes our construction of thin-wall solutions corresponding to figure 2.1 (right). However, we note in passing that a similar analysis indicates that our solutions are unstable. This is to be expected as the interior of our wormhole remains static only due to a delicate balance between the gravitational attraction of the black hole and the gravitational repulsion of the domain wall. Indeed, maintaining the Z_2 reflection symmetry and spherical symmetry but allowing the wall to move with time on a surface $r = R(T)$, the Israel junction conditions imply an equation of motion

$$2\sqrt{f(R) + \dot{R}^2} = \frac{8\pi G_D \sigma}{D-2} R, \tag{2.5}$$

for $f(r) = 1 - \frac{\omega_D M}{r^{D-3}} + \frac{r^2}{\ell^2}$ and $\dot{R}$ the derivative of R with respect to proper time along the shell. Here the first-order nature of the equation is a consequence of restricting to solutions with Z_2 symmetry. Squaring (2.5) and linearizing it around the static solution (2.3), we obtain

$$\left(\frac{d}{d\tau}\delta R\right)^2 = (D-3)\, 4^{\frac{1}{D-3}} \left((D-1)\,\omega_D M\right)^{\frac{-2}{D-3}} \delta R^2 + O(\delta R^3), \tag{2.6}$$

so the static solution is unstable on the timescale

$$\tau = \sqrt{\frac{1}{D-3} 4^{\frac{-1}{D-3}} \left((D-1)\,\omega_D M\right)^{\frac{2}{D-3}}}. \tag{2.7}$$

2.2.2 Mutual Information and Thermalization

As noted in the introduction, physical quantities defined by the geometry of our wormhole must be independent of time. This includes the (leading order) holographic mutual information defined by the Ryu-Takayanagi (RT) [42, 83] or the covariant Hubeny-Rangamani-Takayanagi (HRT) [43] prescriptions. While – as will be discussed in section 2.4 – the derivations of [84] and [85] need not apply to our spacetime, it is nevertheless of interest to investigate what these prescriptions would predict. In particular, we will see that – despite the instability noted above – in a sense these mutual informations (and indeed the entropies of all boundary regions) appear to already be thermalized at any finite t.

We note that such leading-order holographic mutual informations are of more interest in our context than our boundary-to-boundary correlators, as the latter depend on the choice of quantum state for light bulk fields as well as on the classical background geometry. Since we have not constructed our spacetimes as stationary points of a path integral, there is no preferred choice for this quantum state. And due to the large causal shadow between the two event horizons of our time-independent wormholes, we are free to choose the light bulk fields in the left asymptotic region to be completely uncorrelated with those in the right asymptotic region so that all connected correlators vanish when evaluated with one argument on the right boundary and another on the left.

Because the spacetime is not globally static, the RT prescription does not strictly apply. Nevertheless, in a spacetime with time-reversal symmetry, the maximin construction of [86] guarantees the HRT surface to be the minimal surface within the $t = 0$ (i.e., within the hypersurface invariant under $t \to -t$) as one would expect from the RT prescription[1].

We wish to study surfaces anchored both to a region A_R of the right boundary and also to a corresponding region A_L of the left boundary, such that A_R, A_L are interchanged by the Z_2 symmetry of reflection across the wall. In order to compute the entropy $S_{A_L A_R}$ of $A_L \cup A_R$, we must correctly identify the minimal surface. We first consider the case where A_R and A_L are each precisely half of the $t = 0$ sphere at the AdS boundary (note that our solutions correspond to 'global' Schwarzschild-AdS). Referring to A_L, A_R as the 'northern' hemispheres (whose boundaries are thus the equator of the sphere), it is then clear that the smallest connected surface anchored to both A_L and A_R is the surface defined by taking the equator of the sphere at each r. As shown below, it suffices for our purposes to compute the area of the portion of this surface inside our wormhole. Noting that the radius r_0 of the event horizon is defined by

$$1 - \frac{\omega_D M}{r_0^{D-3}} + \frac{r_0^2}{\ell^2} = 0, \tag{2.8}$$

[1]Since this surface is minimal on the $t = 0$ slice, its area can be no larger than that of the maximin surface. But the time-reversal symmetry means that this minimal surface is also an extremal surface in the full spacetime. It can therefore have area no smaller than the maximin surface, as the latter agrees with the area of the smallest extremal surface. We thank Veronika Hubeny for pointing this out to us.

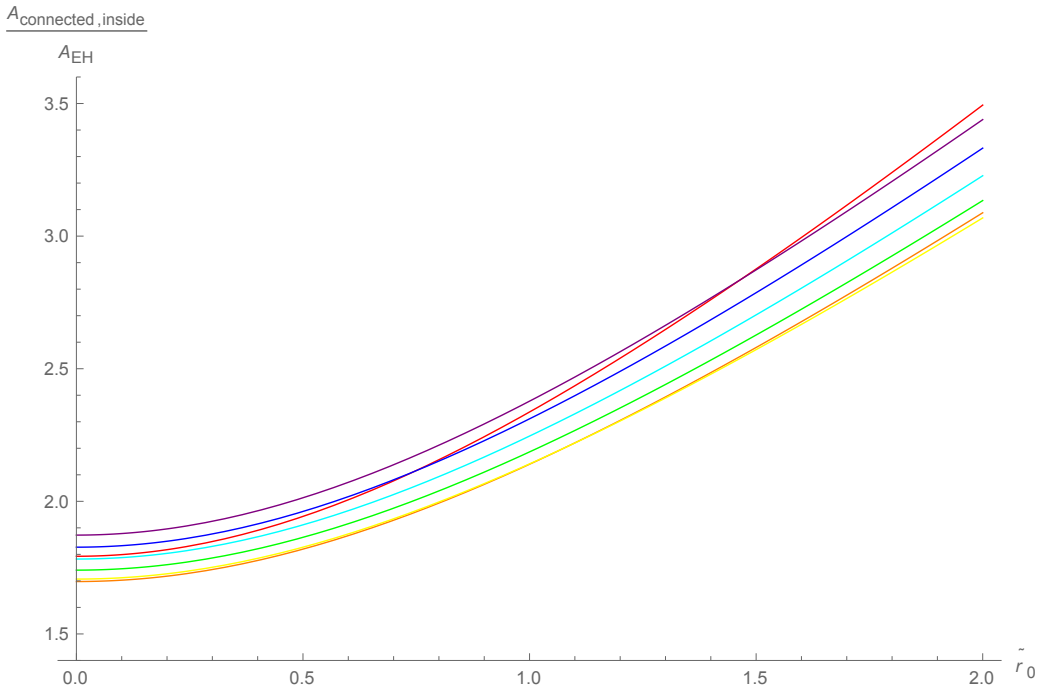

Figure 2.2: The functions (2.9) for $D = 4$ (red), $D = 5$ (orange), $D = 6$ (yellow), $D = 7$ (green), $D = 8$ (cyan), $D = 9$ (blue), and $D = 10$ (purple).

and introducing $\tilde{r} = r/\ell$ and $\tilde{r}_0 = r_0/\ell$, this area satisfies

$$\frac{A_{\text{connected, inside}}}{A_{\text{EH}}} = \frac{2}{\sqrt{\pi}} \frac{\Gamma\left(\frac{D-1}{2}\right)}{\Gamma\left(\frac{D-2}{2}\right)} \int_1^{\left[\frac{D-1}{2}\left(1+\tilde{r}_0^2\right)\right]^{\frac{1}{D-3}}} \frac{\hat{r}^{D-3}}{\sqrt{1 - \frac{1+\tilde{r}_0^2}{\hat{r}^{D-3}} + \left(\tilde{r}_0 \hat{r}\right)^2}} d\hat{r}, \tag{2.9}$$

where we have normalized the quantity by dividing by the area of either event horizon. The area of the full minimal connected surface is then $A_{\text{connected}} = A_{\text{connected, inside}} + A_{\text{connected, Kruskal}}$ where $A_{\text{connected, Kruskal}}$ is the area of the minimal connected surface in the AdS-Kruskal geometry of figure 2.1 (left).

For general D the integral (2.9) can be performed numerically. But for $D = 5$ it

can be performed exactly to obtain

$$\frac{A_{\text{connected, inside, } D=5}}{A_{\text{EH}}} = \frac{2\tilde{r}_0\sqrt{1+\tilde{r}_0^2}\,(1+2\tilde{r}_0^2) - \ln\left(1+2\tilde{r}_0\left(\tilde{r}_0+\sqrt{1+\tilde{r}_0^2}\right)\right)}{\pi\tilde{r}_0^3}. \quad (2.10)$$

As shown in figure 2.2, (2.9) and (2.10) are increasing functions of $\tilde{r}_0$, which are larger than 1.6 for all $\tilde{r}_0$ (at least for $4 \leq D \leq 10$). In particular, there is $\frac{A_{\text{connected, inside}}}{A_{\text{EH}}} > 1$.

However, as usual we must also consider the smallest disconnected surface anchored on A_L, A_R and compare its area to that of the connected surface. Let us first study a single connected component, say the one anchored to A_L. One example of a surface satisfying these boundary conditions is the surface Σ_0 shown in figure 2.3 which consists of the northern hemisphere of the bifurcation surface for the left event horizon together with the equators of all $t = 0$ spheres in the left asymptotic region. In other words, outside the horizon it coincides with the connected surface studied above anchored to both A_L and A_R. So the area of the left component of the actual minimal surface must be less than that of Σ_0.

Adding together the two components, the area of the minimal disconnected surface must satisfy

$$A_{\text{disconnected}} \leq A_{\text{connected, Kruskal}} + A_{\text{EH}}. \quad (2.11)$$

The observation that (2.9) and (2.10) are larger than 1 then implies $A_{\text{disconnected}} < A_{\text{connected}}$. The HRT surface is thus disconnected and, due to e.g. the barrier theorems of [59], lies entirely outside the horizons. The mutual information $I(A_L : A_R)$ is then just what would be obtained from surfaces outside the horizon of AdS-Kruskal (fig. 2.1 left) and $I(A_L : A_R)$ vanishes. Furthermore, the positivity and monotonicity of HRT mutual information derived in [86] then imply vanishing mutual information

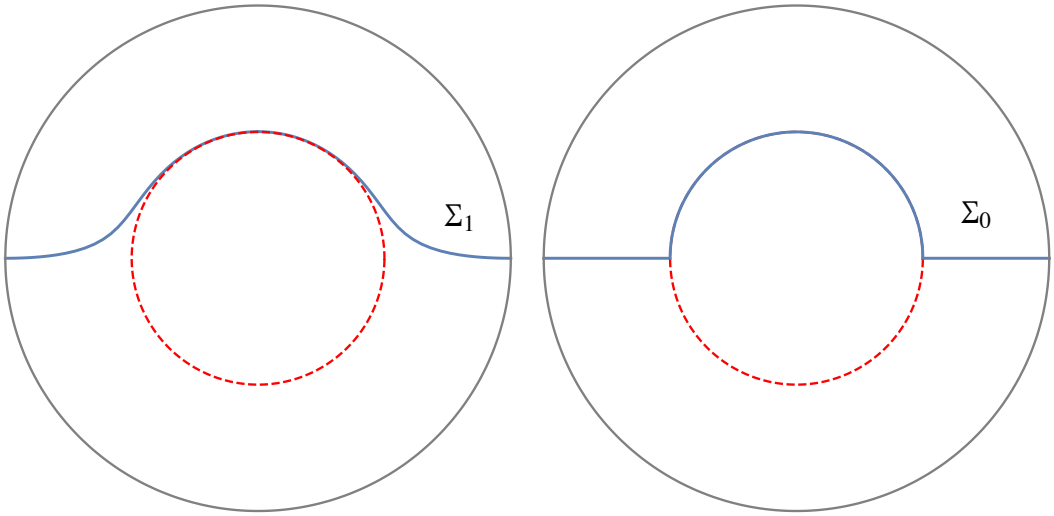

Figure 2.3: On the left, Σ_1 is minimal surface for a hemisphere of the boundary with a black hole (red, dotted) in the bulk. The surface Σ_0 on the right necessarily has larger area than Σ_1. This surface contains a piece (straight segments along the equator) that are part of the connected surface passing through the wormhole; the other piece lies on the black hole horizon.

$I(A_L : A_R)$ for any subsets A_L, A_R of the northern hemisphere, whether or not such A_L, A_R are related by the Z_2 symmetry.

In fact, since $A_L \cup A_R$ is homologous to its complement, the same argument shows that the HRT surface for $S_{A_L A_R}$ is again disconnected (and lies entirely outside the horizon) whenever A_L, A_R both *contain* the entire southern hemisphere. So here too $I(A_L : A_R)$ is what would be obtained from surfaces outside the horizon of AdS-Kruskal (fig. 2.1 left), though due to the homology constraint $I(A_L : A_R)$ no longer vanishes.

Equivalently [75], we may say in both cases that $I(A_L : A_R)$ for the time-dependent wormhole agrees with that for the $t \to +\infty$ limit of AdS-Kruskal. Though there remain certain cases that we have not checked, it is thus natural to conjecture the same to be true of arbitrary A_L, A_R, and thus for the entropies of arbitrary boundary

regions. But the $t \to +\infty$ limit of AdS-Kruskal is naturally interpreted as a thermalized state. So if our conjecture is true, then despite the instability found in section 2.2.1, as measured by such entropies we find that our time-independent wormhole is already thermalized at any finite time t.

2.3 Smooth Solutions

Having constructed time-independent wormholes using thin shells, it is natural to ask if similar solutions can be sourced by smooth scalar fields ϕ. We shall now show that they can, but with an interesting twist. While the solutions are completely smooth, the scalar potential $V(\phi)$ is not. Indeed, near the AdS minimum ϕ_0, our $V(\phi)$ will behave like $(\phi-\phi_0)^2[\ln(\phi-\phi_0)]^3$. We demonstrate the existence of such solutions analytically and construct a particular example numerically. Appendix 2.6 then gives a general argument that spherically symmetric time-independent wormholes cannot be sourced by scalar fields with smooth potentials.

Our smooth solution will bear a strong similarity to our domain wall solution, in that it will be precisely D-dimensional AdS-Schwarzschild outside the horizon and also in the region where the time-translation Killing field is spacelike. In those regions our scalar field will be constant and will sit at a minimum of its potential. The scalar will deviate from this minimum only in the central diamond of figure 2.1 (right) which in section 2.2 contained the domain wall; we refer to this diamond as the wormhole below. Smoothness then requires that all derivatives of ϕ vanish at boundaries of the wormhole.

The wormhole should enjoy both spherical and time-translation symmetry. As a

result, any smooth metric in this region may be written

$$ds^2 = -f(r)dt^2 + \frac{dr^2}{f(r)} + S(r)^2 d\Omega_{D-2}^2, \tag{2.12}$$

where we require f to vanish linearly at the wormhole boundaries to give a smooth bifurcate horizon. Imposing the Z_2 reflection symmetry of figure 2.1 (right), we may set $r = 0$ at the fixed points of this reflection. It then suffices to study the metric only on the right half of the spacetime. We take this to be $r > 0$, with the wormhole boundary at $r = r_h$. Note that (2.12) and these choices still allow the freedom to perform a constant rescaling $(t, r, r_h, f) \to (\alpha t, r/\alpha, r_h/\alpha, f/\alpha^2)$ without changing the geometry. For later reference, we note that AdS-Schwarzschild in these coordinates has

$$S_{AS}(r) = r, \quad f_{AS}(r) = \frac{r^2}{\ell^2} + 1 - (r_h^2 + \ell^2)\left(\frac{r_h}{r}\right)^{D-3}, \tag{2.13}$$

with AdS boundary at $r \to \infty$. From now on, we set $\ell = 1$ so that

$$V(\phi(r_h)) = \Lambda_{AdS} = -\frac{(D-1)(D-2)}{2}. \tag{2.14}$$

In these coordinates, the equation of motion for a single minimally coupled scalar field reads

$$f\phi'' + \left[(D-2)\frac{fS'}{S} + f'\right]\phi' = \frac{dV}{d\phi}. \tag{2.15}$$

and the nontrivial tt, rr, and sphere-sphere, components of the Einstein equation

(with $8\pi G = 1$) may be combined to write

$$\begin{gathered}(D-2)S'' = -S\phi'^2, \\ \left(\frac{S'}{S}\right) f' - \frac{D-3}{S^2}\left(1 - f(S')^2\right) = \frac{2}{D-2}T^r_r = \frac{1}{D-2}(f\phi'^2 - 2V(\phi)), \\ f'' + (D-3)\left(\left(\frac{S'}{S}\right) f' + \frac{1}{S^2} - \left(\frac{S'^2}{S^2}\right) f\right) = \frac{2}{D-2}T^\Theta_\Theta = -\frac{1}{D-2}\left(2V(\phi) + f\phi'(r)^2\right).\end{gathered} \tag{2.16}$$

As usual, (2.15) follows from (2.16) due to the Bianchi identity, so it suffices to consider (2.16).

Rather than choose a form for $V(\phi)$ and solve for the resulting $\phi(r)$, we find it convenient to proceed in analogy with section 4 of [87] and to posit $\phi(r)$. We then take the middle equation from (2.16) as the definition of $V(\phi)$. The requirement that all derivatives of $\phi(r)$ vanish at r_h motivates us to choose the form

$$\phi(r) = b \tanh\left(\frac{kr}{r_h^2 - r^2}\right). \tag{2.17}$$

This leaves us with a pair of second order ODEs (the first and last of (2.16)) to solve for $f(r), S(r)$. The Z_2 reflection symmetry requires the boundary conditions

$$S'(0) = f'(0) = 0. \tag{2.18}$$

We also wish to impose two boundary conditions at r_h. The first of these is simply $f(r_h) = 0$. Using (2.14) and our definition of $V(\phi)$ (the middle equation in (2.16))

gives the second:

$$\frac{df}{dr}|_{r=r_h} = \frac{1}{S'(r_h)S(r_h)} \left((D-1)\, S(r_h)^2 + (D-3) \right). \tag{2.19}$$

We note that (2.19) guarantees the surface gravity at the wormhole boundary to match that of AdS-Schwarzschild with horizon radius $S(r_h)$ if we rescale $(t, r, r_h, k, f) \to (\alpha t, r/\alpha, r_h/\alpha, \alpha k, f/\alpha^2)$ to set $S'(r_h) = 1$. With this understanding, the redshift factor f, the sphere size S, and their first derivatives with respect to r are then continuous at $r = r_h$. So long as $S(r_h) \neq 0$, the ODEs (2.16) then guarantee continuity of all derivatives and the geometry matches smoothly to AdS-Schwarzschild as desired. However, it will be convenient for our later numerics to first choose b, k, r_h arbitrarily and only later to rescale in this manner.

This suffices to prove that the desired solutions exist. So long as $S > 0$, it is clear that our ODEs have no singular points. Furthermore, since we take $\phi(r)$ as given, the first ODE is a homogeneous equation for $S(r)$ alone. Using only $S'(0) = 0$, it is then clear that the resulting one-parameter family of solutions for $S(r)$ will have $S > 0$ on $[0, r_h]$ so long as we choose b sufficiently small for given k, r_h. For each such $S(r)$, the second ODE defines a regular linear 2nd order ODE for $f(r)$, so there a unique solution $f(r)$ satisfying $f'(0) = 0$ and $f(r_h) = 0$. Taking the remaining free parameter to be $S(0)$, and noting that scaling $S(0) \to \beta S(0)$ induces the scalings $S(r), f(r), V(r) \to \beta S(r), \beta^{-2} f(r), \beta^{-2} V(r)$ we may then choose β so as to both satisfy (2.19) and make $S(0)$ positive. Thus smooth time-independent wormholes of this form exist so long as b is sufficiently small. Figure 2.5 displays numerical solutions

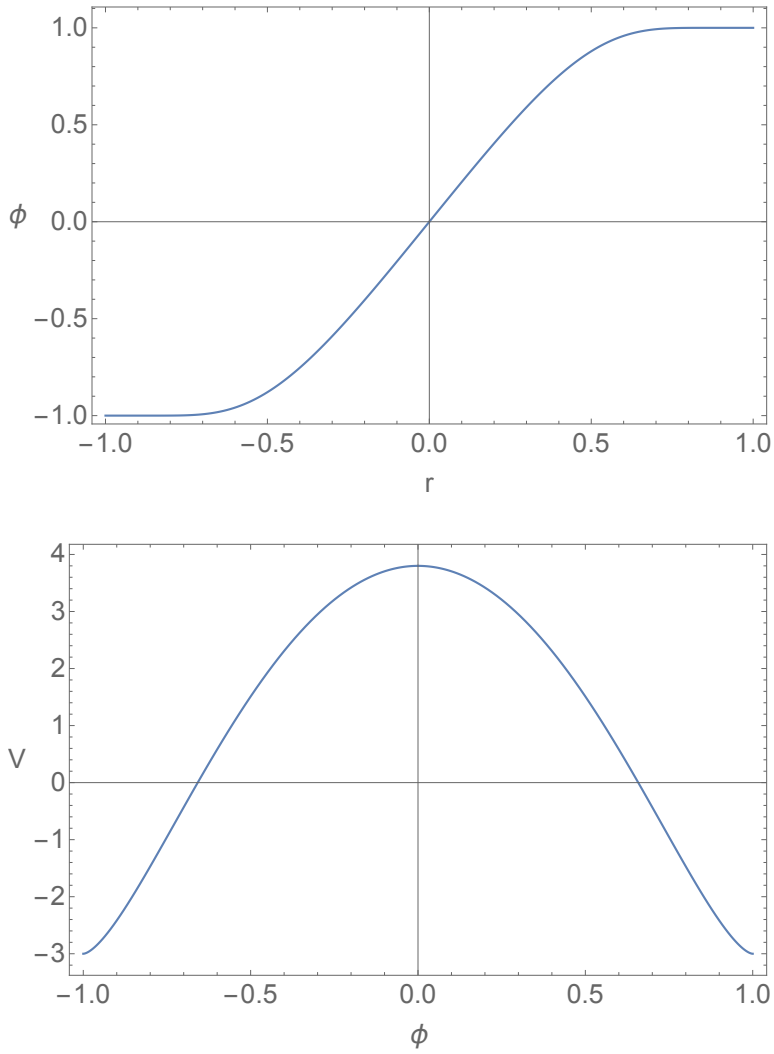

Figure 2.4:

for $f(r)$, $S(r)$ and $V(\phi)$ in $D = 4$ with

$$b = 1, \quad k = 2.05768, \quad S(r_h) = 1, \tag{2.20}$$

where for numerical convenience we have chosen $r_h = 1$.

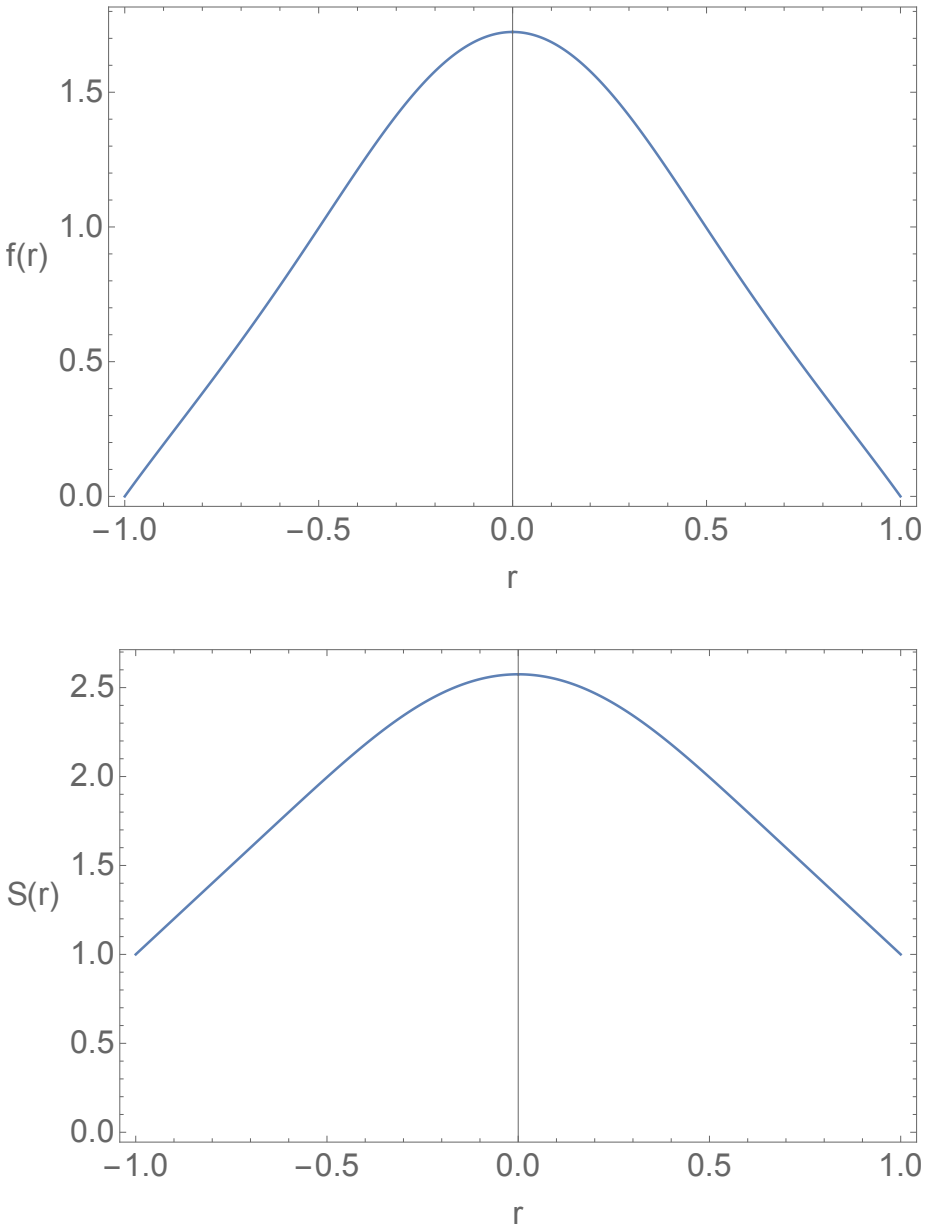

Figure 2.5: Here and in figure 2.4, we plot the numerical solutions to the Einstein-scalar system for the scalar field profile (2.17) with b = 1, k=2.05768. Note that, having set $\ell = 1$, the potential goes to $V = \Lambda_{AdS}$ at the horizons ($r_h = \pm 1$).

It now remains to discuss $V(\phi)$. Since f, S are smooth, our definition of V via (2.16) guarantees that V is a smooth function of r. The ansatz (2.17) then implies that $V(\phi)$ is smooth for $\phi \in (-b, b)$. But the behavior at the minimum b must be determined by expanding S, f, ϕ near $r = r_h$. To simplify this calculation we now set $r_h = 1$ to find

$$\begin{aligned}
\phi &\approx b(1 - 2e^{-k/(1-r)}), \\
\phi' &= b\left(\frac{kr}{1-r^2}\right)' \operatorname{sech}^2\left(\frac{kr}{1-r^2}\right) \approx 2bk\frac{e^{-k/(1-r)}}{(1-r)^2}, \\
\phi'' &= b\left[\left(\frac{kr}{1-r^2}\right)'' - 2\left[\left(\frac{kr}{1-r^2}\right)'\right]^2 \tanh\left(\frac{kr}{1-r^2}\right)\right] \operatorname{sech}^2\left(\frac{kr}{1-r^2}\right) \\
&\approx b\left[\frac{4k}{(1-r)^3} - \frac{2k^2}{(1-r)^4}\right] e^{-k/(1-r)}.
\end{aligned} \tag{2.21}$$

and

$$\begin{aligned}
S^2 f &\approx -f'(1)S(1)^2(1-r) + ... \\
(S^2 f)' &\approx f'(1)S(1)^2 + ...
\end{aligned} \tag{2.22}$$

Using (2.15) then yields

$$\frac{dV}{d\phi} = f'(1)\log^2\left(\frac{b-\phi}{2b}\right)\left(\log\left(\frac{b-\phi}{2b}\right) - 1\right)\frac{b-\phi}{k} + \mathcal{O}[(b-\phi)^2], \tag{2.23}$$

or

$$\begin{aligned}
V(\phi) =& \Lambda_{AdS} + \frac{f'(1)b}{4k}\left(\frac{b-\phi}{2b}\right)^2\left[-5 + 10\log\left(\frac{b-\phi}{2b}\right)\right. \\
&\left. -10\log^2\left(\frac{b-\phi}{2b}\right) + 4\log^3\left(\frac{b-\phi}{2b}\right)\right] + \mathcal{O}[(b-\phi)^3].
\end{aligned} \tag{2.24}$$

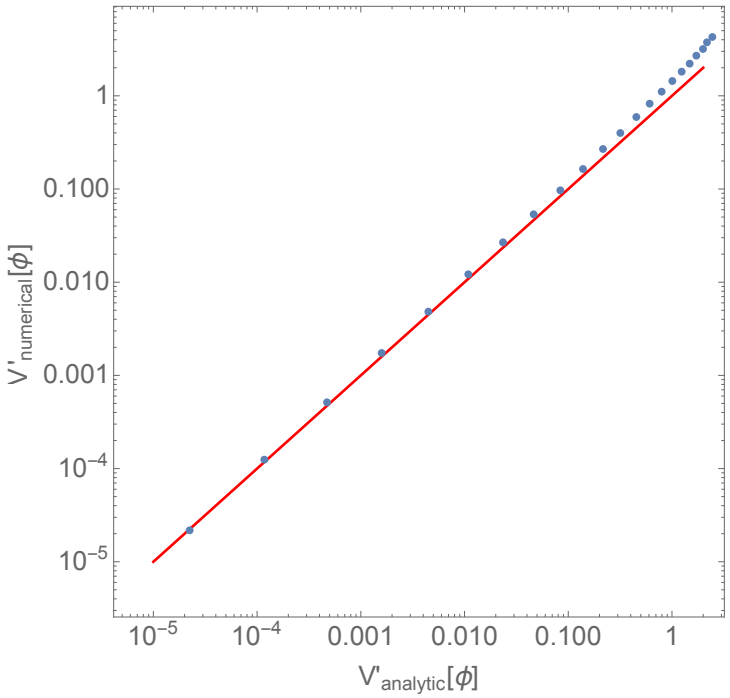

Figure 2.6: A comparison of the numerical results (y-axis) for $\frac{dV}{d\phi}$ to analytic results (x-axis). We have plotted our result (blue) on a log-log plot against a line (red) with slope 1 to show agreement over 4 orders of magnitude. The values of b,k, and r_h are the same as in fig. 2.5.

So our potential is not smooth at its minimum. Instead, $\frac{d^2V}{d\phi^2}$ has a logarithmic singularity, indicating that interactions remain important near the horizon. As shown in figure 2.6, this result is consistent with our numerics.

We remark that the singularity in our potential is not just an artifact of our particular construction. Indeed, appendix 2.6 demonstrates – even when the requirement of a pure AdS-Schwarzschild exterior is dropped – that time-independent spherically-symmetric wormholes cannot be sourced by scalar fields with smooth potentials.

2.3.1 HRT entropies

Finally, we investigate the holographic HRT mutual information between the two boundaries of our smooth time-independent wormhole. Here we consider the particular numerical solution displayed in figure 2.5. As in section 2.2.2, we begin by choosing A_L, A_R to each be the northern hemisphere of the respective boundary at $t = 0$. Repeating the steps describes there, and since the solution is just AdS_4-Kruskal outside the horizon, we focus on the area $A_{\text{connected, inside}}$ of the surface defined by taking the equator of each sphere inside the horizon. Interestingly, as in the thin-wall case, we find $A_{\text{connected, inside}} > A_{EH}$ for all values of k, b that we have explored – and indeed even for other functional forms of $\phi(r)$ such as $\phi(r) = b \tanh\left(\frac{kr}{(r_h^2 - r^2)^{c_2}}\right)^{c_1}$ with c_1, c_2 integer constants. So as in section 2.2.2 we conjecture that for general A_L, A_R the HRT entropy $S_{A_L A_R}$ agrees with the $t \to +\infty$ limit of AdS-Kruskal and that, despite a likely instability analagous to that found for the domain wall solutions, in this sense our time-independent wormholes are already thermalized at any finite t.

Typical results for $A_{\text{connected, inside}}$, A_{EH} are shown in figure 2.7 for the profile (2.17). One might expect that for large k our smooth solutions approximate the thin-shell solutions of section 2.2. At least so far as these areas are concerned, the plot indicates that the agreement is already quite good for any b at $k \sim 1$. Indeed, different scalar profiles in this regime that lead to the same A_{EH} also have nearly identical $A_{\text{connected, inside}}$.

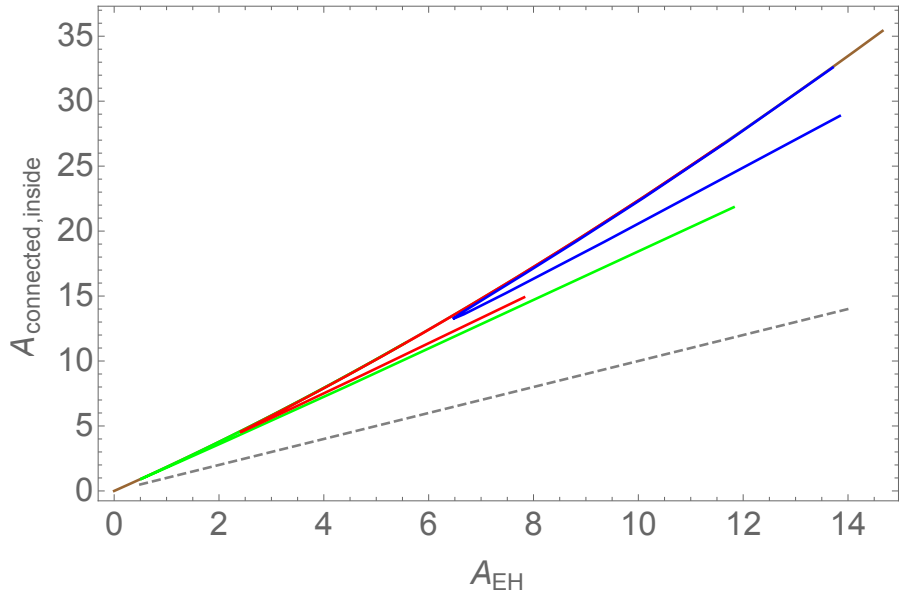

Figure 2.7: A comparison of the areas $A_{\text{connected, inside}}$ of minimal surfaces inside the wormhole to the area A_{EH} of the corresponding black hole. Using the profile in (2.17), each curve corresponds to a fixed value of b ($b = .87$ (green), $b = 1$ (red), $b = 1.2$ (blue)) while k is varied from .2 to 2.1. For each b there are two branches of solutions which join around $k \sim .7$. We have also plotted the $D = 4$ solution from fig. 2.2 in brown which is seen to coincide with the top branch of our solutions for each b; in particular, while the brown curve is hidden by the top branches of the colored curves across much of the figure, it remains visible at both the lower left and upper right ends. All solutions lie above the dashed line which plots $A_{\text{connected, inside}} = A_{EH}$, so the minimal surfaces are disconnected for hemispheres on the boundary of AdS.

2.4 Discussion

We have constructed time-independent spherically symmetric AdS-wormholes sourced by both thin-shell domain walls and smooth scalar fields with potentials $V(\phi)$ that are C^1 but not C^2. The time-translation in such spacetimes translates both wormhole mouths forward in time, instead of shifting them in opposite directions as in familiar AdS-Kruskal black holes. Interestingly, the results of figure 2.7 indicates that, at

least for some purposes, the thin-shell solutions become good approximations to the smooth solutions when the parameter k in (2.17) satisfies $k \gtrsim 1$.

As shown in appendix 2.6, the non-smooth potential $V(\phi)$ is critical to the construction, as there there can be no precisely time-independent such solutions when the scalar potential V is a smooth function of the scalar field ϕ. This feature may be related to the expectation that – even when they exist – the interior of such wormholes will be unstable. The instability was identified explicitly in the thin-shell case.

Nevertheless, as discussed in sections 2.2.2 and 2.3.1, at least for a large set of boundary regions the HRT entropies of boundary regions are already thermalized at any finite t without the above instability having been triggered. By this we mean that the result agrees with that obtained from familiar AdS-Kruskal in the limit $t \to \infty$. This was shown in particular for many cases where the boundary region contains pieces on both boundaries so that the same result holds for cross-boundary mutual informations similar to those studied in [75]. Indeed, we conjecture that it holds for all such entropies and mutual informations. Should one be able to find a stable version of our time-independent wormholes, a feature of this sort would be an interesting consistency check on whether dual gauge theory states thermalize in a universal way.

Such computations raise the question of whether our wormholes can have gauge theory duals in some version of gauge/gravity duality. One question involves the dual description of the logarithm at the minimum of the potentials used in section 2.3. But leaving this aside for now, we might ask if our wormholes define stationary points of Euclidean path integrals in analogy with [13]. At least in the thin-wall context, it is clear that the answer is negative. Constructing a Euclidean thin-wall stationary point amounts to solving an ODE for the Euclidean motion of the wall within Euclidean

AdS-Schwarzschild. Since at $t = 0$ the wall sits at (2.3) with zero velocity, it must do so for all Euclidean time. But since shifting Euclidean time by half a period takes one to the opposite side of the Lorentzian horizon, this is incompatible with the requirement that the wall exist only inside the wormhole and not outside. It would be interesting to determine whether a similar argument applies to our smooth wormhole solutions built from non-smooth potentials.

Finally, we briefly mention the recent discussions of the possible role of complexity in gauge/gravity duality in [78, 79, 80, 81] and the conjectures that gauge-theory complexity is related either to the volume of maximal slices or the action of certain regions in the bulk geometry. In our case, even the renormalized volume of a maximal slice that extends from one boundary to the other is strictly infinite. Although the renormalized volume of the $t = 0$ slice will be finite, for maximal slices there is no analogue of the argument in footnote 1. Indeed, in our case it is clear that a surface of arbitarily large renormalized volume can be obtained by following an orbit of the Killing field in the regions of figure 2.1 (right) in which the time-translation Killing field is spacelike. In particular, the volume of such surfaces grows without bound as the surface nears the topmost point of the dotted line in 2.1 (right). Similarly, the action of the spacetime region inside the wormhole (say, defined as in [88]) should diverge due to the required integral over time and the (non-compact) time-translation symmetry. Interestingly, assuming the wormhole to be unstable as in section 2.2 and choosing a perturbation that collapses the interior even at a very late time would result in finite actions and volumes of maximal surfaces at any given time t, though the resulting breaking of time-translation symmetry would also cause these quantities to grow with time. Indeed, at late times the growth in such quantities should be

dominated by the region near the outermost horizon and so will proceed precisely as in AdS-Kruskal. In contrast, with an instability that causes the wormhole interior to expand both the relevant actions and volumes of maximal slices will continue to diverge. It would be interesting to understand better the meaning of such divergences in the context of the conjectures of [78, 79, 80, 81].

2.5 Acknowledgements

We thank Gary Horowitz, Henry Maxfield, Brian Swingle, and Ying Zhao for useful discussions. DM and ZF were supported in part by the Simons Foundation and by funds from the University of California. EM was supported in part by NSF grant PHY-1504541.

2.6 Appendix: No solutions with smooth scalar potentials

This appendix shows that spherically symmetric time-independent wormholes with a Z_2 reflection cannot be sourced by scalar fields with smooth potentials, and thus that the singular potential found in section 2.3 is not an artifact of our particular construction. Our argument closely follows the work of Bekenstein [89] constraining black holes with scalar hair, though we have rephrased much of the proof in terms of manifestly covariant quantities like the expansion of radial geodesics. We allow a

general scalar action of the form

$$\mathcal{L} = \left[\frac{g^{ab}}{2} M_{AB}(\{\phi^A\})\, \partial_a \phi^A\, \partial_b \phi^B + V(\{\phi^A\}) \right] \sqrt{-g} \tag{2.25}$$

with positive definite M_{AB}. Such fields in particular respects the null energy condition (NEC), which states that the stress tensor T_{ab} satisfies $T_{ab}k^a k^b \geq 0$ for all null k^a.

We again describe the spacetime using the metric (2.12), taking $r = 0$ at the surface invariant under the Z_2 symmetry. We also assume the scalar fields to share the symmetries of the spacetime so that they depend only on the coordinate r. As a result, covariance and the definition $T_{ab} = -\frac{2}{\sqrt{-g}} \frac{\delta S}{\delta g^{ab}}$ require

$$-T_t{}^t = -T_\Theta{}^\Theta = \mathcal{E} = \frac{f}{2} M_{AB}(\{\phi^A\})\, \partial_r \phi^A\, \partial_r \phi^B + V(\phi), \tag{2.26}$$

$$T_r^r = \frac{f}{2} M_{AB}(\{\phi^A\})\, \partial_r \phi^A\, \partial_r \phi^B - V(\phi) \tag{2.27}$$

where $\mathcal{E}$ is the Lagrangian density for the scalars and $T_\Theta{}^\Theta$ is the same for all angular coordinates. Furthermore, the scalar equation of motion takes the form

$$\partial_r \left(M_{AB} f S^{d-1} \partial_r \phi^B \right) = \frac{\partial V}{\partial \phi^A}. \tag{2.28}$$

The Einstein equations remain as in (2.16) with the substitution of (2.26).

Our argument begins not in the wormhole itself, but in the region outside the horizon. Here we recall that the null convergence condition (a consequence of the Einstein equations and the null energy condition) requires the size of the $(d-1)$ spheres to increase monotonically from the horizon to the conformal boundary. The argument is simply that spherical symmetry prevents any outgoing sphere of light rays

from forming a caustic before reaching the conformal boundary, and that a standard calculation shows that such null congruences have vanishing expansion ($\theta = 0$) at the AdS boundary. The Raychaudhuri equation thus forbids them from having $\theta < 0$ at any r outside the horizon and thus implies monotonicity of $S(r)$. In the same way, since $S'(r) = 0$ at $r = 0$, the sphere size S must increase monotonically as one moves from a horizon toward $r = 0$. So the horizon $r = r_h$ must be a local minimum of $S(r)$.

In contrast to section 2.3, we now wish to take $V(\phi)$ to be a fixed smooth function of ϕ and to solve (2.28), (2.16) to generate the spacetime. We seek solutions with $S \neq 0$, so the only singular points of this system of ODEs occur when $f = 0$; i.e., at the horizon. In order for this to be a smooth Killing horizon with finite surface gravity, both f and must be a smooth function of r at r_h. Thus as usual $r - r_h$ is quadratic in the proper distance $s - s_h$ from the horizon, and in fact $(r - r_h)$ may be expanded in even powers of $(s - s_h)^2$. Smoothness of the geometry then requires that f also have an asymptotic series expansion about the horizon, and that this expansion is even.

This suggests that the entire solution will be symmetric about the horizon. Given that on one side we allow no further horizons between r_h and the AdS boundary, such a symmetry would forbid the desired wormhole from being present on the other. Indeed, we will show below that smoothness of $V(\phi)$ prohibits any breaking of this symmetry by S, ϕ^A, or by effects vanishing faster than any power of $r - r_h$ and thus forbids smooth time-independent wormholes.

We begin with perturbative effects. Having shown above that r_h is a minimum of S, smoothness requires $S = S(r_h) + \frac{dS}{dr}|_{r_h}(s - s_h)^2 + O((s - s_h)^3)$ with $\frac{dS}{dr}$ finite

at r_h. The scalar equation of motion (2.28) then also forces $\frac{d\phi^B}{dr}$ to remain finite and in fact constrains its value. Repeated differentiation of (2.28) and the first equation of (2.16) then guarantee that all r-derivatives of S, ϕ^B are finite at r_h as well so that they also admit well-defined asymptotic series expansions involving only even powers of $s - s_h$.

We now consider possible non-perturbative effects. In particular, suppose that two solutions (f_1, S_1, ϕ_1^A) and (f_2, S_2, ϕ_2^A) have identical asymptotic expansions about the horizon. Near r_h, we may then expand our ODEs in powers of $\Delta f = f_1 - f_2, \Delta S = S_1 - S_2$, and $\Delta\phi^A = \phi_1^A - \phi_2^A$. And close enough to r_h, to good approximation we may truncate this expansion to first order and neglect $f\Delta\partial_r\phi^A$ relative to $\partial_r\phi^A$. Doing so results in a linear system of ODEs for $\Delta f, \Delta S$, and $\Delta\phi^A$ with smooth non-vanishing coefficents; in particular, the ODE resulting from (2.28) is only of first order. The boundary condition that $\Delta f, \Delta S$, and $\Delta\phi^A$ all vanish at r_h thus requires them to vanish everywhere. We have thus shown that solutions of our ODEs are uniquely determined by their power series expansion near r_h for smooth $V(\phi)$. As a result, smooth $V(\phi)$ requires a Z_2 symmetry about any smooth bifurcate Killing horizons an forbids the desired time-independent wormholes.

Chapter 3

Sparseness bounds on local operators in holographic CFT_d

3.1 Introduction

There has been a recent surge of interest in precisely characterizing conformal field theories with a weakly coupled Einstein gravity dual, with equations now accompanying folkore from the past. The most quantitative work has focused on conformal field theories in two dimensions, though there has also been progress on higher-dimensional theories. The difficulties brought on by higher dimensions are clear: the constraining infinite-dimensional Virasoro symmetry is absent and modular invariance of the torus partition function does not immediately provide constraints on the space of local operators.

In this paper we will use the familiar thermodynamics of gravity in asymptotically anti-de Sitter spacetimes to provide quantitative sparseness bounds on the spectrum

of local operators of holographic conformal field theories. This approach began with [14], which showed that the thermodynamics of gravity in AdS_3 is reproduced if and only if the spectrum of operators with scaling dimension $\Delta < c/6$ and $\Delta \sim O(c)$ obeys $\rho(\Delta) \lesssim \exp(2\pi\Delta)$. This methodology was subsequently generalized to supersymmetric theories [90], correlation functions [91], and higher-dimensional theories on tori [92]. The universality of the thermodynamics for holographic CFTs on tori can also be derived from the special center symmetry structure of such theories through the Eguchi-Kawai mechanism [93].

In two dimensions, the low-temperature and high-temperature thermodynamics are related to one another by modular invariance. This is what allows one to capture the entire thermodynamic phase structure by constraining only the low-lying ($\Delta < c/6$) operators. Unfortunately, in higher-dimensional theories on S^{d-1}, there is no obvious high-temperature/low-temperature duality. But there is still a universal feature of the gravitational phase structure that we can aim to reproduce from the CFT: the Hawking-Page phase structure [94], where, as a function of some external chemical potentials, the vacuum-subtracted free energy (or the entropy) jumps from $O(1)$ to $O(N^k)$ for k some positive number. (For notational simplicity we will ignore the possibility of intermediate scalings $O(N^m)$ for $0 < m < k$.) More specifically, we will reproduce the fact that the theory is confined ($O(1)$ scaling in the entropy) below the Hawking-Page transition temperature T_{HP}.

To illustrate the basic idea, consider the finite-temperature canonical ensemble

with normalization $E_{\text{vac}} = 0$ and a deconfining phase transition at $\beta_c \sim O(1)$. Then,

$$\log Z(\beta) \sim \begin{cases} \mathcal{O}(1), & \beta > \beta_c \\ \mathcal{O}(N^k), & \beta < \beta_c \,. \end{cases} \tag{3.1}$$

Since $Z(\beta) = \int e^{-\beta\Delta}\rho(\Delta)d\Delta$, the $O(1)$ behavior of $\log Z$ may be ruined if the density of states $\rho(\Delta)$ grows too quickly for states with $\Delta \gtrsim O(N^k)$. More precisely, we have

$$\log Z(\beta > \beta_c) \sim O(1) \qquad \text{if and only if} \qquad \rho(\Delta) \lesssim e^{\beta_c \Delta} \quad \text{for} \quad \Delta \gtrsim O(N^k)\,. \tag{3.2}$$

In the worst-case scenario where the bound is saturated for all states, we have

$$Z(\beta > \beta_c) = \int_0^\infty d\Delta e^{-\beta\Delta} e^{\beta_c \Delta} = \frac{1}{\beta - \beta_c}\,. \tag{3.3}$$

Hence, $\log Z$ is $O(1)$ for all $\beta > \beta_c + \epsilon$ for $\epsilon \ll 1$ as long as ϵ is not exponentially small in N.

While a deconfinement transition is generically expected for large-N adjoint CFTs on compact spaces [12, 95], it is the precise temperature at which the transition occurs which gives us mileage. In particular, applying the above argument to the well known Hawking-Page transition at inverse temperature $\beta_{HP} = \frac{2\pi}{d-1}$ gives us a bound on the spectrum of local operators of holographic CFTs:

$$\rho(\Delta) \lesssim \exp\left(\frac{2\pi\Delta}{d-1}\right) \quad \text{for} \quad \Delta \gtrsim O(N^k) \quad \text{if and only if} \quad \log Z(\beta > \beta_{HP}) \sim O(1) \tag{3.4}$$

This bound applies to the entire spectrum, but above the transition temperature, bulk

thermodynamics tells us that the large-N density of states is given by the degeneracy of the black hole dominating the ensemble, which is generically smaller than our bound (see figure 3.1). Interestingly, our bound must be saturated at the transition point, since at leading order in N we can write

$$F_c = E_c - S_c/\beta_c = 0 \implies S_c = \beta_c E_c \implies \rho(E_c) = e^{\beta_c E_c}\,, \tag{3.5}$$

where we are assuming that immediately above the transition we have equivalence of canonical and microcanonical ensembles, i.e. $E_c \equiv \langle E \rangle_{\beta_c}$ is a well-defined energy level stable to fluctuations. Applied to AdS/CFT, this argument means that our bound will be saturated by the black hole at the Hawking-Page transition. In appendix 3.7, we invert the logic behind this fact to provide a field-theoretic density of states interpretation for the Bekenstein-Hawking entropy.

For the remainder of this paper, we generalize eq. (3.4) using known classical black hole solutions to bound the density of operators of the dual CFT with given scaling dimension Δ, spins J_i and $U(1)$ charge Q. For $d = 2$ the bounds will reduce to those of [14]. Importantly, these bounds are more constraining in $d > 2$ than in $d = 2$, because for $d = 2$ modular invariance implies that, if a single deconfining phase transition occurs, it must occur at $\beta = 2\pi$ independent of coupling. Indeed, free symmetric orbifolds (which are not dual to weakly coupled Einstein gravity theories) have a transition at $\beta = 2\pi$ just like AdS_3 gravity, and α' perturbation theory around AdS_3 gravity leaves the Hawking-Page temperature unchanged [96]. On the other hand, in higher dimensions the deconfining temperature tends to increase as interactions are turned on. For example, in both ABJM theory and $\mathcal{N} = 4$ super Yang-Mills,

it can be checked that $\beta_{HP}(\lambda = 0) > \beta_{HP}(\lambda = \infty)$ for 't Hooft coupling λ [97, 95, 98], with further calculations suggesting monotonic behavior between the free and strongly coupled theories [99, 100, 101]. This means that $\log Z \sim O(1)$ for a smaller range of temperatures as the interaction strength is decreased. By the argument above, this means that weakly coupled CFTs must be less sparse—they *must* have $\rho(\Delta) \gtrsim e^{2\pi\Delta/(d-1)}$ somewhere in their spectrum. The fact that strong interactions are necessary to reproduce the precise low-temperature phase structure of AdS gravity in higher dimensions has been translated into a simple bound on the density of local operators. The violation of our bound is a sharp diagnostic of "how much" interactions have to sparsify a spectrum. There is another interesting aspect to these bounds that we will discuss in section 3.4: they imply an $O(1)$ density of states beyond corresponding BPS/unitarity bounds. For example, taking $\Delta < 0$ implies $\log \rho(\Delta) \sim \mathcal{O}(1)$, which looks like a coarse unitarity bound.

The layout of the rest of the paper is as follows. In section 3.2, we provide the methodology behind obtaining our bounds more carefully. In section 3.3, we provide calculational details for deriving our various bounds. Analytic bounds are possible for three parameters, either mass and two spins or mass, one spin and one $U(1)$ charge, but for four or more parameters, we must resort to numerics. Two-parameter analytic results are summarized in table 3.1. In section 3.4, we discuss the connection of our bounds to BPS/cosmic censorship bounds. In section 3.5, we speculate on the connection between the high-lying spectrum or high-temperature thermodynamics and our bounds on the low-lying spectrum. We will begin with an analysis of the Cardy-Verlinde formula, which correctly gives the entropy above the Hawking-Page temperature T_{HP} for holographic CFT$_d$ on S^{d-1} [102]. After discussing the many

limitations of this formula, we instead focus on a more robust feature of the high-temperature thermodynamics: the extended range of validity of a high-temperature effective field theory. In appendix 3.7, we provide a field-theoretic density of states interpretation for the Bekenstein-Hawking entropy of black holes at Hawking-Page phase transitions. In appendix B, we provide details for calculations in $4 \leq d \leq 6$.

3.2 Method for obtaining bounds

In this section, we explain more carefully our method for obtaining bounds on the allowed density of states of operators with $U(1)$ charge and spin for holographic theories with a confining phase transition. We consider a grand canonical ensemble at finite temperature β, with m angular velocities Ω_i and a single chemical potential for $U(1)$ charge Φ for CFT_d:

$$\log Z(\beta, \Omega_i, \Phi) = \int dE\, dJ_i\, dQ \exp\left[-\beta(E - \Omega_i J_i - \Phi Q)\right] \rho(E, J_i, Q)\,, \tag{3.6}$$

where the integral goes over the spectrum of the theory and we sum over repeated indices in the exponential. Except when otherwise noted, we will always normalize the ground state energy (even for $d = 2$) to zero. The extension to additional chemical potentials is trivial.

A confining phase transition means that $\log Z[\beta > \beta_c(\Omega_i, \Phi)] \sim O(1)$, i.e. the free energy does not scale with N for temperatures below some critical temperature $\beta_c^{-1}(\Omega_i, \Phi)$. The chemical potentials Ω_i, Φ and β span an $(m+2)$-dimensional space, and the confinement-deconfinement phase transition happens on a co-dimension one critical surface $\beta = \beta_c(\Omega_i, \Phi)$. The $O(1)$ scaling of the free energy requires that the

density of states be bounded from above,

$$\rho(E, J_i, Q) \lesssim \exp\left[\beta\left(E - \Omega_i J_i - \Phi Q\right)\right] , \qquad \forall \quad \beta, \Omega_i, \Phi \text{ in the confined phase.} \tag{3.7}$$

It is simple to minimize the right-hand-side with respect to the potentials β, Ω_i, and Φ to provide the tightest bound. In the case of $\Omega_i = \Phi = 0$ the minimization gives $\beta = \beta_c$ for $E > 0$ and the bound becomes $\rho(E) \lesssim e^{\beta_c E}$, while for $E < 0$ gives $\beta \to \infty$ and our bound vanishes. This behavior is generic: the minimum of eq. (3.7) always lies either on the critical surface or at $\beta \to \infty$ which gives vanishing degeneracy. The set of values for charges which separates the two behaviors corresponds to a unitarity/BPS bound. To see the two behaviors in general, we first impose parity symmetry under $\Omega_i \to -\Omega_i$ such that the critical surface is an even function of the chemical potentials Ω_i and Φ. Since eq. (3.7) is invariant under $\{J_i, Q_i, \Omega_i, \Phi\} \to \{-J_i, -Q_i, -\Omega_i, -\Phi\}$, it is then sufficient to consider only operators with $\{J_i, Q\} > 0$ and potentials with $\{\Omega_i, \Phi\} > 0$. For the theories we consider, these potentials Ω_i, Φ have finite range, being bounded below by $\Omega_i = 0$ and $\Phi = 0$ and above by some constants which depend on the theory and dimension. Since β is an overall multiplicative factor, we can minimize it independently, landing on $\beta_c(\Omega_i, \Phi)$ if $E - \Omega_i J_i - \Phi Q > 0$ for all $\{\Omega_i, \Phi\}$ and $\beta \to \infty$ otherwise. In the former case we then minimize along the critical surface, while in the latter case the bound simply vanishes. The minimization along the critical surface is

$$\nabla\left[\beta_c\left(E - \Omega_i J_i - \Phi Q\right)\right] = 0 \tag{3.8}$$

for a given set of charges $\{E, J_i, Q\}$, and $\nabla = (\partial/\partial\Omega_1, \ldots, \partial/\partial\Omega_m, \partial/\partial\Phi)$.

Until this point, the discussion applies to states with general $U(1)$ charge Q and momenta J_i in large-N gauge theories with a confining phase transition. Focusing on local operators in holographic CFTs with a semiclassical Einstein gravitational dual, we restrict to dimensions $2 \leq d \leq 6$ and the spatial manifold S^{d-1}. The Hawking-Page temperature in the bulk will serve as the deconfinement temperature in the CFT. To find the Hawking-Page transition, we compare the on-shell action of the relevant black hole solution to that of vacuum AdS. The vacuum AdS solution will have topological identifications and constant gauge field to match the inverse temperature, angular velocities, and chemical potential for $U(1)$ charge of the black hole. When the black hole has charge and spin, the deconfinement temperature will depend on the chemical potential Φ and angular velocities Ω_j. Below this temperature, the dual CFT is in a confined phase (dual to the AdS vacuum) and above this temperature the dual CFT is deconfined (dual to a black hole).

We consider the most general black holes in $d+1$ dimensions for the cases $d = 2$ through $d = 6$ with a single $U(1)$ charge and $\left\lfloor \frac{d}{2} \right\rfloor$ spins. These black holes are asymptotic to a (spinning) Einstein static universe (ESU) which, in the Lorentzian case, has topology $\mathbb{R} \times S^{d-1}$. Classical solutions for the generically spinning charged black hole in dimensions $d = 5$ and $d = 6$ depend on choice of supergravity truncation and so our results in those cases should be considered in that context. Nevertheless, bounds obtained from these solutions are similar to their lower dimensional counterparts. Analytic results are possible in all dimensions for up to three parameters, while numerics are necessary for four and five parameters. Two-parameter bounds are shown in table 3.1. Analytic expressions are only applicable when they are real

d	$\log\rho(\Delta)$	$\log\rho(\Delta,Q)$	$\log\rho(\Delta,J)$
2	$2\pi\Delta$	N/A	$2\pi\Delta\sqrt{1-J^2/\Delta^2}$
3	$\pi\Delta$	$\pi\Delta\sqrt{1-Q^2/\Delta^2}$	$\pi\Delta(1-J^2/\Delta^2)$
4	$\frac{2\pi\Delta}{3}$	$\frac{2\pi\Delta}{3}\sqrt{1-\frac{3}{4}Q^2/\Delta^2}$	$\frac{2\pi\Delta}{3}\left(2-\sqrt{1+3J^2/\Delta^2}\right)$
5	$\frac{\pi\Delta}{2}$	$\frac{\pi\Delta}{2}\sqrt{1-\frac{2}{3}Q^2/\Delta^2}$	$\frac{\pi\Delta}{4}\left(3-\sqrt{1+8J^2/\Delta^2}\right)$
6	$\frac{2\pi\Delta}{5}$	$\frac{2\pi\Delta}{5}\sqrt{1-\frac{5}{8}Q^2/\Delta^2}$	$\frac{2\pi\Delta}{15}\left(4-\sqrt{1+15J^2/\Delta^2}\right)$

Table 3.1: Bounds on the density of states for charged spinless operators (second column) and uncharged spinning operators (third column). When these expressions become complex or negative, the bound instead is $\log\rho=0$.

and positive; when they become complex or negative it means the charges admit a set of chemical potentials for which $E-\Omega_i J_i-\Phi Q<0$ and the minimization procedure lands at $\beta\to\infty$ instead of the Hawking-Page surface. This leads to an $O(1)$ density of states.

Notable in this table is the absence of a bound for operators with $U(1)$ charge in 2d CFTs. Electrically charged static black holes in three dimensions have interesting but somewhat peculiar thermodynamic properties—see [103, 104]. Among these properties is the fact that if one wants to include a bulk Maxwell field, the black hole mass is not bounded from below [105]. If one wants to consider only a Chern-Simons term – which is necessary to describe a $U(1)$ current on the boundary – there are new difficulties in finding the dominant saddle. It is unclear how to match asymptotics

as any non-zero holonomy of the gauge field remains constant along the radial direction. A holonomy in the spatial direction would lead to a singularity at the origin for the vacuum AdS phase, while a holonomy in the thermal direction would lead to a singularity at the horizon for the black hole phase. If one includes both Maxwell and Chern-Simons terms for the same $U(1)$ gauge field, the spacetimes include closed timelike curves in the asymptotic region [106]. Thus we cannot consistently analyze this situation in Einstein gravity coupled to $U(1)$ Chern-Simons and/or Maxwell gauge fields.

3.3 Bounds on operators

In this section, we derive our bounds for electrically charged operators with spin in CFT dimension $d = 2$ through $d = 6$. We begin with $d = 3$ in section 3.3.1, giving all details of the derivation of the bound. For general d we state our analytic results, without derivation, for single-charge spinless operators in section 3.3.2, single-spin uncharged operators in section 3.3.3, double-spin uncharged operators in section 3.3.4, and single-spin single-charged operators in section 3.3.5.

In the case with four or more parameters, we do not have an analytic bound but present numerical results in 3.3.6. Figures for our numerical results will be presented together at the end of this section to emphasize the similarities between dimensions. The bound on the density of states decreases when charge or spin is added, to the point that no states are allowed beyond a curve that exactly coincides with the BPS bound. As we will see, when the parameters satisfy the BPS condition and admit a

BPS black hole, our bound is saturated by the entropy of the BPS black hole,

$$S_{BH} = max\left[\log \rho(\Delta_{BPS}, Q_{BPS}, J_{BPS,i})\right]. \tag{3.9}$$

This is a special case of the fact that generic black holes at the Hawking-Page transition have an entropy which saturates our bound.

3.3.1 Example: $\rho(\Delta, Q, J)$ in $d = 3$.

In $d = 3$, the AdS-Kerr-Newman black hole is the generic electrically charged, spinning black hole with AdS_4 asymptotics. Its thermodynamics were first studied in [107]. In the limit of zero spin, the thermodynamics reproduces [108, 109], and in the limit of zero charge reproduces [110, 111, 112]. The metric may be written

$$ds^2 = -\frac{\Delta_r}{\rho^2}\left[dt - \frac{a\sin^2\theta}{\Xi}d\phi\right]^2 + \frac{\rho^2}{\Delta_r}dr^2 + \frac{\rho^2}{\Delta_\theta}d\theta^2 + \frac{\Delta_\theta \sin^2\theta}{\rho^2}\left[adt - \frac{r^2+a^2}{\Xi}d\phi\right]^2, \tag{3.10}$$

where the metric functions and Maxwell field, A, are

$$\begin{aligned} &\Delta_r = (r^2+a^2)(1+r^2) - 2mr + q^2, && \Delta_\theta = 1 - a^2\cos^2\theta \\ &\rho^2 = r^2 + a^2\cos^2\theta, && \Xi = 1 - a^2, && A = -\frac{qr}{\rho^2}\left(dt - \frac{a\sin^2\theta}{\Xi}d\phi\right). \end{aligned} \tag{3.11}$$

The mass M, angular momentum J, and electric charge Q—calculated via boundary integrals—are

$$M = \frac{m}{G\Xi^2}, \qquad J = \frac{am}{G\Xi^2}, \qquad Q = \frac{1}{8\pi G}\int_{S^{d-1}_\infty} \star F = \frac{q}{G\Xi}. \tag{3.12}$$

Note that we follow the convention of [113] for the normalization of Killing vectors as the associated conserved charges generate the $SO(d,2)$ algebra. To find the on-shell Euclidean action, we evaluate

$$I_E = \frac{1}{16\pi G}\int d^4x\sqrt{g}(6+F^2) - \frac{1}{8\pi G}\int_{r=\Lambda} d^3x\sqrt{\gamma}K + \frac{1}{8\pi G}\int_{r=\Lambda} d^3x\sqrt{\gamma}\left(2+\frac{1}{2}R[\gamma]\right). \tag{3.13}$$

The second term is the Gibbons-Hawking-York boundary term and the last term is a local boundary counterterm that regularizes the action [114]. The horizon angular velocity and inverse Hawking temperature of these black holes are

$$\Omega_h = \frac{\Xi a}{r_+^2 + a^2}, \quad \beta = \frac{4\pi r_+(r_+^2+a^2)}{r_+^2(1+a^2)+3r_+^4-(a^2+q^2)}. \tag{3.14}$$

The appropriate thermodynamic potential for spin, however, is the difference between Ω_h and Ω_∞, the angular velocity of the boundary ESU. One way to find this Ω_∞ is to boost the boundary metric to a static frame through a coordinate change $T = t - \Omega_\infty\phi$, giving $\Omega_\infty = -a$. We then obtain,

$$\Omega = \Omega_h - \Omega_\infty = \frac{a(1+r_+^2)}{r_+^2+a^2}. \tag{3.15}$$

The parameter Φ is chosen so that the gauge potential vanishes on the outer horizon,

defined by $\Delta_r(r_+) = 0$. Notably, this is the potential difference between the horizon and the conformal boundary, and serves as a chemical potential for $U(1)$ charged operators in the CFT.

$$\Phi \equiv A_a k^a \Big|_{r\to\infty} - A_a k^a \Big|_{r=r_+} = \frac{q r_+}{r_+^2 + a^2}, \tag{3.16}$$

where $k = \partial_t + \Omega_H \partial_\phi$ is the null generator of the horizon. Subtracting the vacuum AdS result from the AdS-Kerr-Newman result gives

$$\Delta I_E = \frac{\beta}{4G\Xi r_+}\left[(a^2 + r_+^2)(1 - r_+^2) + q^2 \frac{a^2 - r_+^2}{r_+^2 + a^2}\right]. \tag{3.17}$$

We can replace $\{r_+, a, q\}$ with $\{\beta, \Omega, \Phi\}$ using eq. (3.14) and (3.16). At fixed $\{\beta, \Omega, \Phi\}$, there are two competing stable phases–a large AdS-Kerr-Newman black hole and vacuum AdS. The bulk undergoes a Hawking-Page phase transition when the two saddle point solutions exchange dominance, in other words when $\Delta I_E = 0$. In the limit of zero charge, the Hawking-Page transition occurs at $r_+ = 1$. In the limit of zero angular momentum, the Hawking-Page transition occurs at $r_+ = \sqrt{1 - \Phi^2}$. For non-zero charge and angular momentum, it is simplest to extremize

$$\beta_{HP}(\Omega, r_+)(\Delta - \Omega J - \Phi_{HP}(\Omega, r_+)Q) \tag{3.18}$$

with respect to Ω and r_+. Obtaining the critical values for Ω and r_+, we find that

$$\log \rho(\Delta, J, Q) \lesssim \frac{\pi\Delta}{\sqrt{2}}\sqrt{\left(1+\hat{J}^2\right)\left(1+\hat{J}^2-\hat{Q}^2\right)+\left(1-\hat{J}^2\right)\sqrt{\left(1+\hat{J}^2-\hat{Q}^2\right)^2-4\hat{J}^2}-4\hat{J}^2}, \tag{3.19}$$

where $\hat{J} = J/\Delta$, $\hat{Q} = Q/\Delta$. Note that if $\hat{J} + \hat{Q} > 1$, eq. (3.19) breaks down and the correct minimization gives an $O(1)$ density of states. This limit corresponds to the BPS bound $\Delta = |J| + |Q|$ for the lightest charged, spinning state. Notably, at $\Delta = |J| + |Q|$, the upper bound on our density of states exactly matches the degeneracy of the corresponding BPS black hole with those charges,

$$S_{BH} = \max\left[\log \rho(\Delta, \pm(\Delta - |Q|), Q)\right] = \pi Q\sqrt{1 - Q/\Delta}. \tag{3.20}$$

Again we see that the upper bound on the density of states is saturated by the degeneracy of the bulk black hole at the Hawking-Page transition and is greater for all other black holes (see figure 3.1). For $\Delta = |J| + |Q|$, in $d = 3$, the black hole at the phase transition is a BPS black hole.

3.3.2 Charged, spinless operators

To bound the density of states of charged, spinless operators, we examine the thermodynamics of $(d+1)$-dimensional AdS-Reissner-Nordström black holes. Using the conventions of [109], the mass, global $U(1)$ charge, $U(1)$ potential, and inverse

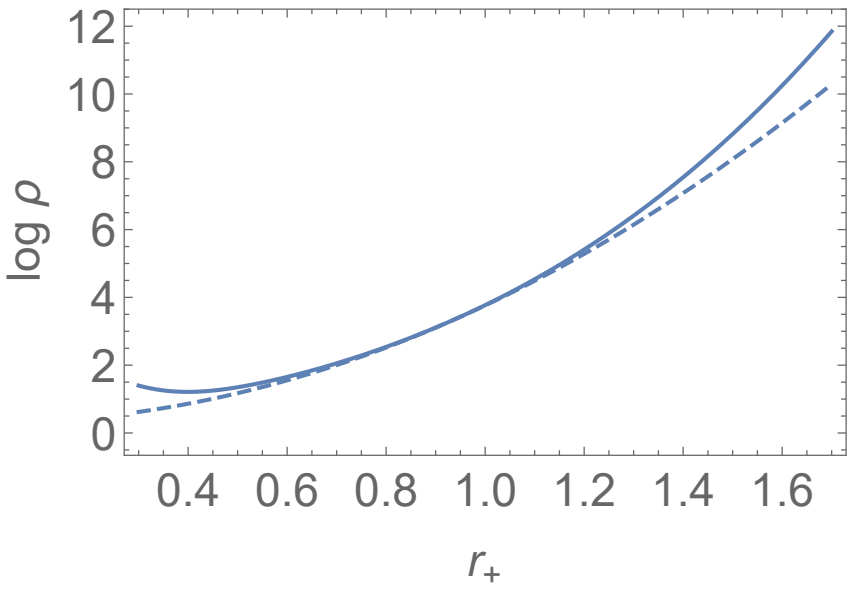

Figure 3.1: As an example, we plot our bound $\log \rho(\Delta, J, Q)$ (thick) and the entropy of the corresponding black hole (dashed) in $d = 3$ for fixed black hole parameters, $a = .3, q = .4$. The two coincide at r_{HP} and our bound is otherwise larger.

temperature for this black hole are

$$M = \frac{(d-1)\omega_{d-1}}{16\pi G} m, \quad Q = \frac{(d-1)\omega_{d-1}}{8\pi G} cq, \quad \Phi = \frac{1}{c}\frac{q}{r_+^{d-2}},$$
$$\beta = \frac{4\pi r_+^{2d-3}}{d r_+^{2(d-1)} + (d-2)[r_+^{2(d-2)} - q^2]}, \tag{3.21}$$

where ω_{d-1} is the area of the unit $(d-1)$ sphere, and $c = \sqrt{2(d-2)/(d-1)}$. The vacuum subtracted Euclidean action is

$$\Delta I_E = \frac{\omega_{d-1}\beta}{16\pi G}\left[(1 - c^2\Phi^2) - r_+^2\right] r_+^{d-2}. \tag{3.22}$$

As before, there are two competing stable phases at fixed Φ, β. The first is the AdS vacuum with $m = q = 0$ and constant gauge potential and the second is a large black hole, both at inverse temperature β. Solving for $\Delta I_E = 0$, it is clear that for $r_+ > \sqrt{1 - c^2\Phi^2}$, black holes dominate the grand canonical ensemble while the vacuum dominates below. The corresponding Hawking-Page temperature is

$$\beta_{HP}(\Phi)\Big|_{r_+=\sqrt{1-c^2\Phi^2}} = \frac{2\pi}{(d-1)\sqrt{1-c^2\Phi^2}}. \tag{3.23}$$

Interestingly, for $\Phi = 1/c$, the Hawking-Page temperature $1/\beta_{HP}$ vanishes and an extremal black hole dominates the grand canonical ensemble. To find our density of states, we extremize $\beta_{HP}(\Phi)(\Delta - \Phi Q)$ and find the bound for charged operators is

$$\log \rho(\Delta, Q) \lesssim \frac{2\pi\Delta}{d-1}\sqrt{1 - \hat{Q}^2/c^2} \tag{3.24}$$

for $\Delta \geq |Q|/c$. The lower limit on the energies is the BPS bound for these black holes. Supersymmetry appears through considering Einstein-Maxwell as a consistent truncation of some supergravity theory. The fact that there cannot exist states lighter than the BPS bound $\Delta > Q/c$, can be seen from our bound eq. (3.24), which vanishes (more precisely, is $\mathcal{O}(1)$) in the BPS limit $\Delta = Q/c$. Unlike the previous subsection, the bound on the density of states *at* the BPS limit vanishes. This is consistent with the nakedly singular nature of these BPS states.

3.3.3 Single spin, uncharged operators

For uncharged operators with a single spin, the dual bulk black hole is the $(d+1)$-dimensional Kerr black hole, analyzed first in [110] for $d > 2$. For $d = 2$, we work with

the spinning BTZ black hole [60]. The relevant thermodynamic parameters for these black holes are the uncharged single spin limit of sections 3.3.1, 3.8.1, 3.8.2, 3.8.3 for $d = 3, 4, 5$, and 6, respectively, where the relevant thermodynamical quantities are listed. The difference of regularized on-shell Euclidean actions becomes

$$\Delta I_E = \frac{\beta_{d+1}\omega_{d-3}}{4G(d-2)\Xi}\left[r_+^{d-4}(r_+^2+a^2)(1-r_+^2)\right], \tag{3.25}$$

so black holes dominate for $r_+ > 1$. The inverse temperature for the Hawking-Page transition is

$$\beta_{HP}(\Omega) = \frac{2\pi}{d-2+\sqrt{1-\Omega^2}}. \tag{3.26}$$

To find the density of states, we extremize $\beta_{HP}(\Omega)(\Delta - \Omega J)$ with respect to β_{HP} and find

$$\log\rho(\Delta, J) \lesssim \frac{2\pi\Delta}{(d-3)(d-1)}\left(d-2-\sqrt{(d-3)(d-1)\hat{J}^2+1}\right), \tag{3.27}$$

where again $\hat{J} = J/\Delta$. The $d = 3$ case is obtained by taking the limit. The unitarity bound is $\Delta \geq |J|$, which can also be understood as a BPS bound by taking the limit of zero $U(1)$ charge.

The result for $d = 2$ agrees with the HKS bound [14]. It is notable that in this case, the bound from cosmic censorship agrees with the BPS bound, $\Delta - c/12 \geq |J|$ [110], where we have normalized $E_{\text{vac}} = -c/12$. However, the HKS bound allows states down to $\Delta = |J|$, which is the saturation point of the unitarity bound $\Delta \geq |J|$. This only occurs in $d = 2$: all higher-dimensional bounds obtained by our method

will coincide with BPS bounds. Because of similarities with multiple spin operators derived in the next sections, we also note that the single spin bound may be written as

$$\log \rho(\Delta, J) \lesssim \pi \Delta s \tag{3.28}$$

where s is the smallest non-negative solution to

$$(d-2)s + \sqrt{s^2 + 4\hat{J}^2} = 2. \tag{3.29}$$

3.3.4 Multiple spin and zero charge operators

Analytic expressions are possible for two spins and zero $U(1)$ charge. Here, the bulk black holes are spinning AdS-Myers-Perry black holes in dimension $d > 3$, whose metrics can be obtained from the zero charge limit of the gauged supergravity solutions[115, 116] in $d = 4, 5$ respectively and from the zero charge, two spin limit of [117] in $d = 6$. The relevant thermodynamics as well as vacuum subtracted Euclidean actions are obtained in these limits from sections 3.8.1, 3.8.2, 3.8.3. Myers-Perry black holes dominate the grand canonical ensemble for $r_+ > 1$. The Hawking-Page temperature is

$$\beta_{HP}(\Omega_a, \Omega_b) = \frac{2\pi}{(d-3) + \sqrt{1-\Omega_a^2} + \sqrt{1-\Omega_b^2}}. \tag{3.30}$$

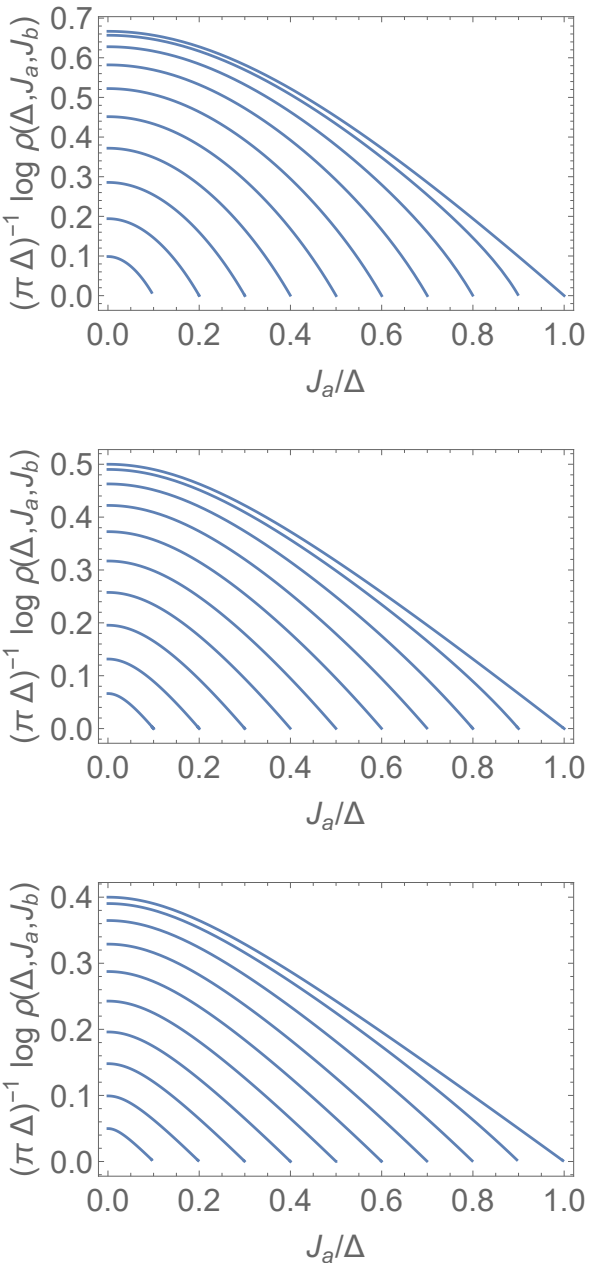

Figure 3.2: The bound for operators with spins J_a and J_b in $d = 4$ (top), $d = 5$ (middle), $d = 6$ (bottom). Curves correspond to $J_b/\Delta = 0$ (rightmost) to $J_b/\Delta = .9$ (leftmost) in increments of .1

We find that extremizing $\beta_{HP}(\Omega_a, \Omega_b)(\Delta - \Omega_a J_a - \Omega_b J_b)$ is equivalent to finding the smallest non-negative solution to

$$(d-3)s + \sqrt{s^2 + 4\hat{J}_a^2} + \sqrt{s^2 + 4\hat{J}_b^2} = 2 \tag{3.31}$$

where $\hat{J}_i = J_i/\Delta$ and our bound is

$$\log \rho(\Delta, J_a, J_b) \lesssim \pi \Delta s. \tag{3.32}$$

For completeness, we will solve eq. (3.31) explicitly. First, define

$$x = 1 + \frac{(d-3)^2}{2}(\hat{J}_a^2 + \hat{J}_b^2), \qquad y = \frac{3}{2}(\hat{J}_a^2 - \hat{J}_b^2). \tag{3.33}$$

In $d = 4$, the bound is

$$\log \rho(\Delta, J_a, J_b) \lesssim \frac{2\pi\Delta}{3}\left(1 - B_4 + \sqrt{\frac{(B_4+2)((2-B_4)B_4 - 6x + 8)}{B_4}}\right) \tag{3.34}$$

where

$$A_4 = \left(\sqrt{3x^3(3x-4)y^2 + 6((x-6)x+6)y^4 + y^6} + x^3 + 3xy^2 - 6y^2\right)^{1/3}, \tag{3.35}$$
$$B_4 = \sqrt{\frac{-2A_4 x + A_4(A_4+4) + x^2 - 1}{A_4}}.$$

In $d = 5$, the bound is

$$\log \rho(\Delta, J_a, J_b) \lesssim \frac{\pi\Delta}{6}\left(6 - x - \left(x^3 - 4\left(\sqrt{36y^4 - 3x^3y^2} + 6y^2\right)\right)^{1/3} - \frac{x^2}{\left(x^3 - 4\left(\sqrt{36y^4 - 3x^3y^2} + 6y^2\right)\right)^{1/3}}\right).$$

In $d = 6$, the bound is

$$\log \rho(\Delta, J_a, J_b) \lesssim \frac{2\pi\Delta}{15}\left(7 - B_6 - \sqrt{\frac{(2 - B_6)\left(B_6^2 + 2B_6 - 2(5x + 4)\right)}{B_6}}\right), \quad (3.36)$$

where

$$A_6 = \left(9(5x + 6)y^2 - x^3 + 3\sqrt{-3x^3(5x + 4)y^2 + 6(5x(5x + 18) + 54)y^4 - 375y^6}\right)^{1/3}, \quad (3.37)$$

$$B_6 = \sqrt{\frac{5A^2 + 5x^2 + 2A(6 + 5x) + 75y^2}{3A}}.$$

One must be careful with these expressions to always take the principal root, which is generally complex, though the bound is always real for $|J_a| + |J_b| \leq \Delta$. For instance, in the no spin limit, $A_6 \to \exp(i\pi/3)$ and $B_6 \to 3$. Like in the previous section, there is a unitarity bound $|J_a| + |J_b| = \Delta$ which can be understood as a BPS bound by taking the limit of zero $U(1)$ charge. It can be shown $|J_a| + |J_b| \to \Delta$, only when $|J_i|, \Delta \to 0$ or they both diverge. In the first case, our bound vanishes and is consistent with the bulk, while in the latter case the bound diverges and is saturated by the divergent entropy of the corresponding black hole. We close this section with a

remark on the triply spinning case. Though it must be solved numerically, the bound on triply spinning operators can be obtained from the simple expression

$$(d-4)s + \sqrt{s^2 + 4\hat{J}_a^2} + \sqrt{s^2 + 4\hat{J}_b^2} + \sqrt{s^2 + 4\hat{J}_c} = 2. \tag{3.38}$$

The smallest non-negative solution to this expression gives our bound,

$$\rho(\Delta, J_a, J_b, J_c) \lesssim \pi \Delta s. \tag{3.39}$$

3.3.5 Single spin and single charge operators

Bounds for single spin and single charge operators exist in $d > 2$. We already derived the bound for $d = 3$ in section 3.3.1. In $d = 4$, we take the single spin limit of the black hole in [115]. In $d = 5$ and $d = 6$, we choose the single spin and single charge black hole from [116] and [117], respectively. It is worth noting that the generically spinning, charged black holes with AdS_6 and AdS_7 asymptotics are not pure Einstein-Maxwell, whose generically spinning solutions are not known in these dimensions, but are rather truncations of minimally gauged supergravity. Their zero-spin limit is not AdS-Reissner-Nordström and so this limit will not agree with section 3.3.2. Relevant thermodynamic quantities and vacuum subtracted Euclidean actions are listed in appendix B, in the single spin and single charge limit. As in $d = 3$, it is easiest to find $\Phi(r_+, \Omega)$ at the Hawking-Page transition and then minimize over $\beta(r_+, \Omega)(\Delta - \Omega J - \Phi(r_+, \Omega)Q)$. In $d = 4$, we have the odd feature (see section 3.8.1) that $b = 0$ does not imply $\Omega_b = 0$ or $J_b = 0$. However, this choice gives a nice analytic

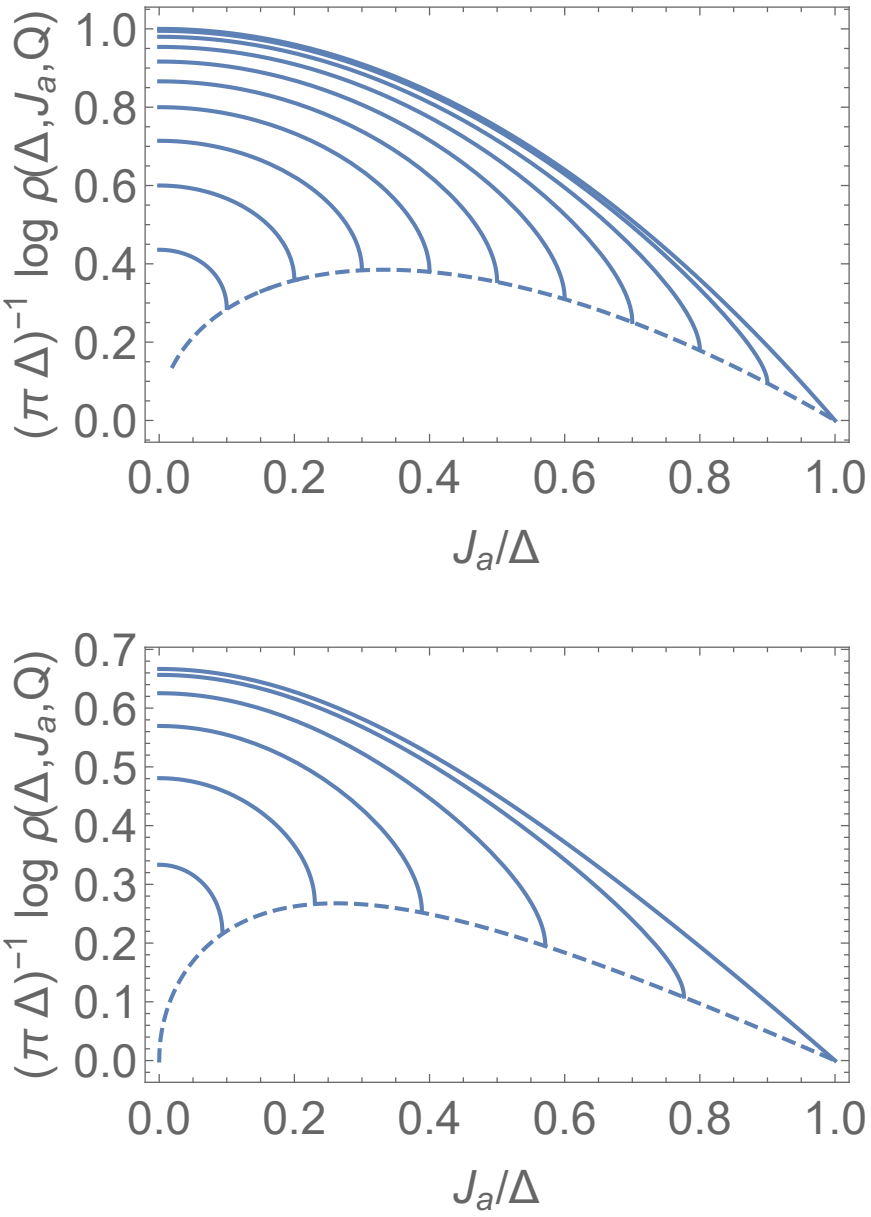

Figure 3.3: The bound for operators with spin J_a and charge Q in $d = 3$ (top) and $d = 4$ (bottom). From right to left, thick curves range from $Q/\Delta = 0$ to $Q/\Delta = 1$ (in $d = 3$) or $Q/\Delta = 1/\sqrt{3}$ (in $d = 4$) in increments of .1. In both plots, the dashed line is the horizon entropy per mass of the BPS black hole $S_{BH}/\pi\Delta$.

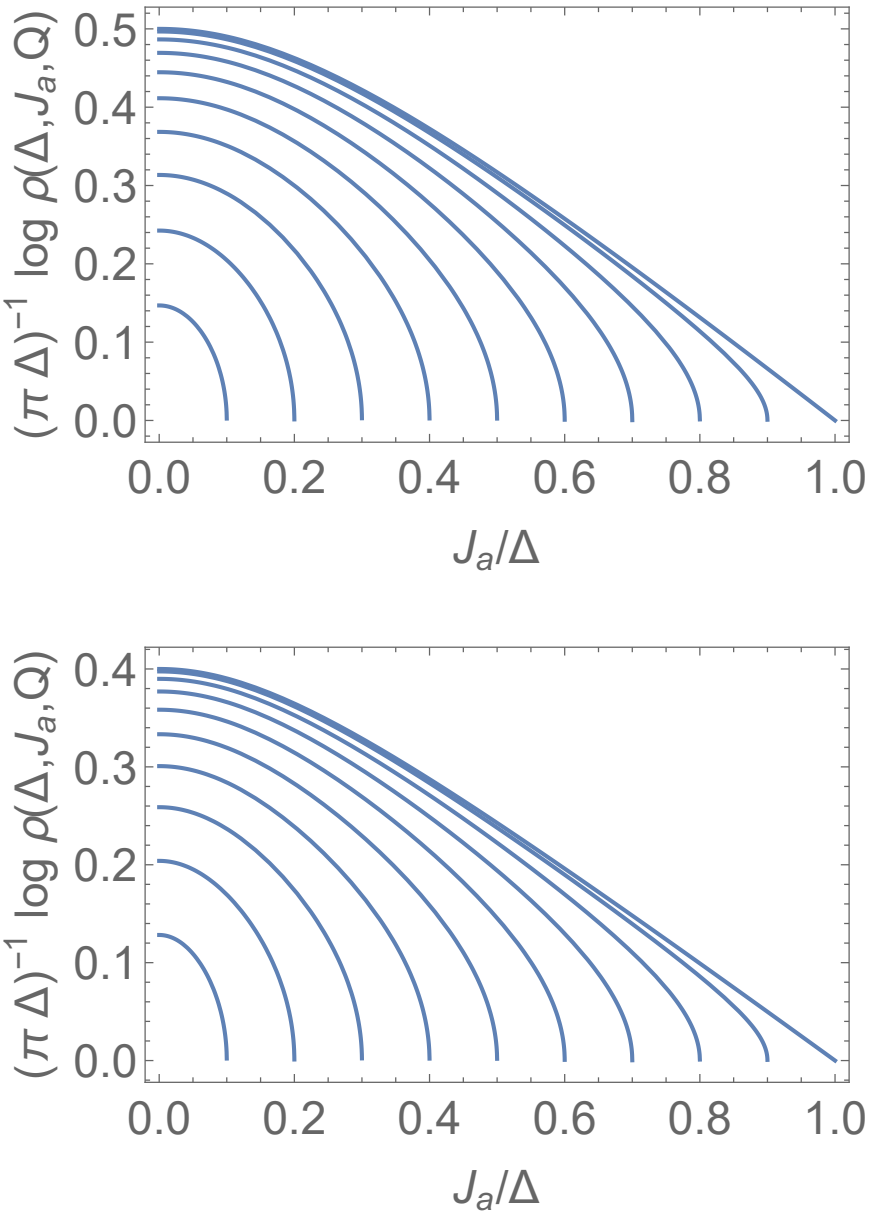

Figure 3.4: The bound for operators with spin J_a and charge Q in $d = 5$ (top) and $d = 6$ (bottom). From right to left, thick curves range from $Q/\Delta = 0$ to $Q/\Delta = 1$. The bound vanishes at the BPS limit $|J| + Q = \Delta$.

bound which can be written purely in terms of Δ, J_a, Q. Defining

$$J_b = \Delta \frac{\left(\tilde{J}-1\right)\hat{Q}}{\sqrt{3}\hat{J}_a} \quad \text{and} \quad \tilde{J} = \sqrt{1+3\hat{J}_a^2}. \tag{3.40}$$

we have

$$\begin{aligned}\rho(\Delta, J_a, J_b, Q) \lesssim & \frac{\pi\Delta}{3\left(1+\tilde{J}\right)^2} \\ & \times \left(\tilde{J}\left(1-\tilde{J}\right)+\sqrt{\left(\tilde{J}(1-\tilde{J})+2+6\hat{Q}^2\right)^2-12\hat{Q}^2\left(1+\tilde{J}\right)^2}+2+6\hat{Q}^2\right) \\ & \times \sqrt{\tilde{J}\left(2\tilde{J}+1\right)-6\hat{Q}^2-1+\sqrt{\left(\tilde{J}\left(1-\tilde{J}\right)+6\hat{Q}^2+2\right)^2-12\hat{Q}^2\left(1+\tilde{J}\right)^2}}\end{aligned} \tag{3.41}$$

Notable in this bound is the BPS limit, $J_a + J_b + \sqrt{3}Q = \Delta$, which does not vanish but, as in $d = 3$, reproduces the entropy of the corresponding BPS black hole,

$$\max\left[\rho\left(J_b + J_a + \sqrt{3}Q = \Delta\right)\right] = \frac{2\pi\Delta\left(1-\hat{J}_a\right)\sqrt{\hat{J}_a\left(\tilde{J}-1\right)}}{\tilde{J}+3\hat{J}_a-1}. \tag{3.42}$$

In $d = 5$, we get the bound

$$\begin{aligned}\log\rho(\Delta, J, Q) \lesssim & \frac{\pi\Delta}{4}\frac{\left(9-\sqrt{72\hat{J}^2-8\hat{Q}^2+9}\right)}{9-9\hat{J}^2+\hat{Q}^2} \\ & \times \sqrt{9(1-\hat{J}^2)^2+\hat{Q}^2\left(\hat{Q}^2-10\hat{J}^2-8-2\sqrt{9+72\hat{J}^2-8\hat{Q}^2}\right)}.\end{aligned} \tag{3.43}$$

Here, the density vanishes in the BPS limit $|J|+Q = \Delta$. Finally, in $d = 6$, our bound

is

$$\log\rho(\Delta,J,Q)\lesssim\frac{2\pi\Delta}{15}\frac{\left(16-\sqrt{240\hat{J}^2-15\hat{Q}^2+16}\right)}{16-16\hat{J}^2+\hat{Q}^2} \times\sqrt{16\left(1-\hat{J}^2\right)^2+\hat{Q}^2\left(\hat{Q}^2-17\hat{J}^2-15-2\sqrt{16+240\hat{J}^2-15\hat{Q}^2}\right)}\,. \tag{3.44}$$

Here too, the density vanishes in the BPS limit $|J|+Q=\Delta$. The vanishing at $|J|+Q=\Delta$ in $d=5,6$ is a consequence of the fact that BPS black holes only exist for J_a, J_b, Q non-vanishing [117, 116].

3.3.6 Numerical Results

In the previous sections, we calculated analytic bounds for operators with up to three parameters. To obtain bounds for operators with four or more parameters, we must resort to numerics. With $\lfloor d/2\rfloor$ angular potentials and one chemical potential, the Hawking-Page temperature is a $\lfloor d/2\rfloor+1$ dimensional hypersurface. For a given set of charges, $\{J_1,J_2,...,J_{\lfloor d/2\rfloor},Q\}$, we then numerically find the minimum value of

$$\beta_{HP}(\Omega_1,\Omega_2,...,\Omega_{\lfloor d/2\rfloor},\Phi)\left[1-\sum_{i=1}^{\lfloor d/2\rfloor}\hat{J}_i\Omega_i-\hat{Q}\Phi\right] \tag{3.45}$$

where for simplicity we have scaled out an overall factor of Δ so that all charges fall in a finite range. In the full ensemble, the BPS bound is $\Delta=\frac{1}{c}|Q|+\sum_{i=1}^{\lfloor d/2\rfloor}|J_i|$.[1] For energies below this bound, the density of states vanishes at leading order in N.

[1]For the $d=5,6$ supergravity solutions, the normalization of the charge is such that $c=1$ rather than the c defined for the Reissner-Nordström black holes

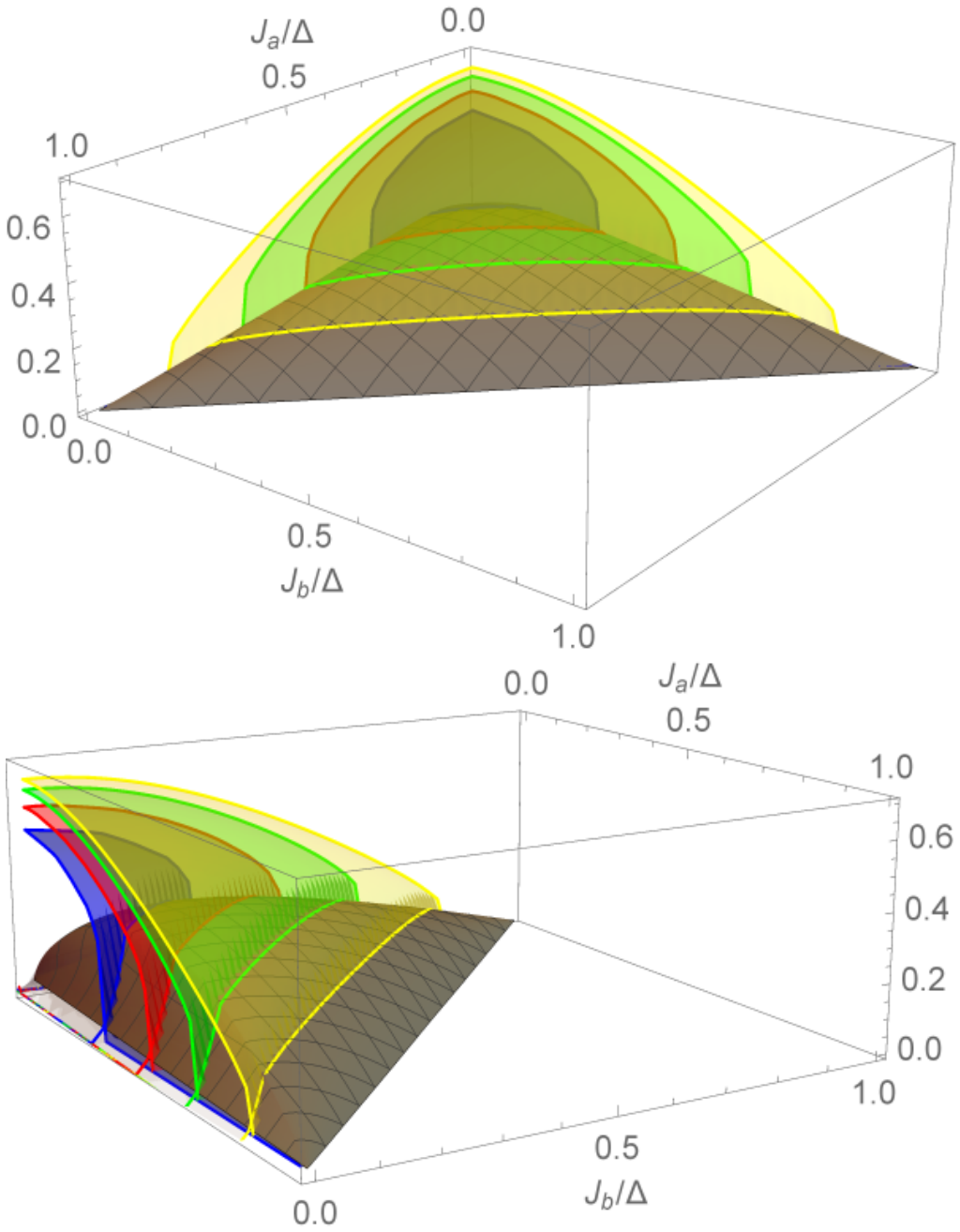

Figure 3.5: $d = 4$: $Q/\Delta = .4, .3, .2, .1$ (blue, red, green, yellow). The BPS condition is $\Delta = J_a + J_b + \sqrt{3}Q$.

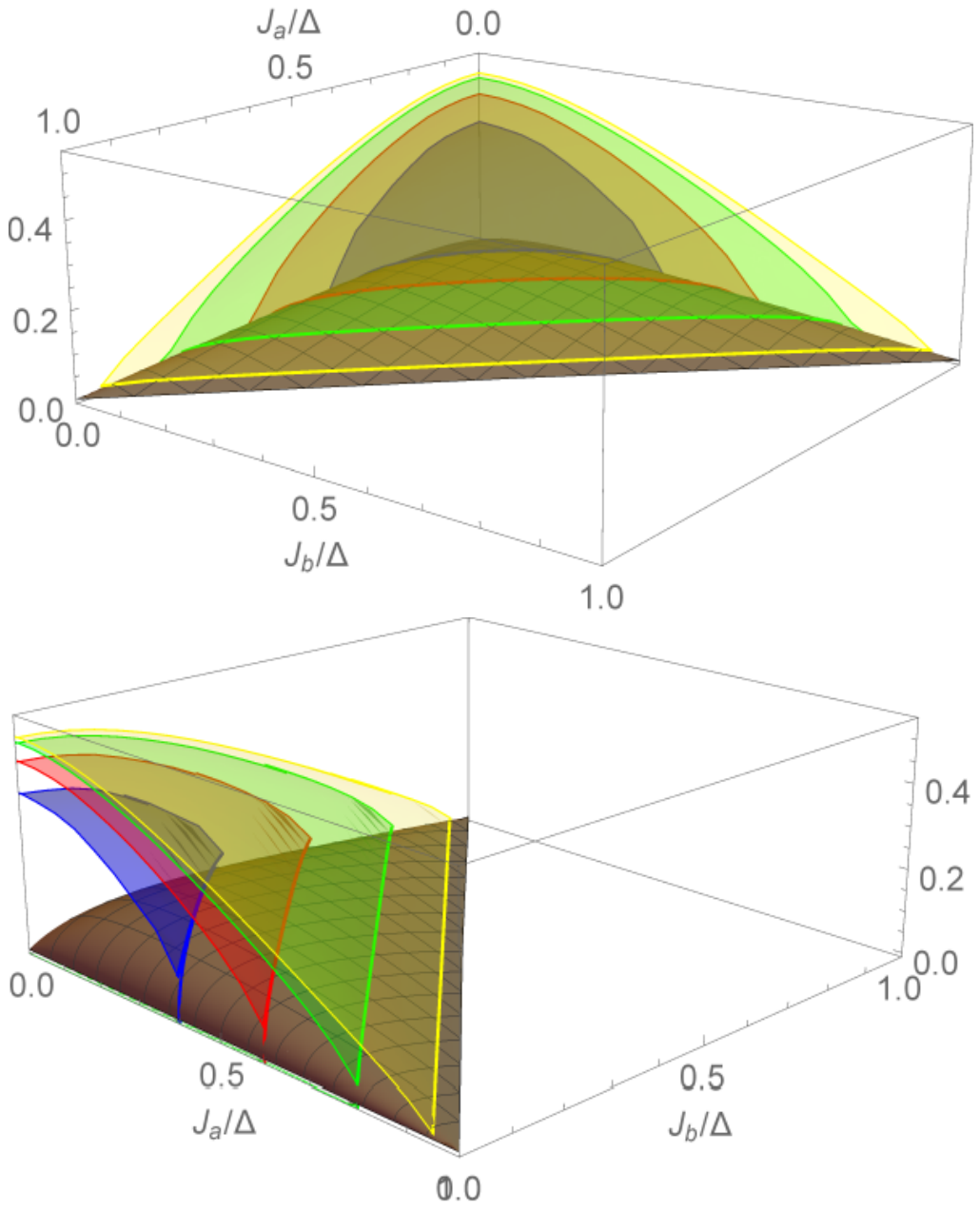

Figure 3.6: $d = 5$: $Q/\Delta = .6, .4, .2, .1$ (blue, red, green, yellow). The BPS condition is $\Delta = J_a + J_b + Q$.

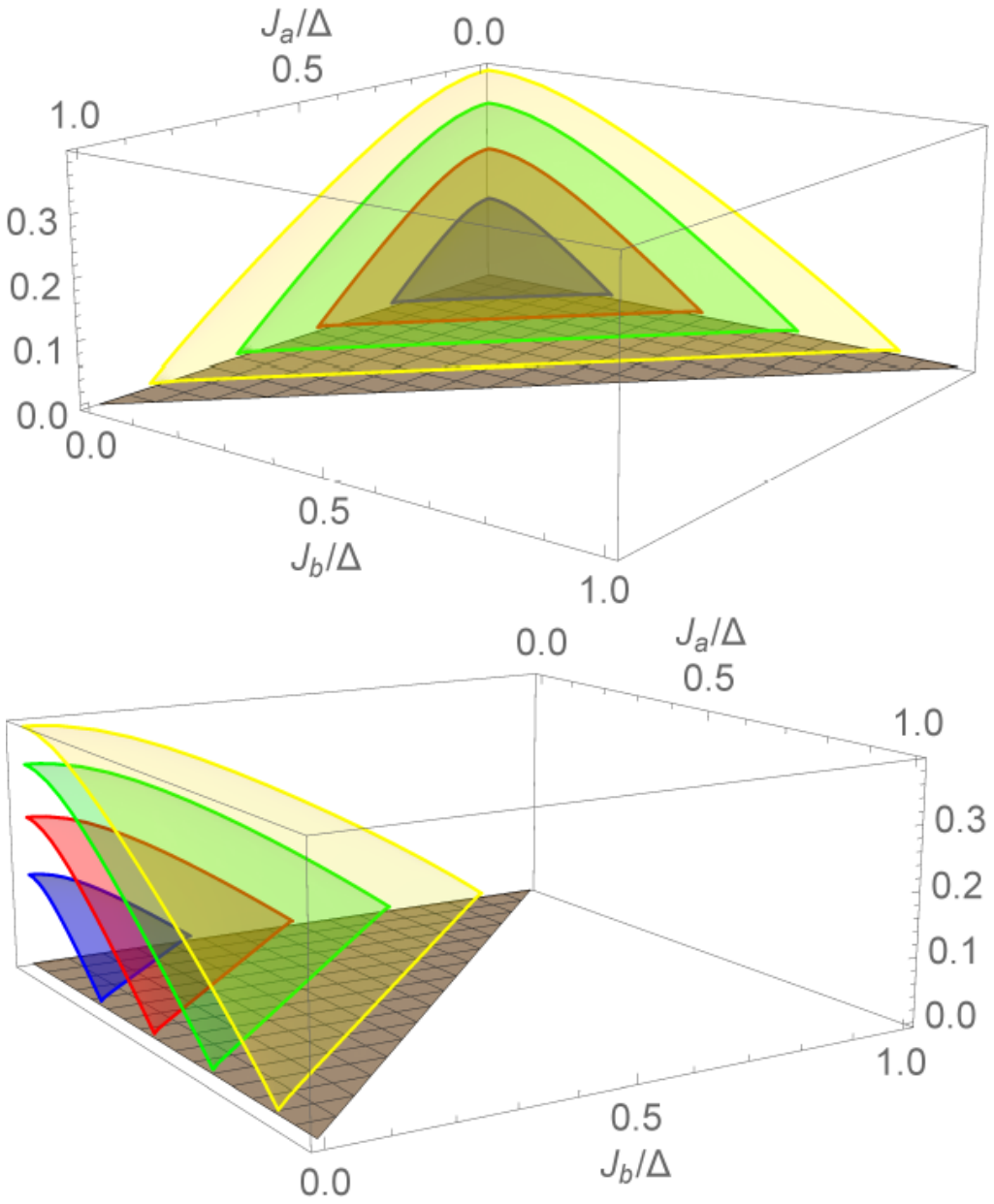

Figure 3.7: $d = 6 : Q = 0$ and $J_c/\Delta = .7, .5, .3, .1$ (blue, red, green, yelow). There are no BPS black holes with vanishing $U(1)$ charge, so the gray surface is $S_{BH} = 0$, where our bound implies $O(1)$ degeneracy of states.

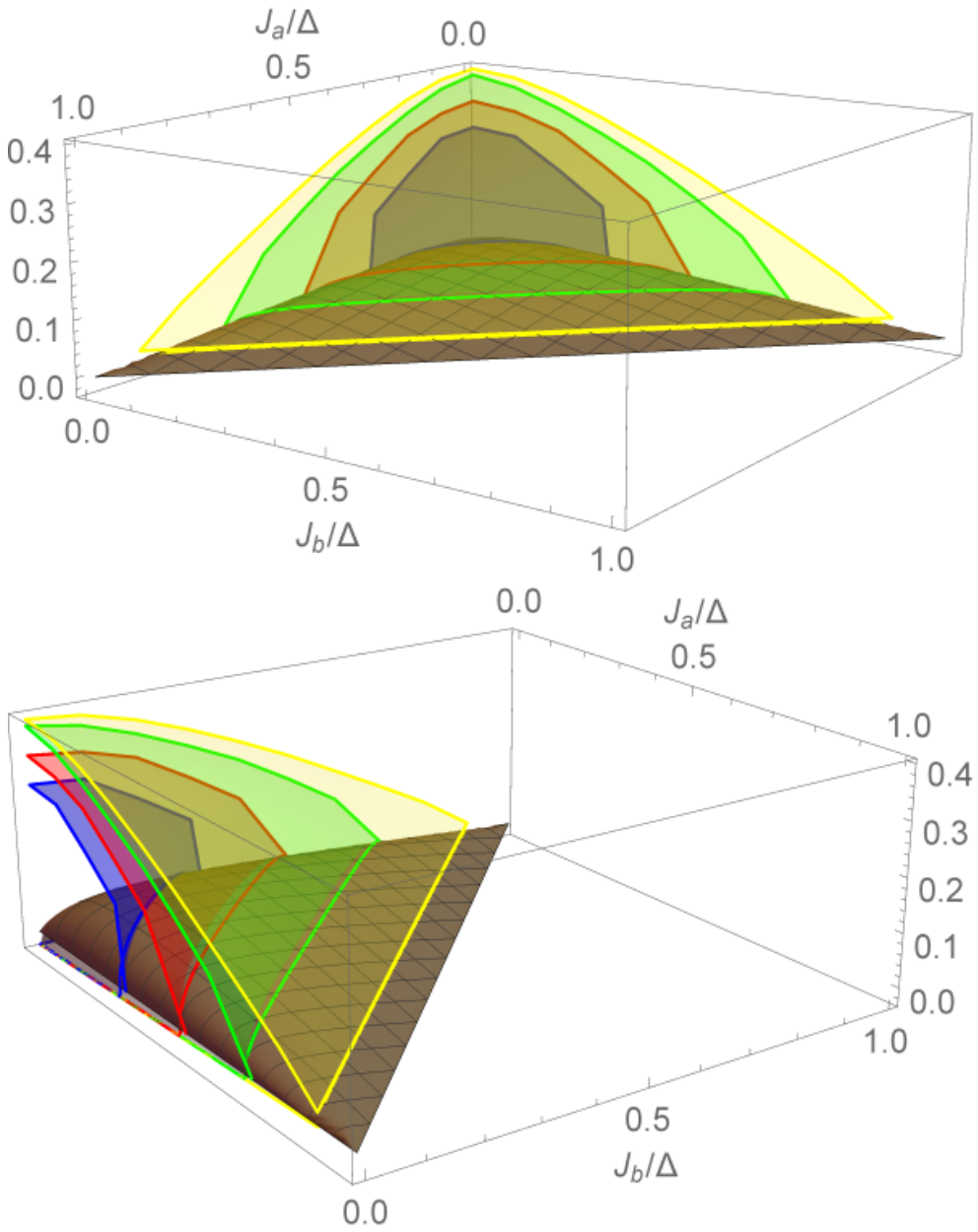

Figure 3.8: $d = 6$: $J_c = 0$ and $Q_c/\Delta = .7, .5, .3, .1$ (blue, red, green, yelow). The BPS condition is $\Delta = J_a + J_b + Q$. Figures 3.5, 3.6, 3.7, 3.8: Plots of $(\pi\Delta)^{-1} \log \rho[\Delta, J_a, J_b, (J_c), Q]$. Gray surfaces are $S_{BH}/(\pi\Delta)$ for corresponding BPS black holes which coincide with our bound at the BPS condition. Beyond this surface, the bound vanishes and no states are allowed (color online).

Because the equations we need to solve are algebraic, no sophisticated numerical techniques are necessary. We discretize the thermodynamic potentials and (hatted) parameters which have finite range. Angular potentials are bounded from above by the speed of light of the boundary ESU, $\Omega_i = 1$ and the electric potential is bounded from above by cosmic censorship. The spins and electric charges, scaled by the energy, also have finite range, typically $\{\hat{J}_i, \hat{Q}\} \in [0, 1]$ but this depends on the normalization of A_μ. The exact limits can be found in the appendix using the BPS bounds. We divide these intervals into equally spaced grids of $N = 100$ points. For each grid point labeled by the potentials' $(\lfloor d/2 \rfloor + 1)$ coordinates, we used the built-in "NSolve" function in Mathematica to obtain the black hole radius at the Hawking-Page transition giving us the critical surface defined in section 3.2. Once obtained, we calculate eq. (3.45) for each grid point in the spins' and charge's $(\lfloor d/2 \rfloor + 1)$ coordinates. Then, for each point $\{\hat{J}_i, \hat{Q}\}$ we searched for the minimum value of eq. (3.45) over the potentials, imposing the lower bound of zero. Because eq. (3.45) is exponentiated for the density of states, the lower bound determines where a single state is allowed–this is the BPS/unitarity bound of the CFT. Beyond this point (or curve), our procedure allows no states.

As checks on the numerics, we verified that our curves did not vary appreciably as a function of the grid sizes and that they agreed with the analytic results in the previous subsections. In figures 3.5 through 3.8, we plot the bound on the density of states in each dimension. Notable in these plots is the entropy of BPS black holes, plotted as a gray surface. Our bounds end on this surface, giving the entropy of these black holes, and then vanish, marking the BPS bound of the CFT. Furthermore, as we pointed out in section 3.3.5, with only one spin and charge, there are no BPS

black holes and hence the gray entropy surface vanishes.

3.4 BPS, cosmic censorship, and sparseness bounds

In previous sections, we saw that our bound on the density of states vanishes at leading order in N for states that violate the BPS bound in $d > 2$. This is intriguing since we generically considered non-supersymmetric (Einstein-Maxwell) theories, without using any embedding into supergravity. The appearance of a coarse BPS condition suggests that bulk thermodynamics knows about the consistent supergravity extension. Its appearance is due to the upper bounds on the chemical potentials in the confined phase of strongly coupled holographic theories. To see this, consider the case of finite temperature and a single angular potential. The confined phase always satisfies $\Omega \leq 1$, which means minimizing $\exp(\beta(E - \Omega J))$ in the confined phase will give zero for $J > E$, since then we can pick $\Omega = 1$ and $\beta \to \infty$. Had the confined phase admitted $\Omega > 1$, then our bound would rule out states with $J > J_c$ where $J_c < E$.

The bulk gravitational theory also has an additional bound – the cosmic censorship (CC) bound, that arises by demanding that there are no naked singularities. In general these two bounds are different: for Δ_{BPS} the lower bound implied by the BPS bound and Δ_{CC} the lower bound implied by cosmic censorship, we have $\Delta_{BPS} < \Delta_{CC}$ for fixed $U(1)$ charge or fixed spins, i.e. BPS states violate cosmic censorship. In the case with both $U(1)$ charge and spin, there is a line $J(Q)$ along which $\Delta_{BPS} = \Delta_{CC}$ if there is at least one spin in $d = 3, 4$ and at least two spins in $d = 5, 6$ (see figure 3.9). We find that in the cases where Δ_{BPS} is strictly smaller than Δ_{CC}, our bound

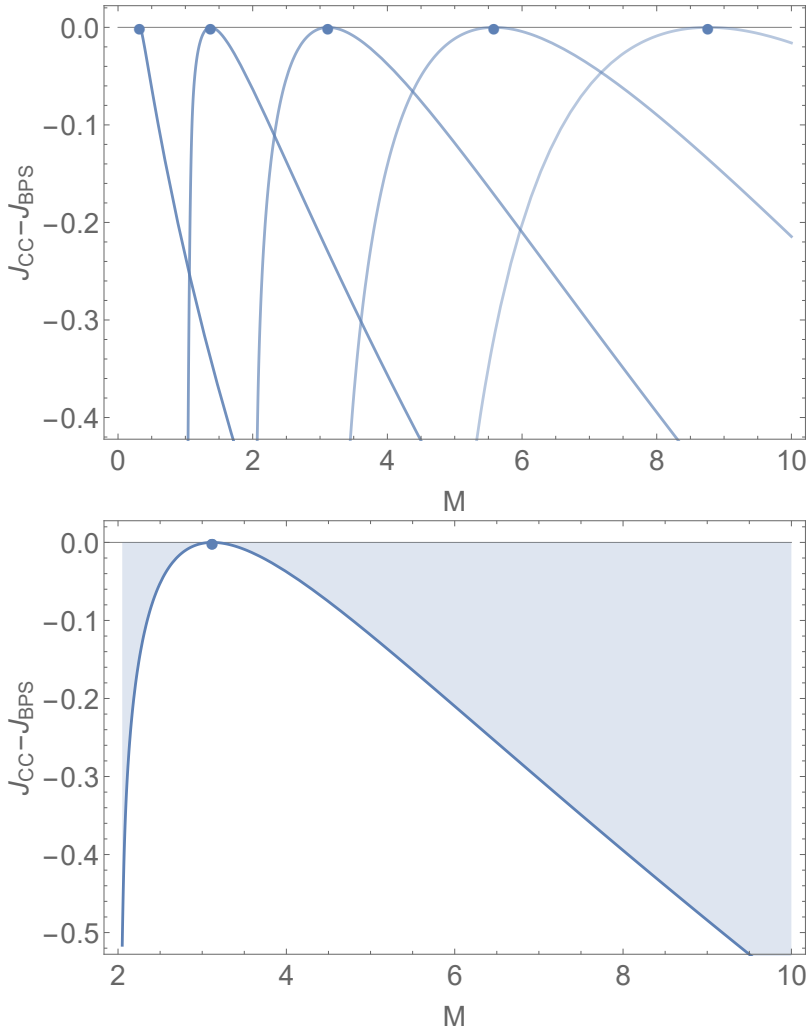

Figure 3.9: (Top) The difference between the BPS and cosmic censorship bound for four-dimensional Einstein-Maxwell-AdS. Curves correspond to fixed $Q = .3, .9, 1.5, 2.1, 2.7$ (left to right, darker to lighter). Circles indicate locations where extremal black holes satisfy the BPS condition $M = |J| + Q$ and BPS states are otherwise superextremal. (Bottom) The $Q = 1.5$ curve. Shaded region corresponds to CFT states with superextremal bulk duals that are not excluded by our bound. The feature $J_{BPS} > J_{CC}$ except at isolated points where $J_{BPS} = J_{CC}$ is characteristic of charged, spinning solutions in $d = 3, 4$ with at least one spin and $d = 5, 6$ with at least two spins. Without both charge and spin the inequality is never saturated.

vanishes at the BPS bound, while in the case where the BPS bound coincides with the CC bound, the maximum of our bound reduces to the entropy of the extremal black hole. Masses between cosmic censorship and BPS must have superextremal bulks but our bound allows for an $O(N^k)$ number of states in this range. In this section, we quickly review the BPS and CC bounds to compare to the sparseness bounds we obtain from the Hawking-Page transition.

For singly spinning black holes, as mentioned in previous sections, there is a unitarity bound that can also be understood as a $Q \to 0$ limit of a BPS bound,

$$\Delta \geq J\,. \tag{3.46}$$

Thus $\Delta_{BPS} = J$ becomes the lower bound on the allowed energy levels. This energy is also found to be strictly less than the cosmic censorship bound. In the limit $\Delta \to \Delta_{BPS}$, we find that our bound gives vanishing degeneracy of states at leading order in N. This is consistent with the fact that the only uncharged spinning BPS states are superextremal, and hence have $O(1)$ entropy. There are no extremal black holes with only one spin in $d \geq 5$, which is easily seen from the emblackening factor of the Kerr metric in Boyer-Lindquist coordinates [110]

$$\Delta_r = (r^2 + a^2)(1 + r^2) - 2mr^{4-d}. \tag{3.47}$$

However, there is still a "speed limit," $a \to 1$, required for stable bulk black holes.

For singly charged black holes, the BPS bound is given by

$$\Delta \geq \sqrt{\frac{d-1}{2(d-2)}}Q. \tag{3.48}$$

At fixed charge, this energy is strictly less than the CC bound. Again we find that as $\Delta \to \Delta_{BPS}$ our bound gives vanishing degeneracy of states at leading order in N. For non-spinning black holes in Einstein-Maxwell theory, the BPS bound is only rigorously known in $d = 3, 4$ where embeddings into supergravity theories have been found.

The same qualitative results are true for charged spinning black holes – at fixed charges the BPS energy is less than or equal to the cosmic censorship bound on energy. In the case of single charge in AdS_{d+1}, single spin single charge or double spin in AdS_6 and AdS_7, BPS states are always superextremal, and we find that our bound vanishes in the BPS limit. However superextremal states that lie between the BPS bound and the cosmic censorship bound, are nakedly singular and have $O(1)$ entropy, but our bound allows for $O(N^k)$ states.

In the case of single spin single charge in AdS_4, single or double spin single charge in AdS_5, double spin single charge in AdS_6, and double spin or triple spin single charge AdS_7, an extremal black hole that saturates the BPS bound exists for specific values of $\{\Delta, J_i, Q\}$. In such cases, the maxima of our bound reduces to the entropy of the extremal black hole. For generic values of $\{\Delta, J_i, Q\}$ between the BPS bound and the CC bound, the black hole is superextremal and has $O(1)$ entropy, but our bound still allows for $O(N^k)$ states. These features are shown for the four-dimensional Einstein-Maxwell-AdS theory in figure 3.9. For fixed Q and Δ, it is clear that there

exist states with $J_{CC} < J < J_{BPS}$ which are allowed by our bound but must be superextremal. That such states can be allowed is not surprising considering the stability of AdS black holes. Charged rotating black holes can often be obtained via dimensional reduction of spinning supergravity black holes in higher dimensions (see sections 3.8.2 and 3.8.3). Spinning black holes have superradiant instabilities by which the black hole should decay to the most stable spinning charged states (i.e. BPS). This instability is reflected in the lower dimension because the extremal black hole is not supersymmetric and hence unstable. Our bound allows for a finite number of superextremal states to which the extremal black hole can decay. Recent work relating BPS and cosmic censorship bounds can be found in [118, 119].

3.5 Comments on the high-lying spectrum

Our bounds imply a range of vacuum dominance ($\beta > \beta_{HP}$) that matches the phase structure of Einstein gravity in the bulk. It is interesting to ask if the high-temperature phase structure ($\beta < \beta_{HP}$) can be reproduced without additional assumptions. This is what was done in [14, 92] by using modular invariance of the torus partition function. Since we are considering theories on S^{d-1}, where ordinary modular invariance is absent, we need other tools.

We begin with an analysis of the Cardy-Verlinde formula [102], which was proposed as a higher-dimensional analog to the Cardy formula on S^{d-1}:

$$S = \frac{2\pi R}{d-1}\sqrt{E_{cas}(2E - E_{cas})} = \frac{4\pi R}{d-1}\sqrt{E_{subext}E_{ext}}. \tag{3.49}$$

R is the radius of S^{d-1} of the CFT, $E = E_{ext} + E_{subext}$, and $E_{cas} \equiv 2E_{subext}$. E_{ext}

and E_{subext} are the extensive and subextensive pieces of the thermodynamic energy. This formula reproduces the entropy of AdS-Schwarzschild black holes above the Hawking-Page transition but is known to fail for generic theories [120].

A very important aspect of this formula is that, unlike the ordinary Cardy formula, it is canonical in nature. E_{cas} is in no sense the ground state energy of the theory—as stated above, it is calculated by extracting the subextensive piece from $E \equiv \langle E \rangle$. That E_{cas} cannot be a single energy level is clear by matching to the high-energy scaling $S \sim E^{(d-1)/d}$, which shows that $E_{cas} \sim E^{(d-2)/d}$ at leading order; in particular it has to scale with E. Furthermore, to compute E_{cas}, one has to have knowledge of $\log Z$ since $\langle E \rangle = -\partial_\beta \log Z$. But this means one already has knowledge of $S = (1-\beta\partial_\beta) \log Z$. So, the Cardy-Verlinde formula should be understood as a repackaging of thermodynamic quantities into a suggestive form. If not for the similarity to the ordinary Cardy formula it would be essentially meaningless. The parameters appearing in the Cardy formula, on the other hand, do not require knowledge of the thermodynamics. To have the Cardy-Verlinde formula reduce to the Cardy formula for $d = 2$, as is often stated, one has to shift the definition of E_{cas} by the vacuum energy $-c/12$.

Nevertheless, the fact that the thermodynamic quantities can be repackaged in this way for holographic theories is nontrivial. It is then natural to ask how general it is—does it depend on the field theory manifold? Can one add potentials for electric charge and angular momentum? It turns out the formula fails for a holographic theory on flat slices, like a torus. This is because $E_{cas} = 0$ for such theories, making the formula meaningless. A constant shift only works for $d = 2$, since for $d > 2$ it would give incorrect asymptotic scaling $S \sim \sqrt{E}$. For this case, one has to instead use the

higher-dimensional Cardy formula, which can be derived from modular invariance and is true for generic conformal theories [121, 122]. On hyperbolic slices, it was shown that the formula fails but can be fixed by defining $E_{sub} = \frac{E_{cas}}{2k}$ [123], where spherical slices have $k = +1$ and hyperbolic have $k = -1$. With this definition, E_{sub} is strictly positive. While no explanation was given for this substitution, we will use a high-temperature effective field theory to explain this result at the end of this section.

The formula fails generally when chemical potentials are added, although it can be fixed by making appropriate modifications in some cases. It has been shown that the entropy of Reissner-Nordström is reproduced by the Cardy-Verlinde formula on substituting E_{ext} for $E_{ext} - \frac{\Phi Q}{2}$, where Φ and Q are the $U(1)$ potential and the electric charge respectively[124]. While for Kerr-Newman black holes, thermodynamic quantities defined with respect to an asymptotically rotating frame can be shown to satisfy the Cardy-Verlinde formula[125]. However in these modified definitions, E_{ext} loses its meaning as being the extensive part of the energy. For more complicated solutions like multi-charged or multiply-spinning black holes in gauged supergravity models, one can still fix the Cardy-Verlinde formula by making changes to E_{cas} and E_{ext}[123], however these changes are quite complicated in terms of the CFT thermodynamic quantities [126]. Thus, there does not seem to exist a universal modification that works for every case. While it is tempting to think the form of the Cardy-Verlinde formula implies a connection between high-lying and low-lying states, the difficulties outlined above, coupled with the fact that E_{cas} is not a fixed low-lying energy, suggest otherwise.

Two approaches, which we will point out but not pursue, are to investigate the notions of "emergent circles" [127] and "detachable circles" [128]. In this context, the

notion of emergent circles says:

$$Z\left[S^1_{2\pi/k\to 0}\times S^{2n+1}/\mathbb{Z}_{p\to\infty}\right]=Z\left[S^1_{2\pi/p\to 0}\times S^{2n+1}/\mathbb{Z}_{k\to\infty}\right],\qquad p/k \text{ fixed} \quad (3.50)$$

The quotient is performed on the Hopf fiber for the odd-dimensional sphere represented as a circle fibered over CP^n. In this highly lensed limit, there is an emergent modular invariance that appears, since a highly lensed sphere behaves like $S^1\times CP^n$ for the purpose of leading-order thermodynamics. Coupling this with the special pattern of center symmetry breaking of strongly coupled holographic CFTs [93] may give an avenue to relating the theory on $S^{2n-1}/\mathbb{Z}_{p\to\infty}$ back to the theory on S^{2n-1}. For $n=3$ there is even a nontrivial Hawking-Page phase structure in the bulk with calculable $\beta(p)_{HP}$ that can be used to provide a bound on the density of states $\rho(E)\lesssim e^{\beta(p)_{HP}E}$ on $S^3/\mathbb{Z}_p$, connecting the round sphere $p=1$ to the case with an emergent modular invariance $p\to\infty$.

The notion of "detachable circles" in this context relates a finite-temperature conformal theory on S^{d-1} to the theory on $\mathbb{H}^{d-1}/\mathbb{Z}$ at some inversely related temperature:

$$ds^2=d\chi^2+d\theta^2+\sin^2\theta d\Omega^2_{d-3}+\cos^2\theta d\phi^2\to\frac{d\chi^2+d\theta^2+\sin^2\theta d\Omega^2_{d-3}}{\cos^2\theta}+d\phi^2\,. \quad (3.51)$$

By restricting our theory to be gapped at finite temperature (which is the generic situation), we can use the effective theory approach introduced in [129]. This approach allows us to write down the following effective action for the theory dimensionally reduced over the thermal circle:

$$\log Z(\beta)=\int d^{d-1}\sqrt{h}\left(c_0\frac{1}{\beta^{d-1}}+c_1\frac{R^{(1)}}{\beta^{d-3}}+c_2\frac{R^{(2)}}{\beta^{d-5}}+\dots\right) \quad (3.52)$$

This is to be understood as a perturbative expansion around $\beta \to 0$. Powers $R^{(n)}$ are to be understood as all possible combinations of contractions of the Riemann tensor, with e.g. different coefficients between $R_{\mu\nu}R^{\mu\nu}$ and R^2 which are suppressed for simplicity.

This effective theory makes clear that the high-temperature theory on a hyperboloid is related to the high-temperature theory on the sphere by sign flips in the terms of the effective theory with odd powers of curvatures. Certain large-N theories may have a sufficiently extended range of validity for this effective theory such that we can relate the theory on $\mathcal{H}^{d-1}/\mathbb{Z}$ back to the theory on S^{d-1}. This effective theory also explains why the Cardy-Verlinde formula works for hyperbolic slices with the definition $E_{sub} = \frac{E_{cas}}{2k}$: this is a simple way to achieve the sign flips implied by the effective theory.

3.6 Conclusion

In this paper, we derived quantitative sparseness conditions on holographic CFTs with a semiclassical Einstein dual. To arrive at these conditions, we used the fact that there generically exists a Hawking-Page transition between vacuum AdS and a large asymptotically AdS black hole at a particular temperature and set of thermodynamic potentials. Such a phase transition implies a discontinuous jump in the free energy from $O(1)$ to $O(N^k)$ and hence the CFT can only support a finite number of states before it deconfines. The difficulty in satisfying such bounds comes from the fact that interactions tend to sparsify a spectrum, so generic weakly interacting theories have dense spectra which violate our bounds.

An interesting aspect of these bounds is that that $\log \rho = O(1)$ for masses below the BPS bound. In situations where a bulk BPS black hole exists at the bound, its entropy saturates our bound, which then discontinuously drops to $O(1)$ consistent with the bulk. It is interesting to see the appearance of the BPS bound in the cases with $U(1)$ charge without inputting supersymmetry.

Sparseness assumptions figure prominently into simplifying limits of conformal bootstrap techniques. The usual style of argument is that a sufficiently sparse spectrum allows you to pick up only the contribution of the vacuum in a particular OPE expansion. This was most recently utilized in the bootstrap approach [130] to the "large charge" expansion [131, 132]. It would be interesting to explore the connection of our quantitative sparseness bounds to these bootstrap techniques.

A sparse low-lying density of local operators is often invoked as a requirement for a CFT to have a semiclassical Einstein dual, but for $d > 2$, a precise definition of "sparseness" was lacking. In this work we have provided a quantitative sparseness bound on the allowed density of local operators in the CFT. This bound enforces vacuum dominance of the gravitational path integral at low temperatures. It is a sharp diagnostic for how much interactions have to "sparsify" a spectrum, since it is *violated* by weakly coupled holographic theories. It would be interesting to connect this sparseness condition to a *different* sparseness condition, the gap to the higher-spin operators [133], both of which need to be satisfied for a weakly coupled Einstein gravity dual, and both of which are violated for weakly interacting holographic CFTs in $d > 2$.

3.7 Appendix A: Black hole entropy from deconfining phase transitions

As we saw throughout this paper, our bounds on the density of states are saturated by the black hole at the deconfining phase transition. We can invert this logic to produce a derivation of black hole entropy from field-theoretic considerations. Since we would have to input a deconfinement temperature (and more assumptions) in the general case, let us focus on $d = 2$ where we can get by with minimal assumptions.

Assume a large-c CFT in $d = 2$ has a single first-order deconfining phase transition. By modular invariance it must occur at $\beta = 2\pi$. We use a normalization consistent with modular invariance, $E_{\text{vac}} = -c/12$. We also know from the modular bootstrap that $\langle E\rangle_{\beta=2\pi} = 0$ [134]. By the generic description of first-order phase transitions as an exchange of saddles, we can use the vacuum energy and $\langle E\rangle_{\beta=2\pi} = 0$ to deduce that $\langle E\rangle_{\beta=2\pi-\epsilon} = c/12$ up to corrections in ϵ. Since $\Delta_c - S_c/\beta_c = O(1) \implies S_c = \beta_c\Delta_c = \beta_c(E_c + c/12)$ at leading order in c, this gives us a prediction for the thermal entropy, where we have deduced $E_c = c/12$ and $\beta_c = 2\pi$ purely from field-theoretic considerations. Notice that "c" is doing double duty here. For $\beta = 2\pi - \epsilon$ we are in the deconfined phase of a large-c theory, so we can coarse grain to translate into a density of states as in [14]. Altogether we have the formula

$$\log \rho(E = c/12) = \pi c/3\,. \tag{3.53}$$

This agrees precisely with the bulk, where the ensemble is dominated by a BTZ black hole below $\beta = 2\pi$, and so by continuity the density of states at $\beta = 2\pi$ is given by the

Bekenstein-Hawking entropy of the BTZ black hole at the Hawking-Page transition. One could also dispense of the assumption that the transition is first order and so described by an exchange of saddles to obtain a formula of the sort $\log \rho(E) = 2\pi E$ where $E \equiv \langle E \rangle_{2\pi-\epsilon}$.

Notice that the Cardy formula $\log \rho(E) = 2\pi\sqrt{cE/3}$, which is true for $E \to \infty$, matches onto the formula given above. This is completely expected, since in the case of $d = 2$ the bound $\rho(\Delta) \lesssim e^{2\pi\Delta}$ implied by the phase transition assumed here can be used to prove the validity of the Cardy formula down to $\Delta \sim c/6$ [14]. So this result is weaker, but the different route taken is illuminating and can potentially be applied in other cases where arguments like that of [14] are absent.

3.8 Appendix B: AdS_5, AdS_6, and AdS_7 details

For interested readers, here is an expanded appendix in which we explicitly write the metric and all thermodynamic quantities.

3.8.1 AdS_5

Here we follow [115]. The metric may be written as

$$ds^2 = -\frac{\Delta_\theta \left[(1+r^2)\rho^2 dt + 2q\nu\right] dt}{\Xi_a \Xi_b \rho^2} + \frac{2q\nu\omega}{\rho^2} + \frac{f}{\rho^4}\left(\frac{\Delta_\theta dt}{\Xi_a \Xi_b} - \omega\right)^2 \tag{3.54}$$

$$+\frac{\rho^2 dr^2}{\Delta_r} + \frac{\rho^2 d\theta^2}{\Delta_\theta} + \frac{r^2+a^2}{\Xi_a}\sin^2\theta d\phi^2 + \frac{r^2+b^2}{\Xi_b}\cos^2\theta d\psi^2 \tag{3.55}$$

with the Maxwell field

$$A = \frac{\sqrt{3}q}{\rho^2}\left(\frac{\Delta_\theta dt}{\Xi_a \Xi_b} - \omega\right). \tag{3.56}$$

The metric functions and one-forms are

$$\begin{aligned}
\nu &= b\sin^2\theta d\phi + a\cos^2\theta d\psi, \qquad & \omega &= a\sin^2\theta\frac{d\phi}{\Xi_a} + b\cos^2\theta\frac{d\psi}{\Xi_b},\\
\Delta_\theta &= 1 - a^2\cos^2\theta - b^2\sin^2\theta, \qquad & f &= 2m\rho^2 - q^2 + 2abq\rho^2,\\
\rho^2 &= r^2 + a^2\cos^2\theta + b^2\sin^2\theta, \qquad & \Xi_a &= 1-a^2, \quad \Xi_b = 1-b^2,\\
\Delta_r &= \frac{(r^2+a^2)(r^2+b^2)(1+r^2) + q^2 + 2abq}{r^2} - 2m.
\end{aligned} \tag{3.57}$$

This metric and Maxwell field solve the equations of motion of minimal gauged five-dimensional supergravity, following from

$$\mathcal{L} = (R+12)\star 1 - \frac{1}{2}\star F\wedge F + \frac{1}{3\sqrt{3}}F\wedge F\wedge A \tag{3.58}$$

where $\star 1$ is the volume form. The vector $k = \frac{\partial}{\partial t} + \Omega_a\frac{\partial}{\partial\phi} + \Omega_b\frac{\partial}{\partial\psi}$ goes null at the outer horizon $\Delta_r(r_+) = 0$. Here,

$$\begin{aligned}
\Omega_a &= \frac{a(r_+^2+b^2)(1+r_+^2) + bq}{(r_+^2+a^2)(r_+^2+b^2) + abq}\\
\Omega_b &= \frac{b(r_+^2+a^2)(1+r_+^2) + aq}{(r_+^2+a^2)(r_+^2+b^2) + abq}.
\end{aligned} \tag{3.59}$$

These are the correct angular potentials for the thermodynamics (note that $q \to 0$ agrees with the lower dimensional cases). The inverse temperatures of these black

holes are

$$\beta = \frac{2\pi r_+[(r_+^2+a^2)(r_+^2+b^2)+abq]}{r_+^4[1+2r_+^2+a^2+b^2]-(ab+q)^2}. \tag{3.60}$$

The chemical potential is

$$\Phi = A_a k^a\Big|_{r\to\infty} - A_a k^a\Big|_{r=r_+} = \frac{\sqrt{3}qr_+^2}{(r_+^2+a^2)(r_+^2+b^2)+abq}. \tag{3.61}$$

The on shell action, with the $m\to 0, q\to 0$ limit of eq. (3.55) background subtracted, is, (note that one must make a gauge transformation on A as in [135] to obtain this result),

$$\begin{aligned} I_E^R =& \frac{\pi\beta}{8G\Xi_a\Xi_b r_+^2} \\ &\times\left[(r_+^2+a^2)(r_+^2+b^2)(1-r_+^2)+2abq+q^2\left(1-\frac{2r_+^4}{(r_+^2+a^2)(r_+^2+b^2)+abq}\right)\right]. \end{aligned} \tag{3.62}$$

Again, the Hawking-Page transition must generically be found numerically. However, when there is just one angular momentum or just one charge, we can perform a similar analysis as in three and four dimensions. With just one spin, the transition occurs at $r_+ = 1$. With just one charge, the transition happens at $r_+ = \sqrt{1-\Phi^2/3}$. The critical density of states in these cases is,

$$\begin{aligned} b=q=0: \quad \log(\rho(E,J)) &= \frac{J^2\left(3-2\sqrt{\frac{3J^2}{E^2}+1}\right)+E^2}{2E^2+\sqrt{E^4+3E^2J^2-4EJ^2\sqrt{E^2+3J^2}+4J^4}+8J^2} \\ a=b=0: \quad \log(\rho(E,Q)) &= \frac{2\pi}{3}\sqrt{E^2-3Q^2} \end{aligned} \tag{3.63}$$

Again, the BPS limit is $E = |J_1| + |J_2| + \sqrt{3}|Q|$ beyond which there are no states. Note, this bound differs slightly from the Chamblin et al. case (see 3.24), because of a factor of 2 in the definition of A_μ.

3.8.2 $\mathbf{AdS}_6$

The bounds on the density of states are meant to serve all holographic CFTs in their respective dimensions. However, there are no bottom-up solutions for Einstein-Maxwell gravity in $d = 5$ and $d = 6$. This may not be surprising as higher form fields and Chern-Simons terms seem natural in higher dimensions, especially in consistent supergravity trunctations. Instead, one must search for the most generic supergravity solution with AdS asymptotics and fewest bulk fields. The most generic choice we could find in the literature is the black hole in [116]. This comes from a dimensional reduction of massive type IIA supergravity on a hemisphere of S^4 [136]. This supergravity theory should arise as the near horizon limit of a D4-D8 brane configuration and is dual to a $d = 5$, $\mathcal{N} = 2$ superconformal field theory. The bosonic field content of six dimensional $\mathcal{N} = 4, SU(2)$ gauged supergravity is a graviton, a two-form potential, a one-form potential, the gauge potentials of $SU(2)$ Yang-Mills and a scalar. We can truncate to the sector where only one $U(1)$ of the SU(2) is excited. Then, the bosonic Lagrangian is

$$\begin{aligned}\mathcal{L} = R \star 1 - \frac{1}{2} \star d\phi \wedge d\phi - X^{-2} \left(\star F_{(2)} \wedge F_{(2)} + \star A_{(2)} \wedge A_{(2)} \right) - \frac{1}{2} X^4 \star F_{(3)} \wedge F_{(3)} \\ + \left(9X^2 + 12X^{-2} - X^{-6} \right) \star 1 - F_{(2)} \wedge F_{(2)} \wedge A_{(2)} - \frac{1}{3} A_{(2)} \wedge A_{(2)} \wedge A_{(2)},\end{aligned} \tag{3.64}$$

with $F_{(2)} = dA_{(1)}$. The black hole solution to the equations of motion derived from this action is, written conveniently in terms of sixbeins,

$$\begin{aligned} ds^2 = H^{1/2}\Bigg[&\frac{(r^2+y^2)(r^2+z^2)}{R}dr^2 + \frac{(r^2+y^2)(y^2-z^2)}{Y}dy^2 + \frac{(r^2+z^2)(z^2-y^2)}{Z}dz^2 \\ &- \frac{R}{H^2(r^2+y^2)(r^2+z^2)}\mathcal{A}^2 \\ &+ \frac{Y}{(r^2+y^2)(y^2-z^2)}\left(dt' + (z^2-r^2)d\psi_1 - r^2z^2 d\psi_2 - \frac{qr\mathcal{A}}{H(r^2+y^2)(r^2+z^2)}\right)^2 \\ &+ \frac{Z}{(r^2+z^2)(z^2-y^2)}\left(dt' + (y^2-r^2)d\psi_1 - r^2y^2 d\psi_2 - \frac{qr\mathcal{A}}{H(r^2+y^2)(r^2+z^2)}\right)^2\Bigg]. \end{aligned} \tag{3.65}$$

The fields are

$$\begin{aligned} X = H^{-1/4}, \quad A_{(1)} &= \frac{2ms_\delta c_\delta r}{H(r^2+y^2)(r^2+z^2)}\mathcal{A} \\ A_{(2)} = \frac{q}{H(r^2+y^2)^2(r^2+z^2)^2}\Bigg[&-\frac{yz[2r(2r^2+y^2+z^2)+2]}{H}dr\wedge\mathcal{A} \\ &+z[(r^2+z^2)(r^2-y^2)+qr]dy \\ &\wedge\left(dt' + (z^2-r^2)d\psi_1 - r^2z^2 d\psi_2 - \frac{qr\mathcal{A}}{H(r^2+y^2)(r^2+z^2)}\right) \\ &+y[(r^2+y^2)(r^2-z^2)+qr]dz \\ &\wedge\left(dt' + (y^2-r^2)d\psi_1 - r^2y^2 d\psi_2 - \frac{qr\mathcal{A}}{H(r^2+y^2)(r^2+z^2)}\right)\Bigg], \end{aligned} \tag{3.66}$$

and the metric functions and one-forms are

$$\begin{aligned}
&R = (r^2+a^2)(r^2+b^2) + [r(r^2+a^2)+q][r(r^2+b^2)+q] - 2mr,\\
&Y = -(1-y^2)(a^2-y^2)(b^2-y^2), \quad Z = -(1-z^2)(a^2-z^2)(b^2-z^2),\\
&H = 1 + \frac{qr}{(r^2+y^2)(r^2+z^2)}, \quad q = 2ms_\delta^2, \quad \mathcal{A} = dt' + (y^2+z^2)d\psi_1 + y^2z^2 d\psi_2.
\end{aligned} \tag{3.67}$$

and $s_\delta = \sinh\delta, c_\delta = \cosh\delta$ are defined in terms of a boost parameter δ which for our purposes serves effectively as a choice of charge.[2] The metric is defined in terms of so-called Jacobi-Carter coordinates. One can move to Boyer-Lindquist coordinates,

$$t' = \tilde{t} - a^4\tilde{\phi}_1 - b^4\tilde{\phi}_2, \quad \psi_1 = -\tilde{t} + a^2\tilde{\phi}_1 + b^2\tilde{\phi}_2, \quad \psi_2 = \tilde{t} - \tilde{\phi}_1 - \tilde{\phi}_2 \tag{3.68}$$

and

$$\tilde{t} = \frac{t}{\Xi_a\Xi_b}, \quad \tilde{\phi}_1 = \frac{\phi_1}{\Xi_a a(a^2-b^2)}, \quad \tilde{\phi}_2 = \frac{\phi_2}{\Xi_b b(b^2-a^2)}. \tag{3.69}$$

As before $\Xi_a = 1-a^2, \Xi_b = 1-b^2$. Finally, y and z are parametrized in terms of direction cosines [137],

$$\mu_1^2 = \frac{(a^2-y^2)(a^2-z^2)}{(a^2-b^2)}, \quad \mu_2^2 = \frac{(b^2-y^2)(b^2-z^2)}{(b^2-a^2)}. \tag{3.70}$$

[2]There is an art to finding charged spinning black holes in higher dimensional supergravity which is covered in many of the references we follow. One particularly effective methods is through repeated dimensional reduction, uplifting, and boosting, which through the typical Kaluza-Klein mechanism leads to U(1) charges in the lower dimensional theory.

It is easily checked that $\mu_1^2+\mu_2^2+\mu_3^2=1$. These direction cosines efficiently parametrize the $(d-1)$ spheres as

$$d\Omega^2 = \sum_{i=1}^{\lfloor (d+1)/2 \rfloor} d\mu_i^2 + \sum_{i=1}^{\lfloor d/2 \rfloor} \mu_i^2 d\phi_i^2 \tag{3.71}$$

where, as before, $\lfloor n \rfloor$ means the nearest integer less than or equal to n. Now, the metric (3.66) is very complicated and calculating the action is messy. It turns out that in this case (and in $d=6$), it is easier to work in terms of thermodynamic charges and potentials to find the Gibbs free energy. First, the Killing vector $k = \frac{\partial}{\partial t}+\Omega_a \frac{\partial}{\partial \phi_1}+\Omega_b \frac{\partial}{\partial \phi_2}$ vanishes at the outer horizon $R(r_+)=0$. This defines

$$\Omega_a = \frac{a[(1+r_+^2)(r_+^2+b^2)+qr_+]}{(r_+^2+a^2)(r_+^2+b^2)+qr_+}, \quad \Omega_b = \frac{b[(1+r_+^2)(r_+^2+a^2)+qr_+]}{(r_+^2+a^2)(r_+^2+b^2)+2r_+}. \tag{3.72}$$

The conjugate charges can be defined through the Komar integral

$$J_i = \frac{1}{16\pi G}\int_{S^4_\infty} \star dK_i = \frac{2\pi m a_i (1+(\Xi_a+\Xi_b-\Xi_i)s_\delta^2)}{3\Xi_i \Xi_a \Xi_b} \tag{3.73}$$

with K_i the dual one-form for $\partial/\partial\phi_i$. Next, the potential at the horizon Φ defined as $\Phi = k\cdot A_{(1)}\Big|_{r=r_+} - k\cdot A_{(1)}\Big|_{r\to\infty}$ is

$$\Phi = \frac{2ms_\delta c_\delta r_+}{(r_+^2+a^2)(r_+^2+b^2)+qr_+} \tag{3.74}$$

and the dual conserved electric charge is

$$Q = \frac{1}{8\pi G}\int_{S^4_\infty} (X^{-2}\star F_{(2)} + F_{(2)}\wedge A_{(2)}) = \frac{2ms_\delta c_\delta}{\Xi_a \Xi_b}. \tag{3.75}$$

Finally, the energy (obtained most efficiently via integration of the first law of black hole mechanics $dE = TdS + \Phi dQ + \Omega_i dJ_i$ [138]), Bekenstein-Hawking entropy, and temperature are

$$\begin{aligned} E &= \frac{\pi}{3\Xi_a\Xi_b}\left[2m\left(\frac{1}{\Xi_a}+\frac{1}{\Xi_b}\right)+q\left(1+\frac{\Xi_a}{\Xi_b}+\frac{\Xi_b}{\Xi_a}\right)\right], \\ S &= \frac{2\pi^2\left[(r_+^2+a^2)(r_+^2+b^2)+qr_+\right]}{3\Xi_a\Xi_b} \\ T &= \frac{2(1+r_+^2)r_+^2(2r_+^2+a^2+b^2)-(1-r_+^2)(r_+^2+a^2)(r_+^2+b^2)+4qr_+^3-q^2}{4\pi r_+[(r_+^2+a^2)(r_+^2+b^2)+qr_+]}. \end{aligned} \tag{3.76}$$

The Gibbs free energy, defined by

$$G = E - TS - \Phi Q - J_a\Omega_a - J_b\Omega_b \tag{3.77}$$

is equivalent to the background subtracted on-shell Euclidean action divided by $-\beta$, $I_E^R = -\beta G$.[3] Plugging everything in, we get

$$\begin{aligned} I_E^R = &\frac{\pi\beta}{\left(6Gr_+\Xi_a\Xi_b\left(r_+^2\left(a^2+b^2\right)+a^2b^2+qr_++r_+^4\right)\right)} \\ &\times\Big[q^2\left(-r_+^2\left(a^2+b^2\right)+a^2b^2-3r_+^4\right) \\ &-qr_+\left(3r_+^2-1\right)\left(a^2+r_+^2\right)\left(b^2+r_+^2\right)-\left(r_+^2-1\right)\left(a^2+r_+^2\right)^2\left(b^2+r_+^2\right)^2-q^3r_+\Big] \end{aligned} \tag{3.78}$$

[3] We also checked that this result agrees with the usual integral method, but this ended up being more straightforward.

This is a complicated result, but in the limit of zero charge, agrees with the generically spinning black holes in six dimensions with no charge [111],

$$I_E^R(q=0) = -\frac{2\pi\beta}{3G\Xi_a\Xi_b r_+}(a^2+r_+^2)(b^2+r_+^2)(r_+^2-1). \tag{3.79}$$

However, it turns out the $a = b = 0$ solution is not the Reissner-Nordström black hole, but rather the black hole in [136]. This gives us

$$I_E^R(a=b=0) = \frac{\beta\pi}{6G}\left[r_+^3 - r_+^5 - 2qr_+^2 - \frac{q^2}{r_+}\right]. \tag{3.80}$$

or in terms of Φ,

$$I_E^R(a=b=0) = -\frac{\pi R^3\left(-\Phi^2 + 2\Phi\coth(\delta) + \left(r_+^2-1\right)\coth^2(\delta)\right)}{6(\Phi-\coth(\delta))^2}. \tag{3.81}$$

The Hawking-Page transition occurs at $r_+ = 1 - \Phi\tanh\delta$. In table 3.1, for the charged static case, we instead present the result from [109], where the action is the one calculated in section 3.3.2.

3.8.3 AdS_7

The $d = 6$ case follows [117]. These solutions come from reducing eleven-dimensional supergravity on S^4 leading to seven dimensional $\mathcal{N} = 4, SO(5)$ gauged supergravity. Note that this can be thought of as coming from the near horizon limit of a stack of $M5$ branes and is dual to the six-dimensional, $\mathcal{N} = (2, 0)$ SCFT. For singly charged black holes, we choose to truncate to the $U(1)^3$ Cartan subgroup. The bosonic fields are a graviton, a self dual 3-form potential, two $U(1)$ gauge fields and two scalars.

Turning off one of the scalars in the gauged theory sets the two $U(1)$ fields equal and the Lagrangian is

$$\begin{aligned}\mathcal{L} =& R \star 1 - \frac{1}{2} \star d\phi_1 \wedge d\phi_1 - X^{-2} \star F_{(2)} \wedge F_{(2)} - \frac{1}{2} X^4 \star F_{(4)} \wedge F_{(4)} \\ &+ 2(8X^2 + 8X^{-3} - X^{-8}) \star 1 + F_{(2)} \wedge F_{(2)} \wedge A_{(3)} + F_{(4)} \wedge A_{(3)},\end{aligned} \tag{3.82}$$

where $X = e^{-\phi_1/\sqrt{10}}$. The self-duality condition reads

$$X^4 \star F_{(4)} = 2A_{(3)} - dA_{(2)} + F_{(2)} \wedge A_{(1)}. \tag{3.83}$$

The solutions to the field equations are, again written in terms of Jacobi-Carter coordinates and sevenbeins,

$$\begin{aligned}ds^2 = H^{2/5} \Bigg[& \frac{(r^2+y^2)(r^2+z^2)}{R} dr^2 + \frac{(r^2+y^2)(y^2-z^2)}{Y} dy^2 + \frac{(r^2+z^2)(z^2-y^2)}{Z} dz^2 \\ & - \frac{R}{H^2(r^2+y^2)(r^2+z^2)} \mathcal{A}^2 \\ & + \frac{Y}{(r^2+y^2)(y^2-z^2)} \left(dt' + (z^2-r^2) d\psi_1 - r^2 z^2 d\psi_2 - \frac{q}{H(r^2+y^2)(r^2+z^2)} \mathcal{A} \right) \\ & + \frac{Z}{(r^2+z^2)(z^2-y^2)} \left(dt' + (y^2-r^2) d\psi_1 - r^2 y^2 d\psi_2 - \frac{q}{H(r^2+y^2)(r^2+z^2)} \mathcal{A} \right) \\ & + \frac{a^2 b^2 c^2}{r^2 y^2 z^2} \Bigg(dt' + (y^2+z^2-r^2) d\psi_1 + (y^2 z^2 - r^2 y^2 - r^2 z^2) d\psi_2 - r^2 y^2 z^2 d\psi_3 \\ & - \frac{q}{H(r^2+y^2)(r^2+z^2)} \left(1 + \frac{y^2 z^2}{abc} \right) \mathcal{A} \Bigg)^2 \Bigg].\end{aligned} \tag{3.84}$$

The fields are

$$
\begin{aligned}
X &= H^{-1/5}, \qquad A_{(1)} = \frac{2ms_\delta c_\delta}{H(r^2+y^2)(r^2+z^2)}\mathcal{A}, \\
A_{(3)} &= qabc[d\psi_1 + (y^2+z^2)d\psi_2 + y^2z^2 d\psi_3] \\
&\quad \wedge \left(\frac{1}{z(r^2+y^2)} dz \wedge (d\psi_1 + y^2 d\psi_2) + \frac{1}{y(r^2+z^2)} dy \wedge (d\psi_1 + z^2 d\psi_2) \right) \\
&\quad - q\mathcal{A} \wedge \left(\frac{z}{r^2+y^2} dz \wedge (d\psi_1 + y^2 d\psi_2) + \frac{y}{r^2+z^2} dy \wedge (d\psi_1 + z^2 d\psi_2) \right).
\end{aligned} \tag{3.85}
$$

The metric functions are

$$
\begin{aligned}
R &= \frac{1+r^2}{r^2}(r^2+a^2)(r^2+b^2)(r^2+c^2) + q(2r^2+a^2+b^2+c^2) - \frac{2qabc}{r^2} + \frac{q^2}{r^2} - 2m \\
Y &= \frac{1-y^2}{y^2}(a^2-y^2)(b^2-y^2)(c^2-y^2), \quad Z = \frac{1-z^2}{z^2}(a^2-z^2)(b^2-z^2)(c^2-z^2) \\
\mathcal{A} &= dt' + (y^2+z^2)d\psi_1 + y^2z^2 d\psi_2, \quad H = 1 + \frac{q}{(r^2+y^2)(r^2+z^2)}, \quad q = 2ms_\delta^2.
\end{aligned} \tag{3.86}
$$

One can derive the two-form potential from the self-duality expression, or look in [117]. Now, thermodynamics is best performed in Boyer-Lindquist coordinates, where

$$
\begin{aligned}
t &= t' + (a^2+b^2+c^2)\psi_1 + (a^2b^2+b^2c^2+c^2a^2)\psi_2 + a^2b^2c^2\psi_3, \\
\phi_1 &= a(t' + \psi_1 + (b^2+c^2)(\psi_1+\psi_2) + b^2c^2(\psi_2+\psi_3), \\
\phi_2 &= b(t' + \psi_2 + (a^2+c^2)(\psi_1+\psi_2) + a^2c^2(\psi_2+\psi_3), \\
\phi_3 &= c(t' + \psi_3 + (a^2+b^2)(\psi_1+\psi_2) + a^2b^2(\psi_2+\psi_3).
\end{aligned} \tag{3.87}
$$

The y, z coordinates again efficiently parametrize the direction cosines,

$$\mu_1^2 = \frac{(a^2-y^2)(a^2-z^2)}{(a^2-b^2)(a^2-c^2)}, \quad \mu_2^2 = \frac{(b^2-y^2)(b^2-z^2)}{(b^2-c^2)(b^2-a^2)}, \quad \mu_3^2 = \frac{(c^2-y^2)(c^2-z^2)}{(c^2-a^2)(c^2-b^2)}. \tag{3.88}$$

As in six dimensions, it is more straightforward to calculate the Gibbs free energy. The relevant thermodynamic quantities are

$$\begin{aligned}
T &= \frac{(1+r_+^2)r_+^2\sum_i\prod_{j\neq i}(r_+^2+a_i^2) - \prod_i(r_+^2+a_i^2) + 2q(r_+^3+abc) - q^2}{2\pi r_+[\prod_i(r_+^2+a_i^2) + q(r_+^2-abc)]}, \\
\Omega_i &= \frac{a_i[(1+r_+^2)\prod_{j\neq i}(r_+^2+a_j^2) + qr_+^2] - q\prod_{j\neq i}a_j}{\prod_i(r_+^2+a_i^2) + q(r_+^2-abc)}, \\
J_i &= \frac{\pi^2 m[a_i c_\delta^2 - s_\delta^2(\Pi_{j\neq i}a_j + a_i\sum_{j\neq i}a_j^2 + abca_i)]}{4\Xi_a\Xi_b\Xi_c\Xi_i}, \\
\Phi &= \frac{2ms_\delta c_\delta r_+^2}{\prod_i(r_+^2+a_i^2) + q(r_+^2-abc)}, \qquad\qquad Q = \frac{\pi^2 m s_\delta c_\delta}{\Xi_a\Xi_b\Xi_c}, \\
E &= \frac{\pi^2}{8\Xi_a\Xi_b\Xi_c}\left[\sum_i\frac{2m}{\Xi_i} - m + \frac{5q}{2} + \frac{q}{2}\sum_i\left(\sum_{j\neq i}\frac{2\Xi_j}{\Xi_i} - \Xi_i - \frac{2(1+2abc)}{\Xi_i}\right)\right].
\end{aligned} \tag{3.89}$$

where $s_\delta = \sinh\delta, c_\delta = \cosh\delta, q = 2m\sinh^2\delta$. For brevity, we used $a_1 = a, a_2 = b, a_3 = c$. Other thermodynamic quantities can be found in [117]. Now the regularized Euclidean action is

$$\begin{aligned}
I_E^R = \frac{\beta\pi^2}{16G\Xi_a\Xi_b\Xi_c}\Bigg[&(1-r_+^2)\prod_i(r_+^2+a_i^2) - 2qr_+^4 - 2qabc \\
&- q^2\left(\sum_i a_i^2 r_+^4 - \sum_{i<j}a_i^2a_j^2r_+^2 - \prod_i a_i^2 + abc(2r_+^4 - 2r_+^2 + q) + r_+^2(r_+^4+q)\right) \\
&(\prod_i(r_+^2+a_i^2) + q(r_+^2-abc))^{-1}\Bigg].
\end{aligned} \tag{3.90}$$

The limit $q \to 0$ agrees with the Myers-Perry-AdS$_7$ solutions, which were calculated using the background subtraction method

$$I_E^R(q=0) = \frac{\pi^2}{16G\Xi_a\Xi_b\Xi_c r_+^2}(r_+^2+a^2)(r_+^2+b^2)(r_+^2+c^2)(1-r_+^2). \tag{3.91}$$

As in all other dimensions, uncharged black holes dominate the grand canonical ensemble for $r_+ > 1$. Furthermore, like $d = 5$, the non-spinning limit does not match the Reissner-Nordström result of Chamblin et al.

Chapter 4

Entanglement entropy in jammed CFTs

4.1 Introduction

The study of quantum field theories on curved spacetimes has historically been a source of both deep and enigmatic discoveries in theoretical physics. For instance, the analysis of an accelerated observer in Minkowski space showed that the field theory in the observer's frame and the field theory in Minkowski spacetime do not share a common vacuum [139, 140, 141]. Furthermore, theories invariant under metric rescaling (Weyl transformations) have classically traceless stress tensors. However, when these theories are quantized on a curved manifold in even spacetime dimensions, it is found that at one-loop order, the trace picks up contributions proportional to geometric invariants of the spacetime [142]. Possibly the most interesting and perplexing discovery, however, is that black holes, when analyzed quantum mechanically, are not

ever-growing cosmic sinks but rather radiate away their energy with a nearly thermal spectrum [143]. This discovery has led to new insights into thermodynamics [144] as well as illuminated fundamental issues in quantum mechanics and the conservation of information [47]. It may not be too surprising to learn that these discoveries are related—for instance, in the context of two dimensional CFTs, Hawking radiation is completely determined by the conformal anomaly [145]. On the other hand, it should be noted that the majority of analysis has been in the context of free fields. Recently, the impact of interactions on these phenomena have begun to be explored [146, 147, 148, 149].

One particularly fruitful avenue for addressing these questions is the AdS/CFT correspondence [5, 8, 26]. Here, one is able to study a strongly interacting d-dimensional $U(N)$ conformal field theory on a fixed spacetime background $\mathcal{B}_d$ by considering a d+1 dimensional solution to Einstein's equations with negative cosmological constant. The d+1 gravitational solution, $\mathcal{M}$, is frequently referred to as "the bulk." The boundary of $\mathcal{M}$ is conformal to the background spacetime on which the conformal field theory lives. In the infinite N limit, the planar graph contributions to expectation values of field theory operators on $\mathcal{B}_d$ may be obtained by solving classical equations of motion for corresponding matter fields in $\mathcal{M}$ [8]. It should be noted that gravity is not dynamical on the boundary. In particular, $\mathcal{B}_d$ serves as a classical background for the field theory, with no backreaction taking place.[1] This limits some of the questions that may be addressed as G_d is now effectively zero. For instance, questions like the black hole information paradox [34, 47] for which the black hole not only radiates but

[1] One may extend the AdS/CFT correspondence to address dynamical gravity by imposing Neumann-like boundary conditions for the CFT metric [150].

also evaporates cannot be addressed by considering a boundary black hole.[2] Nevertheless, we may still think of the black hole as a heat source for the field theory to explore heat transport and use this to characterize unique phases of the interacting field theory.

To analyze properties of Hawking radiation on the CFT, we construct new five, six, and seven dimensional solutions to the Einstein equations for asymptotically locally Anti-de Sitter spacetimes that have Reissner-Nordström metrics on the boundary. These new solutions build upon [146, 147, 148, 149] in which the authors considered spacetimes with boundaries $\mathcal{B}_d$ which contained a hyperbolic black hole of size R_{BH} at temperature T_{BH}. The hyperbolic black hole spacetimes also contained a black hole in the bulk at temperature T_∞. Generally, the bulk horizon is thought to represent the dual of a thermal state in the field theory at the same temperature. However, because of the presence of the boundary black hole, the authors of [151] consider the bulk black hole as governing a thermal plasma at spatial infinity which serves as a heat sink for the CFT. The boundary horizon then serves as a heat source. Our solutions have a Poincaré horizon in the bulk so that $T_\infty = 0$.

There have even been spacetimes, as constructed by [152, 153], with only one Killing vector allowing the CFT to be at a third temperature T_0 in a "detuned" phase. In these so called "flowing funnels", if $T_0 \neq T_{BH}$, the authors of [152, 153] state the stress tensor will be singular at the horizon. In our solutions below, the stress tensor is finite, and so we consider our solution "tuned" with only two temperatures, T_{BH} and T_∞. Even in this case, the authors of [16] suggest that if $T_{BH} \neq T_\infty$, $\mathcal{O}(1/N^2)$ effects in the CFT may introduce singularities at the horizon. In this paper,

[2]At finite N, however, it is expected that AdS/CFT will give valuable insight into this questions when one considers a bulk black hole dual to a thermal field theory.

as we are operating in the planar limit of the field theory, we will not be able to definitively distinguish between these two scenarios. However, we will see that field theory observables are markedly different near the horizon than they are far away, and that the near horizon observables have a strong dependence on T_{BH}.

The presence of two temperatures on the boundary allows one to explore different potential phases of Hawking radiation that the authors of [149] suggest correspond to different vacuum states of the CFT. Varying the dimensionless parameter $R_{BH}T_\infty$ corresponds to adjusting the relative distance between the bulk and boundary horizons. Heuristically, we can see this as follows. Because the spacetimes we construct will correspond to asymptotically flat, spherically symmetric boundary spacetimes, we can consider the bulk horizons to be asymptotically planar. In terms of the so-called "Fefferman-Graham" coordinate [154], z, for which the boundary of our bulk spacetime is at $z = 0$, very far from the rotation axis, the bulk horizon location will roughly be at a location $z_h = 1/T_\infty$. Furthermore, the maximum z location to which the boundary horizon extends into the bulk is roughly $z_b = R_{BH}$. With this in mind, when $R_{BH}T_\infty \ll 1$, we are in a so-called "droplet phase" in which the bulk and boundary horizons are disconnected and very far separated. As this corresponds to a large T_{BH}/T_∞, it is seen that there is very little heat transport in the CFT, a scenario the authors of [151] refer to as "jammed." As we take $R_{BH}T_\infty \to 1$, the separation between the boundary and bulk black holes goes to zero. This may lead to a phase transition to a so-called "funnel phase" in which the bulk and boundary black holes are connected. In this phase, there is only one Killing horizon, and so $T_{BH} = T_\infty$. For the droplets we construct below, we have $T_\infty = 0$ and can use conformal symmetry

to fix $R_{BH} = 1$ so that we always have $R_{BH}T_\infty = 0$, indicative of a droplet phase[3].

These droplet and funnel configurations are conjectured to correspond, respectively, to the Unruh and Hartle-Hawking vacuum states in the CFT. Typically, these states are characterized by regularity conditions of the stress tensor. The Unruh state is empty at past null infinity and regular on the future horizon whereas the Hartle-Hawking state is regular on both the past and future horizons. There is a third state, the Boulware vacuum, which has an empty stress tensor at both past and future null infinity, and is thus singular at both past and future horizons. The "detuned" phase of the CFT discussed earlier is thought to correspond to this vacuum. One can also define these vacua by the matter at null infinity. The Hartle-Hawking state has at null infinity a thermal gas in equilibrium with the black hole—hence $T_{BH} = T_\infty$ and this corresponds to the funnel phase. The Unruh state has a flux of outgoing Hawking radiation at the horizon but is empty at null infinity. This suggests $T_\infty = 0$ and the black hole acts as a heat source. One would expect in this state that the stress tensor vanishes smoothly as one moves away from the horizon. In our solutions, the stress tensor does in fact vanish as one goes to spatial infinity, but is not monotonic and in $d > 4$ even changes sign. As mentioned earlier, the authors of [16] remain ambivalent over whether the $T_{BH} \neq T_\infty$ droplet is in the Unruh or Boulware state, but suggest $\mathcal{O}(1/N^2)$ effects may point toward to the Boulware vacuum.

The boundary stress tensor is just one avenue for analyzing the state of the boundary field theory. Recently, there has been much excitement over the use of another observable, the entanglement entropy, as a means to characterize quantum field the-

[3]The limit $T_{BH} \to 0$ in our solution does not lead to a funnel as R_{BH} is fixed. Nevertheless, we can see some features of how the Unruh state may settle down to the Hartle-Hawking state at zero temperature.

ories. In the context of AdS/CFT, this has been especially exciting because the entanglement entropy of the boundary field theory corresponds to a well-defined geometric quantity in the bulk. On a given time-slice of the field theory background, one may divide the surface into two or more spatial subregions $\{\mathcal{A}, \mathcal{B}, ...\}$. The entanglement entropy of a subregion $\mathcal{A}$ quantifies the entanglement between degrees of freedom in $\mathcal{A}$ and degrees of freedom in its complement $\bar{\mathcal{A}}$. We should emphasize that there is a distinction between the entanglement entropy and von Neumann entropy. In particular, for mixed states such as thermal states of a field theory, the former will vanish when calculated on the whole space while the latter does not. This is because the von Neumann entropy calculates, in addition to the internal correlations of the field theory, correlations between the field theory and the purifying state. For the rest of this paper, we will not distinguish between von Neumann and entanglement entropies. In many cases, especially when the field theory is strongly interacting, the entanglement entropy is difficult to calculate, often requiring the analytic continuation of a path integral on a Riemann surface [155]. Fortunately, for strongly coupled CFTs, we can perform a dual calculation on the gravity side. For static spacetimes, Ryu and Takayanagi [42] have conjectured, and Lewkowycz and Maldacena have proven [84], that the bulk object dual to the entanglement entropy (actually von Neumann entropy) of $\mathcal{A}$ is a co-dimension two minimal surface in the bulk, Σ, anchored to the conformal boundary at $\partial\mathcal{A}$.[4] The entanglement entropy in the field theory is then given by the area of this minimal surface in a formula analogous to the

[4]The extension to stationary spacetimes is given in [43]. First order quantum corrections to this formula were calculated in [156] and extended to all orders in [157].

Bekenstein-Hawking entropy,

$$S(\mathcal{A}) = \frac{\text{Area}(\Sigma)}{4G_{d+1}} \tag{4.1}$$

where G_{d+1} is Newton's constant in $d+1$ dimensions.[5]

The fact that the entanglement entropy is a geometric object in the bulk has inspired many authors to use AdS/CFT to construct bulk spacetimes from knowledge of entanglement in the field theory [61, 159, 160, 161]. Furthermore, it gives an intuitive and visual understanding of entanglement inequalities, renormalization group flow, and confinement-deconfinement phase transitions [56, 162, 163, 83, 164]. While it has been used to understand the properties of thermal field theories on flat backgrounds, studies of entanglement entropy of thermal field theories in black hole backgrounds have been lacking (see [165] for early work) and to our knowledge, this is the first work to report the finite, universal terms in this entropy. We hope that these finite terms, as they have in the work on confinement, may bring some new understanding to the problems discussed above and hopefully provided a nice picture of the "jamming" of the CFT.

Over the last few years, there has been a program of constructing both analytic and numerical funnels and droplets in a journey to understand interacting thermal field theories[146, 147, 148, 149, 16, 166, 151, 152, 153, 167, 168]. Analytic droplets and funnels were constructed in $d = 3$ from the AdS C-metric which include an asymptotically flat boundary black hole which will be reproduced below. An analytic funnel dual to the Unruh state was constructed in d=2. Numerical constructions

[5]It is important to note the RT formula comes with a homology constraint which instructs us to include surfaces that may be disconnected [158].

include a d=4 Schwarzschild droplet, $T_{BH} = T_\infty$ funnels, $d = 5$ rotating droplets, and $d = 2$ "flowing funnels" in which a detuned CFT phase is seen. One challenge to distinguishing vacuum states is the fact that we have a *conformal* field theory on the boundary. For a d=4 boundary Schwarzschild black hole, we note that we can always rescale the metric such that different Schwarzschild radii, R_s, are conformally equal to the $R_s = 1$ spacetime. In this case, then, there is no way to vary T_{BH} in a way visible to the CFT. For this reason, we need another parameter on the boundary. The authors of [151] chose to introduce angular momentum to adjust T_{BH}. To use the Ryu-Takayanagi method for calculating entanglement entropies, we want our spacetime to be static and so instead, we introduce a "charge" by imposing Reissner-Nordström (from here on RN) boundary conditions instead of Schwarzschild. To our knowledge, these droplets have yet to appear in the literature and are therefore new vacuum solutions to the Einstein equations with a negative cosmological constant.

It should be noted that while RN typically corresponds to a black hole with electric charge, the CFT does not couple to this charge. This is because charged operators on the boundary are dual to charged fields in the bulk. However, we have no matter fields in the bulk and so the CFT has vanishing expectation value for the charge. Thus, the only effect of the charge is to vary the temperature for a fixed value of outer horizon while keeping $T_\infty = 0$. Interestingly, variation of T_{BH} does affect both the stress tensor expectation value and the entanglement entropy despite $R_{BH}T_\infty = 0$. For numerically constructed solutions with $d = 4, 5, 6$ RN boundary conditions, as well as in the $d = 3$ analytic C-metric, the stress tensor and entanglement entropy have universal behavior near spatial infinity that matches the boundary Schwarzschild (or in $d > 4$, Tangherlini [169]) black hole. Near the horizon, however, these observables

behave very differently, often including a negative energy density peak that indicates a higher concentration of the jammed plasma. The near horizon behavior is reinforced in the final section where we calculate the entanglement entropy of ball shaped regions on the boundary as a function of both radius and T_{BH} and see interesting behavior at similar locations.

4.2 Quantum Stress Tensors in Spherically Symmetric Static Spacetimes

To understand the numerical results for the boundary stress tensors, we follow the example of [151] and discuss the expectation value of the quantum stress tensor in a static spherically symmetric background. This work extends the analysis of Christensen and Fulling [145] to the case of RN in general spacetime dimension d. To keep the field theory arbitrary, we only require the stress tensor be covariantly conserved,

$$\nabla_\mu \langle T^\mu{}_\nu \rangle = 0. \tag{4.2}$$

To begin, we work with the following metric

$$\begin{aligned} ds^2_{RN} &= -\Delta_d(R)dt^2 + \frac{dr^2}{\Delta_d(R)} + R^2 d\Omega^2_{d-2}, \\ \Delta_d(R) &= \left(1 - \left(\frac{R_+}{R}\right)^{d-3}\right)\left(1 - \left(\frac{R_-}{R}\right)^{d-3}\right). \end{aligned} \tag{4.3}$$

The most general static spherically symmetric, stress tensor is given by

$$\langle T^{\mu}_{\ \nu}\rangle = \begin{pmatrix} T^{t}_{\ t} & T^{t}_{\ R} & 0 \\ T^{R}_{\ t} & T^{R}_{\ R} & 0 \\ 0 & 0 & T^{\Omega}_{\ \Omega}\delta^{i}_{j} \end{pmatrix} \tag{4.4}$$

where all components are functions of only R and spherical symmetry tells us that all angular components are equal. Inserting this into (4.2), we get the following system of equations:

$$\begin{aligned} 0 &= \partial_R T^{R}_{\ t} + \frac{d-2}{R} T^{R}_{\ t} \\ 0 &= \partial_R T^{R}_{\ R} + \left(\frac{d-2}{R} - \frac{\Delta_d'(R)}{2\Delta_d(R)}\right) T^{R}_{\ R} + \frac{\Delta_d'(R)}{2\Delta_d(R)} T^{t}_{\ t} - \frac{d-2}{R} T^{\Omega}_{\ \Omega} \end{aligned} \tag{4.5}$$

The first equation can be integrated to give

$$T^{R}_{\ t} = K\left(\frac{R_+}{R}\right)^{d-2}. \tag{4.6}$$

where K is an integration constant whose physical importance will be discussed below. Next, we use the trace of the stress tensor to write $T^{R}_{\ R}$ in terms of $T^{\Omega}_{\ \Omega}$ and $T^{\mu}_{\ \mu}$.

$$\begin{aligned} T^{R}_{\ R} = &\frac{(R_+/R)^{d-2}}{\Delta_d(R)} \\ &\times \left[Q - K + \frac{1}{2}\int_{R_+}^{R} (\tilde{R}/R_+)^{d-3} \left(\tilde{R}\Delta_d' T^{\mu}_{\ \mu} + (d-2)(2-\tilde{R}\Delta_d') T^{\Omega}_{\ \Omega}\right) \frac{d\tilde{R}}{R_+}\right] \end{aligned} \tag{4.7}$$

where Q is another integration constant to be discussed below. It will be helpful to split the stress tensor into four terms

$$T^{\mu}{}_{\nu} = (T_1)^{\mu}{}_{\nu} + (T_2)^{\mu}{}_{\nu} + (T_3)^{\mu}{}_{\nu} + (T_4)^{\mu}{}_{\nu} \tag{4.8}$$

The first term contains only information about the trace,

$$(T_1)^{\mu}{}_{\nu} = \text{diag}\left\{ -\frac{(R_+/R)^{d-2}}{\Delta_d(R)} H(R) + \frac{1}{2} T^{\mu}{}_{\mu}(R), \frac{(R_+/R)^{d-2}}{\Delta_d(R)} H(R), \frac{1}{2(d-2)} T^{\mu}{}_{\mu}(R) \delta^i_j \right\} \tag{4.9}$$

where

$$H(R) \equiv \frac{1}{2} \int_{R_+}^{R} (\frac{\tilde{R}}{R_+})^{d-3} (\tilde{R}\Delta_d' - \Delta_d) T^{\mu}{}_{\mu}(\tilde{R}) \frac{d\tilde{R}}{R_+}. \tag{4.10}$$

Note that we only construct exteriors of black holes and so the integration is only for $R \geq R_+$. In odd boundary dimensions or Ricci flat spacetimes, there is no conformal anomaly and so the trace of the stress tensor vanishes. However, we construct solutions in both even and odd boundary dimensions which are not Ricci flat and $(T^1)^{\mu}{}_{\nu}$ can contribute.

The next term in the stress tensor tells us that the flux of Hawking radiation at null infinity is proportional to K. In terms of the tortoise coordinate $dR_* = dR/\Delta_d(R)$,

$$(T_2)^{\mu}{}_{\nu} = K \frac{(R_+/R)^{d-2}}{\Delta_d(R)} \begin{pmatrix} 1 & 1 & 0 \\ -1 & -1 & 0 \\ 0 & 0 & 0 \end{pmatrix} \tag{4.11}$$

Since we construct solutions with no heat transfer at infinity, we expect that $K = 0$ for our solutions. In particular, our stress tensor should fall off faster than R^{2-d}.

Below, we will see that our stress tensors fall off as $R^{-(d+1)}$ satisfying this criteria. The third term is proportional to Q and tells us about regularity at the future horizon,

$$(T_3)^{\mu}{}_{\nu} = Q\frac{(R_+/R)^{d-2}}{\Delta_d(R)}\text{diag}\{-1,1,0\} \tag{4.12}$$

In particular, the diverging denominator tells us regularity on this horizon requires that $Q = 0$. Finally, we have a term that determines the pressures. Defining the functions

$$\begin{aligned}\Theta(R) &\equiv T^{\Omega}{}_{\Omega}(R) - \frac{1}{2(d-2)}T^{\mu}{}_{\mu}(r)\\ G(R) &\equiv \frac{d-2}{2}\int_{R_+}^{R}\left((\frac{\tilde{R}}{R_+})^{d-3}(2-\tilde{R}\Delta_d')\right)\Theta(\tilde{R})\frac{d\tilde{R}}{R_+},\end{aligned} \tag{4.13}$$

we may write

$$(T_4)^{\mu}{}_{\nu} = \text{diag}\left\{-\frac{(R_+/R)^{d-2}}{\Delta_d(R)}G(R) - (d-2)\Theta(R), \frac{(R_+/R)^{d-2}}{\Delta_d(R)}G(R), \Theta(R)\delta^i_j\right\} \tag{4.14}$$

For Ricci flat spacetimes regular on both horizons, this is the only part of the stress tensor that is non-vanishing. Because our approach was completely general, any spherically symmetric static quantum stress tensor will have this form, including the strongly interacting one that we consider below. By matching onto this solution, we can draw conclusions about the nature of our jammed CFT. In particular, Christensen and Fulling suggest that states with $Q = K = 0$ which have regular horizons and no flux at null infinity are dual to the Unruh state.

As pointed out by Fischetti and Santos, the notion of single particle states in field theories become ambiguous when put on curved backgrounds. However, currents

such as the stress tensor remain well defined even in the presence of background curvature. External fields like the curvature may couple to these currents and can lead to interesting new behavior like the conformal anomaly. One peculiar feature of the stress tensor in black hole backgrounds that our results exhibit is a negative energy density. From free field theory in Minkowski spacetime, this may seem paradoxical, but as Fischetti and Santos point out, even there, a negative local energy density appears in the Casimir effect. Furthermore, they emphasize that this negative energy density seems to be typical of free field theories near black hole horizons in both the Unruh and Hartle-Hawking states [170, 171]. This, they say, is consistent with the picture of Hawking radiation as pair-production with negative energy particles falling into the black hole and positive energy particles escaping. While the particle-antiparticle picture may not apply to our strongly interacting field theory, we still expect that this negative energy density should be ubiquitous as our results below confirm. Contrary to their results however, this energy density becomes positive away from the black hole horizon for R_-/R_+ sufficiently large. Interestingly, in $d = 6$, we see that the region of negative energy density becomes disconnected from the horizon as the black hole nears extremality.

4.3 Numerical Construction of RN Boundary Black Holes

In order to construct the background spacetimes for our field theory, we solve the DeTurck equations with a negative cosmological constant in d+1 dimensions,

$$R_{AB} - \frac{2\Lambda}{d-1} g_{AB} - \nabla_{(A}\xi_{B)} = 0, \qquad \xi^A = g^{BC}(\Gamma^A_{BC} - \bar{\Gamma}^A_{BC}) \tag{4.15}$$

with $2\Lambda = -(d-1)(d)/L^2_{AdS_{d+1}}$. In this expression, we have introduced Latin letters to denote bulk spacetime indices. The DeTurck vector, ξ^A, is defined in terms of a Levi-Civita connection, $\bar{\Gamma}^A_{BC}$, derived from a reference metric of our choice $\bar{g}$. Equation (4.15) is a deformation of the Einstein field equations which, when evaluated on a solution with $\xi^A = 0$, is analogous to a choice of gauge. As was shown by the authors of [16], this deformation gives an elliptic differential equation which is better suited to numerical evaluation. Furthermore, these authors showed that given a stationary spacetime with Killing horizons, the maximum of $\xi^2 = \xi^A \xi_A$ must occur at the boundaries (or "fictitious boundaries" like symmetry axes and black hole horizons). With a suitable choice of reference metric, $\bar{g}$, that has $\xi^A = 0$ on the boundaries, solutions to the DeTurck equations should also be solutions to the Einstein equations. To confirm this, we monitored the magnitude of ξ^2 and we check that once obtained, our solutions satisfy the Einstein equations to the same precision. Our construction of boundary AdS/RN black holes will closely follow [16] who constructed a five dimensional droplet solution corresponding to a four dimensional boundary Schwarzschild black hole with an extremal bulk horizon at $T_\infty = 0$.

We would like to construct static, asymptotically Anti-de Sitter, spherically symmetric solutions corresponding to an asymptotic field theory plasma at $T_\infty = 0$. From the AdS/CFT correspondence, this tells us that we need a bulk black hole which has an asymptotic planar black hole at $T_\infty = 0$. This is an extremal horizon and we know that this must correspond to the IR horizon of Poincaré-AdS. This horizon is at $z \to \infty$ and so to construct it numerically, we must choose a new AdS radial coordinate. We start with pure Poincaré AdS in d+1 dimensions,[6]

$$ds^2 = \frac{l^2}{z^2}(dz^2 + d\tau^2 + dR^2 + R^2 d\Omega_{d-2}^2). \tag{4.16}$$

Next, we make the coordinate change,

$$R = \frac{x\sqrt{2-x^2}}{1-r^2}, \quad z = \frac{1-x^2}{1-r^2}, \quad 0 \le x \le 1, 0 \le r < 1 \tag{4.17}$$

so that the metric becomes

$$ds^2 = \frac{l^2}{(1-x^2)^2}\left(f(r)^2 d\tau^2 + \frac{4r^2}{f(r)^2}dr^2 + \frac{4}{g(x)}dx^2 + x^2 g(x) d\Omega_{d-2}^2\right) \tag{4.18}$$

where

$$f(r) = 1 - r^2, \quad g(x) = 2 - x^2. \tag{4.19}$$

In these coordinates, the conformal boundary is located at $x = 1$, while the Poincaré horizon is located at $r = 1$. The axis of rotational symmetry is at $x = 0$.

We would like to deform this solution in such a way that the conformal boundary

[6]Note that we have chosen to use Euclidean time, although because our solution is static, we could just as easily construct Lorentzian solutions. Because we will evaluate the stress tensor with one index up and one index down, i.e. $\langle T^\mu{}_\nu \rangle$, this choice of time coordinate will give the same results as for the Lorentzian analysis above.

has the form of a d-dimensional Reissner-Nordström black hole. Since we want this to be a droplet, this horizon extends into the bulk and smoothly ends at the symmetry axis. If we define $r = 0$ as the horizon location, then the following metric ansatz will have such a horizon,

$$ds^2 = \frac{(1-r^2)^2}{(1-x^2)^2}\left(r^2 T d\tau^2 + \frac{4A}{f(r)^4}dr^2 + \frac{4B}{f(r)^2 g(x)}dx^2 + \frac{2rxF}{f(r)^3}drdx + \frac{x^2 g(x) S}{f(r)^2}d\Omega_{d-2}^2\right) \tag{4.20}$$

where $X \equiv \{T, S, A, B, F\}$ are all functions of x and r. Note that smoothness of the metric functions X tells us that pure AdS_d is not within our ansatz as this would require $T = 1/r^2$.

We require that our spacetime, as $x \to 1$, is asymptotically locally AdS with a metric conformal to d-dimensional Reissner-Nordström. In the limit $x \to 1$, (4.17) becomes $R = 1/1 - r^2$. We want this to have dimensions of length, and so we define for our boundary metric,

$$R = \frac{R_+}{1-r^2}. \tag{4.21}$$

As before, the d-dimensional Reissner-Nordström metric is,

$$\begin{aligned} ds^2 &= \Delta_d(R)d\tau^2 + \frac{dR^2}{\Delta_d(R)} + R^2 d\Omega_{d-2}^2 \\ \Delta_d &= 1 - \frac{2M_d}{R^{d-3}} + \frac{Q_d^2}{R^{2(d-3)}} = \left(1 - (\frac{R_+}{R})^{d-3}\right)\left(1 - (\frac{R_-}{R})^{d-3}\right) \end{aligned} \tag{4.22}$$

where $R_\pm^{d-3} = M_d \pm \sqrt{M_d^2 - Q_d^2}$ and M_d, Q_d are related to the energy, μ and charge,

q of the d-dimensional black hole in the following way [172],[7]

$$M_d = \frac{16\pi G_d}{(d-2)\Omega_{d-2}}\mu \qquad Q_d^2 = \frac{8\pi G_d}{(d-3)(d-2)}\frac{q^2}{\Omega_{d-2}^2}. \tag{4.23}$$

These black holes have temperatures (in natural units)

$$T_d = \frac{\kappa_d}{2\pi} \quad \text{where } \kappa_d = \frac{(d-3)\left(1-\left(\frac{R_-}{R_+}\right)^{d-3}\right)}{2R_+} \tag{4.24}$$

After the change of variables the boundary metric becomes

$$ds^2 = g_{\mu\nu}dx^\mu dx^\nu = r^2\delta_d(r)dt^2 + \frac{4R_+^2 dr^2}{(1-r^2)^4\delta_d(r)} + \frac{R_+^2}{(1-r^2)^2}d\Omega_{d-2}^2 \tag{4.25}$$

where

$$\delta_d(r) = \frac{1}{r^2}\left(1-(1-r^2)^{d-3}\right)\left(1-(1-r^2)^{d-3}\left(\frac{R_-}{R_+}\right)^{d-3}\right) \tag{4.26}$$

Near the boundary, we want

$$ds^2 \to \frac{(1-r^2)^2}{(1-x^2)^2}\left(\frac{1}{f(r)^2}dx^2 + g_{\mu\nu}dx^\mu dx^\nu\right) \tag{4.27}$$

Now, we set $l = 1$ and use conformal symmetry to fix $R_+ = 1$. In particular, note that in the limit $R_- \to 0$, we can take $\tau \to R_+\tau$ and the parameter R_+ completely scales out of the metric (4.25). This means that, to the conformally invariant theory, all boundary Schwarzschild black holes are equivalent—hence our need for another parameter, R_-. When we set $R_+ = 1$, we choose a particular branch of RN solutions

[7] The charge comes from considering an electric field $E = q/\Omega_{d-2}r^{d-2}$.

such that

$$\kappa_d = (d-3)(1-M_d) = \frac{(d-3)(1-Q_d^2)}{2} \tag{4.28}$$

Following the above discussion, we impose the following boundary conditions on X. As $x \to 1$,

$$T \to \delta_d(R),\ S \to 1,\ A \to \frac{1}{\delta_d(r)},\ B \to 1,\ F \to 0. \tag{4.29}$$

As $r \to 1$,

$$\begin{gathered} T \to 1 + T_1(1-r),\ S \to 1 + S_1(1-r),\ A \to 1 + A_1(1-r),\ B \to 1 + B_1(1-r), \\ F \to (1-r)F_1,\ (T_1 - A_1)_{r=1} = \text{constant}. \end{gathered} \tag{4.30}$$

The last boundary condition is required to ensure this boundary is an extremal horizon.

The rotation axis and droplet horizon serve as fictitious boundaries. Figueras et al. show that the DeTurck problem is still well defined on these fictitious boundaries. For these boundaries, we require that our solutions be smooth—as we approach the horizon $r \to 0$, X must be functions of r^2, and as $x \to 0$, X must depend only on x^2 so that

$$\partial_r X|_{r=0} = 0, \quad \partial_x X|_{x=0} = 0. \tag{4.31}$$

Furthermore regularity of the Euclidean solution at the horizon requires

$$\frac{T}{A}|_{r=0} = 4\kappa_d^2 \tag{4.32}$$

and regularity at the rotation axis requires

$$\frac{S}{A}|_{x=0} = 1. \tag{4.33}$$

Finally, our choice of reference metric, $\bar{g}_{AB}$ is (4.20) with

$$T = \frac{1}{\delta_d(r)}, \quad A = \delta_d(r), \quad S = B = 1, \quad F = 0. \tag{4.34}$$

To find solutions, we use a Newton-Raphson relaxation algorithm using pseudospectral collocation on a Chebyshev grid. In $d = 5$, we found $\xi^2 \sim 10^{-13}$ for all solutions below. In $d = 4$ and 6, the numerics are slightly more unstable, and more grid points were necessary. For the largest grids we used, 81×81 in $d = 6$ we found $\xi^2 \sim 10^{-10}$ in $d = 4$ and $\xi^2 \sim 10^{-6}$ in $d = 6$. Plots of convergence for two characteristic choices of R_- are shown in figure 4.2. In fig. 4.1, we plot the droplet horizons of our solutions by embedding them in the metric $ds^2 = \frac{l^2}{z^2}(dz^2 + dR^2 + R^2 d\Omega_{d-2}^2)$. In four dimensions, for $R_- = R_+$, the geometry on the horizon exactly matches the surface $R^2 + z^2 = R_+^2$. Importantly, this is a minimal surface in pure AdS, as we will discuss below. In higher dimensions, the horizon approaches this surface, but sufficiently close to extremality, the horizon can no longer be isometrically embedded. The largest R_- we plot is approximately this critical value.

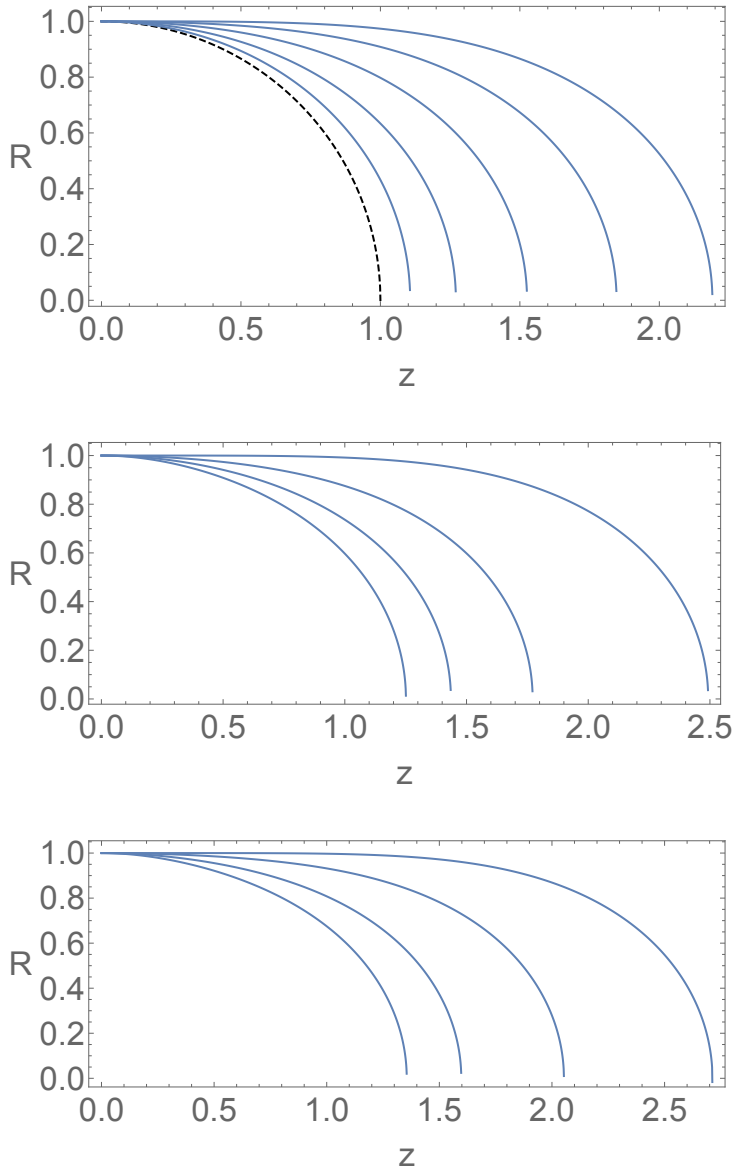

Figure 4.1: In (a)-(c), we embed the horizons into the metric $ds^2 = \frac{l^2}{z^2}(dz^2 + dR^2 + R^2 d\Omega_{d-2}^2)$. In (a), $d = 4$ and we choose (from right to left) $R_-/R_+ = 0,\ .2,\ .5,\ .8,\ .96,\ 1.0$. The extremal black hole is the dotted black line. In (b) ($d = 5$) and (c) ($d = 6$), we choose (R to L) $R_-/R_+ = 0,\ .5,\ .7,\ .8$. Notably, the extremal horizon in $d = 4$ is a minimal surface in the pure AdS where it is embedded.

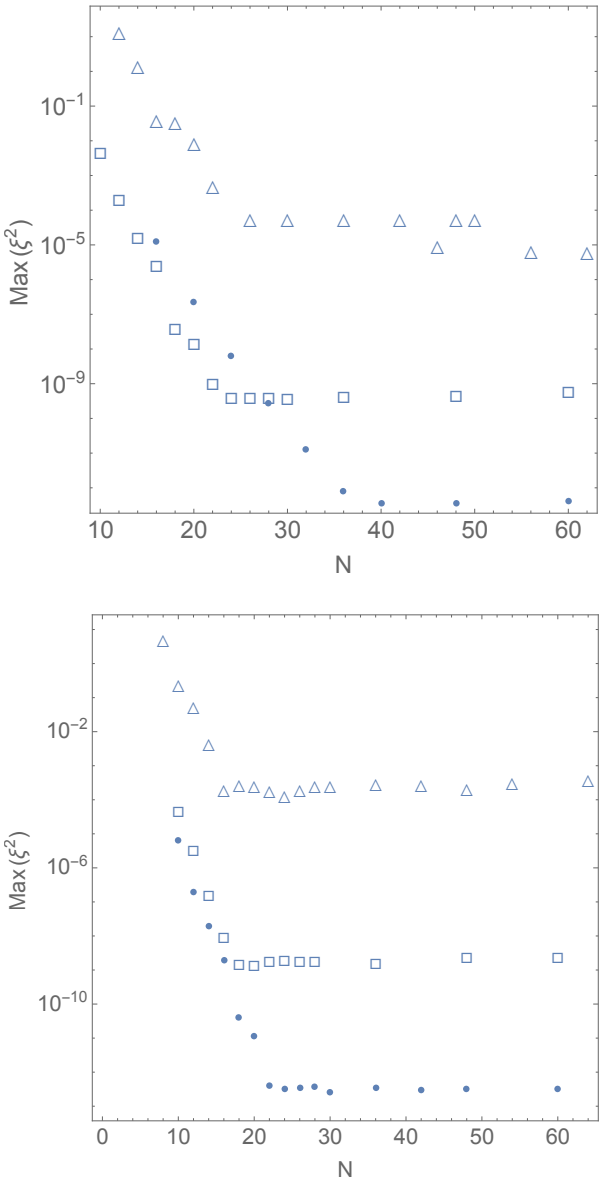

Figure 4.2: The maximum value of ξ^2 for two choices of R_-/R_+ in $d = 4$ (circles), $d = 5$ (squares), and $d = 6$ (triangles). Our numerical method leads to exponential convergence in the number of grid points, N, until saturation. Even boundary dimensions ($d = 4$ and 6) show more numerical error because of the presence of logarithmic terms in the asymptotic expansion (see equation (4.35).) The first figure has $R_-/R_+ = .2$ and the second has $R_-/R_+ = .5$.

4.4 Boundary Stress Tensor

As discussed above, our spacetime is asymptotically locally Anti-de Sitter. This means the metric can be expanded in a neighborhood of the boundary in terms of the Fefferman-Graham coordinate, z [173]. The boundary stress tensor can be determined from the coefficients of z^i for $i \leq d$. The expansion and expressions for the boundary stress tensor in terms of these coefficients is discussed in the appendix. For the boundary stress tensor of our numerical solutions, we need to find an expression for the coordinate z and boundary radial coordinate R in terms of x and r as well as boundary expansions for the functions X. To do so, we write

$$\begin{aligned} z &= (1-x^2)\left(\frac{1}{1-r^2} + \sum_{n=1}^{\infty} z_n(r)(1-x^2)^n\right) \\ R &= \frac{R_+}{1-r^2} + \sum_{n=1}^{\infty} R_n(r)(1-x^2)^n \\ X &= X_0(r) + \sum_{n=1}^{\infty} X_n(r)(1-x^2)^n + \log(1-x^2)\sum_{n=1}^{\infty} \tilde{X}_n(r)(1-x^2)^n \end{aligned} \tag{4.35}$$

where $X_0(r)$ are our Dirichlet boundary conditions (4.29). By inserting the expansion for X into the DeTurck equations and matching with the Fefferman-Graham expansion, we can find the functions z_n, R_n and X_n in terms of x, r for all $n < d$ including potential $\log(1-x^2)^d$ terms in even d. In the appendix, we present the functions X_n relevant to calculating the boundary stress tensor. Importantly, these terms are also sufficient to determine the UV divergences in the entanglement entropy.

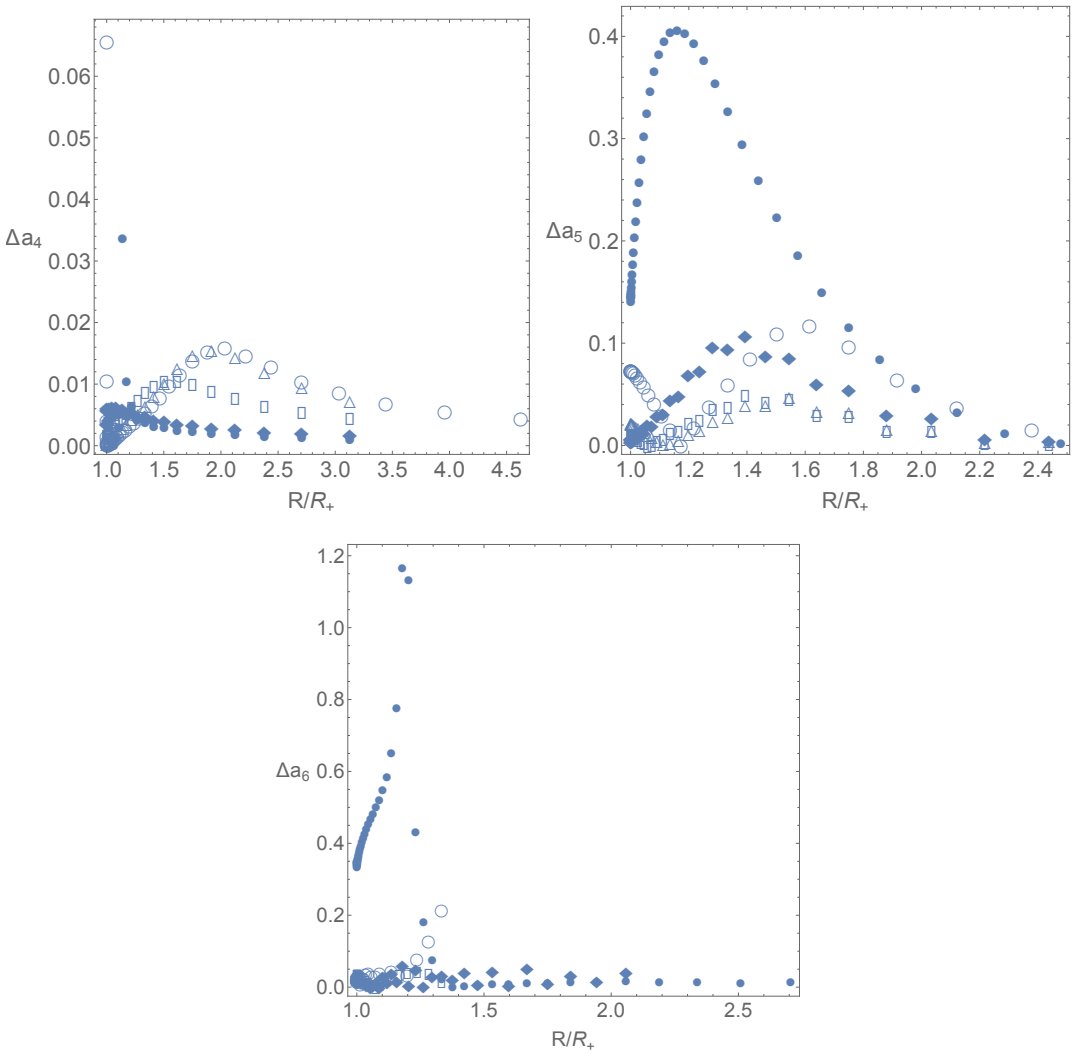

Figure 4.3: In (a)-(c), we plot the error in extracting $A_d(r)$. Regions with large errors (especially in (c)) correspond to places where our calculated $A_d(r)$ vanishes while our theoretical $\mathcal{A}_d(r)$, while small, does not vanish exactly. Away from these points, the errors are a few percent or less. Furthermore, in $d = 6$ as seen in (c), because of large coefficients, errors accumulate quickly. In each plot, the different values of R_-/R_+ match the values used for the energy densities in figs. 4.4, 4.5, and 4.6. In order of increasing R_-/R_+, the symbols are $\bullet, \blacklozenge, \triangle, \square, \bigcirc$. (For $d = 6$, we don't use $\square$.) Note (a) corresponds to $d = 4$, (b) corresponds to $d = 5$, (c) corresponds to $d = 6$.

The $X_d(r)$ terms are relevant to the boundary stress tensor and must be found numerically. Unfortunately, high order derivatives are numerically unstable, and so to find the coefficients $X_d(r)$, we subtract the known expressions for X_n with $n < d$ above from our numerical solution and fit this to the $X_d(r)$ term in the expansion near the boundary,

$$X^{\text{num}}(x,r) - \sum_{n<d} X_n(1-x^2)^n = (1-x^2)^d X_d(r). \tag{4.36}$$

To monitor the numerical accuracy of this method, we note that, because the trace of the stress tensor is known, one of our coefficients can be calculated from knowledge of the other coefficients. We chose to specifically monitor the function $A_d(r)$. The analytic expression for this function, which we call $\mathcal{A}_d(r)$, in terms of the other $X_d(r)$ can be found in the appendix. In fig. 4.3, we plot

$$\Delta a_d(r) \equiv \left| \frac{\mathcal{A}_d(r) - A_d(r)}{A_d(r)} \right| \tag{4.37}$$

for the values of R_-/R_+ that we display in the stress tensors below. In $d = 4$, the errors stay below a few percent for all R and most are less than a percent. In higher dimensions the errors increase, especially close to the horizon. These errors are due, in most cases, to the stress tensor changing sign. If $\mathcal{A}_d$ and A_d cross the axis at different values of R, the denominator of (4.37) blows up. Away from these locations, the errors again become on the order of a few percent or less. For $R_-/R_+ = 0$ in $d = 6$, there is an error close to the horizon where the stress tensor does not vanish. Instead, this can be traced to the large coefficients in $\mathcal{A}_6(r)$ (4.94) which cause errors to accumulate quickly. For this case, we checked that the stress tensor does not

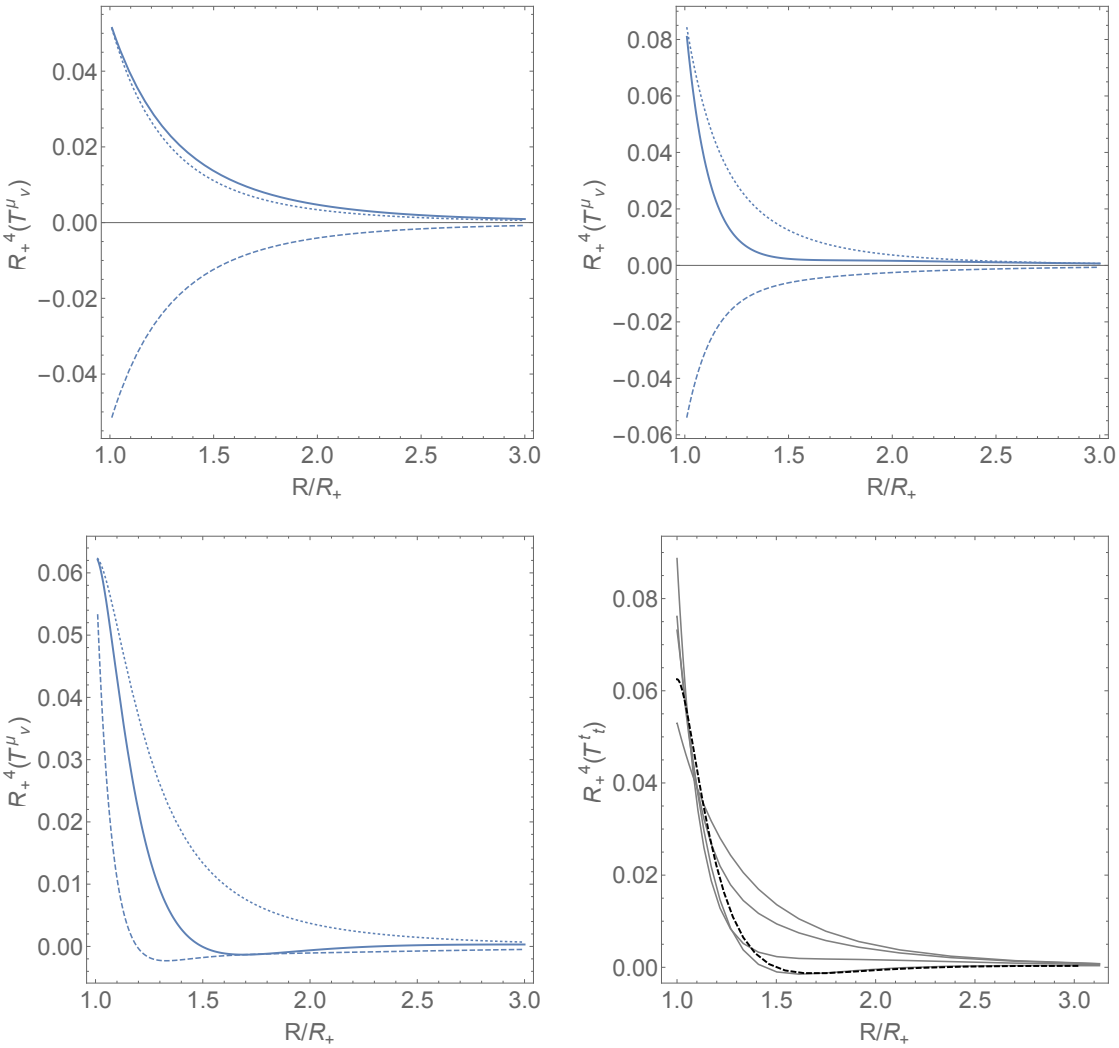

Figure 4.4: (a)-(c) are plots of the four dimensional $\frac{4\pi G_5}{l^3}\langle T^{\mu}{}_{\nu}\rangle$ as a function of R for $R_-/R_+ = 0, .5, 1.0$ respectively. In the plots, the thick line is the energy density $T^t{}_t$, the dotted line is $T^r{}_r$, and the dashed line is $T^{\Omega}{}_{\Omega}$. In (d), we plot the energy densities for $R_-/R_+ = 0$, .2, .5, .9, and 1.0 (black dotted line).

change appreciably as we varied the grid size.

Finally, we write the expressions for the boundary stress tensors. In d=4,

$$\langle T^{\mu}{}_{\nu}\rangle = \frac{l^3}{4\pi G_5}\text{diag}\left\{T^t{}_t, T^R{}_R, T^{\Omega}{}_{\Omega}, T^{\Omega}{}_{\Omega}\right\} \tag{4.38}$$

where

$$T^t{}_t = \frac{1}{R^4}\Bigg(\frac{T_4(R)}{(1-\frac{R_-}{R})} + \frac{3R_+}{4R}(1-\frac{R_+}{R}) + R_-\frac{\big(((78R_+-12R)R-73R_+^2)R_- + R(R(12R-82R_+)+78R_+^2)R_+\big)}{16R^4}\Bigg) \tag{4.39}$$

$$T^R{}_R = \frac{1}{R^4}\Bigg(\frac{3R_+^2}{4R^2} - (\frac{T_4(R)}{1-\frac{R_-}{R}} + 2S_4(R)) + R_-\frac{((2R(6R-17R_+)+35R_+)R_- + 2R(5R-17R_+)R_+)}{16R^4}\Bigg) \tag{4.40}$$

and

$$T^\Omega{}_\Omega = \frac{1}{R^4}\Bigg(-\frac{3R_+}{8R} + S_4(R) + R_-\frac{\big((21R_+-22R)R_+R_- - 2R(3(R-6R_+)R+11R_+^2)\big)}{16R^4}\Bigg) \tag{4.41}$$

Notably, as $R_- \to 0$, this agrees with Figueras et al. Furthermore the trace is

$$\langle T^\mu_\mu \rangle = \frac{l^3}{4\pi G_5}\frac{R_+^2R_-^2}{4R^8} \tag{4.42}$$

agreeing with the conformal anomaly in 4 dimensions.

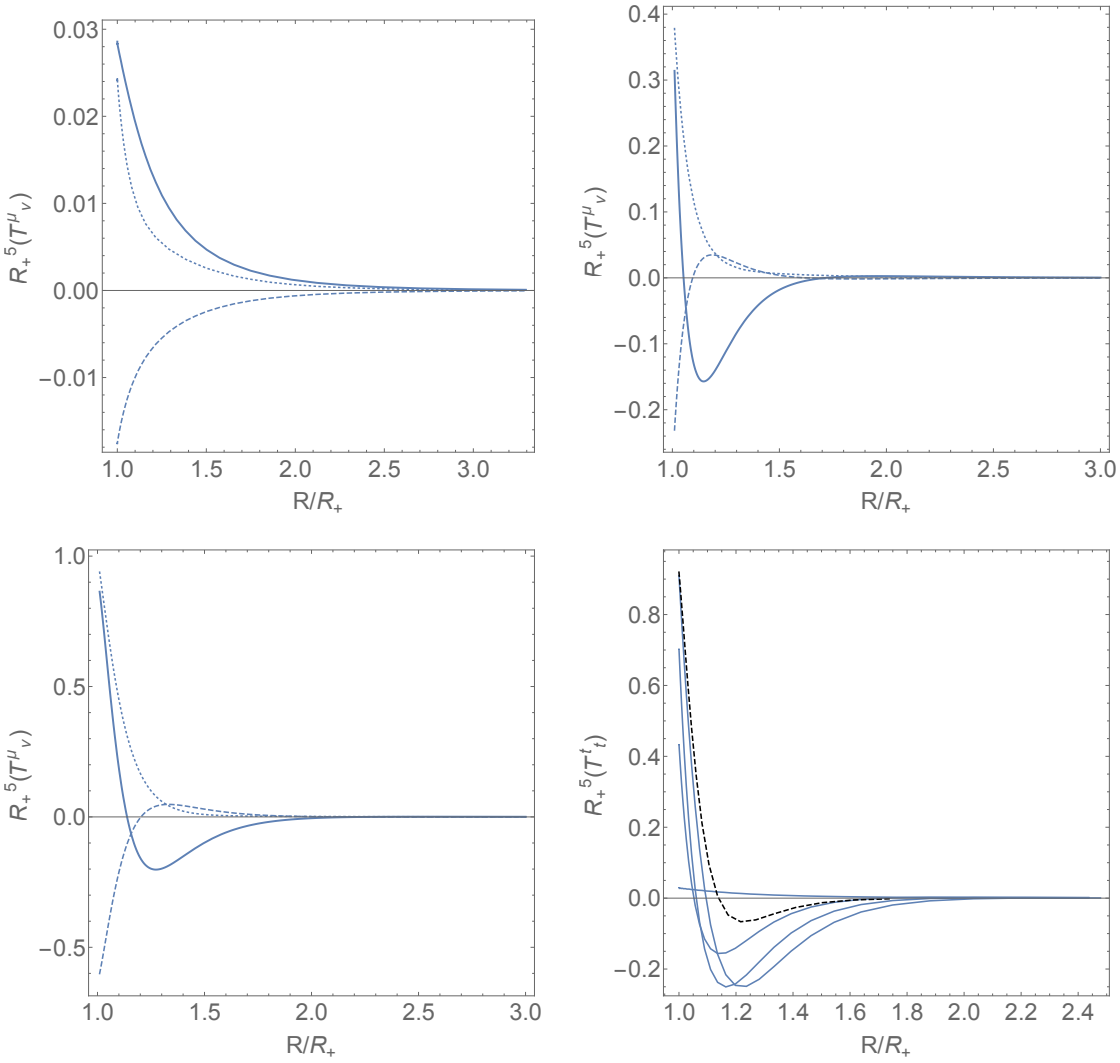

Figure 4.5: (a)-(c) ($R = 0, .5, 1.0$ respectively) are plots of the five dimensional $\frac{16\pi G_5}{5l^4}\langle T^\mu{}_\nu\rangle$ as a function of R for different values of R_-/R_+. In the plots, the thick line is the energy density $T^t{}_t$, the dotted line is $T^r{}_r$, and the dashed line is $T^\Omega{}_\Omega$. In (d), we plot the energy densities for R_-/R_+ =0, .5, .7, .9, and 1.0 (black, dotted line).

In fig. 4.4, we plot this stress tensor for different values of R_-. This stress tensor agrees with results of [16] in the limit $R_- \to 0$. In this limit, it is clear that the trace of the stress tensor vanishes. Furthermore, in the language of section 2, $Q = K = H = 0$

indicative of the Unruh vacuum. Interestingly, we see new behavior in the CFT as R_-/R_+ increases. As mentioned earlier, for all R_-, the stress tensor displays negative energy densities near the horizon[8]. This is typical of the non-classical state we expect from a strongly interacting field theory. On the other hand, we see that as we approach extremality, there is a turning point in the energy density. Furthermore, as this ratio becomes sufficiently large, there is a finite size region near the horizon with positive energy density. In droplets with $T_\infty > 0$, the authors of [168] saw positive energy densities in this same limit. In this limit, the pressure also becomes positive near the horizon but becomes negative far away, matching the $R_- = 0$ behavior. Finally, as seen in fig. **??**, the magnitude of the energy density near the horizon actually decreases as the boundary black hole approached extremality. This is different than what was observed in [151] where the magnitude of the energy density increased monotonically as the black hole approached extremality. We believe this behavior may indicate that the plasma is becoming localized away from the horizon as the Unruh and Hartle-Hawking states degenerate at zero temperature. We propose that the peak in the energy density corresponds roughly to the location of the jammed CFT. This is reinforced by the entanglement entropy calculations.

[8]Recall that in both Euclidean and Lorentzian signature $\langle T^t{}_t \rangle < 0$ would indicate positive energy.

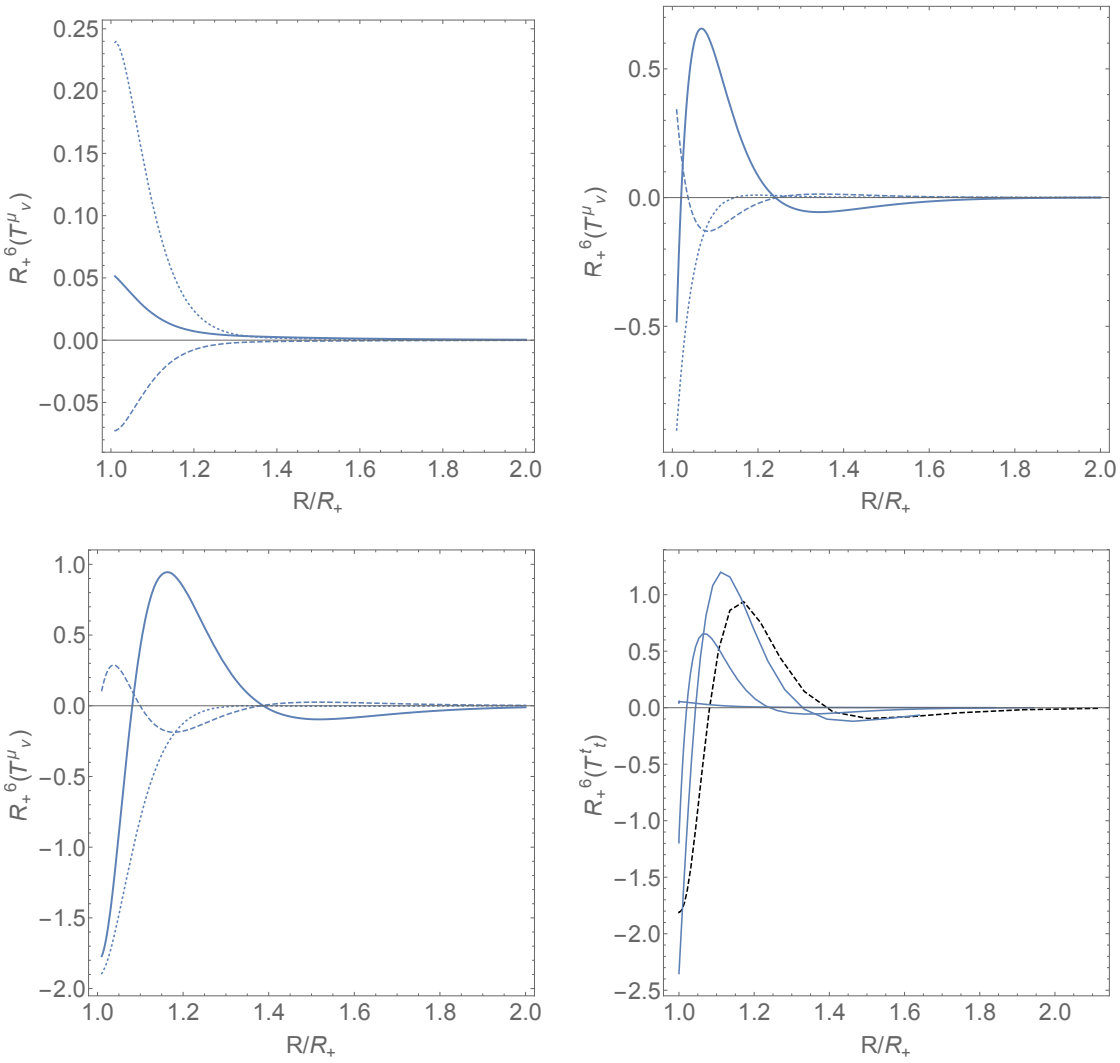

Figure 4.6: (a)-(c) ($R = 0, .5, 1.0$, respectively) are plots of the six dimensional $\frac{8\pi G_6}{3l^5}\langle T^{\mu}{}_{\nu}\rangle$ as a function of R for different values of R_-/R_+. In the plots, the thick line is the energy density $T^t{}_t$, the dotted line is $T^r{}_r$, and the dashed line is T^{Ω}_{Ω}. In (d), we plot the energy densities for R_-/R_+ =0, .5, .9, and 1.0 (black, dotted line).

Next, the five dimensional stress tensor is given by

$$\langle T^{\mu}{}_{\nu}\rangle = \frac{5l^4}{16\pi G_6}\frac{1}{R^5} \times \mathrm{diag}\left\{\frac{T_5(R)}{(1+\frac{R_+}{R})(1-\frac{R_-^2}{R^2})}, -\frac{T_5(R)}{(1+\frac{R_+}{R})(1-\frac{R_-^2}{R^2})} - 3S_5(R), S_5(R), S_5(R), S_5(R)\right\} \tag{4.43}$$

This is traceless, as it should be, because there is no conformal anomaly in odd dimensions. In fig. 4.5 we plot this for some choices of R_-. Here we note some differences from the four dimensional result. The first is that the energy density starts negative near the horizon but becomes positive away from the horizon for smaller ratios of R_-/R_+. In higher dimensions, it seems as though the "jammed" plasma is more easily localized away from the black hole. This is confirmed by the pressure becoming positive in this same region. As in the four dimensional case, the energy density first increases then decreases as $R_-/R_+ \to 1$.

The six dimensional stress tensor is very messy, and so we will leave the full expression to the appendix. Here, we just note that the trace,

$$\langle T^\mu_\mu \rangle = \frac{3l^5}{8\pi G_6} \frac{9R_-^6 R_+^6 \left(280R^6 - 320R^3\left(R_-^3 + R_+^3\right) + 271R_-^3 R_+^3\right)}{200R^{24}} \tag{4.44}$$

exactly matches the conformal anomaly, $a^{(6)}$, in 6 dimensions. In fig. 4.6, we plot this stress tensor for different values of R_-/R_+ as before. Here, we see a new phenomenon. Near the black hole, the energy density is positive, but becomes negative away from the black hole, and then becomes positive again. This reinforces the idea that in higher dimensions there is a stronger tendency for the CFT to localize away from the black hole as $T_{BH} \to T_\infty$.

It is worth pointing out that in all dimensions, the behavior far from the black hole matches the corresponding Tangerlinhi behavior with a $R^{-(d+1)}$ fall-off. This rapid fall off gives a strong indication that the CFT corresponds to an Unruh or Boulware state. Furthermore, the dimension dependence of this fall-off suggests that the black

hole affects the CFT closer to the horizon in higher dimensions. As we will show below, from work done on Wilson loops in holography [163], there is a "confinement" scale for the T_∞ plasma that tends to decrease in size in higher dimensions. These may conspire to explain the dimension dependence of localization seen in the energy densities and in the entanglement entropies below.

4.5 Entanglement Entropies of Droplets

In this section we seek to clarify some of the results of the previous section. In particular, we learned from the boundary stress tensor that there is a region near to the black hole horizon where the CFT energy density becomes negative. This state prevents heat flow between the black hole at temperature T_{BH} and asymptotic plasma at temperature T_∞. In the "jammed" phase, then, there should be very little correlation between degrees of freedom near the horizon and degrees of freedom in the asymptotic plasma.

One measure of these correlations is the entanglement entropy of a spatial subregion in the CFT. To define the entanglement entropy of a spatial subregion, one first takes a time slice of the field theory manifold on which to define a Hilbert space. On this time slice, one then chooses a spatial subregion which we will call $\mathcal{A}$ and divides the Hilbert space into two subspaces, one that contains degrees of freedom purely within $\mathcal{A}$ another that contains only degrees of freedom in $\bar{\mathcal{A}}$, $\mathcal{H} = \mathcal{H}_\mathcal{A} \otimes \mathcal{H}_{\bar{\mathcal{A}}}$. Given a state on the full Hilbert space defined by a density matrix ρ, one can define a reduced density matrix, ρ_A, describing only $\mathcal{H}_\mathcal{A}$ by tracing out the degrees of freedom in $\bar{\mathcal{A}}$. The entanglement entropy is then given by the von Neumann entropy of this density

matrix,[9]

$$S_A = -Tr\rho_A \log \rho_A. \tag{4.45}$$

One may check that if our Hilbert space defines a single entangled pair, the entanglement entropy of a region containing just one member of the pair is 2 but a region containing both pairs is 0. Thus, at least to first order, the entanglement entropy quantifies how correlations are shared across the boundary of the spatial region $\partial\mathcal{A}$.

For free field theories, one can occasionally calculate the entanglement entropy. These calculations often require the computation of so-called Renyi entropies which come from the analytic continuation of path integrals on Riemann surfaces [155, 174]. However, for interacting field theories, such calculations become more burdensome, especially for theories without large numbers of symmetries. In the AdS/CFT correspondence, degrees of freedom on the boundary are often ambiguous and such calculations on the field theory side are prohibitive. Fortunately, for field theories on static spacetimes, Ryu and Takayanagi gave a procedure to calculate these entanglement entropies by solving for surfaces in the bulk [42, 83]. Given a spatial region of the field theory $\mathcal{A}$ with boundary $\partial\mathcal{A}$, one solves for a codimension-two minimal surface which starts on $\partial\mathcal{A}$ and extends into the bulk.[10] The surface which corresponds to the entanglement entropy of $\mathcal{A}$ is that surface which minimizes the area. Occasionally, there may be a "phase transition" between two different types of surfaces which minimize the area at different values of some parameter, for instance the width of the chosen spatial region [163].

Note that due to the short range correlations of quantum field theories, entangle-

[9] As mentioned earlier, this includes entanglement with a purifying system if ρ is not pure.

[10] For our droplet solutions, the horizon stretching into the bulk acts as a barrier that minimal surfaces may not cross [59].

ment entropies are strictly divergent. Defining a UV cutoff in the field theory, ϵ, the leading order divergence is proportional to Area$(\mathcal{A})/\epsilon^{d-2}$ [37]. For the holographic entanglement entropy, the field theory cutoff corresponds, on the bulk side, to evaluating the area of the minimal surface up to a fixed $z = \epsilon$ slice. In the following, we wish to analyze correlations between the jammed and asymptotic plasma and so we calculate the entanglement entropy of ball shaped regions on the boundary as a function of the radius of the ball.[11] We present both the UV divergences of this quantity as well as the regularized entanglement entropies where these divergences are subtracted.

4.5.1 AdS C-metric

The AdS C-metric is an analytic solution to the Einstein equations in four bulk dimensions with negative cosmological constant [147]. For different regions of parameter space, this metric has both droplets and funnel solutions with hyperbolic black holes on the boundary. For one particular choice of parameters, however, the C-metric gives a droplet with an asymptotically flat black hole on the boundary. The metric for this droplet is

$$\begin{gathered} ds^2 = \frac{l^2}{(x-y)^2}\left(-F(y)dt^2 + \frac{dy^2}{F(y)} + \frac{dx^2}{G(x)} + G(x)d\phi^2\right) \\ \text{with } F(y) = y^2 + 2\mu y^3, \quad G(x) = 1 - x^2 - 2\mu x^3 = 1 - F(x) \end{gathered} \tag{4.46}$$

This spacetime is asymptotically locally AdS with conformal boundary at $x = y$. For $x - y \geq 0$ and $-\frac{1}{2\mu} \leq y \leq 0$, the spacetime has black hole on the boundary that

[11] There are different invariant measures of radii on the boundary including the distance from the horizon and the coefficient of $d\Omega_{d-2}^2$ in $\tilde{g}_{\mu\nu}$. We choose the latter as it is finite, even as $R_- \to R_+$

extends into the bulk and touches the axis of rotation symmetry ($G(x_0) = 0$). This black hole has a temperature $T = 1/4\pi\mu$. For $0 \leq y \leq x_0$, we have a similar spacetime with no black hole on the boundary. For a given μ, both spacetimes have an equal conical deficit $\Delta\phi = \frac{4\pi}{|G'(x_0)|}$. They both also have a zero temperature horizon in the bulk at $y = 0$. This spacetime is only well defined for $\mu \geq \frac{1}{3\sqrt{3}}$, below which $G(x)$ is not positive semi-definite.

Conformally rescaling by $1/x^2$ and defining $\xi = -1/x$, we find a boundary metric

$$ds_\partial^2 = -(1 - \frac{2\mu}{\chi})dt^2 + \frac{d\chi^2}{(1 - \frac{2\mu}{\chi})G(-1/\chi)} + \chi^2 G(-1/\chi)d\phi^2. \tag{4.47}$$

As $\chi \to \infty$, $G(-1/\chi) \to 1$ and we see this metric describes flat 3 dimensional Minkowski space. Note that in this conformal frame, the horizon has area $A_h = \frac{8\pi\mu}{|G'(x_0)|}$. For completeness, we also note that for $\mu = 0$, the C-metric gives Poincaré-AdS_4. Defining

$$r = \frac{\sqrt{G(x)}}{y}, \quad z = (\frac{x}{y} - 1) \tag{4.48}$$

the metric (4.46) becomes

$$ds^2 = \frac{l^2}{z^2}(-dt^2 + dz^2 + dr^2 + r^2 d\phi^2). \tag{4.49}$$

To find minimal surfaces, we first need to define a disc shaped region on the boundary. There are a couple choices of invariant radii, but the one that seems to make the most sense is the circumference radii $R = \frac{\sqrt{G(x)}}{x}$.[12] Thus a choice of R defines a choice

[12]This radius only monotonically increases for $\mu \geq \frac{1}{2\sqrt{2}}$ which will be the range we will investigate.

$x_b = y_b$ on the boundary. Then we minimize the area functional

$$\frac{A}{\Delta\phi} = \int_{x_b+\epsilon_x}^{x_0} dx \frac{1}{(x-y(x))^2}\sqrt{\frac{G(x)}{F(y)}y'(x)^2+1} \tag{4.50}$$

where ϵ_x is proportional to the UV cut-off in the field theory. Now, a defining feature of minimal surfaces is that they are normal to the conformal boundary. This tells us that

$$y'(x)|_{x=x_b} = -\frac{F(x_b)}{G(x_b)} \quad \text{and} \quad \epsilon = \frac{\epsilon_x}{x_b G(x_b)} \tag{4.51}$$

where $z = \epsilon$ is the fixed field theory cutoff. We Taylor expand our curve $y(x)$ near $y = x_b$ and plug this into the area functional to see

$$\frac{A}{\Delta\phi} = \int_{x_b+\epsilon_x} \frac{dx}{(x-x_b)^2}(1+\frac{F(x_b)}{G(x_b)})^{-3/2} \to \frac{R_b}{\epsilon} + \text{finite} \tag{4.52}$$

The divergence is the same for both the spacetime with a boundary black hole and without a boundary black hole, but the finite piece is different.

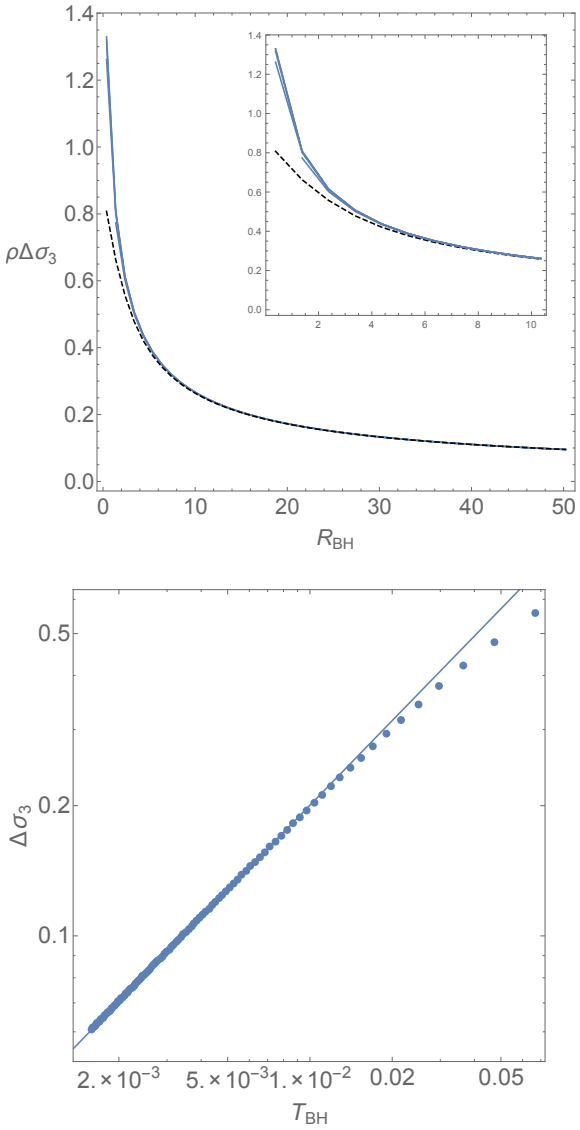

Figure 4.7: In (a), we plot $\rho\Delta\sigma_3$ for $\rho = 1$ (black, dotted line) $, 2, 3, 10, 20, 100$ as a function of R_{BH}. In scaling by ρ, the area curves nearly perfectly overlap and the entanglement entropy has a universal behavior. Near the horizon (inset plot), there is some deviation, especially for $\rho = 1$ (black dotted line) but the discrepancy disappears for ρ larger than ~ 2 (ρ increases from bottom to top). In (b), we show a log-log plot of the horizon entanglement as a function of $T_{BH} = (4\pi\mu)^{-1}$. The line that we plotted shows this grows as $T_{BH}^{2/3}$.

To understand how the black hole affects correlations in the field theory, we want to compare entanglement entropies for equivalent size regions in both spacetimes. A convenient way to do so is to fix the radius of the disc R_b and subtract the entanglement entropy for the field theory with no boundary black hole, S_{NBH}, from the entanglement entropy for the field theory with a boundary black hole.[13] This gives a finite value for the entanglement entropy

$$\Delta\sigma_3 \equiv \frac{A_{BH}(R_b) - A_{NBH}(R_b)}{2\pi}. \tag{4.53}$$

This subtraction is standard in the literature, for instance in understanding thermal correlations in a strongly coupled field theory, one subtracts the entropy of pure AdS from the entropy of AdS-Schwarzschild for identical boundary regions. Conveniently, this method of comparison also gets rid of the divergence in the entanglement entropies. Notably, the cancellation of all divergences is particular to $d = 3$. We will show below that in higher dimensions, it is only the leading order divergence which is cancelled.

In fig. 4.7, we plot the entanglement entropy for a fixed ratio $\rho = R_b/R_{BH}$ and vary the black hole radius $R_{BH} = 2\mu$. For $\mu >\sim 1.5$, or for $\rho >\sim 1.5$, the different entanglement entropies as a function of μ vary only by the ratio of their radii ρ,

$$A(\rho_1, \mu) = \frac{\rho_2}{\rho_1} A(\rho_2, \mu) \tag{4.54}$$

In particular, one can find the entanglement entropy as a function of R if one knows

[13] In this paper, we will write everything in terms of the areas, leaving out the factor of $1/4G_{d+1}$ which would give the entropy. The no black hole spacetime is the $x > 0$ region for a given μ, not three dimensional Minkowski space.

how the entropy of the horizon scales as a function of μ. The dependence on ρ agrees with the picture of a jammed phase where at larger R_b, there are fewer correlations between degrees of freedom at large radius and degrees of freedom near the black hole. Interestingly, as $T_{BH} \to T_\infty$, the difference in entanglement entropy at the horizon also goes to zero. We show a log-log plot of this quantity in fig. 4.7 as a function of the black hole temperature. In this plot, we see that as we approach extremality, the correlations between degrees of freedom inside the horizon and those outside go to zero. Because of the ρ dependence of the entanglement entropy, the vanishing of the horizon entanglement entropy tells us that $\Delta\sigma_3$ vanishes everywhere in the extremal limit. One might expect this if the extremal limit corresponds to the field theory approaching a zero-temperature Hartle-Hawking.

4.5.2 Numerical Solutions

We now seek to answer whether the same behavior occurs in higher dimensions. Like the "charge" μ in the C-metric, we will vary R_- in (4.22) to change T_{BH}. To find the minimal surfaces, we minimize the area functional

$$\frac{A_d}{\Omega_{d-2}} = \int_0^{x_{max}} \frac{dx}{1-x^2}\left(\frac{x^2 g(x) S}{(1-x^2)^2}\right)^{d/2-1} \sqrt{\frac{4A}{(1-r(x)^2)^2}r'(x)^2 + \frac{4B}{g(x)} + \frac{2xr(x)F}{1-r(x)^2}r'(x)} \tag{4.55}$$

where $f(r)$ and $g(x)$ were defined in (4.19). Given a UV cutoff $z = \epsilon$, the cutoff in the coordinate x is $x_{max} = \sqrt{1-\epsilon/R_b}$ where R_b is the radius of the ball whose entanglement we are investigating. The integration limits are consistent with the change of variables for pure AdS. Note that R_b is related to r through the same coordinate definition (4.21). Using the expansions (4.76), (4.79), (4.82) and the fact

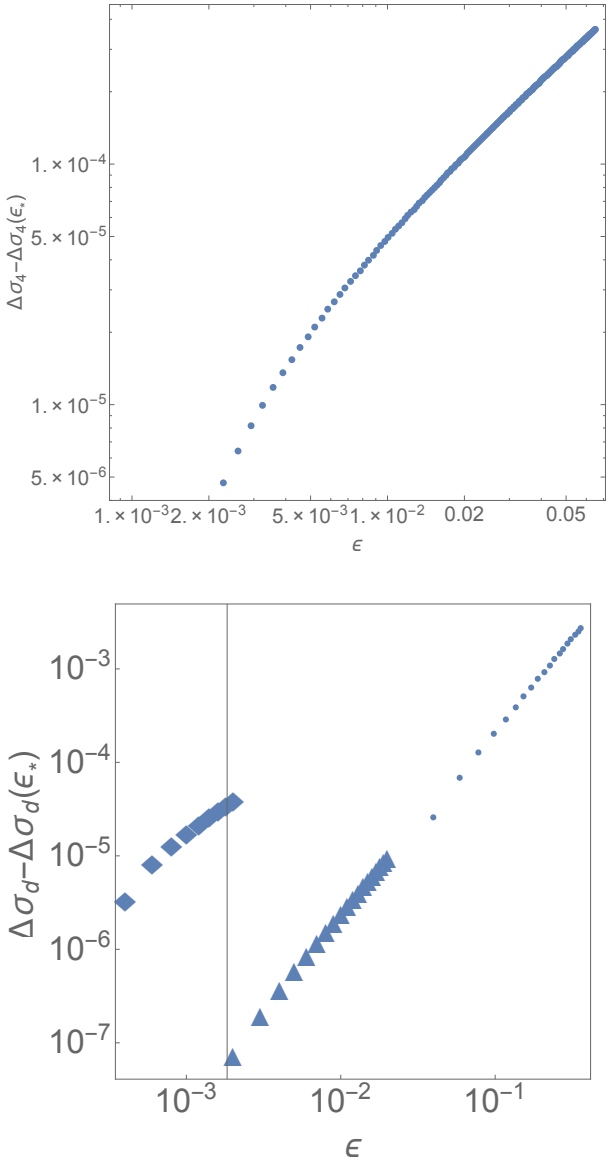

Figure 4.8: Above we show in a log-log plot the error in extracting $\Delta\sigma_d$ as a function of the cutoff, ϵ. In (a), we do this for d=3 for $\mu = 3$ and $R = R_+$. In (b), we do this for $R/R_+ = 3$ in $d = 4$ (♦), $d = 5$ (▲), and $d = 6$ (•). In all cases, we see a power-law convergence.

that the surfaces are normal to the boundary ($r'(x) \to 0$) the divergent terms in the entanglement are,

$$
\begin{aligned}
A_4/\Omega_2 &\to \frac{1}{2}\frac{R_b^2}{\epsilon^2} - \frac{1}{2}(\alpha(r_b)-1)log(\epsilon) + ... \\
A_5/\Omega_3 &\to \frac{1}{3}\frac{R_b^3}{\epsilon^3} - \frac{(8+3\beta(r_b))}{8}\frac{R_b}{\epsilon} + ... \\
A_6/\Omega_4 &\to \frac{1}{4}\frac{R_b^4}{\epsilon^4} - \frac{(2\psi(r_b)+15)}{20}\frac{R_b^2}{\epsilon^2} - \frac{(15+20\chi_r(r_b)-12\psi(r_b)+80\chi_s(r_b))}{40}log(\epsilon) + ...
\end{aligned}
\tag{4.56}
$$

where ... are finite terms. At the black hole horizon, r=0, so that the above expansions are

$$
\begin{aligned}
A_4/\Omega_2 &\to \frac{1}{2}\frac{R_{BH}^2}{\epsilon^2} + \frac{1}{2}(\frac{R_-}{R_+})log(\epsilon) + \text{finite} \\
A_5/\Omega_3 &\to \frac{1}{3}\frac{R_{BH}^3}{\epsilon^3} - \frac{(2+9\frac{R_-^2}{R_+^2})}{8}\frac{R_{BH}}{\epsilon} + \text{finite} \\
A_6/\Omega_4 &\to \frac{1}{4}\frac{R_{BH}^4}{\epsilon^4} - \frac{(5+18\frac{R_-^3}{R_+^3})}{20}\frac{R_{BH}^2}{\epsilon^2} + \frac{50-9\frac{R_-^3}{R_+^3}(40+29\frac{R_-^3}{R_+^3})}{200}log(\epsilon) + \text{finite}
\end{aligned}
\tag{4.57}
$$

In particular, the leading order divergence is proportional to the area of the black hole horizon on the boundary, a similarity to the Bekenstein-Hawking entropy first noted in [165, 175].

One may also ask about the divergences as $R_b \to \infty$. We note that in this limit, $\alpha(r), \beta(r), \psi(r), \chi_r(r), \chi_s(r)$ all vanish and so

$$
\begin{aligned}
A_4/\Omega_2 &\to \frac{1}{2}\frac{R_b^2}{\epsilon^2} + \frac{1}{2}\log(\epsilon) + \text{finite} \\
A_5/\Omega_3 &\to \frac{1}{3}\frac{R_b^3}{\epsilon^3} - \frac{R_b}{\epsilon} + \text{finite} \\
A_6/\Omega_4 &\to \frac{1}{4}\frac{R_b^4}{\epsilon^4} - \frac{3}{4}\frac{R_b^2}{\epsilon^2} - \frac{3}{8}log(\epsilon) + \text{finite}
\end{aligned}
\tag{4.58}
$$

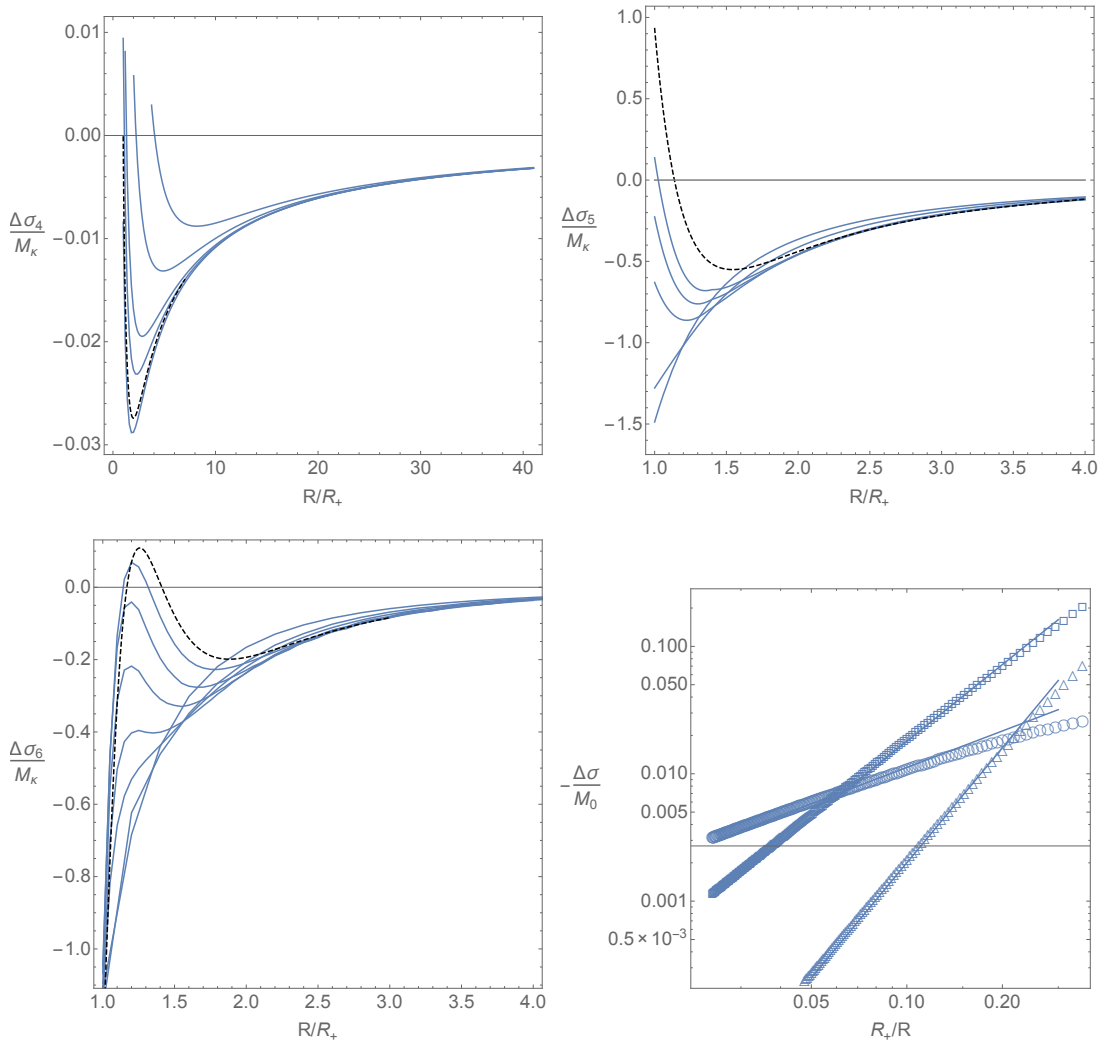

Figure 4.9: In (a)-(c) ($d = 4, 5, 6$, respectively), we plot the finite piece of the entanglement entropies, defined in (4.61), divided by the mass parameter M_κ for a given R_-. As can be seen, far from the black hole, all entanglement entropies agree. In (a), the curves correspond to $R_-/R_+ = 0$, .2, .4, .5, .8, 1.0 (top to bottom). In (b), $R_-/R_+ = 0$, .3, .5, .7, .8, 1.0 (bottom to top). Finally, (c) is the six dimensional case with $R_-/R_+ =$0, .4, .5, .6, .7, .8, .9, 1.0 (bottom to top). In all cases, the result for the extremal boundary black hole is in black and dashed. In (d), we show a log-log plot of the asymptotic part of the entanglement entropies as a function of R_+/R. These are linear (◯), quadratic (□), and cubic (△)for $d = 4, 5, 6$ respectively.

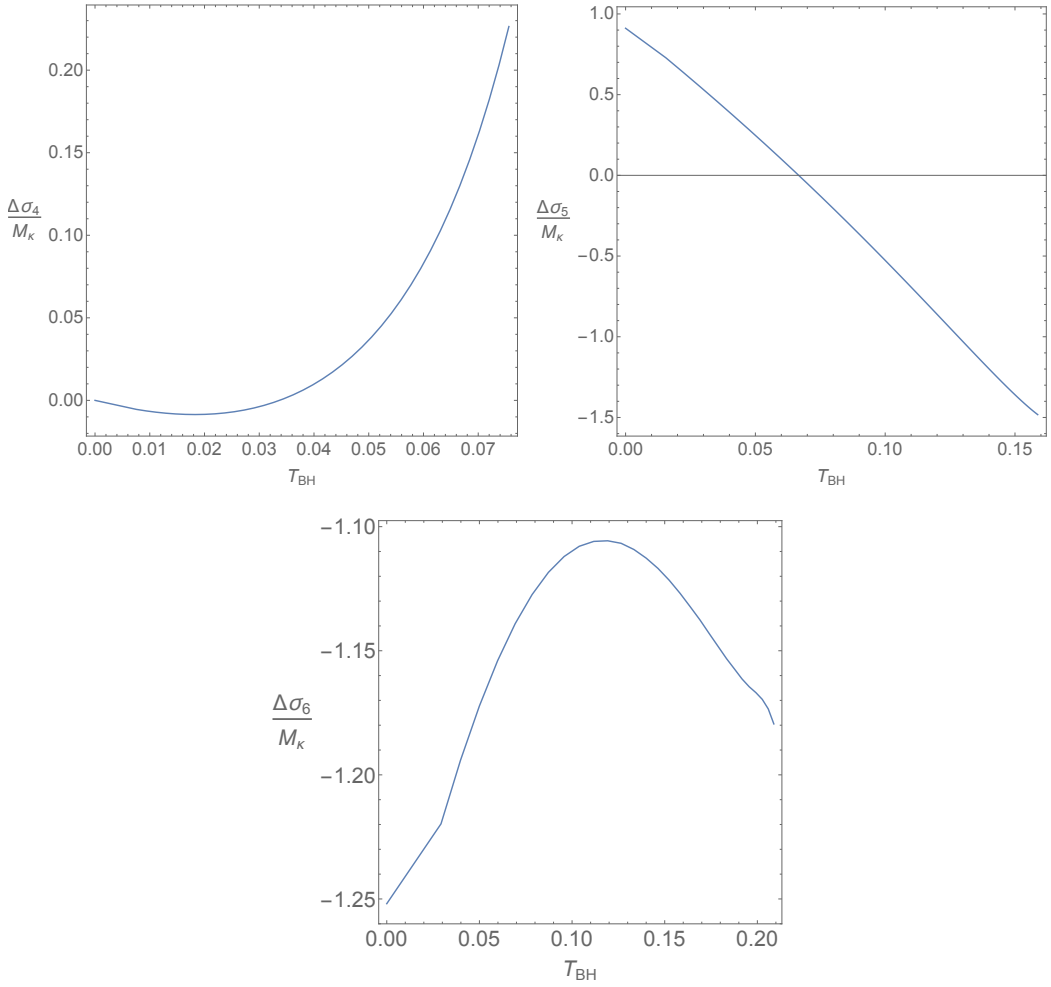

Figure 4.10: In (a)-(c) ($d = 4, 5, 6$, respectively)m we plot the finite piece of the entanglement entropies for the horizon as a function of T_{BH}.

We want to subtract the entanglement entropies for balls of radius R_b in pure AdS_{d+1}.[14]

Here, we minimize

$$A_d = \Omega_{d-2} \int_\epsilon^{R_b} dz \frac{R(z)^{d-2}}{z^{d-1}} \sqrt{R'(z)^2 + 1}. \tag{4.59}$$

[14]In four dimensions, this was calculated for instance in [163] but the higher dimensional results are new

In all dimensions, the minimal surface is $R(z) = \sqrt{R_b^2 - z^2}$. Plugging this into the above expression gives

$$\begin{aligned} A_4/\Omega_2 &= \frac{1}{2}\frac{R_b^2}{\epsilon^2} + \frac{1}{2}log(\epsilon) - \frac{1}{4}(1 + 2log(2)) \\ A_5/\Omega_3 &= \frac{1}{3}\frac{R_b^3}{\epsilon^3} - \frac{R_b}{\epsilon} + \frac{2}{3} \\ A_6/\Omega_4 &= \frac{1}{4}\frac{R_b^4}{\epsilon^4} - \frac{3}{4}\frac{R_b^2}{\epsilon^2} - \frac{3}{8}log(\epsilon) + \frac{3}{32}(3 + 4log(2)) \end{aligned} \tag{4.60}$$

As can be seen, the pure AdS divergences match the asymptotic limit of the droplet divergences (4.58), as would be expected since the boundary spacetime is asymptotically flat.

Now, as we did for the C-metric, we subtract the area of the surface in the no black hole background from the area of the surface in the black hole background. This gives

$$\begin{aligned} \Delta A_4/\Omega_2 &= -\frac{1}{2}\alpha(r_b)log(\epsilon) + \Delta\sigma_4 \\ \Delta A_5/\Omega_3 &= -\frac{3\beta(r_b)}{8}\frac{R_b}{\epsilon} + \Delta\sigma_5 \\ \Delta A_6/\Omega_4 &= -\frac{\psi(r_b)}{10}\frac{R_b^2}{\epsilon^2} - (2\chi_s(r_b) + \frac{1}{2}\chi_r(r_b) - \frac{3}{10}\psi(r_b))\log(\epsilon) + \Delta\sigma_6 \end{aligned} \tag{4.61}$$

where σ_d is the finite part of the d-dimensional area divided by Ω_{d-2}. As can be seen, the leading divergence is gone but we still have to contend with subleading divergences. Our regularization procedure will be to fix a value of ϵ and then subtract these divergences from the area integral of our solutions. As we show in fig. 4.8, we find that $\Delta\sigma_d$ has power law convergence up to some minimum ϵ_*. Below this value, the numerics become unstable. The plots of $\Delta\sigma_d$ come from ϵ slightly above this minimum.

In fig. 4.9, we plot our results for σ_d/M_κ as a function of R/R_+ for various values of R_- in $d = 4, 5, 6$ (M_κ is the mass appearing in Δ_d (4.22)). While the three plots look very similar, there are actually some important differences, especially between the $d = 4$ and $d > 4$ cases. We first note the similarities. In each case, the finite piece of the entanglement entropy is negative far from the black hole. Furthermore, once scaled by the mass, M_κ, the entanglement entropies agree for $R_b \gg R_+$. Note that we have already used conformal symmetry to set $R_+ = 1$ and so this procedure is analogous to the scaling by ρ in the C-metric example. As we saw there, the entanglement entropy becomes universal (i.e. independent of R_-) in this limit. This shows that far from the horizon, the leading order fall-off in the metric determines the entanglement entropy. This is demonstrated in fig. 4.9 where we show that in this region, the entanglement entropies fall off as $(R_+/R)^{d-3}$, exactly following $\Delta_d(R)$ at large R. Importantly, this is not the case near the horizon, where interactions between the CFT and Hawking radiation have a strong influence on the entanglement entropy and as we show below, prevent heat flow from the black hole to spatial infinity.

In particular, near the horizon, we see a minimum (also a maximum in six dimensions) that becomes more exaggerated as $T_{BH} \to T_\infty$. This dip defines a radius, R_{min}, where entanglement between degrees of freedom at $R < R_{min}$ and $R > R_{min}$ is minimized. One explanation for these dips is that the jammed plasma is becoming more localized near these critical radii, R_{min}, more effectively blocking the flux of Hawking radiation to infinity. As discussed above, if a Bell pair is separated across the boundary of our entangling region, the entanglement entropy is two, whereas if both members of the pair are within the entangling region, the entropy is zero. If there is localization in the plasma, then there should be a region where correlations are

dense. At $R = R_{min}$, the internal correlations of the localized plasma are all within our entangling region and so the entanglement entropy is at a local minimum.

4.5.3 Localization in pure AdS

To better understand this picture of localization in the T_{BH} plasma state, we seek to quantify a length scale for confinement in the CFT vacuum (corresponding to the $T_\infty = 0$ state). We extend the work of [163] to find a confining phase transition in $d \geq 4$ Poincaré-AdS. It is worth noting that this spacetime is not compact, so this is not the usual holographic picture of confinement in a CFT [12]. However, it was shown in [176] that using holography one can relate a glueball mass in four-dimensional QCD to a phase transition in the two-point correlator of Wilson loops in $\mathbb{R}^4$ at finite temperature. The correlator can be obtained from finding the minimal surface connecting two loops separated by a distance L. For L larger than some critical L_c, the minimal surface becomes disconnected and the correlator vanishes, an indication of confinement.[15] This transition can also be related to monopole condensation in four dimensions. For monopoles separated by a distance $L > L_c$, the phase transition in the minimal surface shows that the potential between the monopoles goes to a constant, effectively screening the monopoles from each other so that the force between them vanishes. It seems possible, then, that a similar phase transition in the CFT on a black hole background may act to prevent heat exchange between the black hole and an asymptotic plasma.

[15]Nominally, this implies the glueball mass is infinite. In fact, one expects that when the cross section of the minimal surface in this geometry is on the order of the string-scale, the supergravity approximation breaks down and instead the correlator is dominated by supergraviton exchange between the Wilson loops. The extension of this Gross-Ooguri phase transition to holographic geometries dual to confining CFTs was performed in [162]

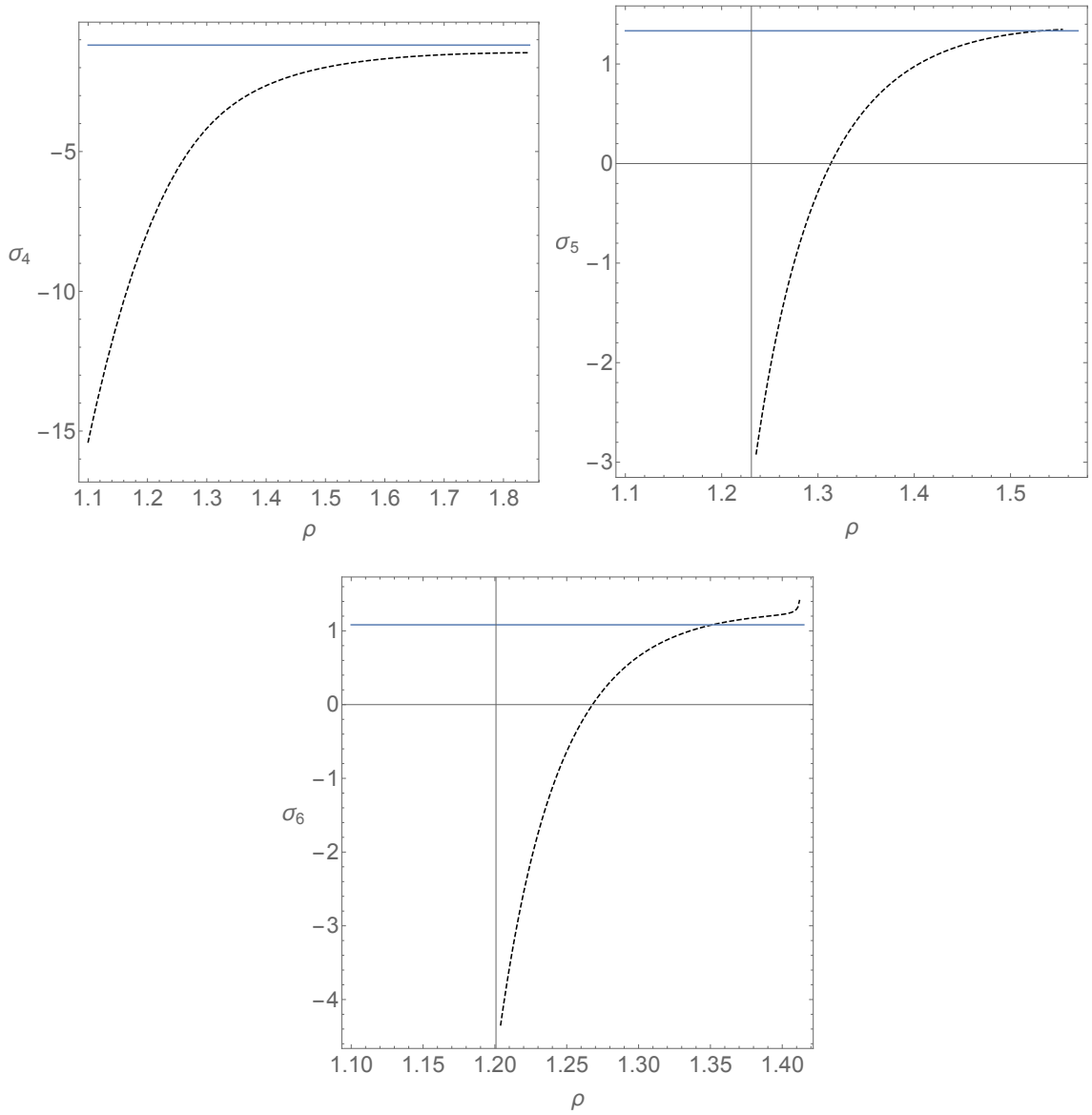

Figure 4.11: We plot the area of the minimal surfaces for boundary annuli as a function of the ratio of outer and inner radii $\rho = \frac{R_2}{R_1}$ for $d = 4, 5, 6$. The dotted line is the area for the "connected" surface while the filled line is the area for two "disconnected" balls. At some critical $\rho_*^{(d)}$ the minimal area surface changes, representing a confining phase transition.

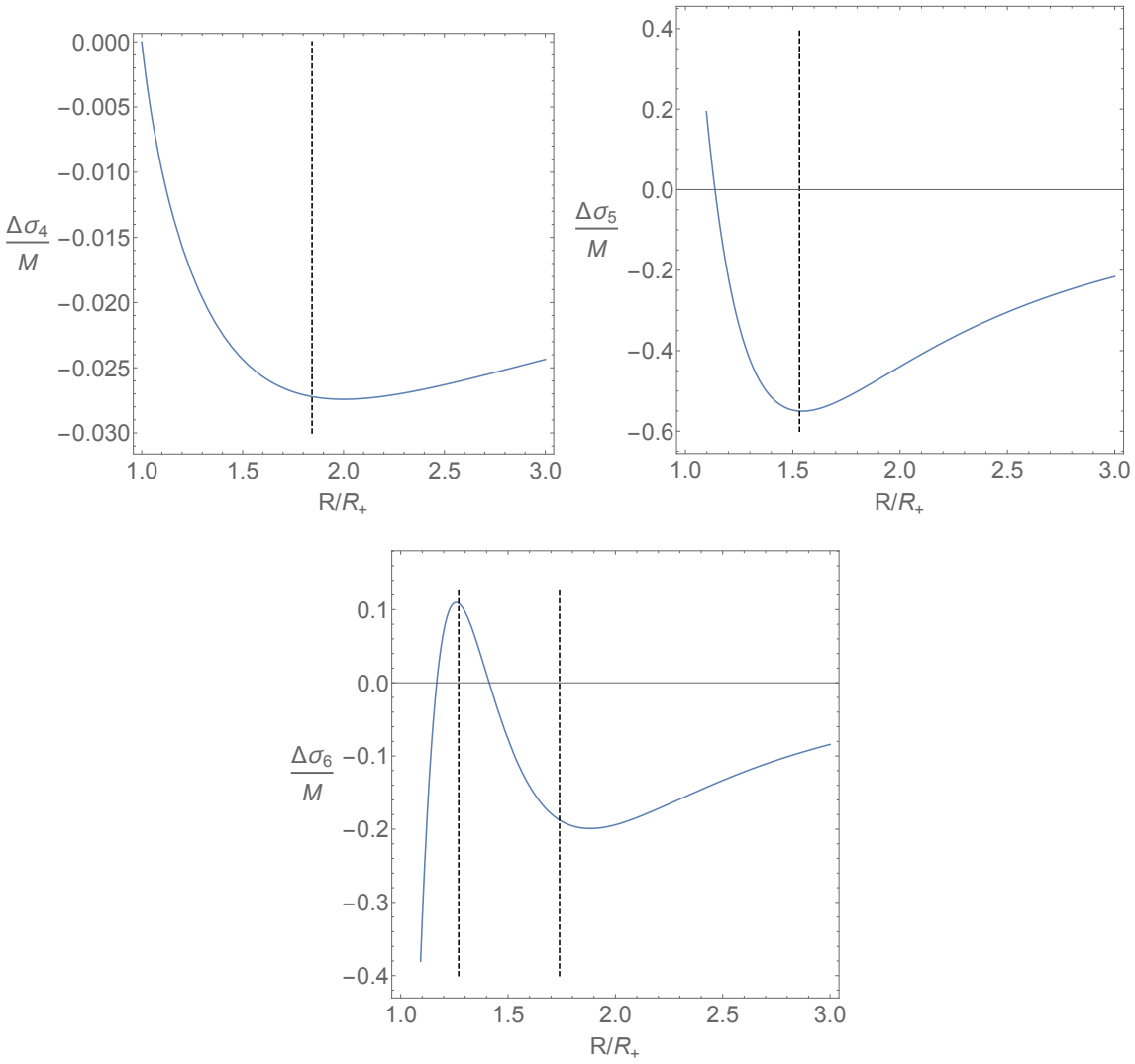

Figure 4.12: We show the entanglement entropy of balls in the extremal black hole background $\Delta\sigma_d$ and mark $\rho_*^{(d)}$. In $d = 6$, the first line marks radius where $\Delta\sigma_6$ is maximized and the second line is $\rho_*^{(6)}$ times this radius.

To find the critical length scale for our droplets, we start with Poincaré-AdS$_{d+1}$ and study the entanglement entropy of annuli on the boundary with inner radius R_1 and outer radius R_2. As we vary the ratio $\rho = (\frac{R_1}{R_2})$, there is again phase transition between "connected" and "disconnected" surfaces. For small ρ, the surfaces which

minimize the area are "connected". Using a conformal transformation to take the plane to a cylinder, this surface can be understood as the string world sheet connecting two Wilson loops analogous to the construction in [176].[16] At some critical $\rho_*^{(d)}$, the minimal area surface for the annuli is instead two disconnected surfaces, each of which corresponds to the ball surfaces discussed above. In the frame of the cylinder, this tells us that the string worldsheet no longer stretches between the two Wilson loops. As before, the area and therefore the two point correlator does not scale with ρ and so this is understood to represent a type of confinement. The critical ratio ρ_* is then understood to correspond to a size for the "glueballs" of the CFT above which heat transport is screened.[17]

As seen in fig. 4.12, in pure AdS, the phase transition for the $d = 4$ plasma occurs at $\rho_*^{(4)} \equiv (R_2/R_1)_* \sim 1.844$. As the boundary black hole nears extremality, we also see that a minimum in the entanglement entropy appears at $R/R_+ \sim \rho_*$. In $d = 5$, we find that $\rho_*^{(5)} \sim 1.53$. Again, as $T_{BH} \to 0$, the minimum in the entanglement entropy occurs at $R/R_+ \sim \rho_*^{(5)}$. We conjecture that this coincidence occurs because the boundary black hole breaks conformal symmetry and in our conformal frame, the event horizon sets a fundamental size for the jammed plasma. This lends some credence to the idea that the jamming occurs because the plasma cannot fit inside the black hole. In the confined phase, where the minimum radius is given by R_+, the jammed plasma can extend only to $\rho_*^{(d)}$. The "glueball" of the plasma is highly entangled with the degrees of freedom behind the horizon. Once the radius that

[16] One important feature of the construction in [176] was that the Euclidean supergravity solution had an S^1 from the Euclidean time circle. In our conformal map, the S^1 of the cylinder is analogous to the thermal circle.

[17] As discussed above, the real length scale actually depends on the map from the plane to the cylinder.

defines the boundary region is larger than $\rho_*^{(d)}$, there are no longer correlations beween the degrees of freedom behind the horizon and the glueball, hence the minimum in the entanglement. The entanglement then grows again because of correlations between degrees of freedom away from the black hole matching onto the Tangerlinhi behavior.

In the $d = 6$ entanglement entropy, the behavior is slightly different and we now see a maximum and a minimum. From the stress tensor (fig. 4.6), we saw that the region of negative energy density has moved away from the horizon, unlike the lower dimensional cases. This suggests that it in this dimension, it may not be accurate to draw conclusions about localization scales in terms of R_+ for the entanglement entropy.[18] In fact, the maximum entanglement occurs at $R_{max}/R_+ \sim 1.25$. Multiplying this radius by $\rho_*^{(6)} \sim 1.346$ gives us approximately the position of the dip in entanglement. In this dimension, it is clear that there is a complicated relationship between the entanglement outside of the horizon and the jammed plasma. The positive energy density near the horizon suggests possible new degrees of freedom which are not highly entangled with the black hole causing the global minimum of entanglement to occur at the horizon in this dimension.[19] As we increase the radius of our entangling surface, the entanglement increases as the surface divides these near horizon degrees of freedom into two regions. This increase continues until R_{max} where the glueball is located. The entanglement then behaves as the $d = 4, 5$ cases, decreasing until eventually reaching a local minimum where the glueball is entirely within the entangling surface and then increasing.

[18] In even dimensions, there is some ambiguity in the regularized entanglement entropy because of the log divergence. While we use the same regularization scheme for each value of R_-, this ambiguity may still play a role. We thank Don Marolf for emphasizing this point to us.

[19] As the energy density is also positive far from the black hole, these degrees of freedom my behave very similarly to the plasma far from the black hole. Note that by dividing the Hilbert space into two spatial regions, we can't distinguish which degrees of freedom are correlated.

Interestingly, in $d > 4$, there are no local minima in the entanglement entropy for sufficiently large temperatures. Here it seems that the Hawking radiation prevents the plasma from confining.[20] In fact, the equality between the location of this dip measured in terms of R_+ and $\rho_*^{(d)}$ is particular to the extremal black hole where the Hawking radiation is at zero temperature and no longer excites the plasma. Here, the jammed CFT should behave similarly to the vacuum state and share the same confining scale. For higher temperature black holes, the plasma should be excited and its pressure should increase. At the same time, there is a stronger gravitational attraction which makes the plasma want to decrease in size. It appears that in four dimensions, the Hawking radiation wins out and the dip in the entanglement entropy moves to larger radii. In $d > 4$, the gravitational attraction wins and the dips move toward the horizon. It is worth noting that the stress tensors (figs. **??**, **??**, 4.6) confirm this behavior as all energy densities have peaks that mirror the temperature dependence of the entanglement entropy.

Now we note some important differences. In $d = 3$, we find $\Delta\sigma_3 > 0$ for all R. However, for $d > 3$, $\Delta\sigma_d$ is negative except near the horizon. This negative $\Delta\sigma_d$ can be explained because the vacuum dual to Poincaré AdS is in a pure state and very highly entangled [178, 179].[21] It is reasonable that far from the black hole, the jammed CFT has less correlations than the vacuum. The new behavior near the horizon can be explained by the breaking of conformal invariance. The vacuum dual to Poincareé-AdS is scale invariant and on a fixed time slice, any division of the boundary into two pieces will give the same value for the finite piece of the entanglement entropy

[20] In [177], it was shown that the critical $\rho_*^{(d)}$ increases with temperature.

[21] It was shown in [178] that the density matrix for ball shaped regions in Poincaré-AdS can be conformally mapped to a thermal density matrix which is known to have maximal entanglement.

(4.60). The droplet spacetime, however, is in general not Ricci flat and breaks this scale invariance. It is worth noting that, in $d = 5, 6$, when the boundary is Ricci flat ($R_- = 0$), the entanglement entropy is monotonic, similar to the three dimensional case, although this is not the case in $d = 4$. Near the black hole, the entanglement becomes positive because the CFT is very localized and has denser correlations than the vacuum. As we increase R away from the horizon, the entanglement decreases until $R/R_+ = \rho_*^{(d)}$ where the glueball of the jammed CFT is completely within our boundary region. From here, the entanglement entropy matches the behavior of the Ricci flat case.

The three dimensional case is unique because neither the black hole nor the no black hole spacetime is scale invariant despite being Ricci flat.[22] While the $\mu = 0$ limit of the C-metric gives Poincaré-AdS$_4$, it is more appropriate to subtract the no boundary black hole state because it has the same leading order divergence and the same conical deficit as the black hole spacetime for a given μ. Furthermore, for large radii, $\Delta\sigma_3 \to 0$. Here it is not clear whether one should expect the no black hole background, which corresponds to an excited state of the CFT, to have more or less entanglement than the black hole background.

The next difference is the behavior of the entanglement on the horizon (fig. 4.10). It is intriguing that the entanglement is not monotonic in T_{BH}. In three and four dimensions, this quantity starts positive and goes to zero as we go to extremality. In four dimensions, the entanglement entropy actually becomes negative at some critical $T_{BH} \sim .02$ but then increases towards zero again. In five and six dimensions, the entanglement starts negative and increases. In five dimensions this continues all the

[22] A scale invariant, spherically symmetric spacetime would have the same value for the entanglement entropy for any choice of R.

way to $T_{BH} = 0$ while the six dimensional case starts decreasing around $T_{BH} \sim .12$. In $d = 5$, the entanglement entropy on the horizon is linear while in $d = 4$ and $d = 6$ it is roughly quadratic. In $d = 3$, as seen in fig. 4.7, the entanglement entropy at the horizon increases as $T_{BH}^{2/3}$. We don't have a good understanding of this behavior. In particular, we note that for $d \geq 4$, $M, Q \to 1$ as $T_{BH} \to 0$, but the three dimensional case has $\mu \to \infty$ as $T_{BH} \to 0$ more similar to a Schwarzschild black hole where the extremal limit is $M \to \infty$. In fig. 4.1, we showed that in $d = 4$, as $T_{BH} \to 0$, the horizon approaches the surface $R^2 + z^2 = 1$. In Poincaré-AdS, this is the minimal surface for a ball with radius $R = 1$. Thus we expect that in the extremal limit, the difference in entanglement entropy should vanish as it does. This is not the case in higher dimensions where the surface cannot be isometrically embedded in this limit. It seems that the extremal limit of the horizon entanglement entropy is dimension dependent. One may hope to gain insight by doing similar calculations in other droplet spacetimes by fixing the boundary black hole temperature and varying T_∞ where we can use a Schwarzschild black hole on the boundary and vary the bulk horizon temperature.[23]

4.6 Discussion

In this paper we sought to clarify some features of jammed CFTs by investigating their holographic duals. To this end, we constructed three new classes of solutions to the Einstein equations with a negative cosmological constant that have boundaries conformal to the d-dimensional Reissner-Nordström metric.

[23]This is a conformal field theory, so that only the ratio T_{BH}/T_∞ should matter. However, the black holes that we constructed have a maximum temperature because we set $R_+ = 1$.

For these solutions, we calculated the boundary stress tensor and compared this to both a theoretical form as well as to existing literature. The calculation of the boundary stress tensor introduced some new features that had not been seen before in the literature, including peaks in the energy densities, positive asymptotic energy densities, and magnitudes near the horizon that were not monotonic as a function of T_{BH}. This new behavior seems to indicate the presence of a CFT phase that becomes localized away from the horizon as $T_{BH} \to T_\infty$.

We also calculated entanglement entropies of balls in these geometries as well as in the analytic example of the AdS C-metric. For these examples, many features of the boundary stress tensor were confirmed, including near horizon behavior indicative of a localized CFT. Furthermore, for $d \geq 4$, the entanglement entropies were smaller in the black hole background than the corresponding entropies in pure AdS far from the black hole showing very little correlation between a near horizon CFT and an asymptotic CFT.[24] Furthermore, by comparing to confining phase transitions in Poincaré-AdS$_{d+1}$, we find critical values in the entanglement entropy which match the proposed "size" of glueballs in units of the horizon radius R_+. At the same time, many features of the entanglement entropy remain enigmatic. One particular example is the behavior of the horizon's entanglement entropy as a function of R_-. The different behavior between the $d = 3$ case and $d \geq 4$ cases suggest that one direction worth pursuing is to choose a Schwarzschild boundary black hole and vary T_∞ instead. Using the construction in [168], one could better compare to the three dimensional case. In particular, one may understand why, in $d = 5, d = 6$, $\Delta\sigma_d$ does not go to

[24]Note that in work done on thermal states dual to the AdS-Schwarzschild black hole, differences are positive. This is because the thermal state, in addition to the vacuum entanglement, has new degrees of freedom from thermally excited entangled pairs.

zero as the boundary black hole approaches extremality.

4.7 Acknowledgments

It is a pleasure to thank Netta Engelhardt, Gary Horowitz, and Don Marolf for helpful discussions on this work and valuable feedback on this manuscript. This work was supported in part by NSF grant PHY-1504541.

4.8 Appendix: Stress Tensor Expansion

In this appendix, we present the expansions used to calculate the boundary stress tensor. As discussed above, our spacetime is asymptotically locally AdS [173]. This suggests that in a finite neighborhood U of the boundary $\partial\mathcal{M}$, we can define a "Fefferman-Graham" coordinate, z, such that

$$z|_{x=1} = 0, \;\; \hat{g}^{MN}\partial_M z \partial_N z = 1/l^2, \quad \text{where } \hat{g} = z^2 g \tag{4.62}$$

This coordinate allows us to construct Gaussian normal coordinates near the boundary such that the metric is given by

$$ds^2 = \frac{l^2}{z^2}(dz^2 + \gamma_{\mu\nu}(x,z)dx^\mu dx^\nu). \tag{4.63}$$

From the Einstein equations, one may show that the metric $\gamma_{\mu\nu}$ can be expanded near the boundary in even powers of z up to order z^d,

$$\gamma_{\mu\nu}(x,z) = \gamma^{(0)}_{\mu\nu} + z^2\gamma^{(2)}_{\mu\nu} + ... + z^d\gamma^{(d)}_{\mu\nu} + z^d\bar{\gamma}^{d}_{\mu\nu}\log z^2 + ... \tag{4.64}$$

where the $\bar{\gamma}^{(d)}_{\mu\nu}$ term only appears for even d. Each term in the expansion up to $\gamma^{(d)}$ can be expressed in terms of geometric quantities determined from the boundary metric $\gamma^{(0)}_{\mu\nu}$. For example,

$$\gamma^{(2)}_{\mu\nu} = -\frac{1}{(d-2)}\left(\mathcal{R}_{\mu\nu} - \frac{1}{2(d-1)}\mathcal{R}\gamma^{(0)}_{\mu\nu}\right) \tag{4.65}$$

where $\mathcal{R}_{\mu\nu\rho\sigma}, \mathcal{R}_{\mu\nu}, \mathcal{R}$ are the Riemann tensor, Ricci tensor, and Ricci scalar of the boundary metric respectively. Other expressions can be found in [180].[25] Furthermore, one can express $\bar{\gamma}^{(d)}_{\mu\nu}$ in terms of these geometric quantities and the covariant derivatives associated with the boundary metric,

$$\begin{aligned}
\bar{\gamma}^{(2)}_{\mu\nu} &= 0 \\
\bar{\gamma}^{(4)}_{\mu\nu} &= \frac{1}{8}R_{\mu\nu\rho\sigma}R^{\rho\sigma} - \frac{1}{48}\nabla_\mu\nabla_\nu\mathcal{R} + \frac{1}{16}\nabla^2 R_{\mu\nu} - \frac{1}{24}\mathcal{R}\mathcal{R}_{\mu\nu} \\
&\quad + \left(-\frac{1}{96}\nabla^2\mathcal{R} + \frac{1}{96}\mathcal{R}^2 - \frac{1}{32}\mathcal{R}_{\rho\sigma}\mathcal{R}^{\rho\sigma}\right)\gamma^{(0)}_{\mu\nu}
\end{aligned} \tag{4.66}$$

Note that the authors of [180, 114] show that in $d = 6$, $\bar{\gamma}^{(d)}$ is regularization scheme dependent and can be cancelled by a local counterterm.[26] Furthermore, this term

[25] These authors use a different convention for the Riemann tensor and some care must be taken to compare to our expressions.

[26] The ambiguity comes from a potential R^2 term in the counter term action leading to a contribution to the trace of the form $\Box R$. The expression above is for a specific choice of regularization scheme.

obeys

$$\gamma^{(0)\mu\nu}\bar{\gamma}^{(d)}_{\mu\nu} = 0 \tag{4.67}$$

and does not contribute to the conformal anomaly. For the d=6 stress tensor, we will not include this term in our expression.

The Einstein equations determine the $\gamma^{(i)}$ up to order z^d where new data first appears, including odd d. The new data appears in the function $\gamma^{(d)}_{\mu\nu}$ which must be determined from our numerical solution. From the Fefferman-Graham expansion, we can find the boundary stress tensor from the coefficients $\gamma^{(i)}_{\mu\nu}$. For odd d, this is simple to evaluate

$$\langle T^{(d)}_{\mu\nu}\rangle = \frac{dl^{d-1}}{16\pi G_{d+1}}\gamma^{(d)}_{\mu\nu}. \tag{4.68}$$

For even dimensions, however, the expression is more complicated. The important expressions for this work are the d=4 expression,

$$\langle T^{(4)}_{\mu\nu}\rangle = \frac{l^3}{4\pi G_5}\Bigg[\gamma^{(4)}_{\mu\nu} - \frac{1}{8}\left((Tr\gamma^{(2)})^2 - Tr(\gamma^{(2)})^2\right)\gamma^{(0)}_{\mu\nu} - \frac{1}{2}\gamma^{(2)\rho}_{\mu}\gamma^{(2)}_{\nu\rho} + \frac{1}{4}Tr(\gamma^{(2)})\gamma^{(2)}_{\mu\nu} + \frac{3}{2}\bar{\gamma}^{(4)}_{\mu\nu}\Bigg]. \tag{4.69}$$

Finally, the six dimensional stress tensor is given by (up to a term proportional to $\bar{\gamma}^{(6)}_{\mu\nu}$.

$$\langle T^{(6)}_{\mu\nu}\rangle = \frac{3l^5}{8\pi G_7}(\gamma^{(6)}_{\mu\nu} - A^{(6)}_{\mu\nu} + \frac{1}{24}S_{\mu\nu}) \tag{4.70}$$

where

$$A^{(6)}_{\mu\nu} = \frac{1}{3}\Bigg((\gamma^{(4)}\gamma^{(2)})_{\mu\nu} - (\gamma^{(2)^3}_{\mu\nu} + \frac{1}{8}\left[Tr(\gamma^{(2)^2}) - (Tr(\gamma^{(2)}))^2\right]\gamma^{(2)}_{\mu\nu} \\ - \left[\frac{1}{8}Tr(\gamma^{(2)^2})Tr(\gamma^{(2)}) - \frac{1}{24}(Tr(\gamma^{(2)}))^3 - \frac{1}{6}Tr(\gamma^{(2)^3}) + \frac{1}{2}Tr(\gamma^{(2)}\gamma^{(4)})\right]\gamma^{(0)}_{\mu\nu} \\ + 2(\gamma^{(2)}\gamma^{(4)})_{\mu\nu} - Tr(\gamma^{(2)})[\gamma^{(4)}_{\mu\nu} - \frac{1}{2}(\gamma^{(2)^2})_{\mu\nu}]\Bigg) \tag{4.71}$$

and

$$S_{\mu\nu} = \nabla^2 C_{\mu\nu} + 2R_{\nu\rho\mu\sigma}C^{\sigma\rho} + 4(\gamma^{(2)}\gamma^{(4)} - \gamma^{(4)}\gamma^{(2)})_{\mu\nu} + \frac{1}{10}(\nabla_\mu\nabla_\nu B - \gamma^{(0)}_{\mu\nu}\nabla^2 B) \\ + \frac{2}{4}\gamma^{(2)}_{\mu\nu}B + \gamma^{(0)}_{\mu\nu}(-\frac{2}{3}Tr(\gamma^{(2)^3}) - \frac{4}{15}(Tr\gamma^{(2)})^3 + \frac{3}{5}Tr\gamma^{(2)}Tr(\gamma^{(2)^2}) \tag{4.72}$$

where

$$C_{\mu\nu} = \left(\gamma^{(4)} - \frac{1}{2}\gamma^{(2)^2} + \frac{1}{4}\gamma^{(2)}Tr(\gamma^{(2)})\right)_{\mu\nu} + \frac{1}{8}\gamma^{(0)}_{\mu\nu}\left(Tr(\gamma^{(2)^2} - (Tr\gamma^{(2)})^2\right). \tag{4.73}$$

In the above expressions, indices are raised with $\gamma^{(0)\mu\nu}$ and lowered with $\gamma^{(0)}_{\mu\nu}$. Expressions like $\gamma^{(2)^2}_{\mu\nu}$ mean $\gamma^{(0)\rho\sigma}\gamma^{(2)}_{\mu\rho}\gamma^{(2)}_{\nu\sigma}$.

To find the coefficients $\gamma^{(i)}_{\mu\nu}$, we need to find an expression for the coordinate z in terms of x and r as well as boundary expansions for X and boundary radial coordinate

R. To do so, we write

$$\begin{aligned} z &= (1-x^2)\left(\frac{1}{1-r^2}+\sum_{n=1}^{\infty} z_n(r)(1-x^2)^n\right), \\ R &= \frac{R_+}{1-r^2}+\sum_{n=1}^{\infty} R_n(r)(1-x^2)^n, \\ X &= X_0(r)+\sum_{n=1}^{\infty} X_n(r)(1-x^2)^n+\log(1-x^2)\sum_{n=1}^{\infty}\tilde{X}_n(r)(1-x^2)^n, \end{aligned} \tag{4.74}$$

where $X_0(r)$ are our Dirichlet boundary conditions (4.29). The expansion coefficients $\tilde{X}_n(r)$ are non-zero for $n \leq d$ in $d = 4, 6$.[27] We insert the expansion for X into the DeTurck equations and match to the known Fefferman-Graham coefficients $\gamma^{(i)}_{\mu\nu}$. From this, we can find the functions z_n, R_n and X_n. Characteristic of asymptotically locally Anti-de Sitter spacetimes, the resulting polynomial contains only even powers of $(1-x^2)$ up to $(1-x^2)^d$. We will omit presenting $z_n,\ R_n,\ B_n$ and F_n because we don't use them explicitly to calculate the stress tensor.

Because they will be useful for the following, we recall that

$$\begin{aligned} \delta_d(r) &= \frac{1}{r^2}(1-(1-r^2)^{d-3})\left(1-(1-r^2)^{d-3}\left(\frac{R_-}{R_+}\right)^{d-3}\right), \\ \delta_4(r) &= (1-(1-r^2)R_-/R_+), \\ \delta_5(r) &= (2-r^2)(1-(1-r^2)^2(R_-/R_+)^2), \\ \delta_6(r) &= (3+3r^2-r^4)(1-(1-r^2)^3(R_-/R_+)^3). \end{aligned} \tag{4.75}$$

[27] There are other logarithmic terms that appear at higher order, for instance in $F(x,r)$, where such terms appear at $(1-x^2)^5$ in $d=4$.

In $d = 4$, the relevant boundary expansion is

$$\begin{aligned}
T &\to \delta_4(r)\left(1-(1-x^2)^2\alpha(r)\right)+(1-x^2)^4\left(T_4(r)+\log(1-x^2)+\tilde{T}_4(r)\right)+...,\\
S &\to 1+\frac{1}{2}(1-x^2)^2\alpha(r)+(1-x^2)^4\left(S_4(r)+\log(1-x^2)\tilde{S}_4(r)\right)+...,\\
A &\to \frac{1}{\delta_4(r)}\left(1-(1-x^2)^2\alpha(r)\right)+(1-x^2)^4\left(A_4(r)+\log(1-x^2)\tilde{A}_4(r)\right)+...,
\end{aligned} \tag{4.76}$$

where

$$\alpha(r) = (\delta_4(r) + r^2 R_-/R_+)(1-r^2) \tag{4.77}$$

and the "..." indicates terms of $\mathcal{O}((1-x^2)^5)$ and higher. For completeness, though they don't appear in the stress tensor, the $\tilde{X}_4$ coefficients can be found analytically to be

$$\begin{aligned}
\tilde{T}_4(r) &= -\frac{3}{2}r^2\left(r^2-1\right)^2\left(\left(r^2-1\right)R_-/R_+ + 1\right)^2 R_-/R_+,\\
\tilde{S}_4(r) &= r^2\left(r^2-1\right)^2\left(\left(r^2-1\right)R_-/R_+ + 1\right)R_-/R_+,\\
\tilde{A}_4(r) &= -\frac{1}{2}r^2\left(r^2-1\right)^2 R_-/R_+.
\end{aligned} \tag{4.78}$$

One can check that as $R_- \to 0$, the above expansion matches Figueras et al.

In $d = 5$,

$$\begin{aligned}
T &\to \delta_5(r)\left(1+\frac{3}{4}(1-x^2)^2\beta(r)\right)+(1-x^2)^4\eta_t(r)+(1-x^2)^5 T_5(r)+...,\\
S &\to 1-\frac{1}{4}(1-x^2)^2\beta(r)+(1-x^2)^4\eta_s(r)+(1-x^2)^5 S_5(r)+...,\\
A &\to \frac{1}{\delta_5(r)}\left(1+\frac{3}{4}(1-x^2)^2\beta(r)\right)+(1-x^2)^4\eta_r(r)+(1-x^2)^5 A_5(r)+...,
\end{aligned} \tag{4.79}$$

where the "..." indicates terms that are $\mathcal{O}((1-x^2)^6)$ and higher. For ease of reading, we have introduced the functions

$$\beta(r) = (1-r^2)^2(-2+(3+5r^2(-2+r^2))\frac{R_-^2}{R_+^2}) \tag{4.80}$$

and

$$\begin{aligned}
\eta_t(r) &= \frac{\delta_5(r)}{112}(-1+r^2)^2 \\
&\times \Bigg[44+204r^2(-2+r^2)-4(76+r^2(-2+r^2)(589+553r^2(-2+r^2)))\frac{R_-^2}{R_+^2} \\
&\qquad +(-1+r^2)^2(227+r^2(-2+r^2)(2258+2235r^2(-2+r^2)))R_-^4R_+^4\Bigg], \\
\eta_s(r) &= \frac{1}{112}(-1+r^2)^2 \\
&\times \Bigg[44+40r^2-20r^4+4(-13+r^2(-2+r^2)(132+161r^2(-2+r^2)))\frac{R_-^2}{R_+^2} \\
&\qquad -(-1+r^2)^2(-59+r^2(-2+r^2)(486+565r^2(-2+r^2)))\frac{R_-^4}{R_+^4}\Bigg], \\
\eta_r(r) &= \frac{1}{112\delta_5(r)}(-1+r^2)^2 \\
&\times \Bigg[4(11+37r^2(-2+r^2))-4(76+r^2(-2+r^2)(379+329r^2(-2+r^2)))\frac{R_-^2}{R_+^2} \\
&\qquad +(-1+r^2)^2(227+r^2(-2+r^2)(1474+1395r^2(-2+r^2)))\frac{R_-^4}{R_+^4}\Bigg].
\end{aligned} \tag{4.81}$$

There are no logarithmic terms in $d=5$.

In d=6, the expansion of X terms are

$$\begin{aligned}
T \to\ & \delta_6(r)\left(1+\frac{2}{5}(1-x^2)^2\psi(r)\right)+(1-x^2)^4\chi_t(r)\\
&+(1-x^2)^6\left(T_6(r)+\log(1-x^2)\tilde{T}_6(r)\right)+...,\\
S \to\ & 1-\frac{1}{10}(1-x^2)^2\psi(r)+(1-x^2)^4\chi_s(r)\\
&+(1-x^2)^6\left(S_6(r)+\log(1-x^2)\tilde{S}_6(r)\right)+...,\\
A \to\ & \frac{1}{\delta_6(r)}\left(1+\frac{2}{5}(1-x^2)^2\psi(r)\right)\\
&+(1-x^2)^4\chi_r(r)+(1-x^2)^6\left(A_6(r)+\log(1-x^2)\tilde{A}_6(r)\right)+...
\end{aligned} \tag{4.82}$$

where the "..." indicates terms that are $\mathcal{O}((1-x^2)^7)$ and higher. For ease of reading, we have defined

$$\psi(r)=\left(r^2-1\right)^3\left(\left(14r^2\left(r^4-3r^2+3\right)-9\right)\frac{R_-^3}{R_+^3}+5\right) \tag{4.83}$$

and

$$\begin{aligned}
\chi_t(r) =\ & \frac{\delta_6(r)}{1000}\left(r^2-1\right)^3\\
&\times\Bigg[\left(r^2-1\right)^3\left(\left(r^4-3r^2+3\right)\left(38374r^2\left(r^4-3r^2+3\right)-40113\right)r^2+5139\right)\frac{R_-^6}{R_+^6}\\
&+5\left(\left(r^4-3r^2+3\right)\left(7327r^2\left(r^4-3r^2+3\right)-8184\right)r^2+1332\right)\frac{R_-^3}{R_+^3}\\
&+25\left(136r^2\left(r^4-3r^2+3\right)-41\right)\Bigg],
\end{aligned} \tag{4.84}$$

$$\begin{aligned}\chi_s(r) &= \frac{1}{500}\left(r^2-1\right)^3 \\ &\times\Bigg[-\left(r^2-1\right)^3\left(r^2\left(r^4-3r^2+3\right)\left(3388r^2\left(r^4-3r^2+3\right)-2781\right)-432\right)\frac{R_-^6}{R_+^6} \\ &\quad-5\left(r^2\left(r^4-3r^2+3\right)\left(799r^2\left(r^4-3r^2+3\right)-688\right)-36\right)\frac{R_-^3}{R_+^3} \\ &\qquad-25\left(7\left(r^4-3r^2+3\right)r^2+8\right)\Bigg],\end{aligned} \tag{4.85}$$

$$\begin{aligned}\chi_r(r) &= \frac{1}{1000\delta_6(r)}\left(r^2-1\right)^3 \\ &\times\Bigg[\left(r^2-1\right)^3\left(\left(r^4-3r^2+3\right)\left(27874r^2\left(r^4-3r^2+3\right)-30363\right)r^2+5139\right)\frac{R_-^6}{R_+^6} \\ &\quad+5\left(\left(r^4-3r^2+3\right)\left(5077r^2\left(r^4-3r^2+3\right)-6084\right)r^2+1332\right)\frac{R_-^3}{R_+^3} \\ &\qquad+25\left(106r^2\left(r^4-3r^2+3\right)-41\right)\Bigg].\end{aligned} \tag{4.86}$$

The logarithmic terms are

$$\begin{aligned}
\tilde{T}_6(r) = & \\
& \frac{1}{50} f(r)^6 p(r) (R_-/R_+)^3 \left(2f(r)^9 p(r) \left(9394 r^2 p(r) - 1917\right) r^2 + 63\right) (R_-/R_+)^9 \\
& + 15 f(r)^6 \left(p(r) \left(3502 r^2 p(r) - 1167\right) r^2 + 42\right) (R_-/R_+)^6 \\
& + 6 f(r)^3 \left(p(r) \left(8137 r^2 p(r) - 3876\right) r^2 + 189\right) (R_-/R_+)^3 \\
& - 5 \left(p(r) \left(3016 r^2 p(r) - 1917\right) r^2 + 126\right), \\
\tilde{S}_6(r) = & \frac{1}{50} \Bigg[\left(p(r) \left(5551 r^2 p(r) - 1194\right) r^2 + 63\right) f(r)^{12} (R_-/R_+)^9 \\
& + \left(p(r) \left(9908 r^2 p(r) - 4305\right) r^2 + 252\right) f(r)^9 (R_-/R_+)^6 \\
& + 5 \left(p(r) \left(884 r^2 p(r) - 597\right) r^2 + 63\right) f(r)^6 (R_-/R_+)^3 \Bigg],
\end{aligned} \tag{4.87}$$

and

$$\begin{aligned}
\tilde{A}_6(r) = & \frac{1}{50 p(r) (f(r)^3 (R_-/R_+)^3 + 1)} \\
& \times \Bigg(2 \left(p(r) \left(1708 r^2 p(r) - 471\right) r^2 + 63\right) f(r)^{12} (R_-/R_+)^9 \\
& - \left(p(r) \left(5890 r^2 p(r) - 3549\right) r^2 + 504\right) f(r)^9 (R_-/R_+)^6 \\
& + 5 \left(\left(r^4 - 3r^2 + 3\right) p(r) \left(520 r^2 p(r) - 471\right) r^2 + 126\right) f(r)^6 (R_-/R_+)^3 \Bigg).
\end{aligned} \tag{4.88}$$

The d=6 stress tensor is

$$\langle T^\mu_\nu \rangle = \frac{3}{8\pi G_7} \mathrm{diag} \Big\{ T^t{}_t, \;\; T^R_R, \;\; T^\Omega_\Omega, \;\; T^\Omega_\Omega, \;\; T^\Omega_\Omega, \;\; T^\Omega_\Omega \Big\} \tag{4.89}$$

where

$$
\begin{aligned}
(T^t{}_t)R^6 = & \frac{\mathrm{T}_6(R)}{\left(1+\frac{R_+}{R}+\frac{R_+^2}{R^2}\right)\left(1-\frac{R_-^3}{R^3}\right)} \\
& + \frac{1}{60000R^{18}}\Big[166250R^{15}\left(R_-^3+R_+^3\right) \\
& - 625R^{12}\left(827R_-^6+6638R_-^3R_+^3+827R_+^6\right) \\
& + 25R^9\left(13335R_-^9+366271R_-^6R_+^3+366271R_-^3R_+^6+13335R_+^9\right) \\
& - 8666482R_-^9R_+^9 - 5R^6R_-^3R_+^3\left(1011065R_-^6+4403462R_-^3R_+^3+1011065R_+^6\right) \\
& + 13441280R^3R_-^6R_+^6\left(R_-^3+R_+^3\right)\Big],
\end{aligned}
\tag{4.90}
$$

$$
\begin{aligned}
(T^R{}_R)R^6 = & -4\mathrm{S}_6(R) - \frac{\mathrm{T}_6(R)}{\left(1+\frac{R_+}{R}+\frac{R_+^2}{R^2}\right)\left(1-\frac{R_-^3}{R^3}\right)} \\
& + \frac{1}{12000R^{24}}\Big[1750R^{15}\left(R_-^3+R_+^3\right)+125R^{12}\left(979R_-^6-1682R_-^3R_+^3+979R_+^6\right) \\
& + 2863126R_-^9R_+^9 - 5R^9\left(22575R_-^9+91367R_-^6R_+^3+91367R_+^6R_-^3+22575R_+^9\right) \\
& + R^6R_-^3R_+^3\left(724225R_-^6+3479278R_-^3R_+^3+724225R_+^6\right) \\
& - 3373640R^3R_-^6R_+^6\left(R_-^6+R_+^6\right)\Big],
\end{aligned}
\tag{4.91}
$$

and

$$
\begin{aligned}
(T^{\Omega}_{\Omega})R^6 = \mathrm{S}_6(R) - \frac{1}{30000R^{18}}\Big[&21875R^{15}\left(R_-^3+R_+^3\right) - 614681R_-^9R_+^9 \\
&- 625R^{12}\left(19R_-^6 - 1040R_-^3R_+^3 + 19R_+^6\right) \\
&+ 175R^9\left(165R_-^9 - 4909R_-^6R_+^3 - 4909R_-^3R_+^6 + 165R_+^9\right) \\
&+ 5R^6R_-^3R_+^3\left(35855R_-^6 + 134423R_-^3R_+^3 + 35855R_+^6\right) \\
&+ 320365R^3R_-^6R_+^6\left(R_-^3+R_+^3\right)\Big].
\end{aligned}
\tag{4.92}
$$

Finally, the expressions for $\mathcal{A}_d(r)$ are (with $R_+ = 1$)

$$
\begin{aligned}
\mathcal{A}_4(r) &= \frac{1}{4}(\delta_4(r)(-(1-r^2)(R_-r^2+\delta_4(r))(-3+5R_-+5r^2(1+(2r^2-3)R_-)) \\
&\qquad - 8S_4(r)) - 4T_4(r))/\delta_4(r)^2, \\
\mathcal{A}_5(r) &= \frac{1}{\delta_5(r)}\left(-3S_5(r) + \frac{T_5(r)}{\delta_5(r)}\right),
\end{aligned}
\tag{4.93}
$$

and

$$\begin{aligned}\mathcal{A}_6(r) = \frac{1}{\delta_6(r)}\Bigg[&-4S_6(r) - \frac{T_6(r)}{\delta_6(r)} \\ &-\frac{f(r)^3 p(r)}{10000}\Bigg(-12250R_+^3 - 17000R_-^3 + 230580f(r)^3R_-^6 \\ &\qquad - 276552f(r)^6R_-^9 - 75222f(r)^9R_-^{12} \\ &+p(r)r^2\big(-82375 + 1137150R_-^3 - 4635720f(r)^3R_-^6 \\ &\qquad + 5992746f(r)^6R_-^9 - 2424051f(r)^9R_-^{12}\big) \\ &+p(r)^2r^4\big(107125 - 2392050R_-^3 + 9669600f(r)^3R_-^6 \\ &\qquad - 12945386f(r)^6R_-^9 + 5478336f(r)^9R_-^{12}\big) \\ &+p(r)^3r^6\big(1284400R_-^3 - 5408835f(r)^3R_-^6 + 7468192f(r)^6R_-^9 - 3236632f(r)^9R_-^{12}\big)\Bigg)\Bigg],\end{aligned} \tag{4.94}$$

where $f(r) = 1 - r^2$ and $p(r) = 3 - 3r^2 + r^4$.

For the sake of completeness, we will also show how to extract the divergences in the entanglement entropies in $d = 4$, as an example. The higher dimensional cases are similar. Near the boundary, $z \approx (1-x^2)R_b$. Next, note that $x^2 g(x) = 2x^2 - x^4 = 1 - z^2/R_b^2$. Finally, $r'(x) = 0$ and $B(x) = 1 + \mathcal{O}(z^4)$ near the boundary. Then we can express the area functional near the boundary as

$$\frac{A_4}{4\pi} = R_b^2 \int_\epsilon \frac{dz}{z} \frac{\left(1 + \frac{1}{2}\frac{z^2}{R_b^2}\alpha(r_b)\right)\sqrt{1 - z^2/R_b^2}}{z^2} = \frac{R_b^2}{\epsilon^2} - \frac{1}{2}(\alpha(r_b) - 1)\log(\epsilon) + \text{finite}. \tag{4.95}$$

It is then just a matter of subtracting the divergent pieces to find the finite entanglement entropy. One must of course check that the finite piece does not vary as a function of the cutoff (for sufficiently small ϵ) which we demonstrate in figure 4.8.

Chapter 5

Holographic stress-energy tensor near the Cauchy horizon inside a rotating black hole

-

5.1 Introduction

One of the outstanding issues in gravity is understanding quantum effects in regions of large spacetime curvature. Although energy densities in typical classical fields such as electromagnetic fields are always non-negative, there have been a number of studies that show the appearance of negative energy density when quantum field effects are taken into account. For instance, it was shown (see, e.g. [181]) that the energy density for an observer falling into a singularity negatively diverges for some physical vacuum state. On the Cauchy horizon deep inside a charged black hole, the

stress-energy tensor was calculated for a two-dimensional massless scalar field model and the energy density diverges at the horizon [182]. Calculations of a conformal scalar field in Taub-NUT-type cosmologies show that the stress-energy tensor negatively diverges on the Cauchy horizon even though the curvature remains small [183]. However, most studies have been made for free massless scalar field models and little attention has been given to strongly interacting field models such as CFTs at strong coupling.

The AdS/CFT duality [7, 5] provides a powerful tool to investigate CFTs at strong coupling on a fixed curved background spacetime. According to the dictionary of the duality, a CFT at strong coupling on a fixed d-dimensional spacetime is dual to a gravitational theory in $d+1$-dimensional AdS spacetime with a timelike boundary conformal to the d-dimensional spacetime. Motivated by the investigation of Hawking radiation in a model of a CFT at strong coupling, two types of black hole solutions were constructed in asymptotically locally AdS spacetimes [184, 146, 148, 147, 185, 153, 152, 167, 151, 166, 2]. One solution is called a "black funnel" in which there is a single connected horizon extending from the conformal boundary to an asymptotically planar horizon in the bulk, and it is dual to the thermal equilibrium Hartle-Hawking vacuum state of the boundary theory. The other is called a "black droplet" solution in which the horizon is disconnected from the planar horizon in the bulk, and it is dual to the Unruh vacuum state. In these models, negative energy density is observed outside the event horizon due to the Hawking effect. However, these solutions are quite complicated and their construction has required numerical methods; hence, it is difficult to analyze general properties of the stress-energy tensor inside the boundary black hole. It is then desirable to have some

analytically constructed solutions for a black funnel/droplet. Recently some attempts along this direction have been made by Haddad [186] [1], who, using a derivative expansion method, has constructed a five-dimensional *static* black droplet solution and computed the holographic stress-energy tensor for the corresponding dual quantum field in the background of a four-dimensional static black hole background [184] (See also for the lower dimensional case ($d \leq 3$) [146, 147, 152]). It is clearly interesting to generalize the line of research [186, 184] performed for the static vacuum case to more general cases. In particular, including rotations would drastically change the causal structure inside the resultant black funnel/droplet motivating a study of the holographic consequences of strong coupling in quantum fields near the inner (Cauchy) horizon.

In this paper, we construct a *rotating* black droplet solution by generalizing the work [184]. In general, including rotation makes the relevant analysis significantly more complicated compared to the static case. For example, if one attempts to add a rotation to the model of [184] so that the corresponding boundary field lives in a four-dimensional Kerr black hole–which is already cohomogeneity-two, then one would have to construct a five-dimensional bulk black droplet by solving a cohomogeneity-three system. In order to avoid this technical difficulty, instead of trying to add a rotation to a five-dimensional black droplet, we attempt to construct a six-dimensional rotating black droplet solution dual to a five-dimensional field theory in the background of the rotating Myers-Perry black hole [189] with equal angular momenta, which is known to be cohomogeneity-one. In this case, the derivative expansion method enables us to reduce the bulk field equations to a set of ordinary differential

[1]Note that this expansion method is essentially the same as the one developed for the "blackfold approach" in [187]. See also e.g. [188], for further applications of this method.

equations, thereby making it possible to compute–analytically and explicitly within our expansion framework–the holographic stress-energy tensor for a CFT at strong coupling and large N inside the five-dimensional rotating black hole. In addition, since quantum field theories in odd-dimensions are not well understood, it is of considerable interest to study the behavior of quantum fields in a five-dimensional spacetime. In fact, motivated from recent interests in five-dimensional conformal field theory (see e. g., [166] for references), the six-dimensional rotating black droplet solutions dual to the rotating Myers-Perry black hole spacetime with equal angular momenta on the boundary were numerically constructed and the holographic stress-energy tensor was derived in region outside the event horizon [151, 166].

Having two rotations, the rotating droplet solution admits not only an outer event horizon but also an inner (Cauchy) horizon. In this paper, we are primarily concerned with the properties of the holographic stress-energy tensor inside the outer horizon and in particular, investigating the quantum instability of the Cauchy horizon. We find that the null-null component of the stress-energy tensor diverges negatively near the Cauchy horizon, in agreement with the study of free massless scalar fields [182, 183]. Our results suggest that the Cauchy horizon suffers from a quantum instability in favor of the strong cosmic censorship. As far as we know, this is the first example of applying the holographic method to study the Cauchy horizon instability due to quantum effects. We also find that negative energy appears just outside the outer horizon, describing particle creation by the Hawking effect. Nevertheless, there is no flux at infinity. This suggests that the dual phase corresponds to a transition from black funnels to black droplets, and that it is reminiscent of soft condensed matter systems representing a transition from a fluid-like behavior to rigid behavior, just like

a "jammed" state [151] (see also [2]).

The paper is organized as follows. In next section, we describe our metric ansatz, derive the equations of motion, and construct a rotating black droplet solution in six-dimensions by using the derivative expansion method. In section 5.3, we perform an analytic computation of the holographic stress-energy tensor for a CFT at strong coupling and large N inside the five-dimensional rotating black hole on the boundary. In section 5.4, we numerically check our results analytically obtained in the previous sections. Section 5.5 is devoted to summary and discussion.

5.2 Derivative expansion method

In this section, we derive the field equations following the derivative expansion method [186] and investigate general properties of the solution. Our bulk field equations are the 6-dimensional vacuum Einstein equations with negative cosmological constant,

$$R_{\mu\nu} = -\frac{5}{L^2} g_{\mu\nu}, \tag{5.1}$$

where L is the AdS radius. We start with the following metric ansatz:

$$
\begin{aligned}
d\bar{s}^2 = &\left[\frac{L^2}{z^2F(z)} - \frac{z^2}{L^2}\left(\frac{rF'(z)}{2F(z)}\right)^2\right]dz^2 + \frac{z^2 r\alpha(r,z)F'(z)}{L^2F(z)}\{\sqrt{F(z)}\,dvdz - drdz\} \\
&+ \frac{z^2}{L^2}\Bigg[-F(z)\frac{f(r,z)}{h(r,z)}dv^2 + 2\sqrt{\frac{F(z)}{h(r,z)}}\,dvdr + \frac{r^2}{4}(d\theta^2 + \sin^2\theta d\phi^2) \\
&\qquad + r^2 h(r,z)\Big(d\psi + \frac{\cos\theta}{2}d\phi - \sqrt{F(z)}\Omega(r,z)dv\Big)^2\Bigg], \\
f(r,z) = &\left(1 - \frac{r_+^2(z)}{r^2}\right)\left(1 - \frac{\kappa^2 r_+^2(z)}{r^2}\right), \qquad h(r,z) = 1 + \frac{\kappa^2 r_+^4(z)}{r^4}, \\
\Omega(r,z) = &\frac{\kappa\sqrt{1+\kappa^2}\,r_+^3(z)}{h(r,z)r^4}, \qquad F(z) = 1 - \frac{\mu^5}{z^5},
\end{aligned}
\tag{5.2}
$$

where α is an unknown function of r and z determined later. In the limit $r_+ \to 0$ and $\alpha \to -1$, this metric reduces to the familiar planar Schwarzschild-AdS spacetime with horizon radius μ after performing the coordinate transformation, $v = t + r/\sqrt{F(z)}$. Furthermore, the metric at each z = const. hypersurface represents the cohomogeneity-one Myers-Perry black hole solution with equal angular momenta [189], where the outer and inner (Cauchy) horizons are located at $r = r_+$ and $r = \kappa r_+$ ($0 \leq \kappa < 1$), respectively. So, the metric (5.2) represents a rotating black string embedded in the background planar Schwarzschild-AdS spacetime in which the horizon is extended along z-direction. The metric (5.2) itself does not satisfy the Eqs. (5.1), and must be corrected order by order in derivatives. To this end, we write

the metric as

$$
\begin{aligned}
ds^2 &= d\bar{s}^2 + ds^2_{(\epsilon)}, \\
ds^2_{(\epsilon)} &= \sum_{n=1}^{\infty} \epsilon^n h^{(n)}_{\mu\nu}(r) dx^\mu dx^\nu,
\end{aligned}
\tag{5.3}
$$

where ϵ is the formal derivative expansion parameter defined below and $h^{(n)}_{\mu\nu}(r)$ is the nth correction of the metric determined by the Einstein equations (5.1). The derivative expansions are valid only when the horizon radius of the string is much smaller than the other scales,

$$
r_+ \ll \mu \sim L. \tag{5.4}
$$

This implies that the background metric (5.2) changes very slowly along the z-direction compared with the radial scale r_+. Thus, the contributions of the first and second derivatives with respect to z-direction to the Einstein Eqs. (5.1) are suppressed by a factor of r_+/L and $(r_+/L)^2$ (or similarly, r_+/μ and $(r_+/\mu)^2$).

Following Ref. [186], we shall expand the metric functions, F, r_+, and α in a series of $z - z_c$ around an arbitrary value z_c as

$$
g(r, z) = g_c + \epsilon g_1 (z - z_c) + \epsilon^2 g_2 (z - z_c)^2 + \cdots, \tag{5.5}
$$

where $g(r, z)$ collectively denotes the metric functions such as F, r_+, and α, and the expansion coefficients are $g_n := \partial_z^n g(z_c)/n!$. Note that the expansion coefficients are functions of only r, but F_n and r_n, are independent of r.

So, the Einstein Eqs. (5.1) are formally modified to

$$r_c^2\, R_{\mu\nu} = -5\epsilon^2 \frac{r_c^2}{L^2} g_{\mu\nu}, \tag{5.6}$$

where $r_c = r_+(z_c)$. This implies that the effect of the cosmological constant appears at second order in the derivative expansion (5.5). Note that the derivative expansion parameter ϵ will be set to unity at the end of our calculations.

5.2.1 First order in derivatives

Substituting Eqs. (5.2) and (5.3) into Eqs. (5.6) one finds that the field Eqs. (5.6) are satisfied at first order by

$$h^{(1)}_{\mu\nu}(r) = 0, \tag{5.7}$$

provided that the following two equations with respect to $\alpha(r; z_c)$

$$\begin{aligned}
&\alpha' + \frac{\alpha}{r} + \frac{(6F_c r_1 + F_1 r_c) r^8 + 24\kappa^2 r_1 F_c\, r_c^4\, r^4 + \kappa^4 r_c^8 (2F_c r_1 - F_1 r_c)}{4F_1 r_c\, r^3 (r^4 + \kappa^2 r_c^4)^{3/2}} = 0, \\
&\alpha'' + \left(\frac{1}{r} + \frac{4r^3}{r^4 + \kappa^2 r_c^4}\right)\alpha' - \left(\frac{1}{r^2} - \frac{4r^2}{r^4 + \kappa^2 r_c^4}\right)\alpha \\
&+ \frac{3F_1 r^8 + 4\kappa^2 r_c^3 (F_1\, r_c - r_1 F_c)\, r^4 + \kappa^4 r_c^7 (4F_c r_1 + F_1 r_c)}{F_1 (r^4 + \kappa^2 r_c^4)^{5/2}} = 0
\end{aligned} \tag{5.8}$$

are satisfied. When

$$r_1 = \frac{r_c F_1}{2F_c} \tag{5.9}$$

is satisfied, the solution α satisfying both two equations (5.8) is given by

$$\alpha(r; z_c) = -\frac{r^2}{\sqrt{r^4 + \kappa^2 r_c^4}} + \frac{C}{r}, \tag{5.10}$$

where C is an integration constant. We discard the integration constant C because it can be eliminated by gauge transformation of $v \to v + C/\sqrt{F}$. In this case, $\kappa \to 0$ limit agrees with the non-rotating four-dimensional black string case [186].

5.2.2 Second order in derivatives

At second order, $O(\epsilon^2)$, we make an ansatz for the non-zero perturbed metric $h^{(2)}_{\mu\nu}$ as

$$\begin{aligned} h^{(2)}_{\mu\nu} dx^\mu dx^\nu = {} & 2\gamma(r) \left(d\psi + \frac{\cos\theta}{2} d\phi \right) dv + h_{vv}(r) dv^2 + 2h_{vr}(r) dv dr \\ & + h_{zz}(r) dz^2 + \beta(r) \left(d\psi + \frac{\cos\theta}{2} d\phi \right)^2 . \end{aligned} \tag{5.11}$$

We derive equations of motion for the metric functions above by substituting Eqs. (5.2), (5.3), and (5.11) into (5.6) and also using α given by (5.10) with r_c replaced by r_+. The equation of motion for h_{zz} is decoupled from the other variables as

$$\begin{aligned} & - \frac{L^2 F_c^2 \, (r^2 - r_c^2)(r^2 - \kappa^2 r_c^2)(r^4 + \kappa^2 r_c^4)^3 z_c^{10}}{5r^2} h''_{zz} \\ & - \frac{L^2 F_c^2 \, z_c^{10} \{3r^4 - r_c^2(1+\kappa^2) r^2 - \kappa^2 r_c^4\} (r^4 + \kappa^2 r_c^4)^3}{5r^3} h'_{zz} + \mathcal{P}(r) = 0, \end{aligned} \tag{5.12}$$

where the source term $\mathcal{P}$ is explicitly given by Eq. (5.49). The general solution

includes two integral constants, one of which is determined by imposing the regularity on the horizon $r = r_c$. Then, we obtain the following analytic solution,

$$
\begin{aligned}
h_{zz} = &-\frac{5r^2}{4L^2} + \frac{25\mu^{10}}{4L^2F_c^2\, z_c^{10}}\left(r^2 + \frac{\kappa^2 r_c^4 - r^4}{\sqrt{r^4+\kappa^2 r_c^4}}\right) \\
&+ \frac{5}{4L^2F_c\, z_c^5}\left\{(z_c^5+5\mu^5)r^2 - 6\mu^5\sqrt{r^4+\kappa^2 r_c^4}\right\} \\
&+ \frac{15(1+\kappa^2)\, r_c^2\, \mu^5}{2L^2F_c\, z_c^5}\ln(r^2-\kappa^2 r_c^2) + C,
\end{aligned}
\tag{5.13}
$$

where C is the remaining integral constant. Hereafter, we discard this constant becuase it can be eliminated by making a gauge transformation [186]. We find that we can solve for h_{vr} in terms of the other variables, so we need only solve three coupled second order differential equations for $\gamma(r)$, $\beta(r)$, and h_{vv}.

$$
\begin{aligned}
h_{vr} = &\frac{\sqrt{F_c}\,(2r^2 - r_c^2(1+\kappa^2))r^3}{4(3r^4-\kappa^2\, r_c^4)\sqrt{r^4+\kappa^2 r_c^4}}\,\beta' - \frac{\kappa\sqrt{1+\kappa^2}\, r_c^3\, r^3}{(6r^4-2\kappa^2\, r_c^4)\sqrt{r^4+\kappa^2 r_c^4}}\,\gamma' - \frac{r^2 h_{vv}}{2\sqrt{F_c}\,\sqrt{r^4+\kappa^2 r_c^4}} \\
&- \frac{(3r^4+\kappa^2\, r_c^4)r^3}{4\sqrt{F_c}\,(3r^4-\kappa^2\, r_c^4)\sqrt{r^4+\kappa^2 r_c^4}}h'_{vv} \\
&+ \frac{\sqrt{F_c}\, r^2\{r_c^6\,\kappa^2(1+\kappa^2) + 3r_c^4\,\kappa^2 r^2 + r_c^2(1+\kappa^2)r^4 - r^6\}}{2(3r^4 - r_c^4\,\kappa^2)(r^4+r_c^4\,\kappa^2)^{3/2}}\beta \\
&+ \frac{\kappa\sqrt{1+\kappa^2}\, r_c^3\, r^2}{(3r^4-\kappa^2\, r_c^4)\sqrt{r^4+\kappa^2 r_c^4}}\gamma + \frac{F_c^{3/2} z_c^4\{\kappa^2 r_c^4 - 2r_c^2(1+\kappa^2)r^2 + 3r^4\}r^3}{4L^4(3r^4-\kappa^2 r_c^4)\sqrt{r^4+\kappa^2 r_c^4}}h'_{zz} \\
&+ \frac{5r^4}{8\sqrt{F_c}L^6 z_c^6(3r^4-\kappa^2\, r_c^4)(r^4+\kappa^2 r_c^4)^{5/2}}\times \\
&\Bigg[8F_c^2 z_c^{10}(r^4+\kappa^2 r_c^4)^2 r^4 + 5\{6r^{12} + 2\kappa^4 r_c^8\, r^4 - 2\kappa^6 r_c^{12} + 3\kappa^4(1+\kappa^2)r_c^{10}r^2 \\
&+ 2\kappa^2 r_c^4((1+\kappa^2)r_c^2 - \sqrt{r^4+\kappa^2 r_c^4})r^6 - ((1+\kappa^2)r_c^2 + 6\sqrt{r^4+\kappa^2 r_c^4})r^{10} \\
&+ 2r_c^2(5\kappa^2 r_c^2 + 2(1+\kappa^2)\sqrt{r^4+\kappa^2 r_c^4})r^8\}\mu^{10} - 8F_c^2 z_c^{10}(r^4+\kappa^2 r_c^4)^2 r^4\Bigg],
\end{aligned}
\tag{5.14}
$$

$$\sqrt{F_c}L^6r^2(r^2-r_c^2)(r^2-\kappa^2r_c^2)(3r^4-\kappa^2r_c^4)(r^4+\kappa^2r_c^4)^2\gamma''$$
$$+\sqrt{F_c}L^6r(r^4+\kappa^2r_c^4)^2\{3r^8-3(1+\kappa^2)r_c^2\,r^6+2\kappa^2r_c^4\,r^4-7\kappa^2(1+\kappa^2)r_c^6\,r^2-r_c^8\kappa^4\}\gamma'$$
$$-4\sqrt{F_c}L^6(r^4+\kappa^2r_c^4)^3\{3r^4-3(1+\kappa^2)r_c^2\,r^2-\kappa^2r_c^4\}\gamma$$
$$+2F_cL^6\kappa\sqrt{1+\kappa^2}\,r_c^3\,r(r^4+\kappa^2r_c^4)^2\{r^4-2(1+\kappa^2)r_c^2\,r^2+\kappa^2r_c^4\}\beta'$$
$$-8L^6\kappa^3\sqrt{1+\kappa^2}\,r_c^7\,r^3(r^4+\kappa^2r_c^4)^2h'_{vv}$$
$$+4F_cL^6\kappa\sqrt{1+\kappa^2}\,r_c^3(r^4+\kappa^2r_c^4)^2\{r^4+2(1+\kappa^2)r_c^2\,r^2+\kappa^2r_c^4\}\beta$$
$$+4F_c^2L^2z_c^4\kappa\sqrt{1+\kappa^2}\,r_c^3\,r^3(r^4+\kappa^2r_c^4)^2\{3r^4-2(1+\kappa^2)r_c^2\,r^2+\kappa^2r_c^4\}h'_{zz}+\mathcal{S}(r)=0, \tag{5.15}$$

$$-F_cL^6r(r^2-r_c^2)(r^2-\kappa^2r_c^2)(3r^4-\kappa^2r_c^4)(r^4+\kappa^2r_c^4)^2\beta''$$
$$+F_cL^6(r^4+\kappa^2r_c^4)^2\{3r^8-9(1+\kappa^2)r_c^2\,r^6+6\kappa^2r_c^4\,r^4-5\kappa^2(1+\kappa^2)r_c^6\,r^2+3r_c^8\kappa^4\}\beta'$$
$$+12F_cL^6r(r^4+\kappa^2r_c^4)^3\{2r^2+(1+\kappa^2)r_c^2\}\beta$$
$$-8\sqrt{F_c}L^6\kappa\sqrt{1+\kappa^2}\,r_c^3\,r^2(3r^4+\kappa^2r_c^4)(r^4+\kappa^2r_c^4)^2\gamma'$$
$$-8L^6\kappa^2r_c^4\,r^2(3r^4+\kappa^2r_c^4)(r^4+\kappa^2r_c^4)^2h'_{vv}$$
$$+16\sqrt{F_c}L^6\kappa\sqrt{1+\kappa^2}\,r_c^3\,r(3r^4+\kappa^2r_c^4)(r^4+\kappa^2r_c^4)^2\gamma$$
$$+8F_c^2L^2\kappa^2z_c^4r_c^4\,r^2(r^4+\kappa^2r_c^4)^2\{3r^4-2(1+\kappa^2)r_c^2\,r^2+\kappa^2r_c^4\}h'_{zz}+\mathcal{R}(r)=0, \tag{5.16}$$

$$
\begin{aligned}
&- L^6 r^2 (r^2 - r_c^2)(r^2 - \kappa^2 r_c^2)(3r^4 - \kappa^2 r_c^4)(r^4 + \kappa^2 r_c^4)^2 h''_{vv} \\
&- L^6 r (r^4 + \kappa^2 r_c^4)^2 \{9r^8 - 9(1+\kappa^2) r_c^2\, r^6 - 6\kappa^2 r_c^4\, r^4 + 7\kappa^2(1+\kappa^2) r_c^6\, r^2 + \kappa^4 r_c^8\} h'_{vv} \\
&- 2F_c L^6 (1+\kappa^2) r_c^2\, r^3 (r^4 + \kappa^2 r_c^4)^2 \{(1+\kappa^2) r_c^2 - 2r^2\} \beta' \\
&+ 4\sqrt{F_c} L^6 \kappa \sqrt{1+\kappa^2}\, r_c^3\, r (r^4 + \kappa^2 r_c^4)^2 \{3r^4 - (1+\kappa^2) r_c^2\, r^2 - \kappa^2 r_c^4\} (r\gamma' - 2\gamma) \\
&- 4F_c L^6 (1+\kappa^2) r_c^2 (r^4 + \kappa^2 r_c^4)^2 \{4r^4 - (1+\kappa^2) r_c^2\, r^2 - 2\kappa^2 r_c^4\} \beta \\
&+ 2F_c^2 L^2 (1+\kappa^2) r_c^2 z_c^4\, r^3 (r^4 + \kappa^2 r_c^4)^2 \{3r^4 - 2(1+\kappa^2) r_c^2\, r^2 + \kappa^2 r_c^4\} h'_{zz} + \mathcal{Q}(r) = 0,
\end{aligned}
\tag{5.17}
$$

where $\mathcal{S}(r)$, $\mathcal{R}(r)$, and $\mathcal{Q}(r)$ are functions of r given by Eqs. (5.50), (5.51), and (5.52) in the Appendix. From the other constraint equations, we obtain the coefficient r_2 as

$$
r_2 = \frac{r_c (4F_2 F_c - F_1^2)}{8F_c^2}. \tag{5.18}
$$

Combining Eqs. (5.9) and (5.18), we obtain

$$
r_+(z) = r_0 \sqrt{F(z)}, \tag{5.19}
$$

up to second order in the derivative expansion, where r_0 is the radius of r_+ at the AdS boundary, $z \to \infty$. Just as in the non-rotating five-dimensional black string case [186], the droplet horizon shrinks to zero at the horizon of the planar Schwarzschild-AdS spacetime, ending on the horizon.

These three equations (5.15), (5.16), and (5.17) have a singular source term $\sim (r - r_c\kappa)^{-1}$ arising from h_{zz} in (5.13). This implies that γ, β, and h_{vv} can be expanded

near the inner (Cauchy) horizon as

$$\gamma(r) \simeq \ln(r-\kappa\, r_c)\{a_0 + a_1(r-\kappa\, r_c) + a_2(r-\kappa\, r_c)^2 + \cdots\} + d_0 + d_1(r-\kappa\, r_c) + \cdots ,$$
$$\beta(r) \simeq \ln(r-\kappa\, r_c)\{b_0 + b_1(r-\kappa\, r_c) + b_2(r-\kappa\, r_c)^2 + \cdots\} + e_0 + e_1(r-\kappa\, r_c) + \cdots ,$$
$$h_{vv}(r) \simeq \ln(r-\kappa\, r_c)\{c_0 + c_1(r-\kappa\, r_c) + c_2(r-\kappa\, r_c)^2 + \cdots\} + f_0 + f_1(r-\kappa\, r_c) + \cdots . \tag{5.20}$$

Note that we have assumed that the black droplet solution is non-extremal, i. e. , $\kappa < 1$, in the expansion. Substituting these into Eqs. (5.15), (5.16), and (5.17), we obtain all the coefficients provided that the coefficients c_0, d_0, e_0, f_0, e_1, and f_1 are given. This implies that six independent mode solutions exist for the second order differential equations (5.15), (5.16), and (5.17). For the discussions in the next section, it suffices to obtain the relation between the leading order coefficients a_0, b_0, and c_0. The remaining subleading coefficients are determined by numerics in Sec. 5.4.

The leading coefficients a_0 and b_0 are determined by c_0 as

$$a_0 = -\frac{r_c\,\kappa\sqrt{1+\kappa^2}\{2L^6 z_c\, c_0 + 15 r_c^2(1+\kappa^2)\mu^5 F_c\}}{2L^6 z_c(1-\kappa^2)\sqrt{F_c}},$$
$$b_0 = \frac{r_c^2\,\kappa^2\{2L^6 z_c\,(1+3\kappa^2)c_0 + 15 r_c^2(3+4\kappa^2+\kappa^4)\mu^5 F_c\}}{2L^6(1-\kappa^2) z_c\, F_c}. \tag{5.21}$$

By Eq. (5.14), we also find the asymptotic behavior of h_{vr} near the Cauchy horizon:

$$h_{vr} \simeq \frac{r_c\,\kappa^2\{2L^6 z_c\,\kappa^2 c_0 + 15(1+\kappa^2) r_c^2\,\mu^5 F_c\}}{4L^6 z_c(1-\kappa^2)\sqrt{1+\kappa^2}\sqrt{F_c}(r-\kappa r_c)}. \tag{5.22}$$

5.2.3 The non-rotating case

In the non-rotating case ($\kappa = 0$), Eqs. (5.15) and (5.16) respectively for γ and β are decoupled from the other variables and we can set $\gamma = \beta = 0$. Furthermore, we obtain analytic expressions for h_{vv} and h_{vr} from Eqs. (5.13), (5.17), and (5.14):

$$\begin{aligned} h_{zz} &= \frac{15 r_c^2\, \mu^5 \ln r}{L^2 F_c\, z_c^5}, \\ h_{vv} &= C_2 - \frac{C_1}{2r^2} - \frac{5\mu^5 F_c\, r_c^2}{L^6 z_c\, r^2}\{r_c^2 - (r^2 - 2r_c^2)\ln r\}, \\ h_{vr} &= \frac{-4C_2 L^6 z_c^6 + 5 r_c^2\, \mu^5 (4 z_c^5 + \mu^5) - 20 r_c^2\, \mu^5 z_c^5\, F_c \ln r}{8 L^6 z_c^6 \sqrt{F_c}}, \end{aligned} \tag{5.23}$$

where C_1 and C_2 are constants that correspond to a global shift in the temperature as explained in [186], so we must set it to zero.

5.3 The holographic stress-energy tensor

In this section, we calculate the holographic stress-energy tensor using the prescription of [190], up to the second order in ϵ. In the six-dimensional bulk theory, the regularized action becomes

$$\begin{aligned} S = {} & \frac{1}{16\pi G_6}\int_{\mathcal{M}} dx^6 \sqrt{-g}\left(R + \frac{30}{L^2}\right) + \frac{1}{8\pi G_6}\int_{\partial\mathcal{M}} dx^5 \sqrt{-q} K \\ & + \frac{1}{8\pi G_6}\int_{\partial\mathcal{M}} dx^5 \sqrt{-q}\left[\frac{4}{L} + \frac{L}{6}\mathcal{R} + \frac{L^3}{18}\left(\mathcal{R}_{ab}\mathcal{R}^{ab} - \frac{5}{16}\mathcal{R}^2\right) + \cdots\right], \end{aligned} \tag{5.24}$$

where $\mathcal{R}$ is the Ricci scalar of the induced metric $q_{ab} = g_{ab} - n_a n_b$ at $z = z_c$ associated with the unit normal outward pointing vector n^a, and K is the trace of the extrinsic curvature defined below. Note that the first three terms in the second line are sufficient

to cancel the divergences. Furthermore, the last two terms are at $O(\epsilon^4)$, since the induced metric is the vacuum Myers-Perry black hole [189] at zeroth order, i. e. , $\mathcal{R}_{ab} = \mathcal{R} = O(\epsilon^2)$. Thus, the holographic stress-energy tensor T_{ab}, given by $T_{ab} = (2/\sqrt{-q})\,\delta S/\delta q^{ab}$, becomes

$$T_{ab} = \frac{L}{8\pi G_6}\left[\frac{1}{3}E_{ab} - \frac{\epsilon}{L}\Big(K_{ab} - q_{ab}K\Big) - \frac{4\epsilon^2}{L^2}q_{ab}\right] + O(\epsilon^4), \tag{5.25}$$

where E_{ab} is the Einstein tensor of the induced metric q_{ab}, and K_{ab} is the extrinsic curvature defined by

$$K_{ab} = q_a{}^c \nabla_c n_b. \tag{5.26}$$

If the metric (5.3) is decomposed into

$$ds^2 = (N^2 + N_a N^a)dz^2 + 2N_a dx^a dz + q_{ab}dx^a dx^b, \tag{5.27}$$

K_{ab} is rewritten by

$$K_{ab} = \frac{1}{2N}(\partial_z q_{ab} - D_a N_b - D_b N_a), \tag{5.28}$$

where D_a is the covariant derivative with respect to the induced metric q_{ab}, and the lapse function N and the shift vector N_a are given by

$$\begin{aligned} &N_v = \frac{5\alpha r\mu^5}{2L^2 z_c^4} + O(z_c^{-9}), \quad N_r = -\frac{5\alpha r\mu^5}{2L^2 z_c^4} + O(z_c^{-9}), \quad \text{the other components} = 0, \\ &N = \frac{L}{z_c\sqrt{F_c}} + O(\epsilon^2). \end{aligned} \tag{5.29}$$

Note that $N_a = O(\epsilon)$, as it includes the derivative with respect to z from Eq. (5.2). Thus, if we expand q_{ab}, K_{ab}, and E_{ab} as

$$\begin{aligned} q_{ab} &= {q^{(0)}}_{ab} + \epsilon^2 {q^{(2)}}_{ab} + \cdots , \\ K_{ab} &= \epsilon K^{(1)}_{ab} + \epsilon^3 K^{(3)}_{ab} + \cdots , \\ E_{ab} &= \epsilon^2 E^{(2)}_{ab} + \cdots , \end{aligned} \tag{5.30}$$

$K^{(1)}_{ab}$ is determined by ${q^{(0)}}_{ab}$ as

$$K^{(1)}_{ab} = \frac{z_c \sqrt{F_c}}{2L} (\partial_z {q^{(0)}}_{ab} - \bar{D}_a N_b - \bar{D}_b N_a), \tag{5.31}$$

where $\bar{D}_a$ denotes the covariant derivative with respect to ${q^{(0)}}_{ab}$. Then, Eq. (5.25) reduces to

$$T_{ab} = \frac{\epsilon^2 L}{8\pi G_6} \left[\frac{1}{3} E^{(2)}_{ab} - \frac{1}{L} \left(K^{(1)}_{ab} - q^{(0)}_{ab} K^{(1)} \right) - \frac{4}{L^2} q^{(0)}_{ab} \right] + O(\epsilon^4). \tag{5.32}$$

This implies that the second order perturbation $h^{(2)}_{\mu\nu}$ contributes to the stress-energy tensor only through the Einstein tensor, up to $O(\epsilon^2)$.

First, we investigate the stress-energy tensor in the static case ($\kappa = 0$). Substitu-

tion of Eqs. (5.23) into Eq. (5.32) yields

$$
\begin{aligned}
T_{vv} &= \epsilon^2 \cdot C \cdot \frac{4r^6 - 9r_c^2\, r^4 + 5r_c^6}{r^6}, \\
T_{vr} &= \epsilon^2 \cdot C \cdot \frac{-4r^4 + 5r_c^2\, r^2 + 5r_c^4}{r^4}, \\
T_{rr} &= \epsilon^2 \cdot C \cdot \frac{5(r^2 - r_c^2)}{r^2}, \\
T_{\psi\psi} &= \frac{2}{\cos\theta} T_{\psi\phi} = \epsilon^2 \cdot C \cdot \frac{r^4 - 5r_c^4}{r^2}, \\
T_{\theta\theta} &= T_{\phi\phi} = \epsilon^2 \cdot C \cdot \frac{r^4 - 5r_c^4}{4r^2},
\end{aligned}
\tag{5.33}
$$

where $C = \mu^5/16\pi G_6 L^3 z_c^3$. It is easily checked that the conservation law $\bar{D}_a T^{ab} = 0$ is satisfied. Near the outer horizon $r = r_c$, negative energy density appears, i.e., $T_{vv} < 0$ ($r > r_c$). This implies that due to the Hawking effect, pair creation of particles occurs near the horizon, and the negative energy particles are absorbed into the horizon. Nevertheless, there is no flux at null infinity. This is verified by checking that the (t, r)-component of the stress-energy tensor in the original coordinate system (t, r) becomes zero at null infinity. This is due to strong coupling effects of the dual CFT in the boundary theory, just as in the five-dimensional case [184]. It is also immediately checked that the trace of our stress-energy tensor vanishes, in agreement with the general argument that odd dimensional CFTs have a vanishing trace anomaly.

Next, we investigate the stress-energy tensor near the inner (Cauchy) horizon in the rotating case. Note that K_{ab} is regular near the Cauchy horizon $r = \kappa r_c$ at $O(\epsilon)$ because ${q^{(0)}}_{ab}$ and the shift vector N_a are regular there. Thus, the dominant term of T_{ab} in Eq. (5.25) near the Cauchy horizon comes from the Einstein tensor E_{ab}. As

shown in Eqs. (5.20), (5.21) and (5.22), the second order metric h_{ab} diverges near the Cauchy horizon. So, the relevant (i.e., (r,r)-) component of the Einstein tensor E_{ab} can be expanded as

$$E_{rr} = \frac{\epsilon^2}{z_c^3}\left[-\frac{15r_c^2(1+\kappa^2)\mu^5}{4L^4(r-r_c\kappa)^2} + \frac{C'}{r-\kappa r_c} + \cdots\right] + O(\epsilon^4), \tag{5.34}$$

where C' is a constant. As for the other components, the leading term in order $O(\epsilon^2)$ behave as $1/(r-\kappa r_c)$, and therefore are irrelevant to the rest of our arguments.

The most striking feature is that E_{rr} in Eq. (5.34) negatively diverges at the Cauchy horizon. This implies that the null energy condition is strongly violated along the null direction, ∂_r near the Cauchy horizon:

$$T_{rr} \simeq -\frac{5\epsilon^2 r_c^2(1+\kappa^2)\mu^5}{32\pi G_6 L^3 z_c^3(r-r_c\kappa)^2} \to -\infty. \tag{5.35}$$

Interestingly, this behavior is very similar to the case of massless scalar field in two-dimensions [182, 183]; in both cases, the stress-energy tensor negatively diverges as $(r-\kappa r_c)^{-2}$.

5.4 Numerical results

When we add rotation to our droplets, we must solve the second order equations numerically. To account for the logarithmic divergences in β, γ and h_{vv}, as well as

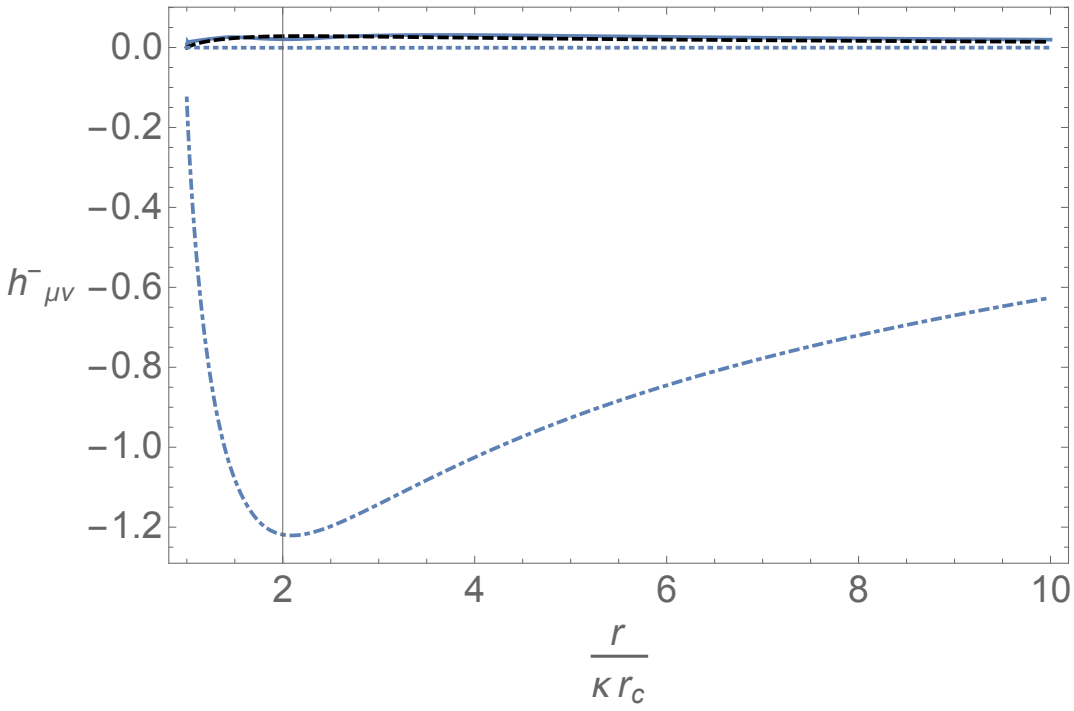

Figure 5.1: Here we plot the finite pieces of $h_{\mu\nu}(r)$ at $\mathcal{O}(\epsilon^2)$. The curves correspond to $\beta^-(r)$ (dotted), $\gamma^-(r)$ (dashed, black), $h^-_{vv}(r)$ (dot-dashed), and $h^-_{vr}(r)$ (thick) for $r_c = .1,\ \mu = 1,\ \kappa = .2,\ z_c = (4\mu)^{1/5}$. Note that γ^- and h^-_{vr} nearly overlap, and β^- is much smaller than the other functions.

the pole in h_{vr}, we make the following ansatz,

$$\begin{aligned}
\beta(r) &= \beta_L(r)\ln(r-\kappa r_c) + \beta_1(r)\\
\gamma(r) &= \gamma_L(r)\ln(r-\kappa r_c) + \gamma_1(r)\\
h_{vv}(r) &= h_{vvL}(r)\ln(r-\kappa r_c) + h_{vv1}(r)\\
h_{vr}(r) &= h_{vrL}(r)\ln(r-\kappa r_c) + \frac{r}{r-\kappa r_c}h_{vr1}(r).
\end{aligned} \tag{5.36}$$

In the last equation, the coefficient of $h_{vr1}(r)$ is required to have $h_{vv1}(r)$ vanish as r goes to infinity, matching the non-rotating case.

We insert these ansatz into (5.14) and find eight equations to solve numerically– four from the coefficients of $\ln(r-\kappa r_c)$ involving only $\beta_L, \gamma_L, h_{vvL}$ and h_{vrL} and four remaining equations involving these variables as well as $\beta_1, \gamma_1, h_{vv1}, h_{vr1}$. It is numerically convenient to also set $L=1$ and work in terms of a variable $R \equiv 1/r$ in order to impose boundary conditions at spatial infinity.

As we did in the analytic case, we can perform a series expansion in powers of $R-(\kappa r_c)^{-1}$ near the Cauchy horizon to find appropriate boundary conditions on our new metric functions,

$$X(R) = \sum_{i=0}^{\infty} x_i (R - \frac{1}{\kappa r_c})^i \tag{5.37}$$

where X refers collectively to $\{\beta_L, \gamma_L, h_{vvL}, h_{vrL}, \beta_1, \gamma_1, h_{vv1}, h_{vr1}\}$. This expansion reflects the fact that the divergences in β, γ, h_{vv} come only from a log term sourced by h_{zz} and there is an extra divergence of $(r-\kappa r_c)^{-1}$ in h_{vr}. Inserting this expansion into our eight differential equations and solving order by order in $(R-\frac{1}{\kappa r_c})$ leads to the following boundary conditions,

$$\begin{aligned}
h_{vrL}\left(R=\frac{1}{\kappa r_c}\right) &= -\frac{1}{4\left(\kappa^2-1\right)^2\left(\kappa^2+1\right)^{3/2}\sqrt{F_c}z_c} \\
&\quad \times \kappa\Bigg(15\left(\kappa^2+1\right)\left(2\kappa^6+7\kappa^4+12\kappa^2+3\right)\mu^5 F_c r_c^2 \\
&\quad + 2\kappa^2\left(5\kappa^4+14\kappa^2+5\right) z_c h_{vvL}\left(\frac{1}{\kappa r_c}\right)\Bigg) \\
h'_{vvL}\left(\frac{1}{\kappa r_c}\right) &= -\frac{\kappa\left(\kappa^2+1\right) r_c\left(15\left(\kappa^2+1\right)\mu^5 F_c r_c^2 + 2 z_c h_{vvL}\left(\frac{1}{\kappa r_c}\right)\right)}{\left(\kappa^2-1\right) z_c}
\end{aligned} \tag{5.38}$$

as well as the previously derived conditions, Eq. (5.21). Furthermore, the expansion

leads to the following constraint at the horizon,

$$
\begin{aligned}
0 = \\
&16\kappa\left(\kappa^2-1\right) r_c^2 z_c\left(2\left(\kappa^2+1\right)\sqrt{F_c}\gamma_1\left(\frac{1}{\kappa r_c}\right)+\sqrt{\kappa^2+1}h'_{vv1}\left(\frac{1}{\kappa r_c}\right)\right)\\
&+5\kappa^2\mu^5 r_c^5\Bigg(-20\kappa\left(\kappa^2-1\right)\left(\kappa^2-2\sqrt{\kappa^2+1}\kappa-1\right)\\
&+3\left(4\kappa^5-8\kappa^3+93\sqrt{\kappa^2+1}\kappa^2+33\sqrt{\kappa^2+1}+19\sqrt{\kappa^2+1}\kappa^6+63\sqrt{\kappa^2+1}\kappa^4+4\kappa\right)F_c\Bigg)\\
&-4\left(\sqrt{\frac{1}{\kappa^2}+1}-\kappa^3\sqrt{\kappa^2+1}\right)\\
&-8\sqrt{F_c}r_c z_c\left(3\kappa\left(\sqrt{\frac{1}{\kappa^2}+1}-\kappa^3\sqrt{\kappa^2+1}\right)\sqrt{F_c}\beta_1\left(\frac{1}{\kappa r_c}\right)-2\left(\kappa^4-1\right)\gamma_1'\left(\frac{1}{\kappa r_c}\right)\right)\\
&F_c z_c\beta_1'\left(\frac{1}{\kappa r_c}\right)+2\kappa^2\sqrt{\kappa^2+1}\left(57\kappa^4+48\kappa^2-1\right)r_c^3 z_c h_{vvL}\left(\frac{1}{\kappa r_c}\right).
\end{aligned}
\tag{5.39}
$$

We can likewise perform a series expansion at spatial infinity in powers of R (recall $R=0$ corresponds to spatial infinity) to find appropriate boundary conditions. This leads to

$$
\begin{aligned}
\beta_L(0)=\gamma_L(0)=0, \qquad & h_{vr1}(0)=\frac{-5\left(\kappa^2+1\right)\mu^5\left(F_c-5\right)r_c^2-4z_c h_{vv1}(0)}{8\sqrt{F_c}z_c},\\
h_{vvL}(0)=\frac{5\left(\kappa^2+1\right)\mu^5 F_c r_c^2}{z_c}, \qquad & h_{vrL}(0)=-\frac{5\left(\kappa^2+1\right)\mu^5\sqrt{F_c}r_c^2}{2z_c},\\
\beta_1(0)=\frac{25\kappa^2\mu^{10}r_c^4}{2F_c z_c^6}, \qquad & \gamma_1(0)=-\frac{25\kappa\sqrt{\kappa^2+1}\mu^{10}r_c^3}{2\sqrt{F_c}z_c^6}.
\end{aligned}
\tag{5.40}
$$

Note that these boundary conditions correspond to imposing a single constraint on the free parameters c_0, d_0, f_0, e_1 and f_1 in Eq. (5.20).

Finally, there are a few boundary conditions which me must impose by hand.

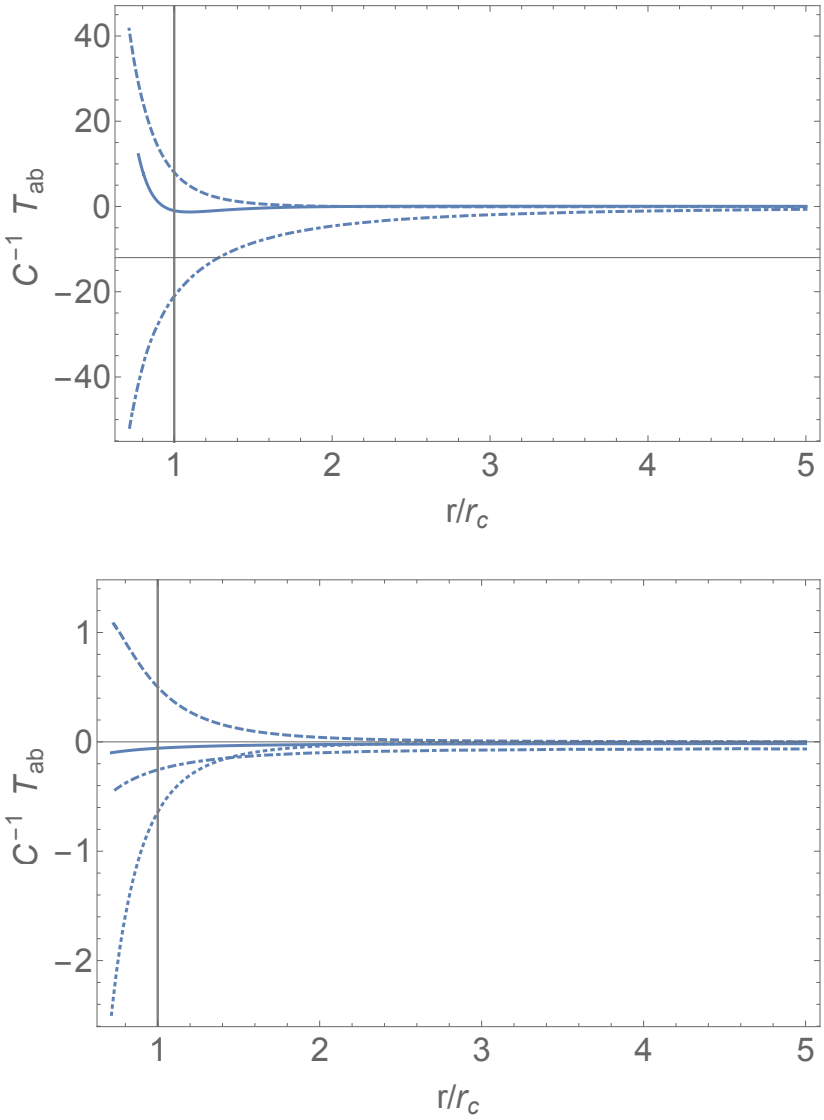

Figure 5.2: Here we plot the components of the holographic stress-energy tensor for the same parameters as figure 5.1 with $\theta = \pi/2$ and $z_c = (10^8\mu)^{1/5}$. In the top plot, we show T_{vr} (dashed), T_{rr} (dot-dashed), and T_{vv} (thick). In the bottom, we show $T_{\psi r}$ (dotted), $T_{\psi v}$ (dashed), $T_{\psi\psi}$ (dot-dashed), and $T_{\theta\theta}$ (thick). For each of these, we have scaled our solution by C^{-1} defined below Eq. (5.33). Notably, each of these components is regular at the outer horizon (labelled by the vertical line at $r/r_c = 1$).

These are analogous to the constants C_1 and C_2 in Eq. (5.23). To smoothly match onto the non-rotating case, we choose $\beta_1(\frac{1}{\kappa r_c}) = \gamma_1(\frac{1}{\kappa r_c}) = 0$ and $h_{vv1}(0) = 0$. This choice is equivalent to imposing $d_0 = e_0 = f_0 = 0$.

These boundary conditions are not sufficient to ensure smooth solutions because the point $R = 3^{1/4}/(r_c\sqrt{\kappa})$ is a (regular) singular point of our differential equations. To accommodate this singularity, we used two numerical regions, $0 \leq R \leq \frac{3^{1/4}}{r_c\sqrt{\kappa}}$ and $\frac{3^{1/4}}{r_c\sqrt{\kappa}} < R < \frac{1}{\kappa r_c}$ (this is only necessary for $\kappa < \sqrt{3}$). We impose continuity of our functions and match the first derivatives of our functions at this point. Regularity of the differential equation, or similarly smoothness of h_{vrL} and h_{vr1} at our singular point, amounts to two constraints. In total, we start with four free constants, $\beta_1(\frac{1}{\kappa r_c}), \gamma_1(\frac{1}{\kappa r_c}), h_{vvL}(\frac{1}{\kappa r_c})$, and $h_{vv1}(0)$ and fix three by hand to smoothly match onto the non-rotating solution. The final constant is fixed by consistency of the two constraints coming from the smoothness of h_{vr1}, h_{vrL}.

To find these numerical solutions, we use the Newton-Raphson method with pseudospectral collocation over a Chebyshev grid in the two numerical domains. In figure 5.1, we have plotted our solutions for $r_c = .1, \mu = 1, \kappa = .2, z_c = (4\mu)^{1/5}$ (reexpressed in terms of the original radial coordinate r). Importantly, we have included only the finite pieces of the solutions, subtracting off the divergent pieces. For example, using the notation of (5.20),

$$\beta^-(r) \equiv \beta(r) - b_0 \ln(r - \kappa r_c), \quad \gamma^- \equiv \gamma^-(r) - a_0 \ln(r - \kappa r_c),$$
$$h^-_{vv}(r) \equiv h_{vv}(r) - c_0 \ln(r - \kappa r_c) \tag{5.41}$$

and similarly for $h^-_{vr}(r)$.

We have also plotted the non-vanishing components of the stress-energy tensor for this solution in figure 5.2. We have only included the part of the stress-energy tensor near $r = r_c$ because the behavior of the stress-energy tensor near the Cauchy horizon can be derived from (5.21) as was done for T_{rr} in (5.35). To verify that we obtained the correct holographic stress-energy tensor, we varied z_c between $(10^4\mu)^{1/5}$ and $(10^8\mu)^{1/5}$ and checked that $C^{-1}(T_{ab})$ did not change.

As pointed out for the non-rotating case, an interesting quantity is the energy density near the outer horizon. The local energy density may be found by diagonalizing the stress-energy tensor $(T^a{}_b)$, as done in [166]. The stress-energy tensor in our spacetime is diagonalizable near the horizon and far from the horizon, but there is an intermediate region

$$r_c\sqrt{1-\kappa+\kappa^2+(1-\kappa)\sqrt{1+\kappa^2}} < r < r_c\sqrt{1+\kappa+\kappa^2+(1+\kappa)\sqrt{1+\kappa^2}} \tag{5.42}$$

where the stress-energy tensor diagonalization breaks down. This is likely a result of our expansion, as in a fully non-perturbative solution like [166], no such region was seen, though it is notable that our solution contains a finite temperature, rather than extremal, bulk horizon. Following [166], In the region where this decomposition is well-defined, we may write

$$T^a{}_b t^b = -\mathcal{E}(r) t^a \tag{5.43}$$

where t^a is the (unique) normalized timelike eigenvector and $\mathcal{E}(r)$ can be interpreted as the energy density observed by the timelike observer with velocity t^a. At leading

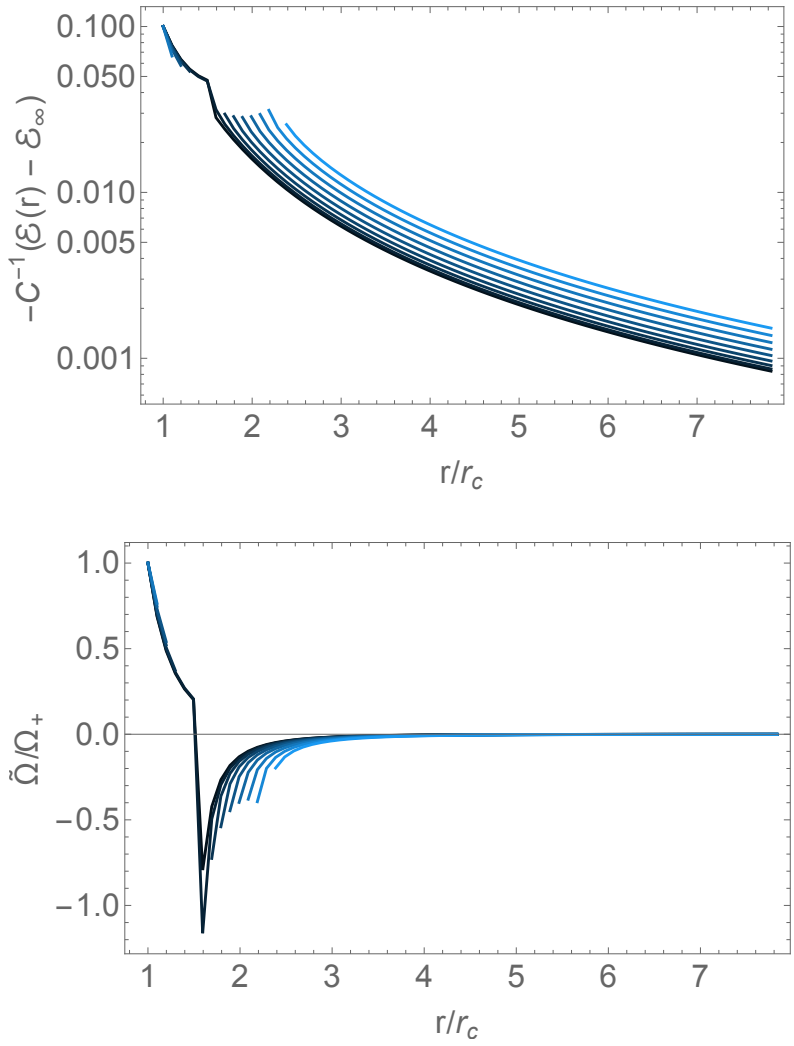

Figure 5.3: (Left) Here we plot $\mathcal{E}(r)$ near the outer horizon for $\kappa = .1,\ .2,\ .3,\ .4,\ .5,\ .6,\ .7,\ .8,\ .9$ with $r_c = .1, \mu = 1, z_c = (10^8\mu)^{1/5}$. The color of the curves gets lighter as κ increases. As before, we have scaled the energy density by C^{-1} and set $\theta = \pi/2$. The upper left of the figure corresponds to the near horizon region. The curves are discontinuous because there is a region set by κ outside the event horizon (Eq. 5.42), where the stress-energy tensor is not diagonalizable. (Right) Here we plot the rotation $\tilde{\Omega}(r)$ for the same values of κ. At the outer horizon, the rotation matches the value $\Omega(r_c, z_c)$ showing that t is the generator for the outer horizon. As before, discontinuities arise because the stress-energy tensor is not diagonalizable.

order in r and z_c,

$$t = \frac{1}{z_c}\left[\left(1 - 2\frac{(1+\kappa^2)r_c^2}{r^2} \pm \frac{\kappa^2 r_c^4}{r^4}\right)\frac{\partial}{\partial v} - \frac{\kappa\sqrt{1+\kappa^2}r_c^3}{r^4}\frac{\partial}{\partial \psi}\right] + \mathcal{O}\left(\frac{1}{r^5}, \frac{\mu^5}{z_c^5}\right). \quad (5.44)$$

The plus sign in this equation corresponds to the near horizon region, while the minus sign corresponds to the region far from the horizon.

The energy density obtained from the decomposition is plotted in figure 5.3 for different values of κ. Just as in the non-rotating case, the region of negative energy density extends all the way from the horizon to spatial infinity. Interestingly, at spatial infinity, the energy density approaches a constant,

$$\mathcal{E}_\infty \equiv \lim_{r\to\infty} \mathcal{E}(r) = \epsilon^2 \cdot \frac{4C}{z_c^2} + \mathcal{O}(r^{-2}). \quad (5.45)$$

This should not be surprising because far from the boundary black hole, the CFT should be in a thermal state, with an energy density corresponding to the temperature of the bulk black hole. In fact, this value matches the energy density for a CFT dual to a 6 dimensional planar-AdS Schwarzschild black brane. Furthermore, this value is independent of κ as it should be, since our boundary black holes are asymptotically flat and a similar result was seen for $\kappa = 0$ in [184]. In figure 5.3, we have subtracted this asymptotic value from the energy density to emphasize that a local observer near the black hole measures an energy density less than the thermal energy density because of quantum effects in the curved background spacetime.

Interestingly, our energy density approaches $\mathcal{E}_\infty$ as r^{-2}, rather than the r^{-7} decay observed in [166]. This less steep fall-off could be a consequence of our derivative expansion method. However, it is also notable that our droplet solution ends on

a finite temperature black brane horizon, whereas in [166], the bulk horizon was extremal (the Poincaré horizon) and the black droplet was disconnected. Similar fall-off discrepancies were seen in numerical constructions of five dimensional static droplets, where the energy density decayed as r^{-5} with an extremal bulk horizon [70], but as r^{-1} for a finite temperature bulk horizon [168]. Importantly, as in the analytic case, for an observer with tangent vector t^a, for all choices of κ, the energy density diverges negatively as $(r - \kappa r_c)^{-2}$ near the Cauchy horizon.

We also can use the stress-energy tensor eigenvalue decomposition to define rotation of the dual plasma. Again, following [166]), we write the timelike eigenvector of the stress-energy tensor as

$$T = \frac{\partial}{\partial v} + \tilde{\Omega}(r, z)\frac{\partial}{\partial \psi} \tag{5.46}$$

and define $\tilde{\Omega}$ to be the rotation. At the outer horizon, this becomes (at zeroth order in ϵ)

$$T_+ = \frac{\partial}{\partial v} + \sqrt{F(z_c)}\Omega(r_c, z_c)\frac{\partial}{\partial \psi} \tag{5.47}$$

which, on the conformal boundary, matches the future generator of the horizon at $r = r_c$. Note that the rotation decays as r^{-4}, rather than the r^{-2} fall-off seen in [166]. The faster fall-off could again be a consequence of our perturbative expansion, though more likely a result of the droplet ending on a finite temperature bulk horizon.

To better understand the energy density in regions of the spacetime where $T^a{}_b$ is not diagonalizable, we instead define a new vector, timelike everywhere outside the

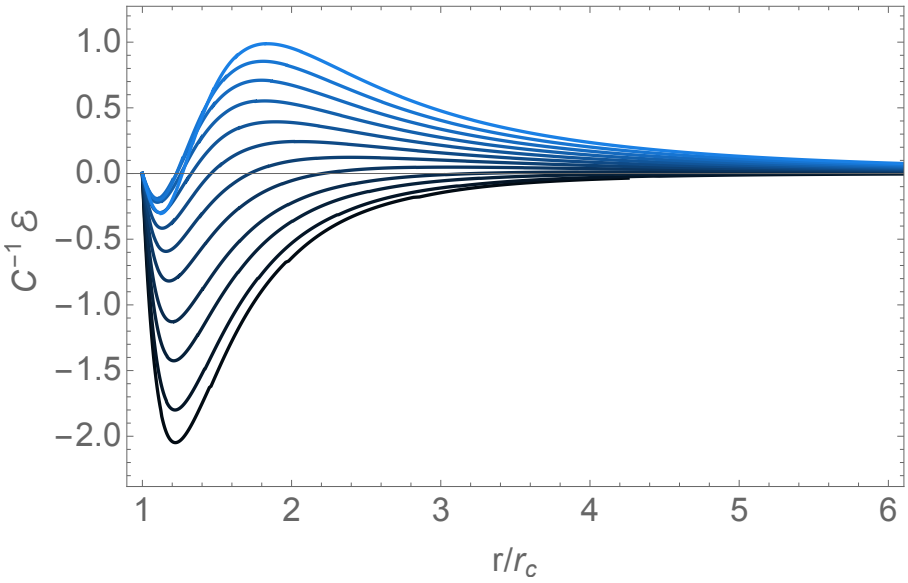

Figure 5.4: The energy density seen by an observer with the tangent vector in Eq. (5.48). Here, we choose $\kappa = .02,\ .05,\ .1,\ .15,\ .2,\ .25,\ .3,\ .35,\ .4,\ .45,\ .5,\ .55$ and $r_c = .1,\ \mu = 1, z_c = 10\mu^{1/5}$. The color of the curves gets lighter as κ increases. For all κ, the energy density is negative near the outer horizon.

outer horizon,

$$K = \frac{\partial}{\partial v} + \sqrt{F(z)}\Omega(r,z)\frac{\partial}{\partial \psi} \tag{5.48}$$

which also approaches T_+ at the outer horizon and goes to $(\partial/\partial v)$ near spatial infinity. An observer with this tangent vector would see the energy density plotted in figure 5.4, which is regular everywhere and still has the important feature of being negative near the event horizon. Furthermore, the localization of negative energy density near the event horizon is reminiscent of [2] and illuminates the "jammed" nature of the dual CFT. Here too, because $K \to \partial/\partial_v$ near spatial infinity, the energy density also approaches $\mathcal{E}_\infty$, indicative of the CFT in a thermal phase. This tangent vector, however, becomes spacelike inside the outer event horizon, and so is not useful to illustrate strong cosmic censorship. In this region, t^a is well-defined and diverges on the Cauchy horizon.

We emphasize that while the stress-energy tensor diverges on the Cauchy horizon, it is finite at $r = r_c$ so that it is regular on the past and future event horizons (shown in figure 5.2). Finally, one can check that the trace of stress-energy tensor vanishes at leading order, as expected for a CFT in odd spacetime dimensions, just as in the non-rotating case. In figure 5.5, we have plotted the diagonal components of the holographic stress-energy tensor, $C^{-1}(T^a{}_a)$ (no sum) as well as the trace. From this figure, it is clear that the sum vanishes as we approach the conformal boundary, (i.e. $z_c \to \infty$). One can also check explicitly from the definition of the stress-energy tensor (5.32) and the equations of motion for $h_{\mu\nu}$ (5.14–5.17), that the trace vanishes as $\mathcal{O}\left((\mu/z_c)^{10}\right)$, exactly following the non-rotating case.

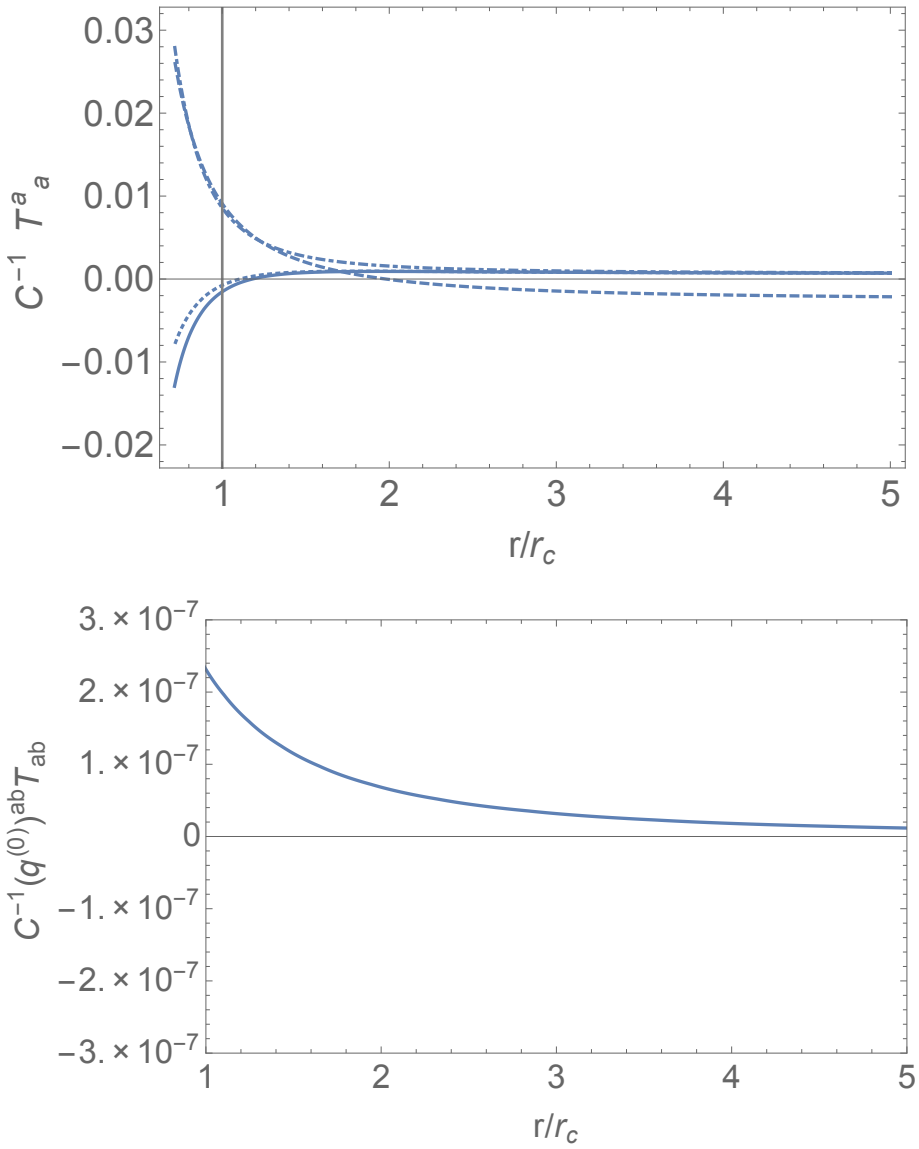

Figure 5.5: The left plot displays the diagonal components of the holographic stress-energy tensor, $T^a{}_a$, for $r_c = .1, k = .2, \mu = 1, z_c = (10^8\mu)^{1/5}$. The curves correspond to $T^\theta{}_\theta = T^\phi{}_\phi$ (dotted), $T^v{}_v$ (dashed), $T^r{}_r$ (dot-dashed), $T^\psi{}_\psi$ (thick). Again, the vertical grey line indicates the outer event horizon. The right plot displays the sum of these components. Notably, the trace of the stress-energy tensor vanishes as $\mathcal{O}\left((\mu/z_c)^{10}\right)$.

To summarize our numerical results, for generic rotation parameter, κ, of our boundary black hole, the CFT plasma exhibits the following features. The stress-energy tensor is traceless to leading order in μ/z_c and regular on the outer event horizon. For a timelike observer, there is a region near the event horizon which has negative energy density. As a timelike observer approaches spatial infinity, the energy density seen by such an observer approaches that of the thermal CFT dual to a six dimensional planar AdS-Schwarzschild black brane. Depending on the observer's velocity, the energy density may remain less than this asymptotic value for all of space, as for the observer with tangent vector t^a, or there may be a region with positive energy density, as in the observer with tangent vector K. In all cases, this negative energy density diverges on the Cauchy horizon, as shown in Eq. (5.35), in favor of strong cosmic censorship.

5.5 Conclusion and discussions

In this paper we have analytically constructed a rotating black droplet solution embedded in the planar Schwarzschild-AdS black brane spacetime by applying the generalized derivative expansion method, which was originally developed for the static case [186]. Our method is valid when the horizon size of the black droplet is much smaller than the horizon size of the planar Schwarzschild-AdS black brane (and the curvature radius of the background AdS space). In this case, the derivative of the metric along the bulk radial direction, z, is much smaller than the one along the droplet radial direction, r (parallel to the planar horizon). Then, order by order in the derivative expansion, we have been able to solve the Einstein equations. The

horizon radius of the thin black droplet solution gradually shrinks toward the planar horizon and caps off smoothly just at the horizon. Since the temperature of the black droplet solution is much higher than the temperature of the background planar horizon, the dual boundary state can be interpreted as the Unruh state [184]. For our black droplet solution, we have–analytically and holographically–computed the null-null components of the stress-energy tensor for a strongly coupled CFT in the boundary five-dimensional rotating Myers-Perry black hole spacetime. First, we have found that the negative energy appears just outside the event horizon, which can be interpreted as a consequence of the particle production by the Hawking effect. We show, however, there is no energy flux at infinity, as in the static case studied in [184], and therefore our boundary CFT can be viewed as a jammed state. We have also studied the behavior of the holographic stress-energy tensor near the inner Cauchy horizon. The null-null component of the stress-energy tensor corresponds to the energy density seen by an observer whose world line is transverse to the Cauchy horizon. We have found that the null-null component negatively diverges at the Cauchy horizon, suggesting that due to quantum effects, the Cauchy horizon would become singular, in favor of strong cosmic censorship.

Although we have not analyzed the classical instability of our droplet solution in the present paper, we expect our solution to show a classical instability or divergence of curvature scalars inside the event horizon. In fact, it was shown in [191] that in general, adding stationary but spatially inhomogeneous linear perturbations makes inhomogeneous black branes unstable, rendering the Kretschmann scalar with respect to the perturbed geometry divergent on the Cauchy horizon. Viewing our black droplet solution as a type of an inhomogeneous black string in the bulk and applying

the general argument of [191], our droplet solution should also exhibit the divergence of curvature scalars at the Cauchy horizon even inside the bulk $z < z_c$. In the spirit of the bulk-boundary duality, our result of the quantum divergence of the stress-energy tensor at the Cauchy horizon in the boundary geometry may be viewed as a holographic realization of the classical divergence of curvatures at the Cauchy horizon in the bulk geometry.

5.6 Acknowledgments

This work was supported in part by JSPS KAKENHI Grant Number 15K05092(AI), 26400280, 17K05451 (KM) as well as by NSF grant PHY-1504541 (EM).

5.7 Appendix: $\mathcal{P}(r)$, $\mathcal{S}(r)$, $\mathcal{R}(r)$, and $\mathcal{Q}(r)$

$\mathcal{P}(r)$, $\mathcal{S}(r)$, $\mathcal{R}(r)$, and $\mathcal{Q}(r)$ appearing in (5.14), (5.15), (5.16), and (5.17) are below.

$$
\begin{aligned}
\mathcal{P}(r) = &-2F_c^2\, z_c^{10}(r^4+\kappa^2 r_c^4)^3 r^2 - 5\Bigg[-2r^{14} + r^{12}(r_c^2(1+\kappa^2) + 2\sqrt{r^4+\kappa^2 r_c^4}) \\
&+ 3\kappa^4 r_c^8\, r^4(r_c^2(1+\kappa^2) + 2\sqrt{r^4+\kappa^2 r_c^4}) + \kappa^6 r_c^{12}(r_c^2(1+\kappa^2) + 3\sqrt{r^4+\kappa^2 r_c^4}) \\
&+ \kappa^2 r_c^4\, r^8(3r_c^2(1+\kappa^2) + 5\sqrt{r^4+\kappa^2 r_c^4}) - r_c^2\, r^{10}(6r_c^2\kappa^2 + (1+\kappa^2)\sqrt{r^4+\kappa^2 r_c^4}) \\
&- r_c^6\, r^6\kappa^2(6r_c^2\kappa^2 + (1+\kappa^2)\sqrt{r^4+\kappa^2 r_c^4}) - 2r_c^{10}\,\kappa^4 r^2(r_c^2\kappa^2 + 3(1+\kappa^2)\sqrt{r^4+\kappa^2 r_c^4})\Bigg]\mu^{10} \\
&+ 2F_c\, z_c^5(r^4+\kappa^2 r_c^4) \\
&\times \Bigg[-6r^8\sqrt{r^4+\kappa^2 r_c^4}\,\mu^5 - 9r^4\kappa^2 r_c^4\sqrt{r^4+\kappa^2 r_c^4}\,\mu^5 - 3r_c^8\,\kappa^4\sqrt{r^4+\kappa^2 r_c^4}\,\mu^5 \\
&+ r^{10}(z_c^5+5\mu^5) + r^2 r_c^6\,\kappa^2\Big\{6(1+\kappa^2)\sqrt{r^4+\kappa^2 r_c^4}\,\mu^5 + r_c^2\,\kappa^2(z_c^5+5\mu^5)\Big\} \\
&+ r^6 r_c^2\Big\{3(1+\kappa^2)\sqrt{r^4+\kappa^2 r_c^4}\,\mu^5 + 2r_c^2\,\kappa^2(z_c^5+5\mu^5)\Big\}\Bigg],
\end{aligned}
\tag{5.49}
$$

$$
\begin{aligned}
\mathcal{S}(r) = \frac{10\kappa\sqrt{1+\kappa^2}r_c^3\, r^2}{z_c^6}\Bigg[& 2F_c^2 z_c^{10} r^2 (r^4+\kappa^2 r_c^4)^3 \\
& + 5\Big\{ r_c^2(-5r_c^2\kappa^2 + (1+\kappa^2)\sqrt{r^4+\kappa^2 r_c^4})r^{10} + \\
& - 3r^{14} + 2(1+\kappa^2)r_c^2\, r^{12} + 2\kappa^4(1+\kappa^2)r_c^{10}\, r^4 \\
& - \kappa^6\sqrt{r^4+\kappa^2 r_c^4}\, r_c^{12} + \kappa^2 r_c^4(4(1+\kappa^2)r_c^2 + 5\sqrt{r^4+\kappa^2 r_c^4})r^8 \\
& + r_c^{10}\,\kappa^4(r_c^2\kappa^2 + 2(1+\kappa^2)\sqrt{r^4+\kappa^2 r_c^4})r^2 \\
& - r_c^6\,\kappa^2(r_c^2\kappa^2 + 5(1+\kappa^2)\sqrt{r^4+\kappa^2 r_c^4})r^6\Big\}\mu^{10} \\
& + 2F_c z_c^5\Big\{ 6\sqrt{r^4+\kappa^2 r_c^4}\,\mu^5 r^{12} + 7r_c^4\kappa^2\sqrt{r^4+\kappa^2 r_c^4}\,\mu^5 r^8 - r_c^{12}\kappa^6\sqrt{r^4+\kappa^2 r_c^4}\,\mu^5 \\
& + r_c^{10}\kappa^4(2(1+\kappa^2)\sqrt{r^4+\kappa^2 r_c^4}\,\mu^5 - r_c^2\kappa^2(z_c^5 - 3\mu^5))r^2 - (z_c^5+5\mu^5)r^{14} \\
& + r_c^6\kappa^2(-5(1+\kappa^2)\sqrt{r^4+\kappa^2 r_c^4}\,\mu^5 - r_c^2\kappa^2(3z_c^5 - \mu^5))r^6 \\
& - r_c^2(3(1+\kappa^2)\sqrt{r^4+\kappa^2 r_c^4}\,\mu^5 + r_c^2\kappa^2(3z_c^5+7\mu^5))r^{10}\Big\}\Bigg],
\end{aligned}
\tag{5.50}
$$

$$
\begin{aligned}
\mathcal{R}(r) = \frac{10\kappa^2 r_c^4\, r}{z_c^6}\Bigg[& 2F_c^2 z_c^{10}\, r^2 (r^4+\kappa^2 r_c^4)^2 (5r^4+\kappa^2 r_c^4) \\
& + 5\Big\{ 4r_c^{10}\,\kappa^4(1+\kappa^2) r^4 - \kappa^6 r_c^{12}\sqrt{r^4+\kappa^2 r_c^4} + 2r_c^{10}\kappa^4(1+\kappa^2)\sqrt{r^4+\kappa^2 r_c^4}\, r^2 \\
& + 5r_c^2(1+\kappa^2)\sqrt{r^4+\kappa^2 r_c^4}\, r^{10} - 5r_c^6\kappa^2(1+\kappa^2)\sqrt{r^4+\kappa^2 r_c^4}\, r^6 \\
& + (4r_c^2(1+\kappa^2) - 6\sqrt{r^4+\kappa^2 r_c^4}) r^{12} + \kappa^2 r_c^4 (8r_c^2(1+\kappa^2) + 3\sqrt{r^4+\kappa^2 r_c^4}) r^8 \Big\}\mu^{10} \\
& - 2F_c z_c^5 \Big\{ -6\sqrt{r^4+\kappa^2 r_c^4}\,\mu^5 r^{12} - 7r_c^4\kappa^2\sqrt{r^4+\kappa^2 r_c^4}\,\mu^5\, r^8 \\
& + r_c^{12}\kappa^6\sqrt{r^4+\kappa^2 r_c^4}\,\mu^5 + (5z_c^5+\mu^5) r^{14} \\
& + \kappa^2 r_c^6 \{ 5(1+\kappa^2)\sqrt{r^4+\kappa^2 r_c^4}\,\mu^5 + r_c^2\kappa^2(7z_c^5 - 5\mu^5)\} r^6 \\
& + \kappa^4 r_c^{10} \{ -2(1+\kappa^2)\sqrt{r^4+\kappa^2 r_c^4}\,\mu^5 + r_c^2\kappa^2(z_c^5 - 3\mu^5)\} r^2 \\
& + r_c^2 \{ 3(1+\kappa^2)\sqrt{r^4+\kappa^2 r_c^4}\,\mu^5 + r_c^2\kappa^2(11 z_c^5 - \mu^5)\} r^{10} \Big\} \Bigg], \qquad (5.51)
\end{aligned}
$$

$$\mathcal{Q}(r) = \frac{5\mu^5 r^2}{z_c^6}\Bigg[6(2z_c^5+3\mu^5)r^{16} - 2\kappa^6(1+\kappa^2)r_c^{14}(2z_c^5+3\mu^5)\sqrt{r^4+\kappa^2 r_c^4}$$
$$- r_c^8\,\kappa^2(1+\kappa^2)\Big\{10(1+\kappa^2)(2z_c^5+3\mu^5)\sqrt{r^4+\kappa^2 r_c^4} + r_c^2\,\kappa^2(8z_c^5+7\mu^5)\Big\}r^6$$
$$- 3\Big\{2(2z_c^5+3\mu^5)\sqrt{r^4+\kappa^2 r_c^4} + r_c^2\,(1+\kappa^2)(8z_c^5+7\mu^5)\Big\}r^{14}$$
$$+ \kappa^4 r_c^{12}\Big\{(4+9\kappa^2+4\kappa^4)(2z_c^5+3\mu^5)\sqrt{r^4+\kappa^2 r_c^4} + r_c^2\,\kappa^2(1+\kappa^2)(8z_c^5+7\mu^5)\Big\}r^2$$
$$- r_c^4\Big\{5r_c^2\,\kappa^2(1+\kappa^2)(8z_c^5+7\mu^5)$$
$$+ \sqrt{r^4+\kappa^2 r_c^4}\,\{2z_c^5(6+19\kappa^2+6\kappa^4) + (-2+17\kappa^2-2\kappa^4)\mu^5\}\Big\}r^{10}$$
$$+ 5r_c^2\Big\{3(1+\kappa^2)(2z_c^5+\mu^5)\sqrt{r^4+\kappa^2 r_c^4} + 2r_c^2(2z_c^5\kappa^2 + (1+5\kappa^2+\kappa^4)\mu^5)\Big\}r^{12}$$
$$- 2r_c^{10}\kappa^4\Big\{(1+\kappa^2)(2z_c^5+3\mu^5)\sqrt{r^4+\kappa^2 r_c^4} + r_c^2(2z_c^5\kappa^2 - (5+7\kappa^2+5\kappa^4)\mu^5)\Big\}r^4$$
$$+ r_c^6\kappa^2\Big\{(1+\kappa^2)(38z_c^5+47\mu^5)\sqrt{r^4+\kappa^2 r_c^4} + 2r_c^2(2z_c^5\kappa^2 + (10+23\kappa^2+10\kappa^4)\mu^5)\Big\}r^8\Bigg]. \tag{5.52}$$

Chapter 6

Simple holographic insulator

6.1 Introduction

Gauge/gravity duality provides a new tool to study strongly correlated systems [192, 193, 194]. In particular, it provides a novel way to study states of matter at zero temperature. Indeed holographic models of superconductors [195], as well as conductors and insulators [196, 197, 198, 199, 200, 201] have all been found, and some have properties similar to what is seen in exotic materials [202, 203].

Previous discussions of holographic insulators fall into three classes. One is based on an asymptotically anti-de Sitter (AdS) solution called the AdS soliton. This solution has a gap for all excitations in the bulk and hence is dual to a gapped system [204, 205]. The second class starts with a system with finite charge density. In this case, translation invariance leads to momentum conservation which implies an infinite DC conductivity, σ_{DC}. (Charge carriers have no way to dissipate their momentum.) If one breaks translation invariance, either explicitly or spontaneously, the DC con-

ductivity is finite. To obtain an insulator, one usually adds a perturbation which becomes large in the IR, leading to a bulk geometry which is singular in the interior. Since $T = 0$, this is not a black hole singularity, but rather a timelike or null naked singularity. Finally, the third class of holographic insulators based on probe D-branes which produce gapped and gapless insulators, see e.g. [206, 207]. These probe models also typically require singular bulk solutions to obtain vanishing conductivity, as in [207].

In this note we show how to obtain a holographic description of an insulator using a nonsingular bulk geometry. Like the AdS soliton, we work at zero net charge density, so we can keep translation invariance and have finite σ_{DC} [1]. However, unlike the approach based on the AdS soliton, at low temperature, the entropy scales like a power of T showing the system is not gapped. The IR geometry is simply another AdS spacetime, so our solution describes a renormalization group flow from one CFT to another. We induce this flow by adding a relevant deformation to the original CFT. We will see that by tuning the interaction between a scalar field and gauge field, we can ensure that $\sigma_{DC} = 0$.

In a little more detail, we construct our holographic insulator by starting with gravity coupled to a scalar field ψ with a "Mexican hat" type potential $V(\psi)$. By modifying the boundary conditions on the scalar in a way corresponding to a relevant double trace deformation, we induce the scalar to turn on at low temperature. The zero temperature solution is then a standard domain wall interpolating between the AdS corresponding to $\psi = 0$ at infinity and the AdS corresponding to the minimum

[1] With an equal number of positive and negative charge carriers, the charge current and momentum decouple since an applied electric field induces a current, but the net momentum stays zero.

of the potential at $\psi = \psi_c$ in the interior (see, e.g., [208]). Finally, we add a Maxwell term to the action with a coefficient $G(\psi)$. This function is chosen to vanish when $\psi = \psi_c$. Since it has been shown that the DC conductivity is simply given by the value of $G(\psi)$ on the horizon [209], it follows immediately that σ_{DC} vanishes at zero temperature and we have an insulator.

We will show that both the DC conductivity at low temperature and the optical conductivity at zero temperature satisfy power laws:

$$\text{Re } \sigma_{DC} \sim T^{2\Delta_\psi} \qquad \lim_{T\to 0} \text{Re } \sigma \sim \omega^{2\Delta_\psi} \tag{6.1}$$

where the exponent Δ_ψ is simply related to the dimension of the operator dual to our scalar in the IR CFT. These results are similar to the behavior found in more complicated constructions of holographic insulators starting with a nonzero charge density [197, 198]. However in those cases the power law is somewhat surprising given the singular nature of the IR geometry, and is the result of an approximate scaling symmetry in an intermediate regime. In contrast, the power law in our case is simply the result of the fact that our low energy theory has no scale.

The organization of this paper is as follows. We will start by introducing our model and discussing how imposing a modified boundary condition for our scalar field can induce an instability which turns on the scalar field. (This corresponds to adding a relevant double-trace deformation of the CFT.) We will then discuss how to compute the conductivity and present both numerical and analytic arguments for the power laws. Finally we show that this same model with a slightly different $G(\psi)$ can also describe a conductor with a standard Drude peak.

6.2 The Model

We will study a $3+1$ dimensional gravitational theory in anti-de Sitter spacetime with a real scalar field ψ and a $U(1)$ gauge field, A_μ. These are dual to a $2+1$ dimensional CFT with a scalar operator $\mathcal{O}$ and a conserved current J^μ, respectively. (The model is easily extended to other dimensions.) The action for these fields is

$$S = \int d^4x\sqrt{-g}\left[R - \frac{1}{4}G(\psi)F^2 - (\nabla\psi)^2 - V(\psi)\right], \tag{6.2}$$

where

$$\begin{aligned} G(\psi) &= (1+g\psi^2)^2, \\ V(\psi) &= -\frac{6}{L^2} + \frac{1}{L^2}\sinh^2(\psi/\sqrt{2})\left[\cosh(\sqrt{2}\psi) - 5\right]. \end{aligned} \tag{6.3}$$

The particular form of $V(\psi)$ is not important. All we need is that it has a local maximum at $\psi = 0$ (with m^2 within a suitable range discussed below), and a global minimum at some nonzero value ψ_c [2]. The particular choice we have made comes from a consistent supergravity truncation [210] and is shown in Fig. 6.1. The particular form of $G(\psi)$ is also not crucial. What we need to model an insulator is a positive function that vanishes at ψ_c. This will hold with the form of G that we have chosen if we set $g = -1/\psi_c^2$. We will see later that this same theory will describe a conductor with standard Drude peak, if we take $g > 0$.

To obtain the background solution, we set $F_{\mu\nu} = 0$ and make an ansatz for an

[2]For stability of the gravity solution, we also require that V can be derived from a certain superpotential, as we will discuss shortly.

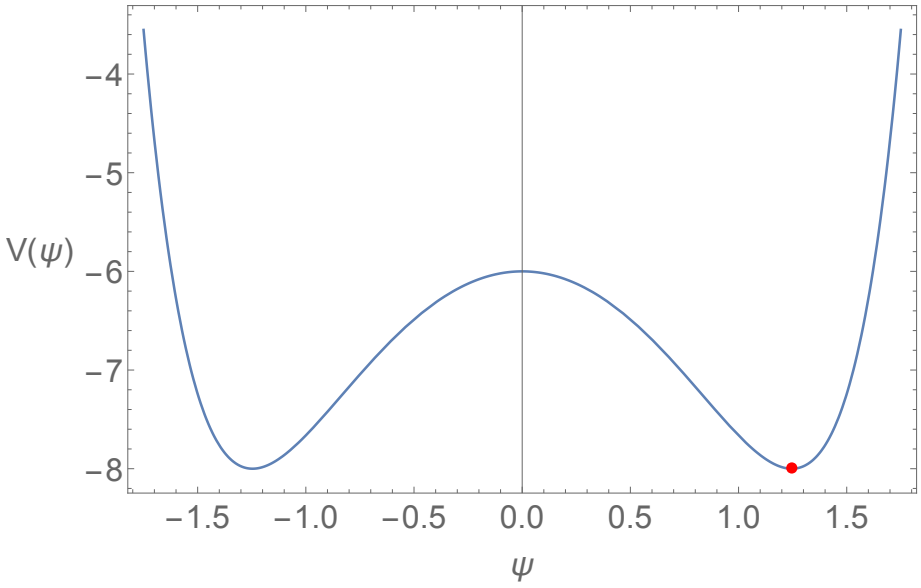

Figure 6.1: A plot of our potential. The minimum is at $\psi_c = \sqrt{2}\ln(1+\sqrt{2})$ with minimum value $V(\psi_c) = -8$.

asymptotically Poincaré AdS_4 metric,

$$ds^2 = -f(r)dt^2 + \frac{dr^2}{f(r)} + h(r)^2 d\vec{x}^{\,2}, \tag{6.4}$$

such that as $r \to \infty$, $f(r) \to r^2/L^2$ and $h(r) \to r/L$. The equations of motion then take the form:

$$\psi''(r) + \left(\frac{f'(r)}{f(r)} + 2\frac{h'(r)}{h(r)}\right)\psi'(r) - \frac{V'(\psi)}{2f(r)} = 0, \tag{6.5a}$$

$$h''(r) + \frac{\psi'(r)^2}{2}h(r) = 0, \tag{6.5b}$$

$$f''(r) + 2\frac{f'(r)h'(r)}{h(r)} + V(\psi(r)) = 0, \tag{6.5c}$$

$$\frac{h'(r)^2}{h(r)} + \frac{f'(r)h'(r)}{f(r)} - \frac{h(r)(\psi'(r))^2}{2} + \frac{h(r)V(\psi)}{2f(r)} = 0. \tag{6.5d}$$

Since we want to consider the low temperature behavior of the conductivity, we are interested in solutions with a small black hole. We will find such solutions numerically by imposing boundary conditions of regularity on the horizon, the above asymptotic conditions on the metric, and a boundary condition for the scalar field which we discuss next.

6.2.1 Double-trace boundary conditions

We can deform our boundary CFT by adding the following double-trace operator to the boundary action,

$$S \to S - \kappa \int d^3x\, \mathcal{O}^2, \tag{6.6}$$

where $\mathcal{O}$ is the operator dual to ψ. This deformation is relevant if the dimension of $\mathcal{O}$ is less than 3/2. If $\kappa > 0$, then this term increases the energy and makes it harder for $\mathcal{O}$ to condense. However, if $\kappa < 0$, we have the opposite behavior and there is some critical temperature T_c below which $\langle\mathcal{O}\rangle \neq 0$ [211]. One might have thought that taking $\kappa < 0$ would destabilize the theory and cause it not to have a stable ground state. However this is not the case. It has been shown that the energy of the

dual gravity solution is still bounded from below, provided V can be derived from a suitable superpotential [212] (which is true for a large class of potentials including the one we have chosen).

Recall that the dimension of the operator $\mathcal{O}$ is related to the mass of the scalar field in the bulk:

$$\Delta_{\pm} = 3/2 \pm \sqrt{9/4 + m^2 L^2} \tag{6.7}$$

and

$$\lim_{r\to\infty} \psi(r) = \frac{\alpha}{r^{\Delta_-}} + \frac{\beta}{r^{\Delta_+}} + ... \tag{6.8}$$

As long as

$$-\frac{9}{4L^2} < m^2 < -\frac{5}{4L^2}, \tag{6.9}$$

both of these modes are normalizable. In order for the operator in (6.6) to be a relevant deformation, we must take $\mathcal{O}$ to have dimension Δ_-.

Our double trace deformation induces the following boundary condition on ψ [213, 214]:

$$\beta = \kappa\alpha. \tag{6.10}$$

Note that expanding our potential in (6.3) to second order in ψ gives a mass $m^2 = -2/L^2$, within the range required by these boundary conditions. Note that this also tells us $\Delta_- = 1, \Delta_+ = 2$, and

$$\langle\mathcal{O}\rangle = \alpha. \tag{6.11}$$

To understand precisely how introducing a double trace deformation with $\kappa < 0$ can cause the Schwarzschild-AdS solution to become unstable at low temperature, we refer the reader to [211]. We will just summarize an important point from that work

motivating the existence of black hole solutions with nonzero scalar field below some critical temperature T_c.

At finite temperature with no scalar field, the spacetime is described by planar AdS-Schwarzschild in $3+1$ dimensions,[3]

$$\begin{aligned} ds^2 &= -f(r)dt^2 + \frac{dr^2}{f(r)} + r^2 d\vec{x}^2, \\ \text{where } f(r) &= r^2\left(1 - \frac{r_0^3}{r^3}\right). \end{aligned} \tag{6.12}$$

with a temperature, $T = 3r_0/4\pi$. We would like to find a condition for when the scalar field can be non-zero. At small values of ψ our potential is approximately $V(\psi) \approx -6 - 2\psi^2 + \mathcal{O}(\psi^4)$. Neglecting the higher order terms, we can exactly solve the scalar wave equation in the AdS-Schwarzschild background:

$$\psi(r) = c_1\left(\frac{r_0}{r}\right)\ {}_2F_1\left[\frac{1}{3}, \frac{1}{3}, \frac{2}{3}, \left(\frac{r_0}{r}\right)^3\right] + c_2\left(\frac{r_0}{r}\right)^2\ {}_2F_1\left[\frac{2}{3}, \frac{2}{3}, \frac{4}{3}, \left(\frac{r_0}{r}\right)^3\right]. \tag{6.13}$$

For this solution to be well behaved on the horizon, we need

$$\frac{c_2}{c_1} = -\frac{\Gamma(2/3)^3}{\Gamma(4/3)\Gamma(1/3)^2} \tag{6.14}$$

to cancel the diverging logarithmic pieces from the hypergeometric functions. The large r expansion of ψ gives

$$\lim_{r\to\infty} \psi(r) = c_1 r_0/r + c_2(r_0/r)^2 + ... \tag{6.15}$$

[3]From here on, we set $L = 1$.

which, written in terms of the multitrace boundary condition gives,

$$\frac{\beta}{\alpha} = \kappa = \frac{c_2}{c_1}(4\pi T/3). \tag{6.16}$$

Since κ is negative and has the same dimensions as temperature, it is convenient to work with the (positive) dimensionless quantity $T/(-\kappa)$. Using (6.14) and (6.17) one finds the critical value at which the static scalar field with double-trace boundary conditions is regular on the horizon:

$$\frac{T_c}{(-\kappa)} = \frac{3}{4\pi}\left(\frac{\Gamma(4/3)\Gamma(1/3)^2}{\Gamma(2/3)^3}\right). \tag{6.17}$$

This corresponds to a critical temperature of $T_c/(-\kappa) \approx .616$. So for any $\kappa < 0$, when $T = T_c$ there is a static linearized mode of the scalar field. This signals the onset of an instability to forming scalar hair. At lower temperature, the scalar field is nonzero outside the black hole. From its asymptotic value, one finds that $\langle \mathcal{O} \rangle$ increases as we lower T and approaches a constant as $T \to 0$ (see Fig. 6.2).

6.2.2 Solutions

Lowering the temperature (or equivalently, decreasing κ) below its critical value causes the scalar field to roll down the potential $V(\psi)$. Since we have chosen $V(\psi)$ (6.3) to have a global minimum at ψ_c, as $T \to 0$ the value of the the scalar on the horizon approaches ψ_c. The zero temperature solution is thus a renormalization group flow from an asymptotic AdS_4 as $r \to \infty$ to a new AdS_4 in the IR as $r \to 0$ whose length scale is determined by the minimum value of the potential. Furthermore, the scalar field will have a new mass given by oscillations about this global minimum

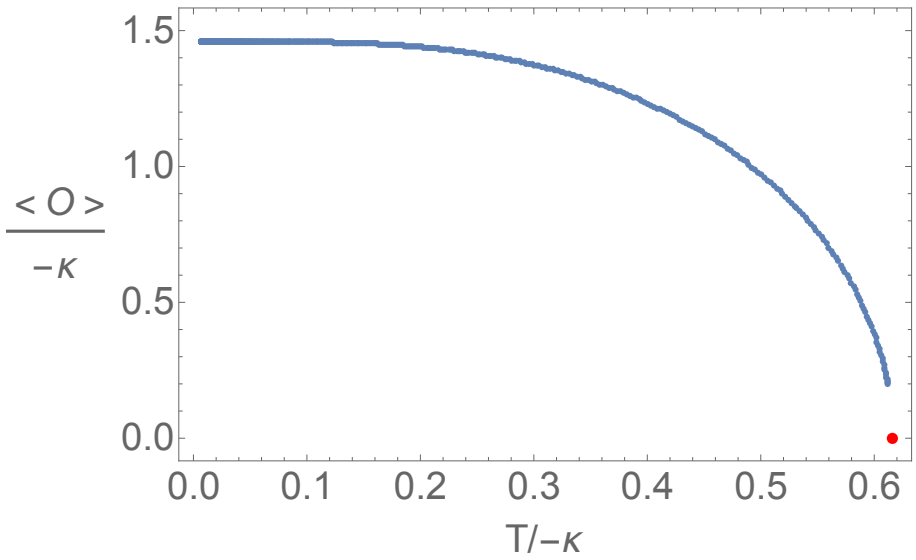

Figure 6.2: The value of $\langle \mathcal{O} \rangle$ vs. $T/(-\kappa)$ with critical value $T_c/(-\kappa) \approx .616$.

which governs its scaling dimension in the deep IR. Expanding about the global minimum of (6.3), we see

$$V(\psi_c + \delta\psi) = -8 + 8\delta\psi^2 + ... \tag{6.18}$$

Setting $V(\psi_c) = -6/L_{IR}^2$, so L_{IR} is the AdS radius in the IR, we have $L_{IR}^2 = 3/4$. Using this, we find from (6.7) that

$$\Delta_{\pm}^{IR} = \frac{3}{2} \pm \sqrt{9/4 + m_{IR}^2 L_{IR}^2} = \frac{3 \pm \sqrt{33}}{2}. \tag{6.19}$$

At zero temperature, the only normalizable solution in the IR scales like

$$\delta\psi(r) \equiv \psi_c - \psi(r) \sim r^{\Delta_\psi}, \quad \text{with} \quad \Delta_\psi \equiv -\Delta_-^{IR} \approx 1.37228. \tag{6.20}$$

At very low temperature, the black hole horizon is at small r_0 where the scalar field is essentially constant $\psi \approx \psi_c$. One thus expects that the spacetime should look like planar AdS-Schwarzschild with the replacement $L^2 \to L_{IR}^2$. One also expects that the scalar field will not be modified much by the horizon, so that the value of the scalar field on the horizon will scale like $\delta\psi(r) \sim r_0^{\Delta_\psi}$.

To check these expectations we solve the equations numerically. (See the end of the next section for a brief discussion of our numerical methods.) As shown in Fig. 6.3 our results confirm these expections. In the top figure, we show a plot of the metric function $f(r)$, and on the bottom is a plot of the scalar field evaluated on the horizon. The black hole has a temperature $T = 3r_0/4\pi L_{IR}^2 = r_0/\pi$, and an entropy scaling like $S \sim T^2$.

6.3 Conductivity

Since our dual theory is conformally invariant in the IR, we would expect the conductivity to be characterized by power laws. We now demonstrate this is the case. As usual, to calculate the conductivity, we perturb our spacetime with a harmonically time varying electric field. To do so, we introduce $\delta A_x = a_x(r)e^{-i\omega t}$. This perturbation back reacts to give at first order a metric perturbation δg_{tx} with no other metric components being affected. Einstein's equation for this component of the metric and the equation of motion for a_x give two coupled second order ODE's which can be combined to give the following equation for a_x,

$$a_x''(r) + \left(\frac{f'(r)}{f(r)} + \frac{G'(\psi)\psi'(r)}{G(\psi)}\right) a_x'(r) + \frac{\omega^2}{f(r)^2} a_x(r) = 0. \tag{6.21}$$

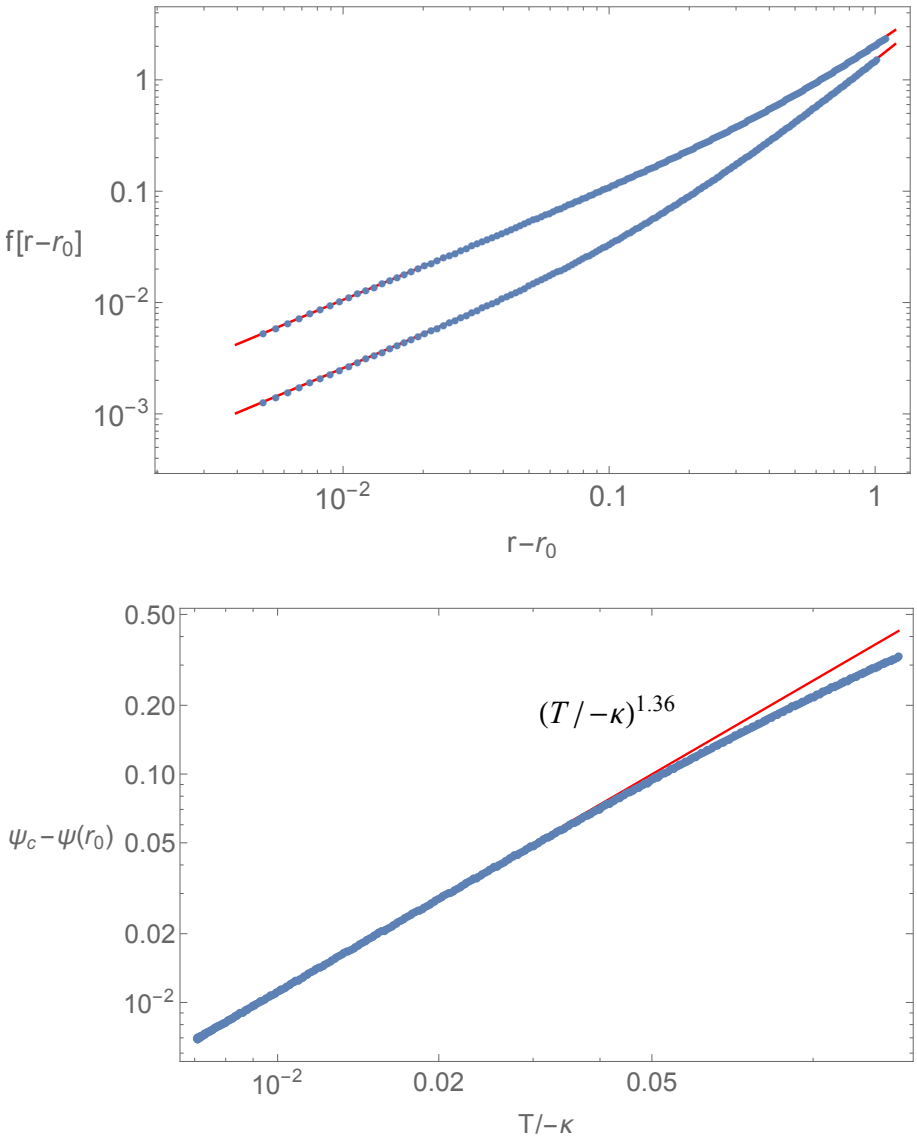

Figure 6.3: (Top figure) Log-log plot of our numerical solution for $f(r)$ in the IR (blue dots). The red line (which goes through all the points) is the analytic planar AdS-Schwarzschild solution. The two curves correspond to $T/(-\kappa) = .037$ (top) and $T/(-\kappa) = 7.06 \times 10^{-3}$ (bottom). One can see the transition from the linear Schwarzschild behavior to the quadratic AdS_4 behavior. (Bottom figure) The scalar field on the horizon as a function of temperature. At low T, it scales like T^{Δ_ψ}.

We can solve this equation numerically using our background solution subject to the boundary condition that the gauge field is ingoing at the horizon [215]. The asymptotic behavior of a_x is given by

$$\lim_{r\to\infty} a_x(r) = a_x^{(0)} + \frac{a_x^{(1)}}{r} + ... \tag{6.22}$$

When our perturbation corresponds to an applied electric field E with harmonic time dependence, then $a_x^{(0)} = -iE/\omega$ and gauge/gravity duality implies [192] $a_x^{(1)} = \langle J \rangle$ so that our conductivity is given by

$$\sigma(\omega) = \frac{a_x^{(1)}}{i\omega a_x^{(0)}}. \tag{6.23}$$

6.3.1 DC conductivity

As first realized by Iqbal and Liu [209], low frequency limits of transport coefficients in the dual field theory are determined by the horizon geometry of the gravity dual. This is a holographic application of the "membrane paradigm" of classical black holes. Applied to a $U(1)$ gauge field, this implies that the DC conductivity is given by the coefficient of the gauge field kinetic term evaluated on the horizon. To see this, assume $T > 0$ and consider the $\omega \ll T$ limit of eq. (6.21). In this limit, the last term can be neglected[4] so that the equation can be rewritten

$$\frac{1}{f(r)G(\psi)}[f(r)G(\psi)a_x'(r)]' = 0. \tag{6.24}$$

[4]Even though this term diverges at the horizon, at nonzero temperature $f(r)$ vanishes linearly, so the horizon is a regular singular point of (6.21). This is no longer true when $T = 0$.

Now, on the boundary, the conserved quantity in this equation becomes

$$\lim_{r\to\infty} f(r)G(\psi)a_x'(r) = r^2\left(\frac{-\langle J\rangle}{r^2}\right) = -\langle J\rangle. \tag{6.25}$$

Normally, we would have to solve eq. (6.21) numerically to find $\langle J\rangle$. However, because this is conserved in the DC limit, we can evaluate it on the horizon,

$$\lim_{r\to r_0} f(r)G(\psi)a_x'(r) = (1+g\psi^2)^2 f(r)a_x'(r)|_{r=r_0}. \tag{6.26}$$

Now, our ingoing boundary conditions tell us that on the horizon, a_x must be a function of the tortoise coordinate, $dr_* = dr/f(r)$ in the combination $v = t + r_*$[5]. This allows us to relate time derivatives to radial derivatives,

$$\partial_t a_x(u)|_{r=r_0} = \partial_v a_x|_{r=r_0} = f(r)\partial_r a_x|_{r=r_0}, \tag{6.27}$$

so that eq. (6.26) becomes

$$\langle J\rangle = -(1+g\psi(r_0)^2)^2\partial_t a_x(r)|_{r=r_0}. \tag{6.28}$$

In the low frequency limit, $dF = 0$ implies that the electric field is essentially constant. We can thus evaluate it near the horizon and see that

$$\begin{aligned}\sigma_{DC} &= \lim_{\omega\to 0}\sigma(\omega) = \frac{i\omega a_x(r_0)(1+g\psi(r_0))^2}{i\omega a_x(r_0)}\\ &= [1+g\psi(r_0)^2]^2.\end{aligned} \tag{6.29}$$

[5]This is of course only valid at nonzero ω where we have harmonic time dependence. We compute the low frequency conductivity and then take $\omega \to 0$.

If we choose $g = -1/\psi_c^2$, then at very low temperatures, with our AdS-Schwarzschild domain wall solution (6.20), we have

$$\sigma_{DC} \sim (\delta\psi(r_0)/\psi_c)^2 \sim r_0^{2\Delta_\psi} \sim T^{2\Delta_\psi}. \tag{6.30}$$

6.3.2 Optical conductivity

We now investigate how the choice of $g = -1/\psi_c^2$ affects the zero temperature optical conductivity. At zero temperature, we have purely AdS_4 in the IR part of the domain wall. In this background, equation (6.21) can be solved exactly to give,

$$a_x(r) \sim i(\omega L_{IR}^2 r)^{-(1+2\Delta_\psi)/2} H^{(1)}_{\frac{1+2\Delta_\psi}{2}}\left(\frac{\omega L_{IR}^2}{r}\right), \tag{6.31}$$

where we have written the solution in terms of a Hankel function, such that as we approach the Poincaré horizon in the IR,

$$H^{(1)}_{\frac{1+2\Delta_\psi}{2}}\left(\frac{\omega L_{IR}^2}{r}\right) \sim \sqrt{\frac{\pi r}{\omega L_{IR}^2}} e^{i\omega L_{IR}^2/r} = i\sqrt{\frac{\pi}{r_*}} e^{-i\omega r_*}. \tag{6.32}$$

as required. Now, it is worth pointing out two important features of this solution. The first is that, because we have a domain wall, this solution only holds for $r < r_D$, where r_D is the location of the domain wall, which must be found numerically. The second point is that the solution above is the zero temperature solution. But we have seen that at low temperature, in the region $r_0 \ll r \ll r_D$ the spacetime is essentially AdS_4, and we have checked numerically that the above solution is still valid.

To calculate the optical conductivity, we will use the matched asymptotic expansion of Gubser and Rocha [216]. The basis of this analysis rests on the presence of a

conserved flux,

$$\mathcal{F} = -fG(\psi)a_x^* \overleftrightarrow{\partial_r} a_x. \tag{6.33}$$

One can check that $\partial_r \mathcal{F}$ does indeed vanish by using the equation of motion (6.21). In the UV, this conserved flux gives

$$\lim_{r\to\infty} \mathcal{F} = -a_x^{(0)} a_x^{(1)*} + a_x^{(0)*} a_x^{(1)}. \tag{6.34}$$

From this we see that we can calculate the real part of the conductivity

$$Re[\sigma(\omega)] = \lim_{r\to\infty} \frac{\mathcal{F}}{2i\omega |a_x^{(0)}|^2}. \tag{6.35}$$

To determine this analytically, we need to find $a_x^{(0)}$. This is possible because we note that in the DC limit (at low temperature), (6.24) allows for $a_x(r)$ to have a constant piece which is undetermined by the equation of motion. However, the low frequency limit of (6.31) should smoothly match onto the DC solution and horizon boundary conditions allow us to fix this constant. A general solution of the DC equation (6.24) in the region $r_0 \ll r \ll r_D$ has the form

$$a_x(r) = Cr^{-(1+2\Delta_\psi)} + D. \tag{6.36}$$

Expanding (6.31) for small $\omega L_{IR}^2/r$, we see

$$a_x(r) \sim (\omega L_{IR}^2)^{-(1+2\Delta_\psi)} \left[\frac{(i + \tan(\Delta_\psi \pi))}{\Gamma(\frac{3+2\Delta_\psi}{2}) 2^{(1+2\Delta_\psi)/2}} (\frac{\omega L_{IR}^2}{r})^{1+2\Delta_\psi} + \frac{2^{(1+2\Delta_\psi)/2}}{\pi} \Gamma(\frac{1+2\Delta_\psi}{2}) \right], \tag{6.37}$$

where we have pulled out an ω dependence as an overall normalization. The expression inside the brackets is matched to the DC solution at low temperature. The second piece corresponds to the D term. Because it has no r dependence, its value in the IR part of the domain wall must match the value in the UV which is $a_x^{(0)}$. We can then use (6.37) to evaluate the conserved flux in a region $r_0 \ll r \ll r_D$. Finally, because the real part of the conductivity is the ratio of two conserved quantities, evaluating these quantites in this region is equivalent to computing the conductivity on the boundary. Doing so gives a power law in the low temperature optical conductivity,

$$\lim_{T\to 0} Re[\sigma] \sim \frac{i\omega^{-(1+2\Delta_\psi)}}{i\omega(\omega^{-2(1+2\Delta_\psi)})} = \omega^{2\Delta_\psi}. \tag{6.38}$$

This behavior is confirmed by our numerical solutions as shown in Fig. 6.4.

6.3.3 Comment on numerical methods

The equations of motion (6.5) and (6.21) are second order differential equations. At non-zero temperatures, these lend themselves well to pseudospectral methods [217, 218]. It is well-known that low temperature black holes are difficult to study numerically because as $T \to 0$, the metric function $f(r)$ vanishes quadratically. For this reason, we found that for low temperatures, we needed a 400 point Chebyshev grid to minimize numerical noise and optimize precision in computing the conductivity. For our pseudospectral methods to cover the full spacetime, we used a variable $z \equiv 1/r$ and rescaled the horizon to $r_0 = 1$. After solving the equations of motion, we rescaled the horizon back to the proper $r_0 = \pi T$. Furthermore, because we fixed

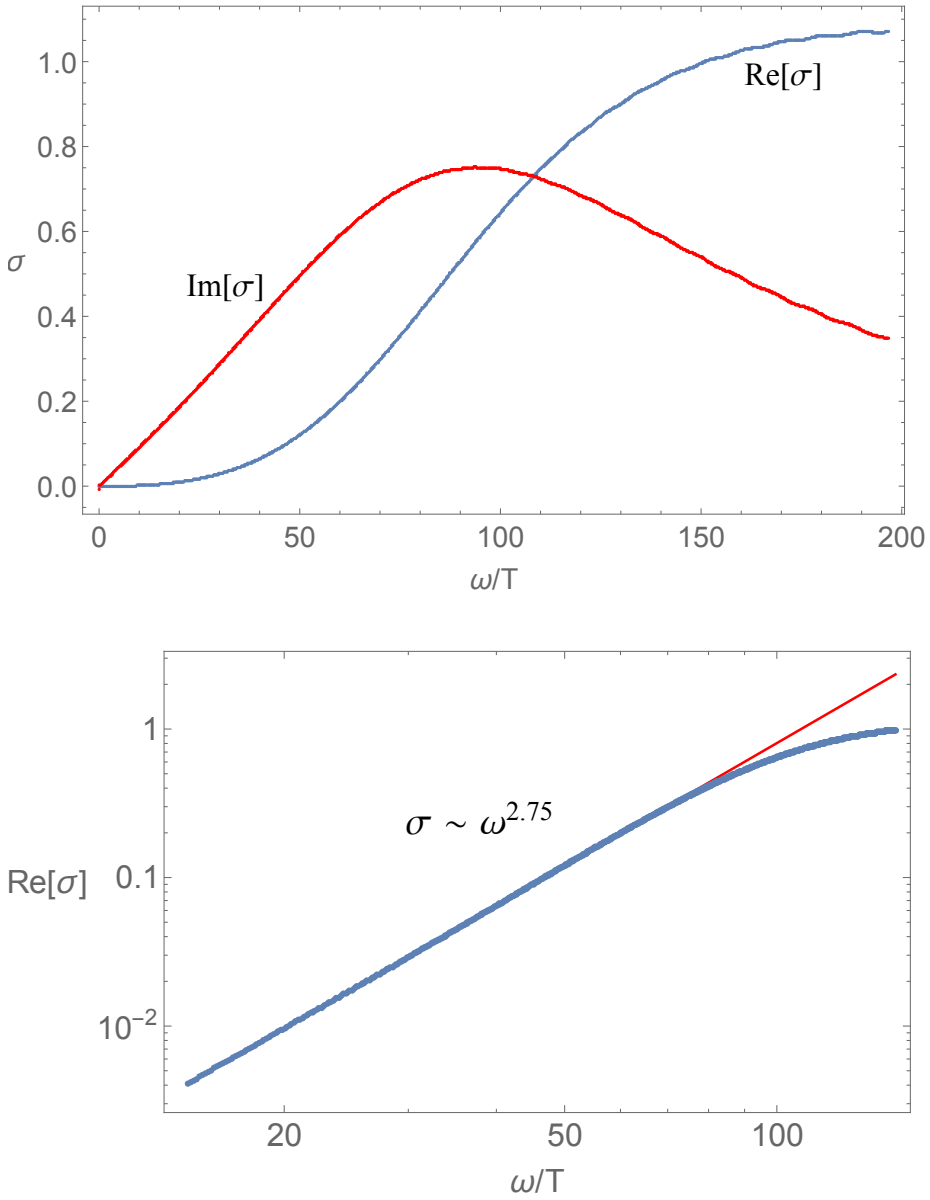

Figure 6.4: (Top figure) A plot of the optical conductivity at $T/(-\kappa) = 7.06 \times 10^{-3}$ and $g = g_c$. The imaginary component vanishes as $\omega \to 0$ rather than diverging as ω^{-1} showing that there is no $\delta(\omega)$ in $\mathrm{Re}[\sigma(\omega)]$. (Bottom figure) Log-log plot of the real component of the optical conductivity above. The line of best fit gives $\sigma \sim \omega^{2.75}$. Our analytic solution says that it should be a power law with an exponent $2\Delta_\psi \approx 2.744$.

r_0, our temperature was varied by adjusting the parameter κ in the boundary conditions for our scalar field. All data showing the temperature dependence is plotted in terms of the dimensionless quantity $T/(-\kappa)$. Finally, we rescaled our functions $f(z) \to F(z)/z^2$ and $h(z) \to H(z)/z$ to be well behaved at the conformal boundary $z \to 0$. We also rescaled the gauge field $a_x(z) \to e^{-i\omega z_*} A_x(z)$ to be better behaved on the horizon. The appropriate boundary condition for the redefined functions are $F'(0) = H'(0) = 0$ on the boundary and $F(1)A'_x(1) = 0$ corresponding to ingoing boundary conditions at the horizon.

6.4 Discussion

We have presented a nonsingular holographic model of an insulator. A key parameter in the model, g, controls the coupling between the kinetic term for the gauge field and a neutral scalar field. A scalar potential with a global minimum at $\psi = \psi_c$ allows us to define a critical $g_c = -1/\psi_c^2$ such that the dual theory has a DC conductivity that goes to zero as a power of the temperature T. This same critical g_c produces a zero temperature optical conductivity that also vanishes as a power of ω. Both exponents agree and are given by the scaling dimension of the scalar field in the IR. This behavior has also been seen in models with nonzero charge density and broken translation invariance [202, 196, 198, 199].

A class of holographic insulators based on probe branes shares similar features with our model–in particular, gapless power law conductivities [207]. One embeds a Dp-brane with non-zero electric flux in a four-dimensional asymptotically AdS spacetime. A radially varying dilaton couples to the Maxwell term in the linearized DBI

action mimicing the $G(\psi)$ term in our action above. The authors of [207] then choose a dilaton profile (eq. (3.44) in their paper) which results in a power law AC conductivity they characterize as a pseudogap insulator. By choosing other dilaton profiles, they can also produce a soft-gap and hard-gap insulators. However, the vanishing conductivity requires a diverging dilaton, whereas our choice of potential keeps the scalar field finite. One useful feature of this comparison is that the authors of [207] point out that the Dp-brane construction does not have a delta function in the real part of the conductivity because the scalar field couples to the A_x' term, just as ours does in (6.21) and not to the A_x term as in AdS-RN constructions. This is easily seen in Fig. 6.4 where the imaginary component vanishes linearly as $\omega \to 0$.

We now ask what happens for other values of g. We know that $g \to g_c$ effectively increases the interactions between the charge carriers causing $\sigma_{DC} \to 0$. As we increase g, σ_{DC} also increases. It reaches one when $g = 0$, which is expected since this is the standard value for the conductivity in AdS-Schwarzschild, and $g = 0$ turns off the coupling between the scalar and gauge field. For $g > 0$, $\sigma_{DC} > 1$. For large g there is a pronounced Drude peak showing that we have a standard metal. This is illustrated in Fig. 6.5.

In Fig. 6.6 on the left, we have plotted our numerical results for the DC resistivity, $\Omega \equiv 1/\sigma_{DC}$, as a function of temperature for different values of $g \geq g_c$. Just for fun, on the right is experimental data from a Bose metal [220]. Bose metallicity is a unique phase exhibited by certain thin film materials which also exhibit high temperature superconductivity. These materials are characterized by strong interactions among their charge carrying quasiparticles and conductivity along two-dimensional planes. By applying a magnetic field transverse to these planes or by adjusting the thickness

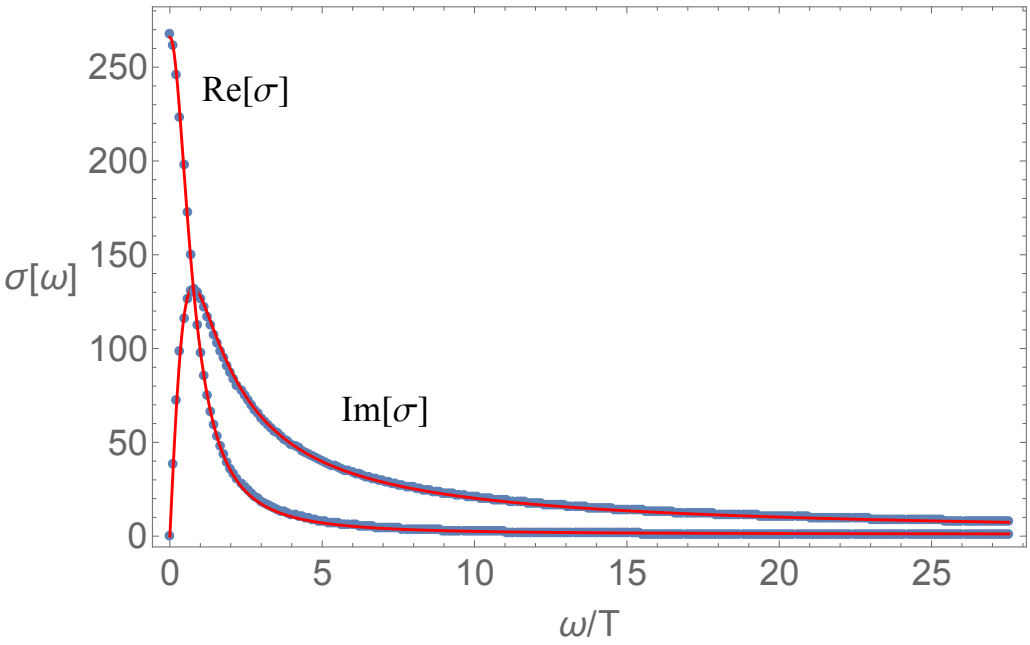

Figure 6.5: Fit of optical conductivity to a Drude type curve, $\sigma(\omega) = \frac{K\tau}{1-i\omega\tau}$. For this plot, we chose $g = 10$ at a temperature $T/(-\kappa) = .037$, and found $K = 540$, $\tau = .485$.

of the thin films, one can create a phase where Cooper pairs (bosons) have condensed but the global $U(1)$ symmetry has not been broken [6]. The lack of phase coherence gives a finite DC conductivity, hence the name Bose metal.

The two sets of curves in Fig. 6.6 show an interesting similarity. However, the experimental curves on the right are obtained by increasing the thickness of a thin film while on the left we are changing a parameter in the bulk Lagrangian and therefore modifying the $2+1$ boundary theory. To better describe a Bose metal, we would need to tune a parameter in the boundary theory instead of the bulk. This could be done by introducing a new bulk field which couples to ψ and effectively modifies

[6] This effect is unique to two (spatial) dimensions where phase coherence fall-offs are algebraic, $G(r) \sim r^{-\eta}$ with $0 < \eta < 1$ [220]

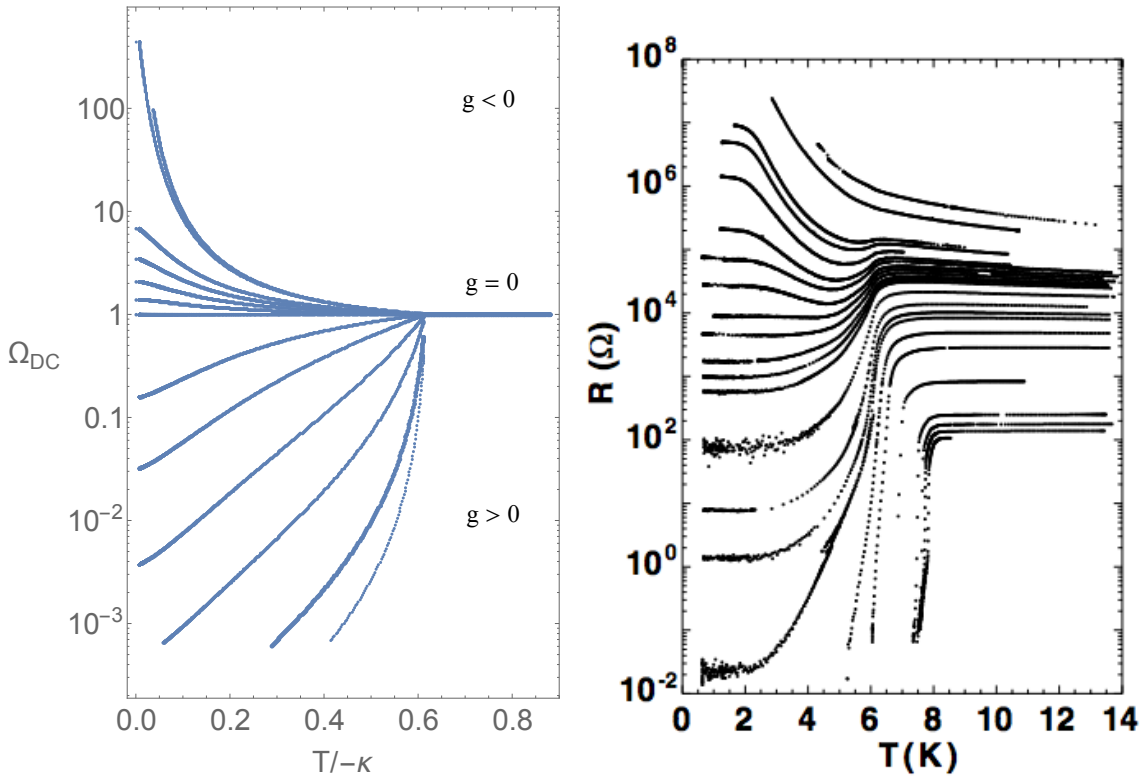

Figure 6.6: (Left) Plot of DC resistivity vs. temperature for different values of our tuning parameter $-1/\psi_c^2 < g < 200$. (Right) Numerical data from [219] showing the DC resistivity of a Ga thin film. The resistivity increases as the thickness of the thin film is decreased (bottom to top).

its potential to have a new minimum at $\psi_c' < \psi_c$. Certain holographic lattice models [198, 199] seem capable of such a deformation.

6.5 Acknowledgments

We would like to thank G. Hartnett and B. Way for help with numerics. This work was supported in part by NSF grant PHY12-05500.

Bibliography

[1] E. Mefford and G. T. Horowitz, *Simple holographic insulator*, *Phys. Rev.* **D90** (2014), no. 8 084042, [arXiv:1406.4188].

[2] E. Mefford, *Entanglement Entropy in Jammed CFTs*, *JHEP* **09** (2017) 006, [arXiv:1605.0936].

[3] M. Srednicki, *Quantum field theory*. Cambridge University Press, 2007.

[4] A. Deur, S. J. Brodsky, and G. F. de Teramond, *The QCD Running Coupling*, *Prog. Part. Nucl. Phys.* **90** (2016) 1–74, [arXiv:1604.0808].

[5] J. M. Maldacena, *The Large N limit of superconformal field theories and supergravity*, *Int. J. Theor. Phys.* **38** (1999) 1113–1133, [hep-th/9711200]. [Adv. Theor. Math. Phys.2,231(1998)].

[6] E. Witten, *Geometric Langlands From Six Dimensions*, arXiv:0905.2720.

[7] O. Aharony, S. S. Gubser, J. M. Maldacena, H. Ooguri, and Y. Oz, *Large N field theories, string theory and gravity*, *Phys. Rept.* **323** (2000) 183–386, [hep-th/9905111].

[8] S. S. Gubser, I. R. Klebanov, and A. M. Polyakov, *Gauge theory correlators from noncritical string theory*, *Phys. Lett.* **B428** (1998) 105–114, [hep-th/9802109].

[9] S. A. Hartnoll, A. Lucas, and S. Sachdev, *Holographic quantum matter*, arXiv:1612.0732.

[10] P. Kovtun, D. T. Son, and A. O. Starinets, *Viscosity in strongly interacting quantum field theories from black hole physics*, *Phys. Rev. Lett.* **94** (2005) 111601, [hep-th/0405231].

[11] V. E. Hubeny, S. Minwalla, and M. Rangamani, *The fluid/gravity correspondence*, in *Black holes in higher dimensions*, pp. 348–383, 2012. arXiv:1107.5780. [,817(2011)].

[12] E. Witten, *Anti-de Sitter space, thermal phase transition, and confinement in gauge theories*, *Adv. Theor. Math. Phys.* **2** (1998) 505–532, [hep-th/9803131].

[13] J. M. Maldacena, *Eternal black holes in anti-de Sitter*, *JHEP* **04** (2003) 021, [hep-th/0106112].

[14] T. Hartman, C. A. Keller, and B. Stoica, *Universal Spectrum of 2d Conformal Field Theory in the Large c Limit*, *JHEP* **09** (2014) 118, [arXiv:1405.5137].

[15] J. McGreevy, L. Susskind, and N. Toumbas, *Invasion of the giant gravitons from Anti-de Sitter space*, *JHEP* **06** (2000) 008, [hep-th/0003075].

[16] P. Figueras, J. Lucietti, and T. Wiseman, *Ricci solitons, Ricci flow, and strongly coupled CFT in the Schwarzschild Unruh or Boulware vacua*, *Class. Quant. Grav.* **28** (2011) 215018, [arXiv:1104.4489].

[17] and, *On crossing the cauchy horizon of a reissner–nordström black-hole*, *Proceedings of the Royal Society of London A: Mathematical, Physical and Engineering Sciences* **384** (1982), no. 1787 301–315, [http://rspa.royalsocietypublishing.org/content/384/1787/301.full.pdf].

[18] W. A. Hiscock, *Stress Energy Tensor Near a Charged, Rotating, Evaporating Black Hole*, *Phys. Rev.* **D15** (1977) 3054–3057.

[19] W. A. Hiscock and D. A. Konkowski, *QUANTUM VACUUM ENERGY IN TAUB - NUT (NEWMAN-UNTI-TAMBURINO) TYPE COSMOLOGIES*, *Phys. Rev.* **D26** (1982) 1225–1230.

[20] R. M. Wald, *General Relativity*. Chicago, Usa: Univ. Pr. (1984) 491p, 1984.

[21] J. G. Bednorz and K. A. Müller, *Possible hightc superconductivity in the balacuo system*, *Zeitschrift für Physik B Condensed Matter* **64** (Jun, 1986) 189–193.

[22] P. W. ANDERSON, *The resonating valence bond state in la2cuo4 and superconductivity*, *Science* **235** (1987), no. 4793 1196–1198, [http://science.sciencemag.org/content/235/4793/1196.full.pdf].

[23] G. T. Horowitz and A. Strominger, *Black strings and p-branes*, *Nuclear Physics B* **360** (1991), no. 1 197 – 209.

[24] J. Maldacena and D. Stanford, *Remarks on the Sachdev-Ye-Kitaev model*, *Phys. Rev.* **D94** (2016), no. 10 106002, [arXiv:1604.0781].

[25] J. Polchinski and V. Rosenhaus, *The Spectrum in the Sachdev-Ye-Kitaev Model*, *JHEP* **04** (2016) 001, [arXiv:1601.0676].

[26] E. Witten, *Anti-de Sitter space and holography*, *Adv. Theor. Math. Phys.* **2** (1998) 253–291, [hep-th/9802150].

[27] J. Penedones, *TASI lectures on AdS/CFT*, in *Proceedings, Theoretical Advanced Study Institute in Elementary Particle Physics: New Frontiers in Fields and Strings (TASI 2015): Boulder, CO, USA, June 1-26, 2015*, pp. 75–136, 2017. arXiv:1608.0494.

[28] G. T. Horowitz and D. Marolf, *A New approach to string cosmology*, *JHEP* **07** (1998) 014, [hep-th/9805207].

[29] S. W. Hawking and G. F. R. Ellis, *The Large Scale Structure of Space-Time*. Cambridge Monographs on Mathematical Physics. Cambridge University Press, 2011.

[30] J. Maldacena, D. Simmons-Duffin, and A. Zhiboedov, *Looking for a bulk point*, *JHEP* **01** (2017) 013, [arXiv:1509.0361].

[31] N. Engelhardt and G. T. Horowitz, *Towards a Reconstruction of General Bulk Metrics*, *Class. Quant. Grav.* **34** (2017), no. 1 015004, [arXiv:1605.0107].

[32] G. 't Hooft, *The Holographic principle: Opening lecture*, *Subnucl. Ser.* **37** (2001) 72–100, [hep-th/0003004].

[33] L. Susskind, *The World as a hologram*, *J. Math. Phys.* **36** (1995) 6377–6396, [hep-th/9409089].

[34] S. W. Hawking, *Breakdown of Predictability in Gravitational Collapse*, *Phys. Rev.* **D14** (1976) 2460–2473.

[35] J. D. Bekenstein, *Black holes and entropy*, *Phys. Rev. D* **7** (Apr, 1973) 2333–2346.

[36] R. Nandkishore and D. A. Huse, *Many body localization and thermalization in quantum statistical mechanics*, *Ann. Rev. Condensed Matter Phys.* **6** (2015) 15–38, [arXiv:1404.0686].

[37] M. Srednicki, *Entropy and area*, *Phys. Rev. Lett.* **71** (1993) 666–669, [hep-th/9303048].

[38] L. Susskind and J. Uglum, *Black hole entropy in canonical quantum gravity and superstring theory*, *Phys. Rev.* **D50** (1994) 2700–2711, [hep-th/9401070].

[39] D. N. Kabat, *Black hole entropy and entropy of entanglement*, *Nucl. Phys.* **B453** (1995) 281–299, [hep-th/9503016].

[40] S. N. Solodukhin, *Entanglement entropy of black holes*, *Living Rev. Rel.* **14** (2011) 8, [arXiv:1104.3712].

[41] R. Bousso, H. Casini, Z. Fisher, and J. Maldacena, *Proof of a Quantum Bousso Bound*, *Phys. Rev.* **D90** (2014), no. 4 044002, [arXiv:1404.5635].

[42] S. Ryu and T. Takayanagi, *Holographic derivation of entanglement entropy from AdS/CFT*, *Phys. Rev. Lett.* **96** (2006) 181602, [hep-th/0603001].

[43] V. E. Hubeny, M. Rangamani, and T. Takayanagi, *A Covariant holographic entanglement entropy proposal*, *JHEP* **07** (2007) 062, [arXiv:0705.0016].

[44] H. Casini, M. Huerta, and J. A. Rosabal, *Remarks on entanglement entropy for gauge fields*, *Phys. Rev.* **D89** (2014), no. 8 085012, [arXiv:1312.1183].

[45] S. B. Giddings, *Hilbert space structure in quantum gravity: an algebraic perspective*, *JHEP* **12** (2015) 099, [arXiv:1503.0820].

[46] A. B. Zamolodchikov, *Irreversibility of the Flux of the Renormalization Group in a 2D Field Theory*, *JETP Lett.* **43** (1986) 730–732. [Pisma Zh. Eksp. Teor. Fiz.43,565(1986)].

[47] A. Almheiri, D. Marolf, J. Polchinski, and J. Sully, *Black Holes: Complementarity or Firewalls?*, *JHEP* **02** (2013) 062, [arXiv:1207.3123].

[48] N. Bao, S. Nezami, H. Ooguri, B. Stoica, J. Sully, and M. Walter, *The Holographic Entropy Cone*, *JHEP* **09** (2015) 130, [arXiv:1505.0783].

[49] C. Holzhey, F. Larsen, and F. Wilczek, *Geometric and renormalized entropy in conformal field theory*, *Nucl. Phys.* **B424** (1994) 443–467, [hep-th/9403108].

[50] P. Calabrese and J. Cardy, *Entanglement entropy and conformal field theory*, *J. Phys.* **A42** (2009) 504005, [arXiv:0905.4013].

[51] G. Vidal, J. I. Latorre, E. Rico, and A. Kitaev, *Entanglement in quantum critical phenomena*, *Phys. Rev. Lett.* **90** (2003) 227902, [quant-ph/0211074].

[52] J. D. Brown and M. Henneaux, *Central charges in the canonical realization of asymptotic symmetries: an example from three-dimensional gravity*, *Comm. Math. Phys.* **104** (1986), no. 2 207–226.

[53] J. Koeller and S. Leichenauer, *Holographic Proof of the Quantum Null Energy Condition*, *Phys. Rev.* **D94** (2016), no. 2 024026, [arXiv:1512.0610].

[54] W. R. Kelly and A. C. Wall, *Holographic proof of the averaged null energy condition*, *Phys. Rev.* **D90** (2014), no. 10 106003, [arXiv:1408.3566]. [Erratum: Phys. Rev.D91,no.6,069902(2015)].

[55] H. Casini, E. Teste, and G. Torroba, *Relative entropy and the RG flow*, *JHEP* **03** (2017) 089, [arXiv:1611.0001].

[56] H. Casini and M. Huerta, *A Finite entanglement entropy and the c-theorem*, *Phys. Lett.* **B600** (2004) 142–150, [hep-th/0405111].

[57] H. Casini, M. Huerta, R. C. Myers, and A. Yale, *Mutual information and the F-theorem*, *JHEP* **10** (2015) 003, [arXiv:1506.0619].

[58] M. Taylor and W. Woodhead, *Renormalized entanglement entropy*, *JHEP* **08** (2016) 165, [arXiv:1604.0680].

[59] N. Engelhardt and A. C. Wall, *Extremal Surface Barriers*, *JHEP* **03** (2014) 068, [arXiv:1312.3699].

[60] M. Bañados, C. Teitelboim, and J. Zanelli, *Black hole in three-dimensional spacetime*, *Phys. Rev. Lett.* **69** (Sep, 1992) 1849–1851.

[61] B. Czech, J. L. Karczmarek, F. Nogueira, and M. Van Raamsdonk, *The Gravity Dual of a Density Matrix*, *Class. Quant. Grav.* **29** (2012) 155009, [arXiv:1204.1330].

[62] A. Strominger and C. Vafa, *Microscopic origin of the Bekenstein-Hawking entropy*, *Phys. Lett.* **B379** (1996) 99–104, [hep-th/9601029].

[63] s. J. C. Dias, J. E. Santos, and B. Way, *Numerical Methods for Finding Stationary Gravitational Solutions*, *Class. Quant. Grav.* **33** (2016), no. 13 133001, [arXiv:1510.0280].

[64] W. H. Press, S. A. Teukolsky, W. T. Vetterling, and B. P. Flannery, *Numerical Recipes in FORTRAN: The Art of Scientific Computing*, .

[65] L. Lehner and F. Pretorius, *Black Strings, Low Viscosity Fluids, and Violation of Cosmic Censorship*, *Phys. Rev. Lett.* **105** (2010) 101102, [arXiv:1006.5960].

[66] R. Gregory and R. Laflamme, *Black strings and p-branes are unstable*, *Phys. Rev. Lett.* **70** (1993) 2837–2840, [hep-th/9301052].

[67] E. Seidel and W.-M. Suen, *Towards a singularity-proof scheme in numerical relativity*, *Phys. Rev. Lett.* **69** (Sep, 1992) 1845–1848.

[68] S. A. Hartnoll, C. P. Herzog, and G. T. Horowitz, *Holographic Superconductors*, *JHEP* **12** (2008) 015, [arXiv:0810.1563].

[69] L. E. Kidder, M. A. Scheel, S. A. Teukolsky, E. D. Carlson, and G. B. Cook, *Black hole evolution by spectral methods*, *Phys. Rev.* **D62** (2000) 084032, [gr-qc/0005056].

[70] P. Figueras, J. Lucietti, and T. Wiseman, *Ricci solitons, Ricci flow, and strongly coupled CFT in the Schwarzschild Unruh or Boulware vacua*, *Class. Quant. Grav.* **28** (2011) 215018, [arXiv:1104.4489].

[71] Z. Fu, D. Marolf, and E. Mefford, *Time-independent wormholes*, *JHEP* **12** (2016) 021, [arXiv:1610.0806].

[72] E. Mefford, E. Shaghoulian, and M. Shyani, *Sparseness bounds on local operators in holographic CFT_d*, *JHEP (to appear)* (2017) [arXiv:1711.0312].

[73] A. Ishibashi, K. Maeda, and E. Mefford, *Holographic stress-energy tensor near the Cauchy horizon inside a rotating black hole*, *Phys. Rev.* **D96** (2017), no. 2 024005, [arXiv:1703.0974].

[74] L. Fidkowski, V. Hubeny, M. Kleban, and S. Shenker, *The Black hole singularity in AdS / CFT*, *JHEP* **02** (2004) 014, [hep-th/0306170].

[75] T. Hartman and J. Maldacena, *Time Evolution of Entanglement Entropy from Black Hole Interiors*, *JHEP* **05** (2013) 014, [arXiv:1303.1080].

[76] J. L. Friedman, K. Schleich, and D. M. Witt, *Topological censorship*, *Phys. Rev. Lett.* **71** (1993) 1486–1489, [gr-qc/9305017]. [Erratum: Phys. Rev. Lett.75,1872(1995)].

[77] G. J. Galloway, K. Schleich, D. M. Witt, and E. Woolgar, *Topological censorship and higher genus black holes*, *Phys. Rev.* **D60** (1999) 104039, [gr-qc/9902061].

[78] D. Stanford and L. Susskind, *Complexity and Shock Wave Geometries*, *Phys. Rev.* **D90** (2014), no. 12 126007, [arXiv:1406.2678].

[79] D. A. Roberts, D. Stanford, and L. Susskind, *Localized shocks*, *JHEP* **03** (2015) 051, [arXiv:1409.8180].

[80] A. R. Brown, D. A. Roberts, L. Susskind, B. Swingle, and Y. Zhao, *Holographic Complexity Equals Bulk Action?*, *Phys. Rev. Lett.* **116** (2016), no. 19 191301, [arXiv:1509.0787].

[81] A. R. Brown, D. A. Roberts, L. Susskind, B. Swingle, and Y. Zhao, *Complexity, action, and black holes*, *Phys. Rev.* **D93** (2016), no. 8 086006, [arXiv:1512.0499].

[82] C. W. Misner, K. S. Thorne, and J. A. Wheeler, *Gravitation*. W. H. Freeman, San Francisco, 1973.

[83] S. Ryu and T. Takayanagi, *Aspects of Holographic Entanglement Entropy*, *JHEP* **08** (2006) 045, [hep-th/0605073].

[84] A. Lewkowycz and J. Maldacena, *Generalized gravitational entropy*, *JHEP* **08** (2013) 090, [arXiv:1304.4926].

[85] X. Dong, A. Lewkowycz, and M. Rangamani, *Deriving covariant holographic entanglement*, arXiv:1607.0750.

[86] A. C. Wall, *Maximin Surfaces, and the Strong Subadditivity of the Covariant Holographic Entanglement Entropy*, *Class. Quant. Grav.* **31** (2014), no. 22 225007, [arXiv:1211.3494].

[87] C. A. R. Herdeiro and E. Radu, *Asymptotically flat black holes with scalar hair: a review*, *Int. J. Mod. Phys.* **D24** (2015), no. 09 1542014, [arXiv:1504.0820].

[88] L. Lehner, R. C. Myers, E. Poisson, and R. D. Sorkin, *Gravitational action with null boundaries*, arXiv:1609.0020.

[89] J. D. Bekenstein, *Novel no-scalar-hair theorem for black holes*, *Phys. Rev.* **D51** (1995), no. 12 R6608.

[90] N. Benjamin, M. C. N. Cheng, S. Kachru, G. W. Moore, and N. M. Paquette, *Elliptic Genera and 3d Gravity*, *Annales Henri Poincare* **17** (2016), no. 10 2623–2662, [arXiv:1503.0480].

[91] P. Kraus, A. Sivaramakrishnan, and R. Snively, *Black holes from CFT: Universality of correlators at large c*, arXiv:1706.0077.

[92] A. Belin, J. de Boer, J. Kruthoff, B. Michel, E. Shaghoulian, and M. Shyani, *Universality of sparse $d > 2$ conformal field theory at large N*, *JHEP* **03** (2017) 067, [arXiv:1610.0618].

[93] E. Shaghoulian, *Emergent gravity from Eguchi-Kawai reduction*, *JHEP* **03** (2017) 011, [arXiv:1611.0418].

[94] S. W. Hawking and D. N. Page, *Thermodynamics of black holes in anti-de sitter space*, *Comm. Math. Phys.* **87** (1982), no. 4 577–588.

[95] O. Aharony, J. Marsano, S. Minwalla, K. Papadodimas, and M. Van Raamsdonk, *The Hagedorn - deconfinement phase transition in weakly coupled large N gauge theories*, *Adv. Theor. Math. Phys.* **8** (2004) 603–696, [hep-th/0310285].

[96] P. Kraus and F. Larsen, *Microscopic black hole entropy in theories with higher derivatives*, *JHEP* **09** (2005) 034, [hep-th/0506176].

[97] B. Sundborg, *The Hagedorn transition, deconfinement and N=4 SYM theory*, *Nucl. Phys.* **B573** (2000) 349–363, [hep-th/9908001].

[98] T. Nishioka and T. Takayanagi, *On Type IIA Penrose Limit and N=6 Chern-Simons Theories*, *JHEP* **08** (2008) 001, [arXiv:0806.3391].

[99] K. Landsteiner, *String corrections to the Hawking-Page phase transition*, *Mod. Phys. Lett.* **A14** (1999) 379–386, [hep-th/9901143].

[100] M. Spradlin and A. Volovich, *A Pendant for Polya: The One-loop partition function of N=4 SYM on R x S**3*, *Nucl. Phys.* **B711** (2005) 199–230, [hep-th/0408178].

[101] G. Papathanasiou and M. Spradlin, *The Morphology of N=6 Chern-Simons Theory*, *JHEP* **07** (2009) 036, [arXiv:0903.2548].

[102] E. P. Verlinde, *On the holographic principle in a radiation dominated universe*, hep-th/0008140.

[103] K. Jensen, *Chiral anomalies and AdS/CMT in two dimensions*, *JHEP* **01** (2011) 109, [arXiv:1012.4831].

[104] P. Kraus, *Lectures on black holes and the AdS(3) / CFT(2) correspondence*, *Lect. Notes Phys.* **755** (2008) 193–247, [hep-th/0609074].

[105] C. Martinez, C. Teitelboim, and J. Zanelli, *Charged rotating black hole in three space-time dimensions*, *Phys. Rev.* **D61** (2000) 104013, [hep-th/9912259].

[106] M. Banados, G. Barnich, G. Compere, and A. Gomberoff, *Three dimensional origin of Godel spacetimes and black holes*, *Phys. Rev.* **D73** (2006) 044006, [hep-th/0512105].

[107] M. M. Caldarelli, G. Cognola, and D. Klemm, *Thermodynamics of Kerr-Newman-AdS black holes and conformal field theories*, *Class. Quant. Grav.* **17** (2000) 399–420, [hep-th/9908022].

[108] A. Chamblin, R. Emparan, C. V. Johnson, and R. C. Myers, *Holography, thermodynamics and fluctuations of charged AdS black holes*, *Phys. Rev.* **D60** (1999) 104026, [hep-th/9904197].

[109] A. Chamblin, R. Emparan, C. V. Johnson, and R. C. Myers, *Charged AdS black holes and catastrophic holography*, *Phys. Rev.* **D60** (1999) 064018, [hep-th/9902170].

[110] S. W. Hawking, C. J. Hunter, and M. Taylor, *Rotation and the AdS / CFT correspondence*, *Phys. Rev.* **D59** (1999) 064005, [hep-th/9811056].

[111] G. W. Gibbons, H. Lu, D. N. Page, and C. N. Pope, *The General Kerr-de Sitter metrics in all dimensions*, *J. Geom. Phys.* **53** (2005) 49–73, [hep-th/0404008].

[112] G. W. Gibbons, H. Lu, D. N. Page, and C. N. Pope, *Rotating black holes in higher dimensions with a cosmological constant*, *Phys. Rev. Lett.* **93** (2004) 171102, [hep-th/0409155].

[113] V. A. Kostelecky and M. J. Perry, *Solitonic black holes in gauged N=2 supergravity*, *Phys. Lett.* **B371** (1996) 191–198, [hep-th/9512222].

[114] V. Balasubramanian and P. Kraus, *A Stress tensor for Anti-de Sitter gravity*, *Commun. Math. Phys.* **208** (1999) 413–428, [hep-th/9902121].

[115] Z. W. Chong, M. Cvetic, H. Lu, and C. N. Pope, *General non-extremal rotating black holes in minimal five-dimensional gauged supergravity*, *Phys. Rev. Lett.* **95** (2005) 161301, [hep-th/0506029].

[116] D. D. K. Chow, *Charged rotating black holes in six-dimensional gauged supergravity*, *Class. Quant. Grav.* **27** (2010) 065004, [arXiv:0808.2728].

[117] D. D. K. Chow, *Equal charge black holes and seven dimensional gauged supergravity*, *Class. Quant. Grav.* **25** (2008) 175010, [arXiv:0711.1975].

[118] G. T. Horowitz, J. E. Santos, and B. Way, *Evidence for an Electrifying Violation of Cosmic Censorship*, *Class. Quant. Grav.* **33** (2016), no. 19 195007, [arXiv:1604.0646].

[119] T. Crisford, G. T. Horowitz, and J. E. Santos, *Testing the Weak Gravity - Cosmic Censorship Connection*, arXiv:1709.0788.

[120] D. Kutasov and F. Larsen, *Partition sums and entropy bounds in weakly coupled CFT*, *JHEP* **01** (2001) 001, [hep-th/0009244].

[121] E. Shaghoulian, *Modular forms and a generalized Cardy formula in higher dimensions*, *Phys. Rev.* **D93** (2016), no. 12 126005, [arXiv:1508.0272].

[122] E. Shaghoulian, *Black hole microstates in AdS*, *Phys. Rev.* **D94** (2016), no. 10 104044, [arXiv:1512.0685].

[123] R.-G. Cai, *The Cardy-Verlinde formula and AdS black holes*, *Phys. Rev.* **D63** (2001) 124018, [hep-th/0102113].

[124] R.-G. Cai, Y. S. Myung, and N. Ohta, *Bekenstein bound, holography and brane cosmology in charged black hole backgrounds*, *Classical and Quantum Gravity* **18** (2001), no. 24 5429.

[125] R.-G. Cai, L.-M. Cao, and D.-W. Pang, *Thermodynamics of dual CFTs for Kerr-AdS black holes*, *Phys. Rev.* **D72** (2005) 044009, [hep-th/0505133].

[126] G. W. Gibbons, M. J. Perry, and C. N. Pope, *Bulk/boundary thermodynamic equivalence, and the Bekenstein and cosmic-censorship bounds for rotating charged AdS black holes*, *Phys. Rev.* **D72** (2005) 084028, [hep-th/0506233].

[127] E. Shaghoulian, *Modular Invariance of Conformal Field Theory on $S^1 \times S^3$ and Circle Fibrations*, *Phys. Rev. Lett.* **119** (2017), no. 13 131601, [arXiv:1612.0525].

[128] G. T. Horowitz and E. Shaghoulian, *Detachable circles and temperature-inversion dualities for CFT_d*, arXiv:1709.0608.

[129] E. Shaghoulian, *"Nonlocal operators in CFT,"* to be published.

[130] D. Jafferis, B. Mukhametzhanov, and A. Zhiboedov, *Conformal Bootstrap At Large Charge*, arXiv:1710.1116.

[131] S. Hellerman, D. Orlando, S. Reffert, and M. Watanabe, *On the CFT Operator Spectrum at Large Global Charge*, *JHEP* **12** (2015) 071, [arXiv:1505.0153].

[132] A. Monin, D. Pirtskhalava, R. Rattazzi, and F. K. Seibold, *Semiclassics, Goldstone Bosons and CFT data*, *JHEP* **06** (2017) 011, [arXiv:1611.0291].

[133] I. Heemskerk, J. Penedones, J. Polchinski, and J. Sully, *Holography from Conformal Field Theory*, *JHEP* **10** (2009) 079, [arXiv:0907.0151].

[134] S. Hellerman, *A Universal Inequality for CFT and Quantum Gravity*, *JHEP* **08** (2011) 130, [arXiv:0902.2790].

[135] H. K. Kunduri and J. Lucietti, *Notes on non-extremal, charged, rotating black holes in minimal D=5 gauged supergravity*, *Nucl. Phys.* **B724** (2005) 343–356, [hep-th/0504158].

[136] M. Cvetic, H. Lu, and C. N. Pope, *Gauged six-dimensional supergravity from massive type IIA*, *Phys. Rev. Lett.* **83** (1999) 5226–5229, [hep-th/9906221].

[137] W. Chen, H. Lu, and C. N. Pope, *General Kerr-NUT-AdS metrics in all dimensions*, *Class. Quant. Grav.* **23** (2006) 5323–5340, [hep-th/0604125].

[138] G. W. Gibbons, M. J. Perry, and C. N. Pope, *The First law of thermodynamics for Kerr-anti-de Sitter black holes*, *Class. Quant. Grav.* **22** (2005) 1503–1526, [hep-th/0408217].

[139] S. A. Fulling, *Nonuniqueness of canonical field quantization in Riemannian space-time*, *Phys. Rev.* **D7** (1973) 2850–2862.

[140] P. C. W. Davies, *Scalar particle production in Schwarzschild and Rindler metrics*, *J. Phys.* **A8** (1975) 609–616.

[141] W. G. Unruh, *Notes on black hole evaporation*, *Phys. Rev.* **D14** (1976) 870.

[142] D. M. Capper and M. J. Duff, *Trace anomalies in dimensional regularization*, *Nuovo Cim.* **A23** (1974) 173–183.

[143] S. W. Hawking, *Black hole explosions*, *Nature* **248** (1974) 30–31.

[144] J. D. Bekenstein, *Black holes and entropy*, *Phys. Rev.* **D7** (1973) 2333–2346.

[145] S. M. Christensen and S. A. Fulling, *Trace Anomalies and the Hawking Effect*, *Phys. Rev.* **D15** (1977) 2088–2104.

[146] V. E. Hubeny, D. Marolf, and M. Rangamani, *Hawking radiation in large N strongly-coupled field theories*, *Class. Quant. Grav.* **27** (2010) 095015, [arXiv:0908.2270].

[147] V. E. Hubeny, D. Marolf, and M. Rangamani, *Black funnels and droplets from the AdS C-metrics*, *Class. Quant. Grav.* **27** (2010) 025001, [arXiv:0909.0005].

[148] V. E. Hubeny, D. Marolf, and M. Rangamani, *Hawking radiation from AdS black holes*, *Class. Quant. Grav.* **27** (2010) 095018, [arXiv:0911.4144].

[149] D. Marolf, M. Rangamani, and T. Wiseman, *Holographic thermal field theory on curved spacetimes*, *Class. Quant. Grav.* **31** (2014) 063001, [arXiv:1312.0612].

[150] G. Compere and D. Marolf, *Setting the boundary free in AdS/CFT*, *Class. Quant. Grav.* **25** (2008) 195014, [arXiv:0805.1902].

[151] S. Fischetti and J. E. Santos, *Rotating Black Droplet*, *JHEP* **07** (2013) 156, [arXiv:1304.1156].

[152] S. Fischetti and D. Marolf, *Flowing Funnels: Heat sources for field theories and the AdS_3 dual of CFT_2 Hawking radiation*, *Class. Quant. Grav.* **29** (2012) 105004, [arXiv:1202.5069].

[153] S. Fischetti, D. Marolf, and J. E. Santos, *AdS flowing black funnels: Stationary AdS black holes with non-Killing horizons and heat transport in the dual CFT*, *Class. Quant. Grav.* **30** (2013) 075001, [arXiv:1212.4820].

[154] C. Fefferman and C. R. Graham, *The ambient metric*, arXiv:0710.0919.

[155] P. Calabrese and J. L. Cardy, *Entanglement entropy and quantum field theory*, *J. Stat. Mech.* **0406** (2004) P06002, [hep-th/0405152].

[156] T. Faulkner, A. Lewkowycz, and J. Maldacena, *Quantum corrections to holographic entanglement entropy*, *JHEP* **11** (2013) 074, [arXiv:1307.2892].

[157] N. Engelhardt and A. C. Wall, *Quantum Extremal Surfaces: Holographic Entanglement Entropy beyond the Classical Regime*, *JHEP* **01** (2015) 073, [arXiv:1408.3203].

[158] M. Headrick and T. Takayanagi, *A Holographic proof of the strong subadditivity of entanglement entropy*, *Phys. Rev.* **D76** (2007) 106013, [arXiv:0704.3719].

[159] V. Balasubramanian, B. D. Chowdhury, B. Czech, J. de Boer, and M. P. Heller, *Bulk curves from boundary data in holography*, *Phys. Rev.* **D89** (2014), no. 8 086004, [arXiv:1310.4204].

[160] T. Faulkner, M. Guica, T. Hartman, R. C. Myers, and M. Van Raamsdonk, *Gravitation from Entanglement in Holographic CFTs*, *JHEP* **03** (2014) 051, [arXiv:1312.7856].

[161] B. Swingle and M. Van Raamsdonk, *Universality of Gravity from Entanglement*, arXiv:1405.2933.

[162] I. R. Klebanov, D. Kutasov, and A. Murugan, *Entanglement as a probe of confinement*, *Nucl. Phys.* **B796** (2008) 274–293, [arXiv:0709.2140].

[163] T. Hirata and T. Takayanagi, *AdS/CFT and strong subadditivity of entanglement entropy*, *JHEP* **02** (2007) 042, [hep-th/0608213].

[164] N. Drukker, D. J. Gross, and H. Ooguri, *Wilson loops and minimal surfaces*, *Phys. Rev.* **D60** (1999) 125006, [hep-th/9904191].

[165] R. Emparan, *Black hole entropy as entanglement entropy: A Holographic derivation*, *JHEP* **06** (2006) 012, [hep-th/0603081].

[166] P. Figueras and S. Tunyasuvunakool, *CFTs in rotating black hole backgrounds*, *Class. Quant. Grav.* **30** (2013) 125015, [arXiv:1304.1162].

[167] J. E. Santos and B. Way, *Black Funnels*, *JHEP* **12** (2012) 060, [arXiv:1208.6291].

[168] J. E. Santos and B. Way, *Black Droplets*, *JHEP* **08** (2014) 072, [arXiv:1405.2078].

[169] F. R. Tangherlini, *Schwarzschild field in n dimensions and the dimensionality of space problem*, *Nuovo Cim.* **27** (1963) 636–651.

[170] H. Epstein, V. Glaser, and A. Jaffe, *Nonpositivity of energy density in Quantized field theories*, *Nuovo Cim.* **36** (1965) 1016.

[171] P. C. W. Davies and S. A. Fulling, *Radiation from Moving Mirrors and from Black Holes*, *Proc. Roy. Soc. Lond.* **A356** (1977) 237–257.

[172] G. T. Horowitz, ed., *Black holes in higher dimensions*. Cambridge Univ. Pr., Cambridge, UK, 2012.

[173] D. Marolf, W. Kelly, and S. Fischetti, *Conserved Charges in Asymptotically (Locally) AdS Spacetimes*, in *Springer Handbook of Spacetime* (A. Ashtekar and V. Petkov, eds.), pp. 381–407. 2014. arXiv:1211.6347.

[174] I. R. Klebanov, S. S. Pufu, S. Sachdev, and B. R. Safdi, *Renyi Entropies for Free Field Theories*, *JHEP* **04** (2012) 074, [arXiv:1111.6290].

[175] S. N. Solodukhin, *Entanglement entropy of black holes and AdS/CFT correspondence*, *Phys. Rev. Lett.* **97** (2006) 201601, [hep-th/0606205].

[176] D. J. Gross and H. Ooguri, *Aspects of large N gauge theory dynamics as seen by string theory*, *Phys. Rev.* **D58** (1998) 106002, [hep-th/9805129].

[177] H. Kim, D. K. Park, S. Tamarian, and H. J. W. Muller-Kirsten, *Gross-Ooguri phase transition at zero and finite temperature: Two circular Wilson loop case*, *JHEP* **03** (2001) 003, [hep-th/0101235].

[178] H. Casini, M. Huerta, and R. C. Myers, *Towards a derivation of holographic entanglement entropy*, *JHEP* **05** (2011) 036, [arXiv:1102.0440].

[179] B. Czech, J. L. Karczmarek, F. Nogueira, and M. Van Raamsdonk, *Rindler Quantum Gravity*, *Class. Quant. Grav.* **29** (2012) 235025, [arXiv:1206.1323].

[180] S. de Haro, S. N. Solodukhin, and K. Skenderis, *Holographic reconstruction of space-time and renormalization in the AdS / CFT correspondence*, *Commun. Math. Phys.* **217** (2001) 595–622, [hep-th/0002230].

[181] L. H. Ford, M. J. Pfenning, and T. A. Roman, *Quantum inequalities and singular negative energy densities*, *Phys. Rev.* **D57** (1998) 4839–4846, [gr-qc/9711030].

[182] W. A. Hiscock, *Stress Energy Tensor Near a Charged, Rotating, Evaporating Black Hole*, *Phys. Rev.* **D15** (1977) 3054–3057.

[183] W. A. Hiscock and D. A. Konkowski, *QUANTUM VACUUM ENERGY IN TAUB - NUT (NEWMAN-UNTI-TAMBURINO) TYPE COSMOLOGIES*, *Phys. Rev.* **D26** (1982) 1225–1230.

[184] N. Haddad, *Hawking Radiation from Small Black Holes at Strong Coupling and Large N*, *Class. Quant. Grav.* **30** (2013) 195002, [arXiv:1306.0086].

[185] M. M. Caldarelli, O. J. C. Dias, R. Monteiro, and J. E. Santos, *Black funnels and droplets in thermal equilibrium*, *JHEP* **05** (2011) 116, [arXiv:1102.4337].

[186] N. Haddad, *Black Strings Ending on Horizons*, *Class. Quant. Grav.* **29** (2012) 245001, [arXiv:1207.2305].

[187] R. Emparan, T. Harmark, V. Niarchos, and N. A. Obers, *World-Volume Effective Theory for Higher-Dimensional Black Holes*, *Phys. Rev. Lett.* **102** (2009) 191301, [arXiv:0902.0427].

[188] J. Armas, *How Fluids Bend: the Elastic Expansion for Higher-Dimensional Black Holes*, *JHEP* **09** (2013) 073, [arXiv:1304.7773].

[189] R. C. Myers and M. J. Perry, *Black Holes in Higher Dimensional Space-Times*, *Annals Phys.* **172** (1986) 304.

[190] R. Emparan, C. V. Johnson, and R. C. Myers, *Surface terms as counterterms in the AdS / CFT correspondence*, *Phys. Rev.* **D60** (1999) 104001, [hep-th/9903238].

[191] K. Maeda, T. Okamura, and J.-i. Koga, *Inhomogeneous charged black hole solutions in asymptotically anti-de Sitter spacetime*, *Phys. Rev.* **D85** (2012) 066003, [arXiv:1107.3677].

[192] S. A. Hartnoll, *Lectures on holographic methods for condensed matter physics*, *Class.Quant.Grav.* **26** (2009) 224002, [arXiv:0903.3246].

[193] J. McGreevy, *Holographic duality with a view toward many-body physics*, *Adv.High Energy Phys.* **2010** (2010) 723105, [arXiv:0909.0518].

[194] S. Sachdev, *What can gauge-gravity duality teach us about condensed matter physics?*, *Ann.Rev.Condensed Matter Phys.* **3** (2012) 9–33, [arXiv:1108.1197].

[195] S. A. Hartnoll, C. P. Herzog, and G. T. Horowitz, *Building a Holographic Superconductor*, *Phys.Rev.Lett.* **101** (2008) 031601, [arXiv:0803.3295].

[196] S. A. Hartnoll and D. M. Hofman, *Locally Critical Resistivities from Umklapp Scattering*, *Phys.Rev.Lett.* **108** (2012) 241601, [arXiv:1201.3917].

[197] A. Donos and S. A. Hartnoll, *Interaction-driven localization in holography*, *Nature Phys.* **9** (2013) 649–655, [arXiv:1212.2998].

[198] A. Donos and J. P. Gauntlett, *Holographic Q-lattices*, *JHEP* **1404** (2014) 040, [arXiv:1311.3292].

[199] A. Donos and J. P. Gauntlett, *Novel metals and insulators from holography*, *JHEP* **1406** (2014) 007, [arXiv:1401.5077].

[200] B. Goutéraux, *Charge transport in holography with momentum dissipation*, *JHEP* **1404** (2014) 181, [arXiv:1401.5436].

[201] Y. Ling, C. Niu, J. Wu, Z. Xian, and H.-b. Zhang, *Metal-insulator Transition by Holographic Charge Density Waves*, arXiv:1404.0777.

[202] A. Donos and S. A. Hartnoll, *Universal linear in temperature resistivity from black hole superradiance*, *Phys.Rev.* **D86** (2012) 124046, [arXiv:1208.4102].

[203] G. T. Horowitz, J. E. Santos, and D. Tong, *Optical Conductivity with Holographic Lattices*, *JHEP* **1207** (2012) 168, [arXiv:1204.0519].

[204] T. Nishioka, S. Ryu, and T. Takayanagi, *Holographic Superconductor/Insulator Transition at Zero Temperature*, *JHEP* **1003** (2010) 131, [arXiv:0911.0962].

[205] G. T. Horowitz and B. Way, *Complete Phase Diagrams for a Holographic Superconductor/Insulator System*, *JHEP* **1011** (2010) 011, [arXiv:1007.3714].

[206] A. Karch and A. O'Bannon, *Metallic AdS/CFT*, *JHEP* **0709** (2007) 024, [arXiv:0705.3870].

[207] S. Ryu, T. Takayanagi, and T. Ugajin, *Holographic Conductivity in Disordered Systems*, *JHEP* **1104** (2011) 115, [arXiv:1103.6068].

[208] D. Freedman, S. Gubser, K. Pilch, and N. Warner, *Renormalization group flows from holography supersymmetry and a c theorem*, *Adv.Theor.Math.Phys.* **3** (1999) 363–417, [hep-th/9904017].

[209] N. Iqbal and H. Liu, *Universality of the hydrodynamic limit in AdS/CFT and the membrane paradigm*, *Phys.Rev.* **D79** (2009) 025023, [arXiv:0809.3808].

[210] S. S. Gubser, S. S. Pufu, and F. D. Rocha, *Quantum critical superconductors in string theory and M-theory*, *Phys.Lett.* **B683** (2010) 201–204, [arXiv:0908.0011].

[211] T. Faulkner, G. T. Horowitz, and M. M. Roberts, *Holographic quantum criticality from multi-trace deformations*, *JHEP* **1104** (2011) 051, [arXiv:1008.1581].

[212] T. Faulkner, G. T. Horowitz, and M. M. Roberts, *New stability results for Einstein scalar gravity*, *Class.Quant.Grav.* **27** (2010) 205007, [arXiv:1006.2387].

[213] E. Witten, *Multitrace operators, boundary conditions, and AdS / CFT correspondence*, hep-th/0112258.

[214] M. Berkooz, A. Sever, and A. Shomer, *'Double trace' deformations, boundary conditions and space-time singularities*, *JHEP* **0205** (2002) 034, [hep-th/0112264].

[215] D. T. Son and A. O. Starinets, *Minkowski space correlators in AdS / CFT correspondence: Recipe and applications*, *JHEP* **0209** (2002) 042, [hep-th/0205051].

[216] S. S. Gubser and F. D. Rocha, *The gravity dual to a quantum critical point with spontaneous symmetry breaking*, *Phys.Rev.Lett.* **102** (2009) 061601, [arXiv:0807.1737].

[217] M. Headrick, S. Kitchen, and T. Wiseman, *A New approach to static numerical relativity, and its application to Kaluza-Klein black holes*, *Class.Quant.Grav.* **27** (2010) 035002, [arXiv:0905.1822].

[218] P. Figueras, J. Lucietti, and T. Wiseman, *Ricci solitons, Ricci flow, and strongly coupled CFT in the Schwarzschild Unruh or Boulware vacua*, *Class.Quant.Grav.* **28** (2011) 215018, [arXiv:1104.4489].

[219] C. Christiansen, L. M. Hernandez, and A. M. Goldman, *Evidence of Collective Charge Behavior in the Insulating State of Ultrathin Films of Superconducting Metals*, *Physical Review Letters* **88** (Jan., 2002) 037004, [cond-mat/0108315].

[220] P. Phillips and D. Dalidovich, *The Elusive Bose Metal*, *Science* **302** (Oct., 2003) 243–247, [cond-mat/0310316].